The role of Lymphoblastic leukemia 1 (Lyl1) in *Mycobacterium tuberculosis* (*Mtb*) infection

Shelby-Sara Ann Jones

JNSSHE006

Thesis Presented for the Degree of DOCTOR OF PHILOSOPHY in the Department of Pathology, Faculty of Health Science, University of Cape Town

Cytokines and Disease Group (Prof. Frank Brombacher),
International Centre for Genetic Engineering and Biotechnology (ICGEB),
Cape Town Component and Institute of Infectious Diseases and Molecular Medicine (IDM), Division of Immunology,
Faculty of Health Sciences, University of Cape Town,
Cape Town, South Africa.

SEPTEMBER 2020

Table of Contents

Table of Contents ..... **ii**
Declaration ..... **v**
Acknowledgements ..... **vi**
Conferences ..... **viii**
List of Abbreviations ..... **ix**
List of Figures ..... **xii**
Abstract **1**
Chapter 1 ..... **2**
Literature Review **2**
1.1. Bacteria and the Immune System 2
1.1.1. The threat of bacterial infections 2
1.1.2. Immune response to bacterial infections 3
1.1.2.1. Innate immunity 3
1.1.2.2. Adaptive immunity 4
1.1.2.3. Macrophage response to bacterial infections 5
1.1.3. Tuberculosis 6
1.1.3.1. History 6
1.1.3.2. Epidemiology 8
1.1.3.3. Macrophages during *Mtb* infection 10
1.1.4. Listeriosis 12
1.1.4.1. History 12
1.1.4.2. Epidemiology 13
1.1.4.3. Macrophages during *Lm* infection 14
1.2. Host-Directed Therapy for Tuberculosis 16
1.2.1. HDT potential targets 16
1.2.2. Using transcriptomics to identify HDT targets 18
1.2.2.1. FANTOM5: Identifying *Mtb* targeted genes 19
1.3. Lymphoblastic leukemia 1 (Lyl1): A potential host protective gene against bacteria 21
1.3.1. Discovery 21
1.3.2. Lyl1 and its paralog, Scl/Tal1 21
1.3.3. Role of Lyl1 in leukemia 22
1.3.4. Lyl1 mouse models 23
1.4. Project Rationale 24
1.4.1. Problem statement 24
1.4.2. Hypothesis 24
1.4.3. Aim and Objectives 25
CHAPTER 2: Manuscript in preparation **26**
Lyl1-deficient mice are immunologically comparable to wild-type mice at steady state **26**
2.1. Abstract 27
2.2. Introduction 27
2.3. Methods 28
2.3.1. Mouse strains 28
2.3.2. Mouse genotyping 29
2.3.3. Ethical statement 29
2.3.4. Single cell suspension of organs upon euthanasia 29

2.3.5. Quantitative real-time polymerase chain reaction (qRT-PCR) 30
2.3.6. Flow cytometry 30
2.3.7. Measurement of cytokines and/or antibodies in organ homogenates and/or serum 31
2.3.8. Histopathology and immunohistochemistry 31
2.3.9. Statistical analyses 31
2.4. Results 31
2.4.1. The neomycin cassette in the published Lyl1-deficient ($Lyl1^{Mg}$) mouse has been omitted, yet they remain viable and express no physiological difference compared to wild-type mice 31
2.4.2. Lyl1-deficiency causes imbalances during thymopoiesis, however, express similar single positive T-cells compared to WT 32
2.4.3. Lung and lymph node (LN) immune cell populations are comparable between WT and Lyl1-knockout mice 33
2.4.4. Globally deleted Lyl1 and WT mice demonstrate comparable immune cell populations in the spleen and liver tissues 33
2.4.5. The cytokine/antibody profile is minimally affected by the absence of Lyl1 at steady state…… 34
2.5. Discussion and Conclusion 34
2.6. Acknowledgements 36
CHAPTER 3: Manuscript in preparation 48
Lymphoblastic leukemia 1 (Lyl1): It is more than just a cancer gene 48
3.1. Abstract 49
3.2. Introduction 49
3.3. Methods 50
3.3.1. Mouse strains 50
3.3.2. Ethical statement 51
3.3.3. Bone marrow-derived macrophages (BMDM) generation and infection 51
3.3.4. Generation and infection/stimulation of monocyte-derived macrophages (MDM) 51
3.3.5. BMDM pathway stimulation and inhibition 52
3.3.6. Quantitative real-time polymerase chain reaction (qRT-PCR) 53
3.3.7. Western blot 53
3.3.8. *Listeria monocytogenes* (*Lm*) infection in mice 54
3.3.9. Measurement of nitric oxide and cytokines/chemokine in culture supernatants and homogenates 54
3.3.10. Flow cytometry 54
3.3.11. Statistical analyses 55
3.4. Results 55
3.4.1. Lyl1 expression is significantly downregulated in response to bacterial infections and immune stimulants 55
3.4.2. MAPk and NFκB signaling pathways are key regulators of Lyl1 expression 56
3.4.3. Lyl1-deficient macrophages are less inflammatory in response to LPS *in vitro* 57
3.4.4. MAPk and NFκB p50-p65 signaling pathways are not regulated by Lyl1 57
3.4.5. Lyl1-deficient mice are more susceptible to *Lm* infection *in vivo* 58
3.5. Discussion and Conclusion 59
3.6. Acknowledgements 62
CHAPTER 4: Manuscript in preparation 76
Lyl1-deficiency promotes inflammatory responses and increased bacterial burden in response to *Mycobacterium tuberculosis* infection 76

4.1. Abstract 77
4.2. Introduction 77
4.3. Methods 78
4.3.1. Mouse strains 78
4.3.2. Ethical statement 79
4.3.3. Bone marrow-derived macrophages (BMDM) generation, activation and infection *in vitro* 79
4.3.4. *Mtb* infection in mice (*in vivo*) 79
4.3.5. Bacterial loads in BMDM and organs 80
4.3.6. Quantitative real-time polymerase chain reaction (qRT-PCR) 80
4.3.7. Measurement of nitric oxide and cytokines/chemokine in culture supernatants and homogenates 80
4.3.8. Flow cytometry 81
4.3.9. Histopathology and immunohistochemistry 81
4.3.10. Data deposition 81
4.3.11. Statistical analyses 82
4.4. Results 82
4.4.1. Lyl1 is required to circumvent *Mtb* infection in macrophages *in vitro* 82
4.4.2. Lyl1$^{-/-}$ mice are highly susceptible to chronic hypervirulent *Mtb* HN878 infection *in vivo* 83
4.4.3. The absence of Lyl1 increases neutrophil recruitment during chronic hypervirulent *Mtb* HN878 infection *in vivo* 83
4.4.4. Lyl1-deficiency alters cytokine-chemokine secretion and promotes lung inflammation/pathology in response to hypervirulent *Mtb* HN878 infection *in vivo* 84
4.4.5. Lyl1-deficient neutrophils, monocytes and macrophages experience a significantly different cytokine profile *in vivo* compared to WT in response to *Mtb* H37Rv infection .. 85
4.4.6. Lyl1 cannot be used as a biomarker for TB diagnosis 86
4.5. Discussion and Conclusion 87
4.6. Acknowledgements 91
Concluding Remarks 112
References 114
Appendix 125

Declaration

I, *Shelby-Sara Ann Jones*, hereby declare that the work on which this dissertation/thesis is based is my original work (except where acknowledgements indicate otherwise) and that neither the whole work nor any part of it has been, is being, or is to be submitted for another degree in this or any other university.

I empower the university to reproduce for the purpose of research either the whole or any portion of the contents in any manner whatsoever.

Signature: Signed by candidate

Date: 7 September 2020

Acknowledgements

بسم الله الرحمن الرحيم

لا إله إلا الله محمد رسول الله

Two years into this degree, my life took a major turn.

Writing these acknowledgements and it still feels so surreal. It's probably a common emotion many Ph.D. students feel when they finally see that light begin to illuminate brighter with each paragraph. Light, as a symbolism, has been my source of stability, guidance, motivation and determination to push through all the negative data and finally finish this degree.

If it wasn't for that brightest light shone my way, I'm not sure where I would have been today, which is why for whatever I achieve and am blessed with, ***Allah SWT will always be the first I thank and appreciate***.

Shukr Allah. Shukr Allah. Shukr Allah.

The decisions we make in life will always impact the ones we love, whether it be positively or negatively. Hence, before I make mention of anyone, I need to express my gratitude to my parents, **Gillian Bredeveldt** and **Wayne Jones**. As a tertiary student for nine years, I am immensely grateful for the continuous emotional and financial support I've received throughout my education. I promise I'm done now. Pending examiners that is. Don't give up my room just yet. However, most importantly, my heart fills with gratitude for guiding and supporting all the personal decisions I've made in my life. May Allah SWT bless me with many more years with both of you. May Allah SWT always guide us all and grant you your heart's desires. Thank you for being my stability light.

With the change in research fields from Plant Biotechnology for a master's degree to Clinical Science and Immunology for a Ph.D. degree, I would not have been able to breeze through the challenge without the help of my co-supervisor, **Dr. Mumin Ozturk**. Thank you for taking me under your wing and guiding me through the field. For always answering my basic immunological questions with respect and for your selflessness in assisting me throughout this degree. I will forever be grateful for the impact you had and have on my scientific career. A noble soul as yourself deserves nothing but immense success. May you always achieve your dreams and I wish you nothing but a victorious future ahead. Thank you for being my guidance light.

This would not be possible if my supervisor, **Prof. Frank Brombacher** and co-supervisor, **A.Prof. Reto Guler**, did not see the slightest potential in my abilities and grant me the opportunity to grow as a scientist.

Thank you for this career-altering opportunity and continuous guidance and support. The transfer between laboratories has taught me so much and it's an experience I will forever be grateful for.

In addition to expanding my scientific knowledge, I was afforded the opportunity to meet amazing colleagues and friends that either physically or emotionally supported the completion of this degree. Thank you to **Nathan Kieswetter**, **Sibongiseni Poswayo**, **Shandre Pillay**, **Thabo Mpotje**, **Suraj Parihar**, **Raygaana Jacobs**, **Saiyukti Naidoo**, **Ousman Tamgue**, **Maxine Hoft, Julius Chia** and all the **Brombacher Lab Members**. I wish you all easy completion of your degrees and/or great success for the future. Thank you for being my motivational light.

The experimental component of this thesis would not be possible if it were not for the **UCT Animal Staff**, especially **Rodney Lucas** for training me and later assisting me in project-specific experiments. Additionally, the Brombacher Lab would not function without the staff. I express my immense gratitude to **Wendy Green**, **Zarinah Sonday-Jattiem**, **Munadia Ansarie**, **Marlon Petersen and George Jacobs**, as well as all the **ICGEB, IDM and post-graduate staff members**. Furthermore, I acknowledge the **National Research Foundation (NRF)** for the continuous financial support as well as the **Medical Research Council (MRC), ICGEB** and **Welcome Trust** for supporting research running costs.

I have so many people to thank for emotional support including my siblings, **Chloe Thomas**, **Troy Jones**, **Connor Meinking**, **Skye Jones** as well as my Father's wife, **Dominique Jones**. Thank you for always being there for me and joining me on this roller-coaster ride. I wish you all successful careers ahead. To the **Addinall Family**, **Stegmann Family** and **Hamza Family**, words cannot express the gratitude I feel for these families. The support throughout my journey is something I will be forever grateful for, but most importantly shukran for all your dua's. I was blessed with an amazing support structure and the best thing I can offer in return are my prayers. Thank you for being determination light.

Finally, to **Riyaad Addinall**, my pillar. You offered me the entire sun to complete this degree. You were there when my data seemed most promising, but you were also there when it felt like this project was leading nowhere. From the day I decided to change research fields, to the day you took me to my interview, right up until my submission, you have stuck by my side. You have motivated and uplifted me countless times. You filtered me with light through my darkest times. Shukran. As I mentioned in my MSc, may Allah SWT grant your kind soul a successful future ahead.

This thesis is dedicated to my late Grandmother who returned home earlier this year.

"Allah is the light of the heavens and the earth" ~ Quran 24:35

Conferences

Title of Proceeding:	2nd Annual World TB Day NanoSymposium: Intervening along the spectrum of TB II
Title of Contribution:	Lyl1 deficiency contributes to susceptibility during *Mycobacterium tuberculosis* infection
Location & Date:	Cape Town, South Africa; March 2019
Format:	Poster Presentation
Award:	First Prize

Title of Proceeding:	Keystone Symposia A3 – Tuberculosis: Mechanisms, Pathogenesis and Treatment
Title of Contribution:	Lyl1 deficiency contributes to susceptibility during *Mycobacterium tuberculosis* infection
Location & Date:	Calgary, Canada; January 2019
Format:	Poster Presentation
Award:	No Award Structure

Title of Proceeding:	Infectious Diseases in Africa (IDA): Measurement of Immune Responses 2018
Title of Contribution:	Lyl1 deficiency contributes to susceptibility during *Mycobacterium tuberculosis* infection
Location & Date:	Cape Town, South Africa; November 2018
Format:	Poster Presentation
Award:	Did not place

List of Abbreviations

AIM	Apoptosis Inhibitor of Macrophages
AML	Acute Myeloid Leukemia
ANG-2	Angiopoietin-2
APC	Antigen Presenting Cell
BCG	Bacillus Calmette-Guerin
bHLH	basic Helix-Loop-Helix
BMDM	Bone Marrow-Derived Macrophages
CAGE	Cap Analysis of Gene Expression
CDC	Centers for Disease Control and Prevention
cDNA	Complementary Deoxyribonucleic Acid
cGAS/cGAMP	cyclic GMP-AMP Synthase
COX1/2	Cyclooxygenase 1/2
CpG ODN	CpG Oligodeoxynucleotide
CREB1	Cyclic-AMP Receptor Element Binding Protein 1
DC-SIGN	DC-Specific Intercellular Adhesion Molecule-3 Grabbing Nonintegrin
DMEM	Dulbecco's Modified Eagle Medium
DN	Double Negative
DNA	Deoxyribonucleic Acid
EGFR	Epidermal Growth Factor Receptor
ELISA	Enzyme-Linked Immunosorbent Assay
ENCODE	Encyclopedia of DNA Elements
ESX	Early Secretory Target (ESAT6) Secretion
FANTOM	Functional Annotation of the Mammalian genome
Gfi1	Growth Factor Independent 1 Transcriptional Repressor
GTEx	Genotype-Tissue Expression
H&E	Haemotoxylin and Eosin
HDT	Host-Directed Therapy
HIV/AIDS	Human Immunodeficiency Virus/Acquired Immunodeficiency Virus
HPRT	Hypoxanthine Phosphoribosyltransferase
HSC	Hematopoietic Stem Cell
iFBS	inactivated Fecal Bovine Serum
IL-	Interleukin

IRAK	IL-1 Receptor-Associated Kinases
LAM	Liparabinomannan
LDL	Low-Density Lipoprotein
LLO	Listeriolysin O
Lm	*Listeria monocytogenes*
LM	Lipomannan
Lmo1/2	Lim-Only-Domain 1/2 oncogenic genes
LMPP	Lymphoid Primed Multipotent Progenitor
LPS	Lipopolysaccharide
Lyl1	Lymphoblastic Leukemia 1
M1	Classically Activated Macrophage
M2	Alternatively Activated Macrophage
mAGP	mycolyl-arabinogalactan-peptidoglycan
MAMP	Microbe-Associated Molecular Pattern
ManLAM	Mannosylated Liparabinomannan
MAPk	Mitogen-Activated Protein (MAP) Kinase
MARCO	Macrophage Receptor with Collagenous Structure
MDM	Monocyte-Derived Macrophages
MDP	Muramyl Dipeptide
MDR-TB	Multi-Drug Resistant Tuberculosis
medLN	Mediastinal Lymph Node
Mincle	Macrophage inducible Ca^{2+}-dependent lectin receptor
Mox	Oxidized Phospholipid Induced Macrophage
MR	Mannose Receptor
Mreg	Regulatory Macrophages
MSK1/2	Mitogen- and Stress-Activated Protein Kinases 1 and 2
Mtb	*Mycobacterium tuberculosis*
MyD88	Myeloid Differentiation Primary Response Protein 88
NFκB	Nuclear Factor κB
NLR	NOD-Like Receptor
NO	Nitric Oxide
PAMP	Pathogen-Associated Molecular Pattern
PAS	Para-Aminosalicylic Acid
PBMC	Peripheral Blood Mononuclear Cells
PBS	Phosphate Buffered Saline

PCR	Polymerase Chain Reaction
PDIM	Phthiocerol Dimycocerosate
PEST	Proline (P), Glutamic Acid (E), Serine (S), Threonine (T)
PRR	Pattern Recognition Receptors
qRT-PCR	Quantitative Real-Time Polymerase Chain Reaction
RNA	Ribonucleic Acid
ROS	Reactive Oxygen Species
SANS	South African National Standard
Scl	Stem Cell Leukemia
SEM	Standard Error of the Mean
SP	Single Positive
SRA	Scavenger Receptor A
STING	Stimulator of Interferon Genes
STMN1	Stathmin 1
T-ALL	T-cell Acute Lymphoblastic Leukemia
TAK1	TGF-β-Activated Protein Kinase 1
Tal1	T-cell Acute Lymphoblastic Leukemia Protein 1
TB	Tuberculosis
TDM	Trehalose-6,6-dimycolate
Th1/2/17	T helper 1/2/17 cells
TLR	Toll-Like Receptors
TMB	Tetramethylbenzidine
TRAF	TNF Receptor-Associated Factor 6
TREM	Triggering Receptors Expressed on Myeloid cells
UCT	University of Cape Town
US	United States
WHO	World Health Organization
WT	Wild-Type
XDR-TB	Extensive Drug Resistant Tuberculosis

List of Figures

Figure 1.1. Global estimated TB incidences in 2018.

Figure 1.2. A Venn diagram illustrating the three high-burdened country lists including TB, TB/HIV and MDR-TB, declared by the World Health Organization (WHO) for the 5-year period (2016-2020).

Figure 1.3. Potential PRR that bind to *Mtb* PAMP.

Figure 1.4. National distribution of the largest Listeriosis outbreak in South Africa between 2017 and 2018.

Figure 1.5. The activation of innate immune cells by *Listeria monocytogenes* (*Lm*).

Figure 1.6. Potential host-directed therapeutic targets against *Mtb*.

Figure 1.7. Experimental layout of CAGE experiment contributed by the Brombacher Laboratory, Cape Town, to the FANTOM5 project.

Figure 1.8. Lymphoblastic leukemia (Lyl1) expression in murine macrophages in response to *Mtb* HN878.

Figure 1.9. Schematic diagram comparing the two Lyl1 mouse models.

Figure 2.1. Confirmed globally deleted Lyl1$^{-/-}$ mice experience no physiological differences compared to wild-type (WT) mice.

Figure 2.2. Lyl1-deficient mice experiences a perturbance in thymopoiesis, but comparable single positive T-cells.

Figure 2.3. Naïve lung immune cell populations in the absence of Lyl1 is similar to WT.

Figure 2.4. Immune cell population in the lymph node (LN) of Lyl1$^{-/-}$ is comparable to that of WT mice.

Figure 2.5. Lyl1$^{-/-}$ spleens show no defect in immune cell population in comparison to WT spleens.

Figure 2.6. Liver immune cell population is comparable between Lyl1$^{-/-}$ and WT mice.

Figure 2.7. Lyl1-deficiency has minimal effect on the immune cytokine/antibody profile compared to WT mice at steady state.

Figure 3.1. Lyl1 is downregulated in multiple immune stimulated environments *in vitro* and *in vivo*.

Figure 3.2. Lyl1 expression is downregulated by MAPk and NFkB signaling pathways in macrophages.

Figure 3.3. Pro-inflammatory responses are reduced in LPS-stimulated Lyl1$^{-/-}$ macrophages *in vitro*.

Figure 3.4. Lyl1 activity does not regulate MAP kinase and p50-p65 NFκB pathways.

Figure 3.5. Murine models are more susceptible to *Listeria monocytogenes* (*Lm*) in the absence of Lyl1 compared to WT mice *in vivo*.

Figure 3.6. Lyl1$^{-/-}$ mice display increased dendritic cell recruitment in spleen and decreased NK cell recruitment in the liver.

Figure S3.1. All agonists induced the targeted pathway and demonstrated no cell toxicity.

Figure S3.2. All agonists induced the target pro-inflammatory cytokine production.

Figure S3.3. Cytokine gene expression evaluation confirm the inhibition of various MAPk subunits, NFκB and MSK1/2 during *in vitro* experiments.

Figure 4.1. Lyl1-deficiency increases macrophage bacterial burden with differential effects on proinflammatory gene expression in response to hypervirulent *Mtb* HN878 *in vitro*.

Figure 4.2. Lyl1-deletion renders increased susceptibility to hypervirulent *Mtb* HN878 infection *in vivo*.

Figure 4.3. No differences in the lung lymphoid population is observed after hypervirulent *Mtb* HN878 infection in the absence of Lyl1.

Figure 4.4. Lyl1-deficiency does not impair lung T-cell memory in response to *Mtb* HN878 infection.

Figure 4.5. Lyl1-deletion enhances lung neutrophil and monocyte recruitment in response to chronic hypervirulent *Mtb* HN878 *in vivo*.

Figure 4.6. Lyl1-deletion promotes inflammatory responses during chronic hypervirulent *Mtb* HN878 *in vivo*.

Figure 4.7. Lyl1-deletion induces CXCL1 and CXCL5 levels in response to chronic hypervirulent *Mtb* HN878 *in vivo*.

Figure 4.8. Lyl1-deficiency induces severe lung inflammation during chronic hypervirulent *Mtb* HN878 infection.

Figure 4.9. Lyl1-deficiency alters myeloid cell cytokines gene expression in response to *Mtb* H37Rv.

Figure 4.10. Lyl1 cannot be used as a biomarker for TB diagnosis but has great potential for viral infected patients.

Figure S4.1. No changes in the lymph node (LN) lymphoid population was observed after hypervirulent *Mtb* HN878 infection (*in vivo*) in the absence of Lyl1.

Figure S4.2. Changes in T-cell memory was observed in Lyl1$^{-/-}$ lymph nodes (LN) after hypervirulent *Mtb* HN878 infection.

Figure S4.3. Lyl1-deletion enhances macrophage recruitment to the lymph nodes (LN) in response to chronic hypervirulent *Mtb* HN878.

Figure S4.4. Lyl1-deficient lymphoid population is unaffected by *Mtb* H37Rv infection after 6 weeks.

Figure S4.5. Neutrophil recruitment is enhanced during *Mtb* H37Rv infection in the absence of Lyl1.

Appendix A Thymus lymphoid gating strategy

Appendix B Lung, Lymph Node (LN), Spleen and Liver lymphoid gating strategy

Appendix C Lung myeloid gating strategy

Appendix D Lymph Node myeloid gating strategy

Appendix E Spleen myeloid gating strategy

Appendix F Liver myeloid gating strategy

Appendix G Primer pairs for qPCR

Abstract

Lymphoblastic leukemia 1 (Lyl1) is a well-studied transcription factor known to exhibit oncogenic potential during various forms of leukemia. Since its discovery in 1989, many reports have been published describing its relationship with cancer as well as demonstrating its function during hematopoiesis. Lyl1 has been shown to serve a significant role during thymopoiesis by contributing to T-cell development. However, it has been recently reported that irrespective of its significance during T-cell development, mature comparable single positive T-cells are observed in mouse models. The use of murine models has been crucial in identifying potential targets for host-directed therapies (HDT) which has been shown to provide great potential in treating tuberculosis (TB). It is evident that *Mycobacterium tuberculosis* (*Mtb*), the causative agent for TB, is capable of developing resistance to various treatments that target the bacterium itself. Therefore, by designing therapies that directly target host factors could assist in circumventing *Mtb* resistance. By analyzing *Mtb*-infected bone marrow-derived macrophages (BMDM) that have been subjected to genome-wide transcriptional deep sequencing of total RNA using a single molecule sequencer in conjunction with the cap analysis gene expression (CAGE) technique, various differentially expressed genes were identified, including the oncogenic transcription factor, Lyl1. With the use of murine models, we investigated whether Lyl1 is important for various immunological responses at steady state, the regulation of Lyl1 in response to various immune stimulants including LPS and whether this transcription factor is relevant in bacterial infections including *Listeria monocytogenes* (*Lm*) and *Mtb*.

The data in this thesis demonstrate comparable immunological responses, including cellular recruitment by means of flow cytometry and cytokine responses by means of ELISA, between naïve littermate control and Lyl1-deficient mice. Further evaluation of Lyl1 regulation revealed the influence of MAPk and NFκB signaling on Lyl1 expression upon LPS stimulation by significantly downregulating this transcription factor in immune stimulated macrophages. A role for Lyl1 during bacterial infections was observed in *Lm*-infected mice whereby $Lyl1^{-/-}$ mice succumbed earlier to listeriosis compared to the littermate controls. We further established a functional role for this transcription factor during *Mtb* infection *in vitro* and *in vivo*. The early surrender of Lyl1-deficient mice to *Mtb* HN878 infection, accompanied by increased bacterial burden during chronic *Mtb* infection, demonstrated enhanced susceptibility in the absence of Lyl1. We show that Lyl1-deficient host susceptibility is a consequence of enhanced inflammatory responses and increased bacterial growth. This is demonstrated by increased neutrophilic inflammation, pro-inflammatory cytokine and chemokine secretion along with a reduction in anti-inflammatory cytokine release during chronic *Mtb* infection. Here, we demonstrate the first non-leukemia role for Lyl1 by suggesting a role and requirement for this transcription factor during bacterial infections. Given the significant role during *Mtb* infection, our studies suggest the use of Lyl1 associated pathways as a potential HDT target for TB.

Chapter 1

Literature Review

1.1. Bacteria and the Immune System

1.1.1. The threat of bacterial infections

In 2013, the Centers for Disease Control and Prevention (CDC) published their first Antibiotic Resistance (AR) Threat Report classifying various bacterial species as urgent, serious and concerning threats. *Mycobacterium tuberculosis* (*Mtb*) was reported as a serious threat given their continuous development of drug resistance [1]. In 2017, the World Health Organization (WHO) released a follow-up communique reporting an estimate of 700 000 individuals succumbing to the effects of antibiotic-resistant bacteria worldwide. This demands extensive research into circumventing antibiotic-resistant bacterial infections, as experts predict this number to increase to 10 million by 2050 [2]. Furthermore, the second and updated AR Threat Report (CDC November 2019) confirms more than 2.8 million antibiotic-resistant infections yearly, of which more than 35 000 die as a result in the United States (US) alone [3].

In the early twentieth century, the use of antibiotics was a great tool to circumvent life-threatening infections [3]. However, the rapid emergence of bacterial antibiotic resistance, due to overuse or inappropriate use of prescribed treatments, as well as a decline in the availability of new antibiotics [4], has resulted in one of the greatest global public health challenges to date [3]. It is possible that we will soon be beyond antibiotic development given that between 2013 – 2014, the CDC and the WHO declared the human race to be experiencing the "post-antibiotic era," simultaneously, emphasizing the seriousness of antibiotic drug-resistance, respectively [5].

South Africa, specifically, is at a greater risk. The rise in bacterial drug-resistance increases population vulnerability, as South Africa is one of the leading countries suffering from a high prevalence of tuberculosis (TB), including HIV-associated TB. In fact, the first XDR-TB outbreak to initiate global concern occurred in Kwazulu-Natal, South Africa in 2005 [6]. Thus, this demands immediate coordinated efforts to research and develop alternate routes of prevention and treatment to assist in what is now referred to as the "antibiotic resistance crisis."

1.1.2. Immune response to bacterial infections

Both Gram-positive and Gram-negative bacterial walls contain protective barriers that consist of peptidoglycan and lipopolysaccharide, respectively [7]. However, this highly conserved rigid and complex structure of carbohydrates and amino acids are easily recognized by the immune system. Bacterial infections usually occur when either normal flora or foreign bacteria enter the sterile cavities of the human body and replicate at an uncontrollable rate [8]. As a response to infection, the primary function of the immune system is to prevent replication, as well as expel foreign bacterial invaders as rapidly as possible. This is achieved by the activation of two responses: the pathogen-associated molecular pattern (PAMP) recognizing innate immunity as well as the antigen-specific adaptive immune response [7, 8].

1.1.2.1. Innate immunity

The innate immune response is considered the first line of defense [7]. When a bacterial species surpasses the physical and chemical barriers of the innate immune response, the complement system is activated to avoid bacterial spread, followed by the initiation of phagocytotic and cytotoxic mechanisms to expel the bacteria. Finally, if the innate system is unable to effectively eradicate the bacteria, it activates the adaptive immune system via cytokine release, antigen presentation and ligand co-stimulation [7]. The innate immunity is not specific to the invading pathogen or bacteria. This immune response focuses on eliminating and reducing the harmful effects of pathogenic species. This is achieved by stimulating a generic response whereby innate cells identify highly conserved structures present across various pathogens/microorganisms known as pathogen/microbe-associated molecular patterns (PAMP/MAMP). These are recognized by pattern recognition receptors (PRR) which are present on innate effector cells, such as monocytes, macrophages as well as dendritic cells and are therefore classified as antigen-presenting cells (APC) [7, 8]. The four commonly described PRR include the Toll-like Receptor (TLR), the NOD-like Receptor (NLR), the Triggering Receptors Expressed on Myeloid cells (TREM) and the RIG-like Receptor [9]. Each bacterial species has the potential to express more than one PAMP, resulting in the synchronous activation of more than one pathway.

The most described PRR are the TLR. These have been identified by binding preference to various PAMP including TLR2 which recognizes the lipoteichoic acid on Gram-positive cocci cell walls and bacterial zymosan, TLR4 that binds to Gram-negative lipopolysaccharide (LPS) situated on the outer cell membrane, TLR5 that adheres to Gram-negative flagellin and TLR9 which recognizes the CpG bacterial DNA oligonucleotides [9]. Once these PRR recognize the invading PAMP, it signals a cascade of intracellular events that recruits myeloid differentiation primary response protein 88 (MyD88) to

intracellular TLR domains. This is followed by the recruitment of TGF-β-activated protein kinase 1 (TAK1), TNF receptor-associated factor 6 (TRAF), IL-1 receptor-associated kinases (IRAK), as well as mitogen-activated protein (MAP) kinases and subsequent transcription of inflammatory response genes including various pro- and anti-inflammatory cytokines and chemokines [9, 10].

The induction of these cytokines and chemokines activate various immune responses to impede bacterial load by minimizing bacterial replication and spread by means of phagocytosis. This immune response involves "sentinel" cells, including macrophages, that circulate the body targeting potential threats. Upon foreign molecule recognition and successful surface receptor binding, these sentinel cells engulf the bacteria, followed by phagolysosome formation and pH reduction to ultimately eliminate the threat. Simultaneously, foreign antigen presentation by APC activates the adaptive immune response to assist in bacterial eradication [11, 12]. This becomes especially helpful in cases whereby these pathogens bypass the killing effector functions of the innate immune cells.

1.1.2.2. Adaptive immunity

Unlike the innate immune response, adaptive immunity is highly specific to the pathogen that activated the response. This specificity allows provision for long-lasting protection from the harmful invader. These involve two key responses: the antibody response and the cell-mediated response [13, 14]. Both these defenses are potentially destructive and are only required when the innate immunity deems the foreign molecule as harmful and uncontainable through generic responses. Given the specificity of this response, the adaptive immunity is only activated after a few days. During this time, the efforts of innate immunity allows for the production of specific immunoglobulins (antibody response) and activated T-cells directed to the antigen presented (cell-mediated response). Later, the secretion of these specialized molecules eliminates the bacteria by inactivating microbial toxins, as well as reducing bacterial replication by phagocytosis. This is followed by the release of various signaling molecules that activate the killing effectors of the innate immune system [13, 14]. With a specific adaptive immune response, innate cells, such as macrophages, can target the pathogen more effectively and induce their pathogen killing effector functions. In addition to these functions, macrophages are one of the main cell types that bridge innate and adaptive immunity through the processing and presentation of antigens [14].

1.1.2.3. Macrophage response to bacterial infections

Macrophages were first described as phagocytic cells by Elie Metchnikoff in 1983 [15]. Today, these powerful cells are described as heterogenic in nature and express tissue-specific and environment-specific functions [16, 17]. Many of the tissue-resident macrophages originate from the yolk sac and are able to persist through adulthood, independently of monocytes [18].

As described above, macrophage recognition of foreign, harmful invaders is achieved through PAMP and PRR binding, resulting in the activation and transcription of various immune components to combat the bacterial infection. The uniqueness of macrophages, in addition to their tissue-specific functional properties, is in their polarizing capabilities in response to distinct microenvironmental signals. The activation and polarization of macrophages by various means was described by many researchers including the well-known M1 classically activated and M2 alternatively activated macrophages in conjunction with the Th1/Th2 paradigm by Mills *et al*. in 2002 [19]. M2 macrophages were later subdivided into M2a, b and c by Mantovani *et al*. in 2004 [20]. Moreover, Nathan *et al*. earlier described the classical activation of macrophages by IFNγ [21], followed by Stein *et al*., who demonstrated the alternate activation of macrophages by IL-4 [22]. More recently, novel macrophage phenotypes, distinct from M1 and M2, have been described. These include regulatory macrophages (Mreg) [23], oxidized phospholipid induced macrophage (Mox) [24] and the unique macrophage transcriptome induced by CXCL4 (M4) [25].

However, the most widely accepted macrophage subsets are the M1/M2 macrophages which are highly distinct in functionality. M1 classically activated macrophages are known to influence a pro-inflammatory phenotype with pathogen killing effector functions [26]. These include the induction of nitric oxide (NO), reactive oxygen species (ROS), various lysosomal enzymes [27], as well as the release of pro-inflammatory cytokines which is essential for bacterial progression control. Furthermore, M1 macrophages exhibit distinct antigen presentation properties by increasing MHCII and costimulatory molecule expression which trigger Th1 and Th17 cell differentiation [28]. Alternatively, M2 macrophages express a rather anti-inflammatory phenotype known for tissue remodeling and cell proliferation [26, 29]. This was further characterized as Th2 cytokine-induced M2a, LPS-, immune complexes- and IL-1R ligand-induced M2b and IL-10-, TGF-β- and glucocorticoid-induced M2c macrophages [20, 27]. However, as the heterogeneity of macrophage responses are better understood with different stimulations, it has recently been advised to rather refer to macrophage subtypes by their stimulating factor instead of the M1/M2 nomenclature [30].

In addition to signal-induced macrophage diversity, resident tissue macrophages also contribute to their plasticity. These macrophages have been shown to be transcriptionally different, expressing distinct genes for distinct tissue-specific functions to maintain homeostasis in its local environment [31, 32]. To

distinguish the different tissue-resident macrophages, they have tissue-specific nomenclature, such as microglial cells in the central nervous system, alveolar and interstitial macrophages in the lungs, Kupffer cells in the liver, marginal zone, red pulp and metallophilic macrophages in the spleen, Langerhans cells on the skin and sinus histiocytes in the lymph node [12, 22, 33].

When encountering a bacterium, macrophage differentiation and activation is dependent on the bacterial species and site of infection. However, regardless of the macrophage subtype, as front-line professional phagocytes and antigen-presenting cells (APC), specializing in pathogen engulfment and digestion, all macrophages have two generic responses upon microbial stimuli recognition. Macrophages begin with phagocytosis and lysosomal inactivation of the bacterium and consequently, release either immune regulatory messenger or antimicrobial effector molecules [12]. Meanwhile, for early elimination of these pathogenic bacteria, macrophages also undergo programmed cell death, known as apoptosis [34]. This is a non-inflammatory effective way to control bacterial replication and dissemination as the bacteria are contained within these apoptotic bodies and engulfed by neighbouring uninfected macrophages by efferocytosis [34, 35]. Contrastingly, some bacterial pathogens can avoid pathogen inactivation and death, using host cell death to their advantage. This allows the bacteria to viably exit the host cell, spread and infect neighbouring cells, and ultimately cause bacterial tissue dissemination [34]. These include necrosis, an uncontrolled cell death, as well as necroptosis and pyroptosis, which are considered programmed cell death [36]. A necrotic cell is morphologically different from an apoptotic cell whereby it experiences nuclear and cellular swelling, as well as chaotic DNA fragmentation with no chromatin condensation, compared to a shrunken cell with preserved plasma membrane integrity, chromatin condensation and nuclear fragmentation in apoptotic cells. Necrotic cells release uncontrolled inflammatory mediators and promote bacterial dissemination and spread. However, recent research describes a controlled form of necrosis known as either, based on molecular pathways , necroptosis or pyroptosis. Contrasting to apoptosis, these processes are lytic cell death modalities that promote the release of potential immunostimulatory molecules and thus, are highly inflammatory in nature [34, 36]. Many bacterial pathogens, such as *Mycobacterium tuberculosis* (*Mtb*) and *Listeria monocytogenes* (*Lm*), are capable of the above-mentioned manipulations.

1.1.3. Tuberculosis

1.1.3.1. History

Mycobacterium tuberculosis (*Mtb*), the bacterial causative agent for the well-known tuberculosis (TB), has challenged the public health system since the 17th century. This disease plagued mankind, causing great

epidemics during the 17th to the mid-19th century, killing more individuals than any other microbial pathogen [37]. The earliest evidence of *Mycobacterium* detection dates back 150 million years ago [38]. However, with recent technology, initial traces of *Mycobacterium tuberculosis*, specifically, dates back 17 000 years through its discovery in the bones of the extinct bison from Wyoming [39]. The first human-tuberculosis interaction was evident in an infant and mother buried in an Eastern Mediterranean village with indications of animal domestication 9000 years ago. This supports the theory of zoonotic transmission of *Mycobacterium bovis* to humans as *Mycobacterium tuberculosis* [40, 41].

As this disease ended many European and North American lives during the 18th century, with a mortality as high as 900 per 100 000 individuals per year, targeting the younger generation, it was given the sobriquet as "The Robber of Youth." Later, when the TB epidemic was most fatal, killing one in four individuals, the nickname "Captain Among These Men of Death" was used. However, the most commonly reported nomenclature for TB was "consumption," "phthisis," and during the most erratic epidemic, the "white plague" [37, 42].

The severity of this disease demanded in-depth research on the most unpredictable, challenging, unknown, long-term, sometimes lifetime, disease that consumed and affected many individuals lives in earlier years. Hence, many researchers are documented and praised for their efforts in uncovering valuable breakthroughs in the disease we continue to fight in the 21st century, now known as tuberculosis (TB). TB was originally assumed to be genetically transmitted. However, Benjamin Marten was the first to describe the infectious nature of TB in his 1720 publication titled "A New Theory of Consumption" [43]. Later, Matthew Baille physiologically described tubercles in his 1793 publication "A Morbid Anatomy of the Human Body," followed by Gaspard-Laurent Bayle who clinically characterized the symptoms of the disease and reported that it was rather a "general infection" that does not only invade the lungs ("Recerches sur la phthisie pulmonaire" in 1810) [42]. With the invention of the stethoscope, Rene Theophile Hyacinthe Laënnec elucidated the pathogenesis of pulmonary and extrapulmonary diseases, including TB in 1819 [44]. After the first anti-TB sanatorium discovery in 1854 with just "fresh air and good nutrition" suggested by Hermann Brehmer [45], Jean-Antione Villemin proved Benjamin Marten's infectious theory by inoculating rabbits with tuberculous matter from human cadavers in 1865 [46]. Prior to Robert Koch, the first scientist to attempt the isolation of the TB bacillus with partial success was Theodor Albrecht Edwin Klebs in 1867 [42]. With the successful isolation of tubercle bacillus and identification of the causative agent in 1882, Robert Koch became a world-renown scientist with a Nobel Peace Prize in 1905. His breakthrough discovery in a two-century long disease was a massive milestone in the fight against TB and his postulates are still widely used today to understand the causative relationship between the microbe and the disease [42, 47].

Robert Koch's breakthrough lead to many historical TB discoveries and developments, including the Pirquet and Mantoux tuberculin skin test in 1908 [42], the first *Mycobacterium* vaccine using *Mycobacterium bovis* known as BCG (Bacille Calmette-Guerin) by Albert Calmette and Camille Guerin in the early 20th century [48] as well as the discovery of many therapeutic agents. These included streptomycin by Albert Schatz and Selman Waksman in 1944 [49], para-aminosalicylic acid (PAS) by Jorgen Lehmann in 1949 [50], TB chemotherapy by introducing a combination of streptomycin, PAS and isoniazid by Sir John Crofton in 1952 [51] as well as the discovery of rifampicin in 1957 [52] and ethambutol in 1961 [53]. By 1966, rifampicin was introduced into the TB drug line and has become an essential component of TB treatment regimens [54]. However, albeit all these discoveries over the last three centuries, the complex pathogenic structures of *Mtb*, in addition to its infectious nature and ability to cause chronic disease which demands long-term treatment, TB is still considered a major public health problem. In recent years, we face a rather challenging microbe as it continues to develop drug resistance, as well as infect immunocompromised individuals resulting in the TB-HIV epidemic. Thus, in addition to various social implications, the "TB crisis" continues into the 21st century and remain to be a permanent challenge throughout human history [42].

1.1.3.2. Epidemiology

Following centuries of attempting to combat TB, the World Health Organization (WHO) implemented "The End TB Strategy" in 2016 with the aim of ending the global tuberculosis epidemic and to create a world free of TB-related disease, suffering and deaths by the year 2035 [55]. The strategy describes milestone goals by 2020, including a 35% reduction in TB-related deaths and a 20% reduction in TB incidences compared to 2015. However, in their latest Global Tuberculosis Report 2019, it was reported that we are not on schedule to achieve these milestone goals of The End TB Strategy [56]. In the 21st century, *Mtb*-causing TB continues to infect millions of people worldwide. A total of 10 million people contracted the disease in 2018, of which 1.5 million died, classifying TB as one of the top ten causes of death. A total of 87% of infected patients in 2018 was reported from the 30 high TB-burdened countries. However, eight specific countries accounted for two-thirds of these cases, of which South Africa was listed (*Figure 1.1*) [56].

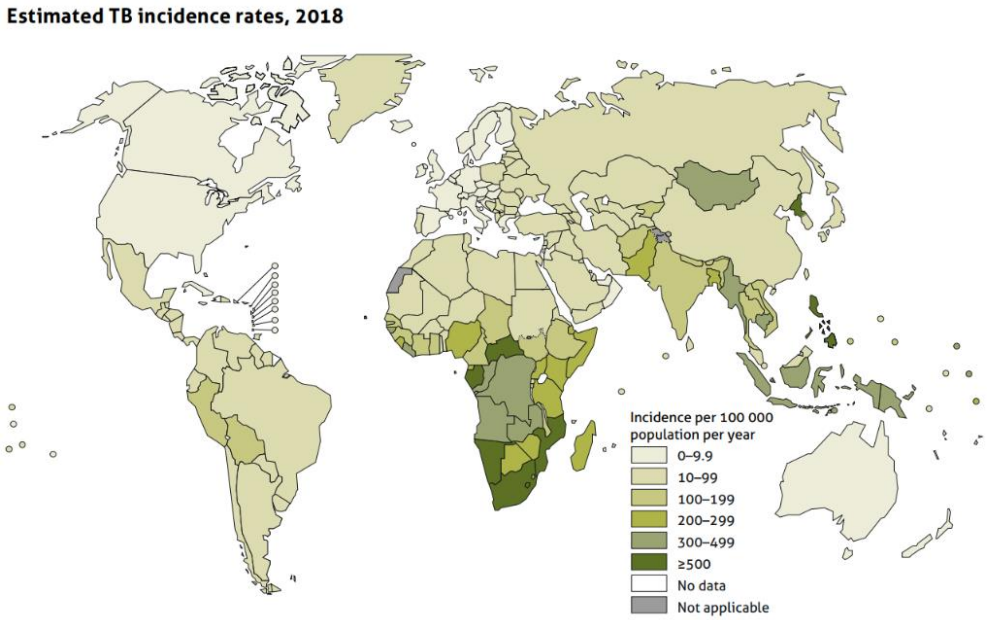

Figure 1.1. **Global estimated TB incidences in 2018.** Severity is based on the annual number of reported TB cases relative to the population size. *Image sourced from the WHO Global Tuberculosis Report 2019 [56].*

TB is currently recognized as a poverty-related disease, hence the high TB burden countries are mainly low-income, third-world countries suffering from high poverty [57]. Not only does South Africa suffer from rising poverty, but it is also an HIV/AIDS-burdened community, thus increasing the vulnerability of the population. HIV-positive individuals are nineteen times more likely to contract TB in comparison to HIV-negative people. In 2018, a total of 862 000 new TB cases were HIV associated of which 251 000 died [56].

Aside from social disadvantages, the TB causative agent has been able to overcome research trends over the last few decades, developing, what we refer to now as, either MDR-TB (Multidrug-Resistant TB) or XDR-TB (Extensive Drug-Resistant TB). Patients that contract MDR-TB are resistant to isoniazid and rifampicin, resulting in the failure of the standard first-line treatment. More severely, XDR-TB patients do not respond to both first-line treatment and second-line injectable drugs as well as fluoroquinolones [58]. Although minority in numbers, drug-resistant TB continues to challenge the global public health system with a total of 484 000 cases reported as rifampicin-resistant of which 78% was declared MDR-TB in 2018. Further, 6.2% of the MDR-TB reported cases were later registered as XDR-TB [56]. In the End TB Strategy report, WHO generated three country lists that are considered high TB-burdened including HIV and MDR-TB (*Figure 1.2*). A total of 14 countries, including South Africa, appear in all three lists, suffering from both HIV/TB coinfection and MDR-TB alongside drug-susceptible TB. Thus, in order to overcome one of

the most vigorous microbes in human history, given its survival throughout the technological era, researchers emphasized the greater need to understand TB immunopathology, especially the interplay between the *Mtb* bacterium and the human macrophage.

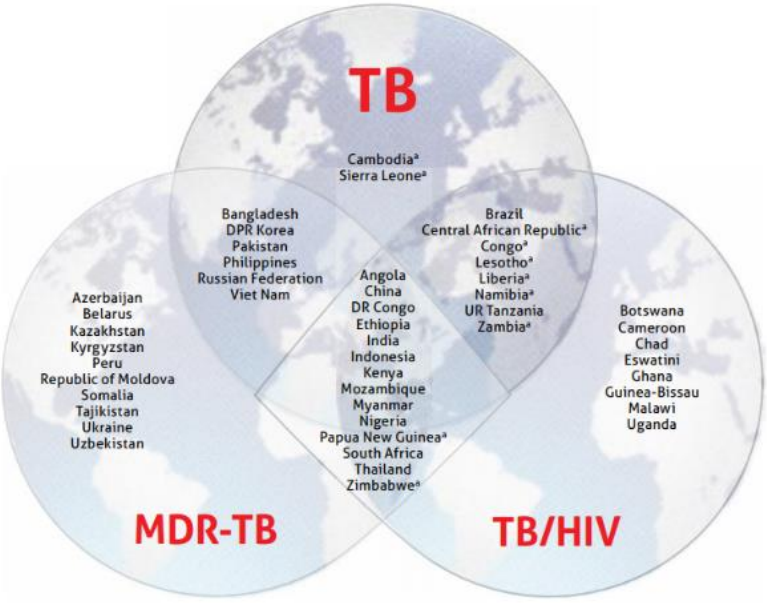

Figure 1.2. **A Venn diagram illustrating the three high-burdened country lists including TB, TB/HIV and MDR-TB, declared by the World Health Organization (WHO) for the 5-year period (2016-2020)**. The "a" depicts the high-burdened countries that are included in the top 30 which is based on the severity of TB burden as opposed to the top 20 which is based on the absolute number of TB cases per year. *Image sourced from the WHO Global Tuberculosis Report 2019 [56].*

1.1.3.3. Macrophages during *Mtb* infection

The *Mtb*-host interaction is an interesting, complex relationship involving the activation and stimulation of multiple components of the immune system. When *Mtb* infects the host through aerosol inhalation, the first immune cells to recognize the pathogen-associated molecular pattern (PAMP) are the lung resident alveolar macrophages [59]. This is followed by the phagocytosis of the bacteria and subsequent cytokine release. Normally, the bacteria would be subjected to increasing acidic environments and lysosomal degradation through various phagosome trafficking pathways and additional nitric oxide and ROS exposure. This would ideally induce pro-inflammatory cytokines, which would augment further host responses. These involve the recruitment of additional immune cells to the site of infection as well as adaptive immunity activation which would ultimately contain the bacterial spread through granuloma formation [10, 60]. However, these immune responses are dependent on the initial PAMP-PRR interaction between the *Mtb* and host immune cells.

Mtb produces many antigens common to most bacteria, hence the innate response can recognize and assist in containing the spread prior to the adaptive response. Additionally, the *Mtb* cell wall expresses unique antigens, including lipomannan (LM), lipoarabinomannan (LAM) with its mannosylated form (ManLAM), various lipoproteins and mycolic acids as well as phthiocerol dimycocerosate (PDIM). Furthermore, *Mtb* can secrete various effector proteins which have been shown to be secreted via the Sec secretion system as well as the ESAT-6 (ESX) system. These antigens or PAMP are recognizable by macrophage PRR, including TLR, scavenger receptors and C-type lectin receptors (*Figure 1.3*) [10].

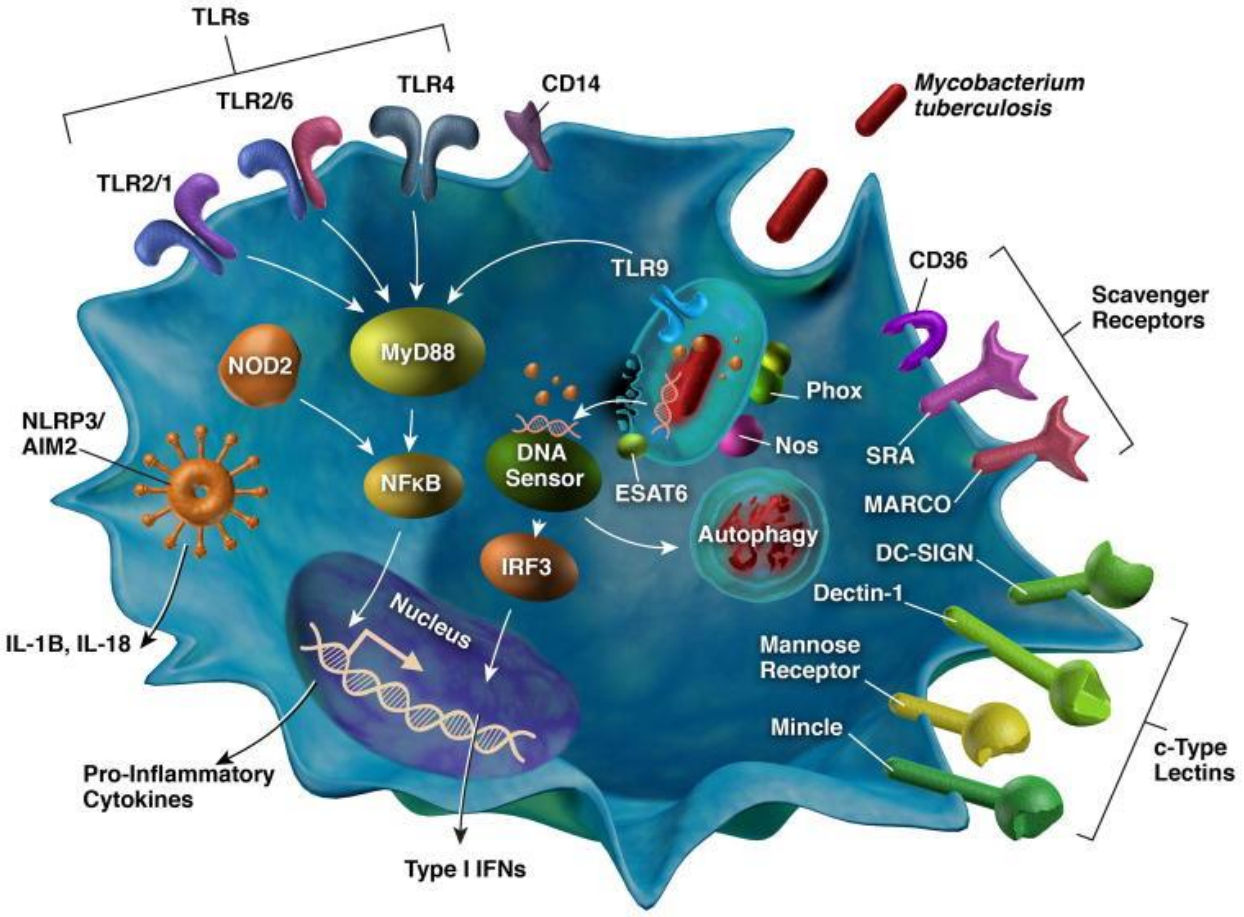

Figure 1.3. **Potential PRR that bind to *Mtb* PAMP**. Schematic diagram showing the major receptors involved in recognizing mycobacterial PAMP including surface-bound and intracellular receptors. These include Toll-like receptors (TLR), C-type lectin receptors scavenger receptors on the surface as well as cytoplasmic receptors that bind to secreted proteins and DNA once *Mtb* accesses the cytoplasm. The diagram also demonstrates various signaling pathways in response to *Mtb*, including autophagy activation, NFκB and IRF3 mediated cytokine release as well as the inflammasome-mediated IL-1β secretion system. *Image sourced from Stamm and co-authors, 2015 [10].*

Toll-like receptors (TLR) recognize a wide range of microbial products of which surface-expressed TLR2, TLR4 and cellular internally expressed TLR9 mainly respond to *Mtb*. However, TLR2 is the

dominant responder to *Mtb* [10]. Other *Mtb*-related PRR include various C-type lectins which are plasma molecules that bind to carbohydrate moieties on *Mtb* surfaces, specifically the DC-specific intercellular adhesion molecule-3 grabbing nonintegrin (DC-SIGN), Dectin-1, mannose receptor (MR) and Mincle. Furthermore, scavenger receptors, which are cell surface-expressed or secreted from macrophages, involved in *Mtb* recognition, include CD36, scavenger receptor A (SRA), macrophage receptor with collagenous structure (MARCO) as well as the secreted scavenger receptor known as apoptosis inhibitor of macrophages (AIM) [10]. Additionally, *Mtb* has been shown to activate various intracellular receptors. These include the activation of the stimulator of interferon genes (STING) pathway which plays a big role in cytosolic surveillance as well as nucleotide-binding oligomerization domain-like receptors (NOD-like receptors) [10]. STING activation is achieved via the ESX-1 secretion system which induces phagosome permeabilization. This grants *Mtb* access to the cytosolic compartment after which their DNA is recognized by cyclic GMP-AMP synthase (cGAS) and consequently activating STING [61, 62], whereas NOD-like receptors bind to mycolyl-arabinogalactan-peptidoglycan (mAGP) complex on *Mtb* cell walls [10].

Therefore, *Mtb* stimulates a variety of immune responses, inducing many pathways simultaneously, creating an immunological storm that could be harmful to the bug itself, or the host. Interestingly, aside from how complex and direct these host defense mechanisms are, *Mtb* is still able to evade these host defense mechanisms by various processes that involve blocking immune cell trafficking, phagolysosome formation and acidification, inhibiting apoptosis and autophagy, as well as delaying antigen-presentation and ultimately inhibiting the adaptive immune response [60]. Although these processes have been identified, the complete mechanisms behind these evasion techniques remain elusive today.

1.1.4. Listeriosis

1.1.4.1. History

Unlike *Mtb*, *Bacterium monocytogenes* was only successfully identified and characterized 100 years ago by Murray, Webb and Swan [63] after which Pirie renamed the listeriosis causative agent as *Listeria monocytogenes* (*Lm*) in 1940 [64]. However, there is strong evidence suggesting the emergence of this bacterium long before its discovery, potentially causing diseases which was then referred to as pseudotuberculosis and neonatal septicemia [65].

For the following two decades after its discovery, *Lm* was mainly found in animals and was extremely rare in humans [65]. Thus, considerable research on this bacterial species was not performed. It was not until the emergence of the first human listeriosis epidemic in Germany 1949 causing a total of 85 stillborn babies, revealing granulomas in most organs including the spleen, skin, liver, lung and brain, that sparked

a new era of listeriosis research [66]. Following this outbreak, Seeliger invested a great deal in creating an awareness and stressing the importance of this bacterium to an extent where he compiled the first overview of this disease in a book titled "Listeriosis" in 1961 [67]. Although many other researchers contributed to understanding the *Lm*-causing listeriosis, Seeliger continued to compile and report new developments globally and thus is considered the "Father of Listeriosis Research" [65, 68].

After many years of minor animal and human outbreaks corresponding to sporadic listeriosis research, Schlech and co-authors finally provided distinct evidence of listeriosis transmission sourced from food after an outbreak in Canada between 1971 and 1981 [69]. In addition to *Lm*-causing studies, this bacterium served as a great model for immunological studies as it is relatively safe to work with, easy to culture and is guaranteed infection in laboratory mice. One of the first studies using *Lm* demonstrated the importance of macrophages and T-lymphocytes during bacterial infections [70]. Today, *Lm* is considered a foodborne disease exhibiting pathogenic characteristics in both animals and humans and continues to be a useful model for bacterial immunological studies.

1.1.4.2. Epidemiology

Listeria monocytogenes (*Lm*) has the potential to cause rather invasive human listeriosis of which the clinical manifestations are stillbirth or abortion in pregnant women, meningitis, septicemia and meningoencephalitis. The lethalness of this disease is evident in the 20-40% fatality rate irrespective of treatment. As a foodborne disease, it is challenging to identify the source of infection. This bacterium is characterized as a psychrotrophic, facultative anaerobic, Gram-positive bacterium capable of surviving in vacuum-packed foods [71]. Given their ability to survive in temperatures as low at 4°C [65], storing these foods in refrigerators does not prevent bacterial growth. In fact, these chilled "ready-to-eat" foods with prolonged shelf lives, could potentially increase *Lm* growth, guaranteeing listeriosis after consumption [71]. Furthermore, *Lm* exhibit mesophilic potential resulting in resistance to temperatures used for pasteurization (71-74°C), causing many previous outbreaks sourced from milk products [65]. In addition to ready-to-eat foods and milk, other high-risk foods include soft and fresh cheese, sausages, raw meat (particularly chicken and turkey), seafood, raw mushrooms, lettuce and any industrially prepared meals that are conserved [68].

After the 20th century discovery, repeated listeriosis outbreaks with an extremely high mortality rate in comparison to *Salmonella* and *Escherichia coli* was observed. This included the outbreak in France in 2000 (27% mortality rate) [72], Canada in 2008 (39% mortality rate) [73] and the US in 2011 (22% mortality rate) [74]. However, one of the largest listeriosis outbreaks occurred between 2017 and 2018 in South Africa with a total of 937 laboratory-confirmed cases of which 193 died of the 728 known outcomes (27%

mortality rate) (*Figure 1.4*) [75]. More recently, as of November 2019, a total of 24 listeriosis cases were reported in the US of which 2 were fatal [76]. Therefore, with these sporadic, fatal, and occasionally resistant listeriosis outbreaks, it has become an alarming infectious disease. Thus, many researchers have invested in deciphering the immunological mechanism used by this pathogen to develop a more effective treatment, especially in pregnant women.

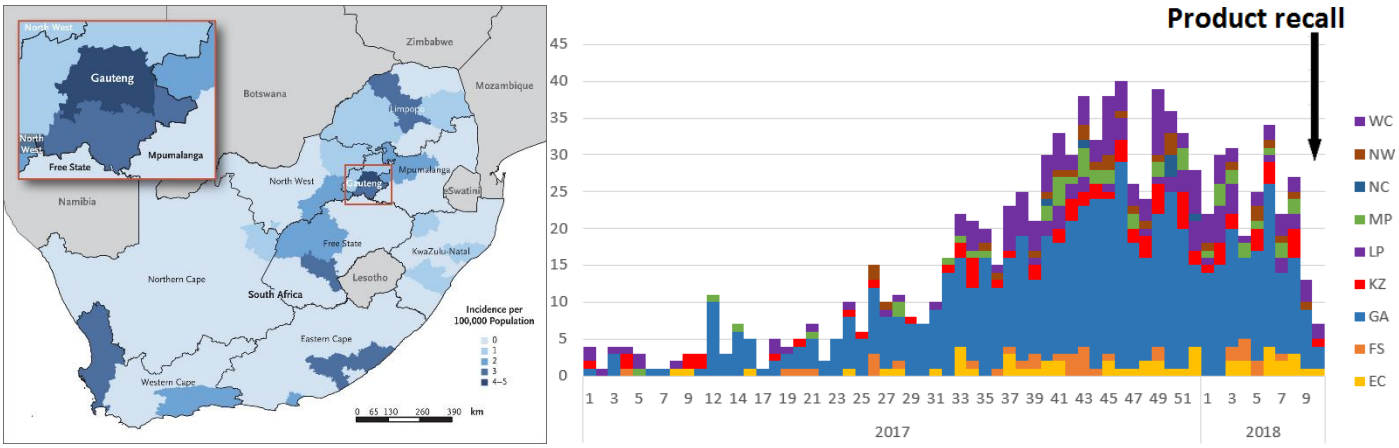

Figure 1.4. **National distribution of the largest Listeriosis outbreak in South Africa between 2017 and 2018.** Laboratory confirmed listeriosis cases in South Africa according to district demonstrates the most burdened provinces included Gauteng (59%), Western Cape (12%) and KwaZulu-Natal (7%) [77]. The figure on the right display disease distribution every two weeks until the source of infection was identified in March 2018. *Images sourced from Thomas and co-authors, 2020 [75] (left) and the WHO [77] (right), respectively.*

1.1.4.3. Macrophages during *Lm* infection

In a similar manner to *Mtb*, *Lm* has evolved mechanisms to evade or circumvent host protective immune responses. When the bacterium enters the host, generally orally and through the gastrointestinal tract, *Lm* initiates infection in the intestinal epithelial cells through the internalin-A – E-cadherin interaction expressed on the bacterium and the cell surface, respectively. This is followed by traversing the epithelial cell layer and entering the bloodstream, creating a systemic infection. This allows for the dissemination of *Lm* into neighbouring organs such as the liver and spleen whereby macrophages are activated and begin phagocytosing [78]. Given the systemic nature of listeriosis, many immunologically studied models are based on intraperitoneal inoculation of *Lm* into laboratory mice to examine immune responses.

TLR2 and TLR5 are key receptors in recognizing *Lm* lipoprotein and flagellin, respectively. However, controversial data rejects the reported relationship between TLR2 and *Lm* infection *in vivo* [79].

Nonetheless, MyD88, a crucial adapter protein in many TLR-mediated signals, has been reported to be essential in controlling *Lm* infection [79, 80]. The virulent components of the *Lm* bacterium activates the innate immune response in a multistep process shown in *Figure 1.5*. Once *Lm* enters the bloodstream, circulating macrophages or tissue-resident macrophages internalize the bacteria after which *Lm* secretes listeriolysin O (LLO), a known virulence factor that destroys the phagosomal membrane. This secretion induces vacuole membrane lysis and ultimately stimulate NFκB-mediated transcription of various immune signals (*Figure 1.5*) [78].

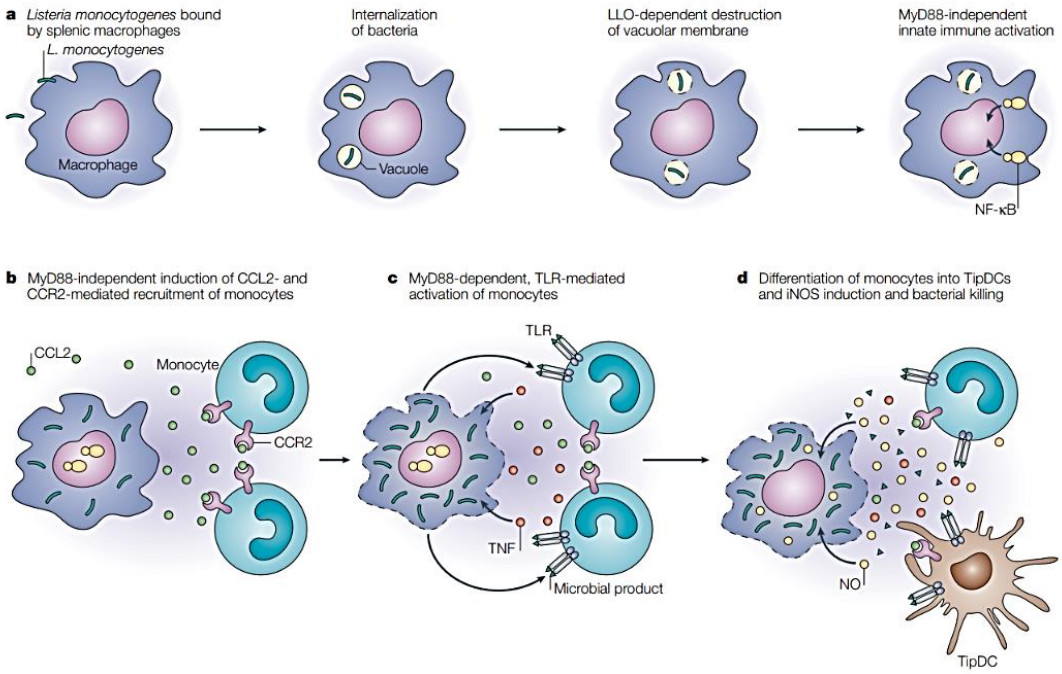

Figure 1.5. **The activation of innate immune cells by *Listeria monocytogenes* (*Lm*). (A)** *Lm* binds to macrophages after which they are internalized. Thereafter, the bacteria secrete LLO resulting in vascular membrane destruction and subsequent activation of NFκB-mediated immune signals such as CCL2 secretion. **(B)** CCL2 then recruits CCR2 expressing monocytes. **(C)** This is followed by the release of microbial products which activates monocytes via TLR in a MyD88-dependent manner. **(D)** Monocytes are later differentiated into TNF- and iNOS-producing dendritic cells (TipDCs) that promote bacterial killing. *Image sourced from Pamer, 2004 [78].*

Overall, bacterial infections, such as tuberculosis and listeriosis, caused by *Mtb* and *Lm*, respectively, continue to be life-threatening in many cases, contributing to unique public health challenges. With the continuous spread of TB in various communities in addition to sporadic listeriosis outbreaks, extensive research efforts in eliminating these infectious agents are required. Although listeriosis has a greater mortality rate compared to that of TB, the unpredictable, persistent and emerging drug-resistant *Mtb*, that

claims many lives yearly, necessitates urgent and novel therapeutics. Thus, many researchers have embarked on alternative routes of treatment interventions, including host-directed therapy (HDT).

1.2. Host-Directed Therapy for Tuberculosis

Given the success of anti-microbial research for the last two centuries, undoubtedly, research efforts into developing drugs directly targeting the pathogen must continue. However, as previously stated, the CDC has declared the 21st century as the "post-antibiotic era" [5]. Thus, in addition to anti-microbial research, an urgent demand for alternative approaches are required to fulfill the goals outlined in The End TB Strategy [55]. By directly targeting host factors and responses to an infectious agent, host-directed therapy (HDT) has great potential to assist in achieving these goals [81]. HDT uses small molecules or biologics to yield anti-microbial or host-beneficial responses [82]. Given the continuous emergence of drug-resistant TB strains, the limitations in anti-mycobacterial research have become a frustrating challenge in developing effective drugs. Redirecting the drug target with the use of HDT could yield more encouraging outcomes and therefore facilitate in achieving a TB-free world as outlined by WHO [55]. The use of HDT presents many advantages, but the primary benefit is the inability or less likely a chance of therapy resistance. As previously stated, the great disadvantage of pathogen-directed therapy is the continuous development of drug resistance. Thus, with HDT targeting host immune responses, the pathogen is less likely to develop a mutation that would prevent compound binding [83].

The outlined goals for TB HDT include the improvement of drug efficacy, especially in drug-resistant TB. Furthermore, to reduce the number of agents involved in combination drug therapy since one of the reasons for drug resistance is the incompletion of the long-term therapy. An additional goal for TB HDT is shortening the treatment regimen while preserving lung function with reduced tissue damage [84]. The immunopathology of *Mtb* allows for a great reservoir in TB HDT research as *Mtb* is able to activate and stimulate multiple immune responses [10], therefore presenting many targets for HDT.

1.2.1. HDT potential targets

There are multiple routes in which HDT can reduce disease progression and/or tissue damage, including the destruction of granulomas, inducing autophagy, anti-inflammatory responses, cell-mediated responses as well as facilitating the use of anti-*Mtb* monoclonal antibodies (*Figure 1.6*). These known HDT targets are briefly described below.

Granulomas are robust structures with rigid epithelioid macrophages on the periphery. They function by enclosing the *Mtb* bacterium and in turn restrict antibiotic access, thereby extending treatment periods. Since this process is controlled by TNFα, the first HDT described is the use of an anti-TNFα antibody (Enbrel) for TNFα neutralization that would disrupt granuloma integrity and augment drug accessibility and subsequent bacterial clearance (*Figure 1.6 A*) [85]. Secondly, the induction of autophagy has been described as a potential target for HDT development (*Figure 1.6 B*). A promising study demonstrated the use of gefitinib which inhibits the epidermal growth factor receptor (EGFR). The inhibition of this EGFR-mediated p38 MAPk signaling pathway induces autophagy and consequently reduces intracellular *Mtb* growth in murine macrophages *in vivo* [86]. Furthermore, various immunomodulators such as vitamin D (1,25-dihydroxyvitamin D_3 [$1,25(OH)_2D_3$]) are known to upregulate innate immune response as well as mediate inflammatory responses, ultimately enhancing bacterial killing [87]. Many studies have shown the protective effects of Vitamin D in *Mtb*-infected macrophages which has been summarized by Kolloli and Subbian in 2017 [88]. However, this did not translate to Vitamin D supplementation clinical trials [89]. Thirdly, a balance between the pro-inflammatory and anti-inflammatory responses is crucial when encountering a pathogen (*Figure 1.6 C*). An aggressive shift in either direction could result in poor bacteria control and severe disease development with potential tissue damage. One of the many research outcomes targeting inflammatory responses as a potential HDT is the use of Ibuprofen. This immunomodulatory drug inhibits cyclooxygenase 1/2 (COX1/2) and suppresses thromboxane and prostaglandin H2 production. The use of this drug without standard anti-TB drugs has shown to reduce TB bacterial loads as well as reduce lung pathology in murine models [90]. Although this drug has great potential for TB therapy, it still requires clinical validation. The fourth HDT target described is the cell-mediated response which is the central component of the adaptive immune response to *Mtb*. There are many routes to target within the cell-mediated response including the use of statins which inhibits 3-hydroxy-3-methylglutaryl-CoA known to reduce serum low-density lipoprotein (LDL) cholesterol levels in humans (*Figure 1.6 D*) [91]. Parihar and co-authors showed a significant reduction in *Mtb* bacterial loads and lung pathology after statin treatment in mouse models. They further demonstrated that this protective phenotype was a consequence of reduced membrane cholesterol levels [92]. The last technique described in *Figure 1.6*, is the use of anti-*Mtb* monoclonal antibodies that would ultimately suppress *Mtb* growth. Many HDT reported studies targeted this area of research testing different antibodies [88], including anti-Lipoarabinomannan (LAM) antibodies. Precoating the bacillus with a serum rich in these antibodies augments phagolysosomal fusion and subsequent IFNγ-expressing $CD4^+$ and $CD8^+$ T-cells (*Figure 1.6 E*) [93]. Therefore, multiple routes in which HDT can target to reduce and eliminate *Mtb* have been explored. However, there are limited clinically successful approaches that can be incorporated into a standard TB drug regimen.

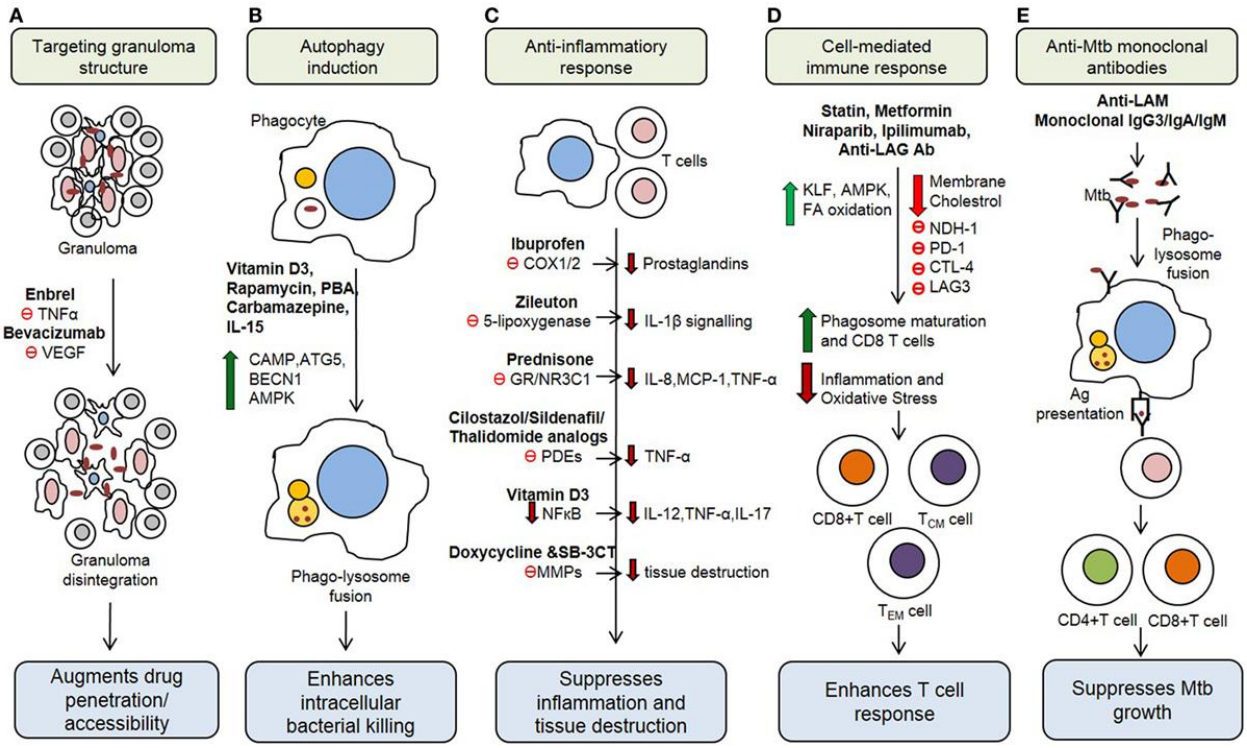

Figure 1.6. **Potential host-directed therapeutic targets against *Mtb*. (A)** Drugs targeting the disruption of granuloma integrity could allow for drug accessibility and reduce treatment length. **(B)** HDT targeted at increasing autophagy could yield increased intracellular bacterial killing, thus reducing spread. **(C)** Therapies that mediate proinflammatory responses by inducing anti-inflammatory molecules to suppress inflammation and reduces tissue damage. **(D)** Drugs aimed at the core of *Mtb* control to enhance the cell-mediated response. **(E)** HDT research directed at anti-*Mtb* monoclonal antibodies to suppress *Mtb* growth. *Image sourced from Kolloli and Subbian, 2017 [88]. Full descriptions and abbreviations can be sourced directly from the publication [88].*

1.2.2. Using transcriptomics to identify HDT targets

Host transcriptomics is a powerful tool that could aid in novel therapeutic design. Using high-throughput technologies to study a complete set of RNA transcripts in response to *Mtb* contributes to the identification of differentially expressed genes and ultimately generating a disease signature, which could be used for the development of diagnostic tools [94]. With the use of microarrays and RNA-sequencing (RNA-seq), it is already known that *Mtb*-infected macrophages exhibit a distinct transcriptomic profile compared to non-infected macrophages [95]. Novel RNA-seq methods are continuously undergoing modifications and improvements to better understand how bacterial pathogens cause disease. These techniques are currently beyond standard mRNA profiling comparing diseased states with healthy environments [96]. Single cell

RNA-seq allows for the analysis of individual host cell heterogeneity accompanied by its contribution to disease progression [96]. This technique was used to identify differentially expressed genes between restrictive and permissive human macrophages in response to *Mtb* infection. These authors demonstrated the importance of GM-CSF to direct macrophages toward an inflammatory state to assist in mycobacterial control [97]. More recently, dual RNA-seq permits the investigation of both the host and pathogen simultaneously [96, 98]. This technique was employed by Pisu and co-authors in 2020, exploring the *in vivo* molecular dynamics of *Mtb*-infected mouse models, after which they describe a distinct transcriptional host-bacteria response between alveolar and interstitial macrophages [98]. With the advent of RNA sequencing transcriptomics, sanctioning more robust and sensitive outcomes (described in [99]), various consortiums, including Encyclopedia of DNA Elements (ENCODE) [100] and Functional Annotation of Mammalian Genome (FANTOM) [101-103] unveiled comprehensive expression profiles.

1.2.2.1. FANTOM5: Identifying *Mtb* targeted genes

Using Cap Analysis of Gene Expression (CAGE) technology, which exploits next-generation sequencing of the 5' end of capped RNA species to obtain genome-wide RNA profiles comprehensively and quantitatively, the FANTOM5 project was aimed to capture the transcriptome of various biologically diverse mammalian cells [101-103]. To identify differentially expressed genes in *Mtb*-infected murine macrophages, bone marrow-derived macrophages (BMDM) were polarized and infected. Thereafter, RNA was extracted at various timepoints and subjected to CAGE sequencing as outlined in *Figure 1.7* [102].

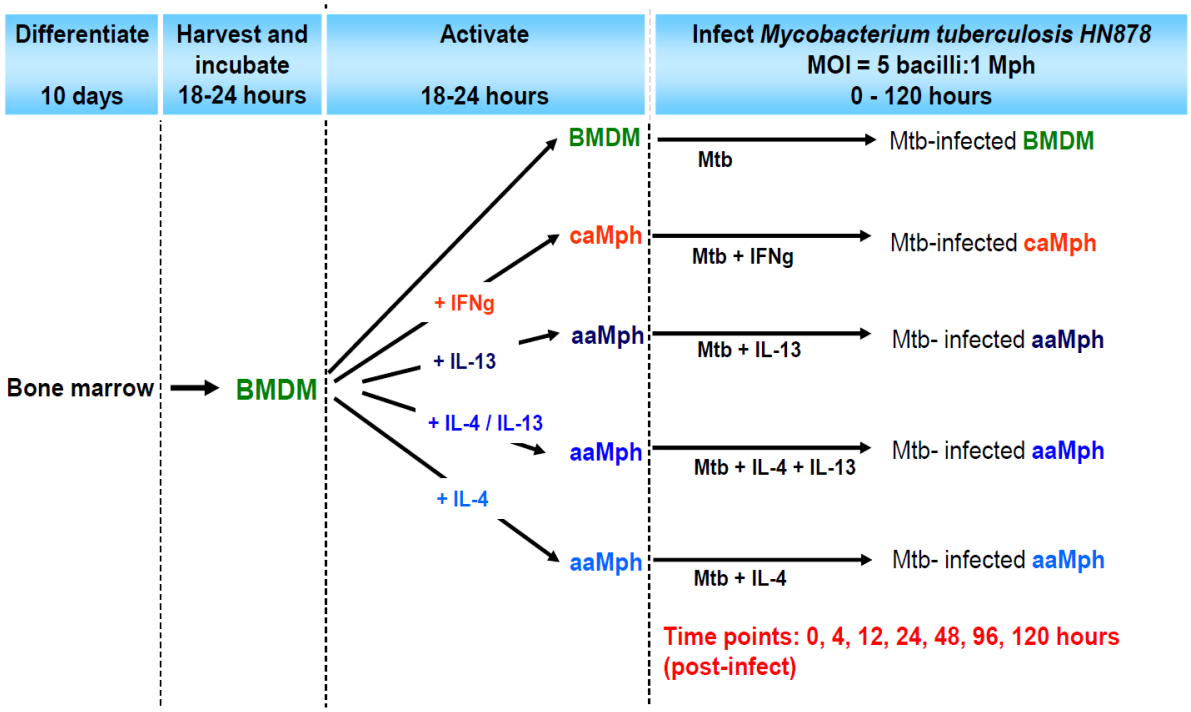

Figure 1.7. **Experimental layout of CAGE experiment contributed by the Brombacher Laboratory, Cape Town, to the FANTOM5 project.** Bone marrow cells were collected from BALB/c mice and differentiated into bone marrow-derived macrophages (BMDM) in the presence of M-CSF conditioned media for 10 days *in vitro*. Cells were harvested, seeded ($3x10^6$ cells/well in a 6-well plate) and polarized into either classically activated macrophages (caMph) with 100U/ml IFNγ or alternatively activated macrophages (aaMph) with 100U/ml IL-4 and/or 100U/ml IL-13, along with untreated control (BMDM) for approximately 24 hrs. They were later infected with hypervirulent Beijing HN878 *Mtb* strain (MOI:5) and RNA was collected at indicated timepoints and subjected to CAGE sequencing. *Image sourced from Anita Schwegmann Ph.D. thesis submitted in 2017*.

This technology has presented the opportunity to identify many immune signatures in various diverse biological states. Therefore, this publicly available dataset provided a platform to identify potential *Mtb*-specific host protective or immune evasion genes by evaluating their expression patterns. With the help of a bioinformatician, Dr. Sebastian Schmeier at Massey University, we were able to graphically view the expression patterns of various genes on the publicly available site TBvis (*Figure 1.8*) [104]. With differential expression algorithms (DESeq2), various potential protein targets were identified. Given the significantly downregulation within 4 hours of hypervirulent Beijing *Mtb* HN878 exposure, Lymphoblastic leukemia 1 (Lyl1) was highlighted. Intriguingly, it was downregulated in both M1 (IFNγ) and M2 (IL-13/IL-4) macrophage subsets, suggesting a potential role of this gene during host *Mtb* infection (*Figure 1.8*) [104].

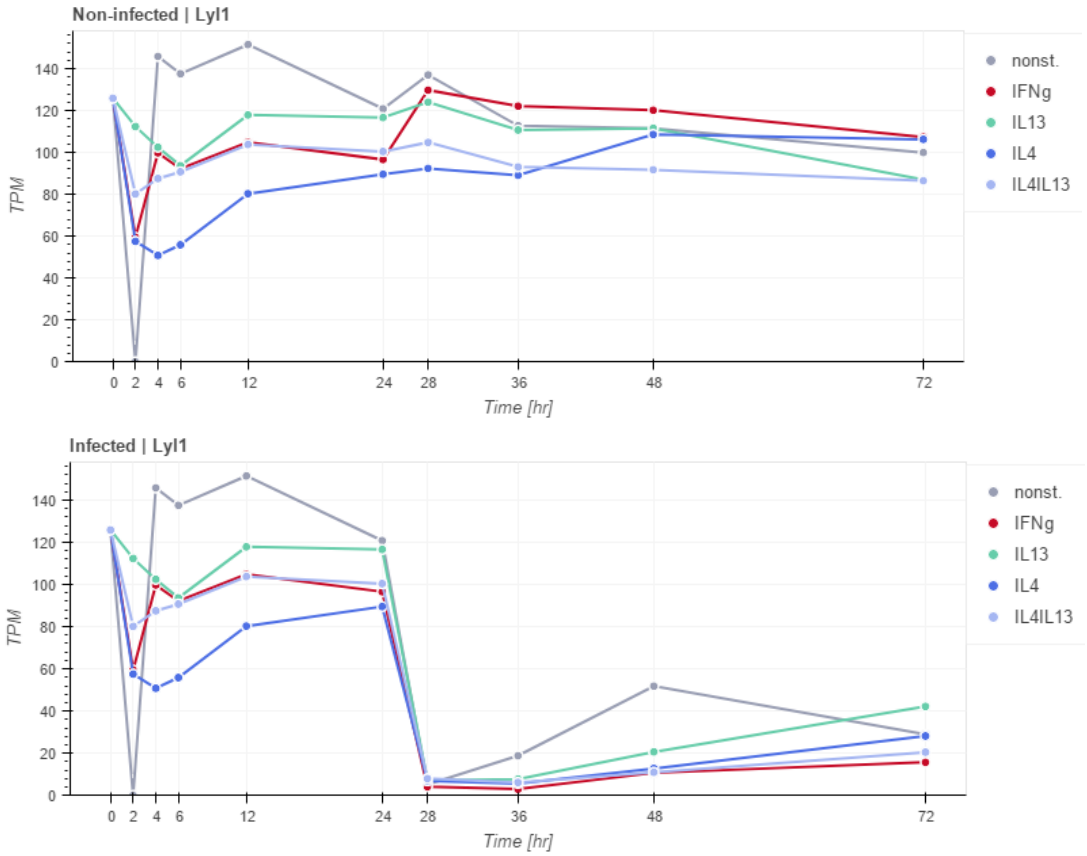

Figure 1.8. **Lymphoblastic leukemia (Lyl1) expression in murine macrophages in response to *Mtb* HN878 infection.** As depicted in *Figure 1.7*, BMDM cells were stimulated with the indicated stimulants for 24 hours after which they were infected with hypervirulent Beijing *Mtb* HN878 strain (MOI:5). Thus, in this figure, the introduction of *Mtb* is illustrated at the 24-hour timepoint, and therefore the 28-hour timepoint represents 4 hours post-infection. Lyl1 expression between the different macrophage subsets were relatively unchanged (*upper panel*). However, in the presence of *Mtb* HN878, the expression of Lyl1 significantly reduces in all macrophage subsets (*lower panel*). *Data adapted from CAGE database [102] and image sourced from TBvis at http://compbio.massey.ac.nz/apps/tbvis2/home/ [104].*

1.3. Lymphoblastic leukemia 1 (Lyl1): A potential host protective gene against bacteria

1.3.1. Discovery

Lymphoblastic leukemia (Lyl1) was initially discovered and characterized by Mellentin, Cleary and Smith in 1988 and 1989 [105, 106]. The aim was to identify genes disrupted in chromosomal translocations with the potential to cause pathogenesis in leukemia patients. The authors described great oncogenic potential for Lyl1 given its translocation on t(7;19)(q35;p13) resulting in the augmentation of abnormally-sized RNA transcripts [105]. Lyl1 was then characterized and classified as a Class II basic helix-loop-helix (bHLH) transcription factor that exhibit tissue-specific expression patterns [106]. Class II bHLH transcription factors are known to regulate genetic transcription (activation/repression) by binding to various target gene sequences as heterodimers with E-proteins [107]. Both Lyl1 and its paralog, Scl/Tal1, revealed heterodimer formation with E2A [108].

1.3.2. Lyl1 and its paralog, Scl/Tal1

Shortly after the discovery of Lyl1 in acute leukemia patients, a highly similar bHLH transcription factor was discovered upon chromosomal translocation at t(1;14)(p32;q11) during stem cell leukemia, known as Scl or T-cell acute lymphoblastic leukemia 1 (Tal1) [109]. Lyl1 and Scl/Tal1 share 82% bHLH amino acid identity, suggesting similar biological functions and target genes [110, 111]. Both transcription factors exhibit overlapping expression patterns across various hematopoietic lineages and are expressed in developing endothelial cells. Furthermore, they also interact with the lim-only-domain oncogenic genes referred to as Lmo1 and Lmo2. However, many studies have demonstrated distinct functions between these two proteins [110]. Extensive research has been published describing the importance of Scl/Tal1 in early hematopoietic stem cell (HSC) specification, including the neuronal and vascular development [112-114]. Further studies have shown the importance of Scl/Tal1 in short-term repopulation activity of HSC, yet simultaneously insignificant in self-renewal and/or long-term repopulation of adult HSC [115, 116]. Contrastingly, Lyl1-deficient mice are viable with standard blood cell counts and serve a rather important

function in B- and T-cell reconstitution after lethal irradiation [110]. Furthermore, various compensatory studies have shown that irrespective of their distinct sequence similarity, Lyl1 cannot compensate for Scl/Tal1 during early developmental hematopoiesis [117]. However, in Lyl1-Scl/Tal1 double knockout mice, HSC function can be restored by one allele of Lyl1 which was not observed for Scl/Tal1 [118]. Collectively, these reports suggest that Scl/Tal1 is required for HSC generation, whereas Lyl1 is rather crucial in the maintenance of adult stem cell properties during lymphoid reconstitution.

Aside from the functionality and expression patterns in different stages of hematopoiesis, various comparative downstream targets have been evaluated. With the use of human Jurkat T-cell line, Pirot and co-authors have demonstrated the interaction of Lyl1 with NFκB1 (p50/p105). An ectopic expression of Lyl1 was shown to reduce NFκB-dependent genetic transcription. However, this was not translated to Scl/Tal [119]. Furthermore, San-Marina and co-authors demonstrate that Lyl1 transactivates a completely different set of genes compared to Scl/Tal1 based on its ability to bind to cyclic-AMP receptor element binding protein 1 (CREB1) via its N-terminal domain which completely differs from Scl/Tal [120]. Since that the absence of Scl/Tal1 results in embryonic lethality, extensive reports on Scl/Tal1 are available. However, given the oncogenic potential of Lyl1 and its distinct role compared to Scl/Tal1, recent studies have focused more on Lyl1-specific functionality and regulatory mechanisms. Chan and co-authors have shown that Lyl1 can be regulated by Ets and GATA factors [111], while a few other authors have demonstrated Lyl1 regulation of many genes including Angiopoietin-2 (ANG-2) [121], Growth Factor Independent 1 Transcriptional Repressor (Gfi1) [122], Stathmin (STMN1) [123] and RhoA expression [124]. Moreover, MAP kinase phosphorylates Lyl1 [125], Lyl1 negatively regulates spleen erythropoiesis [126], and a later paper of Pirot and co-authors demonstrates increased lung vascular permeability in the absence of Lyl1 in mouse models [124]. The mechanisms responsible for the oncogenic potential of these transcription factors also differ whereby Lyl1 interacts with the well-known oncogenic transcription factor Lmo2, contributing to its oncogenicity, whereas Scl/Tal1 is dispensable for Lmo2-driven leukemia [127].

1.3.3. Role of Lyl1 in leukemia

The role of Lyl1 in leukemia is well documented. Given the overexpression of Lyl1 in leukemia patients [128], the use of transgenic mice was used to determine its role in leukemia. Zhong and co-authors show that Lyl1 overexpression induces T- and B-cell lymphoma in murine models after 352 days, suggesting its role in lymphomagenesis [129]. This was followed by another study that demonstrated increased T-cells in peripheral blood and hematopoietic progenitor expansion in bone marrow in response to Lyl1 overexpression [130]. However, these authors argue that Lyl1 is not directly oncogenic but rather

predisposes mice towards lymphoma after which secondary mutations occur to develop leukemia. As previously stated, Lyl1 can directly interact with Lmo2, which is described as an oncogenic transcription factor found in elevated levels during T-cell Acute Lymphoblastic Leukemia (T-ALL). Using Lmo2-transgenic mice deficient in Lyl1 in the thymus, McCormack and co-authors show that the oncogenic potential of Lmo2 is dependent on Lyl1 expression and interaction [127]. In addition to T-ALL, Lyl1 has also been shown to play a significant role in Acute Myeloblastic Leukemia (AML). Meng and co-authors demonstrated Lyl1 overexpression in most AML cell lines [131]. Later, they showed that, with the use of lentiviral short hairpin RNA to silence Lyl1 in CD34-expressing cells directly from AML diagnosed patients, the absence of Lyl1 significantly reduces myeloid cell proliferation [132]. Thus, suggesting the oncogenic potential of Lyl1 during AML as well. Finally, previously mentioned studies by San-Marina and co-authors involving Lyl1 and CREB1 interaction and its regulation of CREB1 target gene expression [120], followed by Lyl1-CREB1 interaction co-regulating STMN1 expression, it was suggested that this Lyl1-CREB1-STMN1 interaction may contribute to malignant leukemia [123].

1.3.4. Lyl1 mouse models

Currently, there are two globally deleted Lyl1 murine models available for immunological studies (*Figure 1.9*). Originally, to study the role of the Lyl1 bHLH transcription factor in hematopoiesis, Capron and co-authors generated a Lyl1-deleted mouse using a β-galactosidase/Neomycin cassette containing a LacZ reporter gene to replace the HLH-expressing fourth exon on the 3' end of murine Lyl1 gene, referred to as $Lyl1^{LacZ}$ [110]. This allowed for Lyl1 expression tracking via β-galactosidase expression/activity [117]. Although the bHLH domain is thought to exhibit the critical functions of bHLH-type proteins, Lyl1, harbours a highly evolutionary conserved N-terminus. This prompted Goodell and her team to investigate as to whether the N-terminus, which was still present in the $Lyl1^{LacZ}$ mouse along with the DNA-binding region, served any functional role. Surprisingly, they discovered that the proline-rich region within the N-terminus of Lyl1, expresses a PEST motif. They demonstrated that this motif is responsible for Lyl1 protein stability by regulating degradation through the proteasome. Thus, concluding that the presence of the N-terminus in the $Lyl1^{LacZ}$ mouse model could potentially cause a hypomorphic allele [125]. Consequently, Goodell and her team generated a complete Lyl1-knockout mouse model whereby they deleted the entire Lyl1 coding region, namely $Lyl1^{Mg}$, and replacing it with a lox-P-flanked Neomycin cassette [107]. They confirmed mice to be viable and fertile with no developmental defects and later haematopoietically characterized the new Lyl1-knockout mouse model. Here they show that the loss of full Lyl1 encoding regions does not affect the myeloid population as well as B-cell development. However, although T-cell

development seem to be impaired, interestingly Lyl1^{Mg} mice still have comparable single positive CD4^{+} and CD8^{+} T-cells, suggesting no defect in differentiation [122].

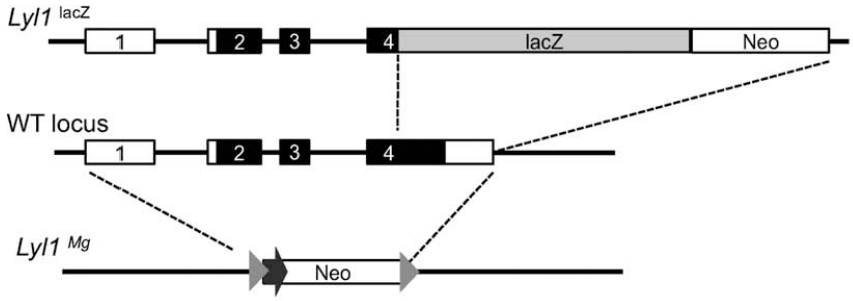

Figure 1.9. **Schematic diagram comparing the two Lyl1 mouse models.** The original model, Lyl1^{LacZ}, has a LacZ/Neo cassette inserted into the fourth exon only disrupting the HLH domain and C-terminus, retaining the basic DNA-binding domain and the N-terminus. The alternative model, Lyl1^{Mg}, eliminates all four exons, thus deleting the entire coding region with the use of a lox-P-flanked Neomycin cassette. *Schematic sourced from Goodell team publication [107].*

1.4. Project Rationale

1.4.1. Problem statement

TB continues to challenge the global health system for reasons described above. As declared by the CDC, we are amidst the "post-antibiotic era" and the demand for new methods of research are required to achieve the WHO End TB Strategy. Given the success of pathogen-targeted therapeutics in the last few decades, therapeutic research directly targeting the pathogen must continue. However, research on novel routes of therapeutics is encouraged. The use of HDT could help circumvent the disadvantages we are facing with current anti-bacterial therapeutic designs, such as resistance and the duration of the treatment regimen. Thus, uncovering the roles and functions of key genes in response to various bacterial agents, especially *Mtb*, could assist in identifying an immunological target to help control bacterial replication, dissemination, exaggerated inflammatory responses and ultimately prevent severe diseases.

1.4.2. Hypothesis

CAGE transcriptomic data (*Figure 1.8*) show significant downregulation of Lyl1 expression following *Mtb* HN878 infection in both M1 (IFNγ) and M2 (IL-13/IL-4) polarized macrophage subsets. Therefore, we hypothesize that the downregulation of Lyl1 expression is mediated by mycobacterial virulence factors.

The *Mtb*-mediated decrease in Lyl1 mRNA levels potentiates the presence of Lyl1 to be beneficial for host protection. Therefore, we hypothesize that, with the use of Goodell's Lyl1-deficient mice (*in vivo*), as well as harvested BMDM (*in vitro*), we will observe enhanced *Mtb* progression and subsequent increased susceptibility to *Mtb* infection. Moreover, contrary to cancer patients, we expect to see significant downregulation of Lyl1 in active TB patients which would conclude that the decreasing of Lyl1 mRNA levels would be an immune evasion mechanism and thus serve as an interesting target for host-directed adjunct TB therapies.

1.4.3. Aim and Objectives

This project aims to identify and characterize the novel candidate gene, Lymphoblastic leukemia 1 (Lyl1), involved in macrophage-specific pathogen killing effector functions, during bacterial infections, including *Mycobacterium tuberculosis* and *Listeria monocytogenes*. This aim is to be achieved by executing the following objectives:

1. To characterize the globally deleted Lyl1^{Mg} mouse model on a pure C57BL/6 background.
2. To understand the regulation and action of Lyl1 *in vivo* and in *vitro* using various PRR activation and *Lm* as immunological models.
3. To investigate the role of Lyl1 during *Mtb* infection.

CHAPTER 2: Manuscript in preparation

Lyl1-deficient mice are immunologically comparable to wild-type mice at steady state

Shelby-Sara Jones[1,2], Mumin Ozturk[1,2], Nathan Kieswetter[1,2], Harukazu Suzuki[4], Reto Guler[1,2,3*], Frank Brombacher[1,2,3*]

[1] International Centre for Genetic Engineering and Biotechnology, Cape Town Component, Cape Town 7925, South Africa.

[2] Department of Pathology, University of Cape Town, Institute of Infectious Diseases and Molecular Medicine (IDM), Division of Immunology and South African Medical Research Council (SAMRC) Immunology of Infectious Diseases, Faculty of Health Sciences, University of Cape Town, Cape Town 7925, South Africa.

[3]Wellcome Centre for Infectious Diseases Research in Africa (CIDRI-Africa), Institute of Infectious Disease and Molecular Medicine (IDM), Faculty of Health Sciences, University of Cape Town, Cape Town 7925, South Africa.

[4]RIKEN Center for Integrative Medical Sciences, Yokohama, Japan.

*Correspondence: Frank Brombacher, frank.brombacher@icgeb.org and Reto Guler, reto.guler@uct.ac.za

Keywords: $Lyl1^{Mg}$ ($Lyl1^{-/-}$), steady state, characterization

2.1. Abstract

Lymphoblastic leukemia 1 (Lyl1) was first identified upon chromosomal translocation during leukemia studies and thus hypothesized to express strong oncogenic potential. Lyl1 has only been studied and described during either hematopoietic function or expression patterns during leukemia. Here, we examined the effects of Lyl1-deficiency on the adult immune system at steady state. We achieve this by fully characterizing the globally deleted Lyl1 mouse model ($Lyl1^{Mg}$) across the thymus, lung, lymph node, spleen and liver, investigating cell recruitment via flow cytometry and cytokine expression by ELISA. Our data reveal minimal differences in the immune cell population across all organs when comparing littermate control (WT) with Lyl1-deficient mice. Furthermore, cytokine expression patterns do not reveal any alarming differences between these two mouse models across all organs. Altogether, our data provide a platform for further Lyl1 functional studies in various other infectious models using the Lyl1 globally deleted mouse model.

2.2. Introduction

Lymphoblastic leukemia 1 (Lyl1) is a basic helix-loop-helix (bHLH) domain-containing transcription factor that was initially discovered through its ectopic expression in the lymphoblasts of T-cell acute lymphoblastic leukemia (T-ALL) patients [105, 106]. This was a result of chromosomal translocation (t(7;19)(q35;p13)) with the T-cell receptor gene [105], similar to its paralog, Tal1 (T-cell Acute Lymphoblastic leukemia protein 1) t(1;14)(p33;q11) [109]. Tal1 was originally identified as the Scl (Stem Cell Leukemia) gene, and later studies demonstrated a highly conserved bHLH domain to that of Lyl1 (82%), suggesting that these two transcription factors share biological functions [110, 111, 133]. However, numerous reports describe the distinctiveness between these two transcription factors, including, a contrasting effect on embryonic lethality whereby Lyl1 does not share the essential role of Scl/Tal1 in embryonic hematopoiesis [110]. Simultaneously, Lyl1 is unable to rescue the Scl/Tal1-null mice lethality effect, despite the similar embryonic expression [111, 117]. The general function of Lyl1 has been described in thymopoiesis by serving a significant role in the lymphoid specification and maintaining homeostasis of immature hematopoietic cells [118, 122]. Additional studies have shown the importance of both, the earlier researched Scl/Tal1 [113, 134] and more recently studied Lyl1 [110, 117, 118, 135] at different stages of hematopoiesis.

The majority of the Lyl1-related studies were performed using the $Lyl1^{lacZ}$ mouse model, which is a Lyl1-knockout mouse that was generated by inserting a Neomycin/β-galactosidase cassette into the fourth exon, replacing the HLH domain and conserving the N-terminus and basic (b) DNA-binding region [110,

117]. However, studies have suggested a functional role of the evolutionary conserved N-terminus in Lyl1. The presence of the PEST regulatory motif located within the proline-rich region of the N-terminus later strengthened the view that the N-terminus can also be functionally significant for Lyl1 [125]. The same research group later designed and generated an alternate Lyl1-knockout mouse that removed the entire coding sequence (all four exons), now referred to as $Lyl1^{Mg}$ [107].

Given the role of Lyl1 in the hematopoietic system, the characterization of the $Lyl1^{Mg}$ mouse was limited to progenitor development whereby the only tissue characterization included the investigation of B-cells, T-cells and overall myeloid population in the spleen, bone marrow and thymus [122]. Although, the Lyl1-null mice ($Lyl1^{Mg}$, hereon referred to as $Lyl1^{-/-}$) exhibit significant defects in lymphoid progenitor development, including in the lymphoid primed multipotent progenitor (LMPP) cells in the thymus, they still express comparable mature $CD4^+$ and $CD8^+$ T-cells during thymopoiesis [122]. Therefore, to use this Lyl1-knockout mouse as a tool for various infectious models, such as bacteria, we aimed to investigate the impact of Lyl1-deficiency on adult immunological responses by focusing on tissue immune cell populations, histopathology and cytokine/antibody concentrations in comparison to a murine Lyl1-inclusive immune system.

Although many studies describe the importance of Lyl1 in various developmental processes during naïve states, our research demonstrate no major immunological defects during adult development or differences in the Lyl1-deficient mice compared to wild-type mice at steady state. This data avails the $Lyl1^{Mg}$ mouse for any immune protection or evasion studies.

2.3. Methods

2.3.1. Mouse strains

To study the function of Lymphoblastic leukemia 1 (Lyl1), we acquired a Lyl1 global knockout mouse whereby the entire coding region was deleted using a lox-P-flanked Neomycin cassette. This mouse ($Lyl1^{Mg/Mg}$) was generated by the Margaret A. Goodell laboratory at Baylor College of Medicine, Houston, Texas [107] by injecting the correctly targeted clones into blastocytes of 129 AB2.2 mice and further back-crossed to the C57BL/6 strain for ten generations. Once received at the University of Cape Town (UCT), $Lyl1^{Mg/Mg}$ was back-crossed with in-house C57BL/6J strains for three generations to generate $Lyl1^{-/-}$, $Lyl1^{-/+}$ and littermate control, $Lyl1^{+/+}$ in the Animal Research Facility, UCT. Animals were housed, monitored and experimentally handled within strict accordance with the guidelines approved by the Animal Research Ethics Board of UCT. All experiments included mice aged 8 – 12 weeks and were sex-matched.

2.3.2. Mouse genotyping

For genotypical identification of mice, genomic DNA was extracted and amplified, by PCR, from mouse tails as described [136, 137] using the following primer pairs (final): Lyl1 forward 5'-TGCAGCCCAATTCCGATCATA-3' and Lyl1 reverse 5'-TGTCCTAGCGGAATGCAAGT-3' along with the WT forward 5'-CGCAGACCAAGCCATAGTGA-3' and WT reverse 5'-TGGCTG TTGTAT GTGTGGCT-3' for the multiplex PCR in a T100™ Thermal Cycler (Bio-Rad). Optimal PCR conditions included an initial denaturing step at 94°C for 2 minutes followed by 39 cycles of denaturation at 94°C (20 seconds), annealing at 58°C (30 seconds), extension at 72°C (90 seconds) and a final acquisition at 72°C for 5 minutes. Thereafter, the PCR products were separated on a pre-stained (SYBR Safe DNA gel stain; Thermofisher) 1.6 % agarose gel and viewed under UV light using the Syngene G:Box and GeneSnap software (Syngene, Cambridge).

2.3.3. Ethical statement

All animals used in this study were subjected to experimental procedures that were in strict accordance with the South African National Standard (SANS 10386:2008) and the Animal Research Ethics Committee of the Faculty of Health Sciences, University of Cape Town (Protocol Permit No: 015/040 and 019/023).

2.3.4. Single cell suspension of organs upon euthanasia

Upon euthanasia of naïve mice, indicated organs were collected, weighed and prepared for single cell suspension as previously described [138]. Briefly, the lymph node (LN) and thymic organs were collected in 1.5 ml of filter-sterilized Dulbecco's Modified Eagle Medium (DMEM) supplemented with 10% inactivated fetal bovine serum (iFBS). Single cell suspensions were achieved by mechanically sieving the organ through a 70 µM cell strainer followed by a 40 µM cell strainer to remove excess debris and clumping. The cells were pelleted, resuspended in DMEM and proceeded to cell counts after which they were finalized to 10 million cells/ml. The spleen was subjected to the same protocol as the LN and thymus aside from subjecting the cell suspension to red blood cell lysis buffer (155 mM NH_4Cl, 12 mM $NaHCO_3$ and 0.1 mM EDTA) for 3 minutes prior to cell counts. Finally, both the lung and the liver was severed into 10 mm^3 pieces using the scalpel, collected in either lung digestion buffer (DMEM supplemented with 13 U/mg DNase I and 220 U/mg Collagenase I (both from Sigma-Aldrich)) or liver digestion buffer (DMEM supplemented with 13 U/mg DNase I, 110 U/mg Collagenase I and 110 U/mg Collagenase II (all from Sigma-Aldrich)) and incubated at 37°C with rotation for 30 minutes or 1 hour, respectively. Thereafter, the

suspension was mechanically passed through a 100 µM cell strainer, followed by a 70 µM cell strainer, after which the cells were pelleted (400 x g for 5 minutes at 4°C) and incubated in red cell lysis buffer for 3 minutes. The cell suspension was finalized as per conditions stated above.

2.3.5. Quantitative real-time polymerase chain reaction (qRT-PCR)

Single cell suspension of each organ was combined with 350 µl of RLT lysis buffer and later extracted RNA using the RNeasy Mini Kit (Qiagen catalogue no. 74106). RNA was extracted according to the manufacturer instructions and normalized to 300 ng. Thereafter, RNA was reverse transcribed by the Transcriptor First Strand Complementary DNA Synthesis Kit (Roche catalogue no. 04 379 012 001) using both anchored oligo dT primers and random hexamer primers according to the manufacturer instructions to yield complementary DNA (cDNA). Later, various transcripts were amplified by qPCR using LightCycler® 480 SYBR Green I Master Mix with the Lyl1 primer pair: Lyl1 forward 5'-CCCCTTCCTCAACAGTGTCTAC-3'; Lyl1 reverse 5'-TATGGCTTGGTCTGCGCTTC-3' and Hprt primer pair: Hprt forward 5'- GTTGGATATGCCCTTGAC-3'; Hprt reverse 5'-AGGACTAGAACACCTGCT-3' in the LightCycler® 480 Instrument II (Roche). The PCR reaction was first pre-incubated for 5 minutes at 95°C followed by amplification (denaturing at 95° for 10 seconds; annealing at 60°C for 15 seconds; extension at 72°C for 15 seconds and the final acquisition step at 80°C for 1 second) for 45 cycles. Targeted expressions were normalized to Hprt expression levels.

2.3.6. Flow cytometry

Single cell suspensions were surface stained for the identification of the lymphoid and myeloid cell populations. The following antibodies, purchased from BD Biosciences, BioLegend and eBioScience. were used to surface phenotype various cell populations: PD-1 (FITC); CD4 (BV421/V450); CD44 (PE); NK1.1 (APC-Cy7); CD3 (A700); CXCR5 (PE-Cy7); CD62L (APC); CD19 (PerCP-Cy5.5); CD8 (V500); KLRG1 (BV786); CD64 (PE-Cy7); Ly6C (PerCP-Cy5.5); CD11b (V450); MHC II (A700); CD11c (APC); SiglecF (APC-Cy7); Ly6G (FITC); MerTK (BV786); CD103 (PE); F4/80 (PE-Cy7); CD169 (eFluor780). Cells were stained and acquired according to [138] using the BD LSR Fortessa (BD Biosciences Immunocytochemistry Systems), and the data analysis were performed with FlowJo v10.6.1 Software (Treestar, US). All panels are outlined in the appendix: *A*-thymus lymphoid; *B*-lung, lymph node, spleen and liver lymphoid; *C*-lung myeloid; *D*-lymph node myeloid; *E*-spleen myeloid; and *F*-liver myeloid.

2.3.7. Measurement of cytokines and/or antibodies in organ homogenates and/or serum

Lung, spleen and liver homogenate as well as serum cytokine and antibody concentrations were examined using the standard sandwich ELISA protocol (coating and detection antibodies obtained from BD Biosciences, BioLegend and R&D Scientific) using either TMB Microwell Peroxidase Substrate (KPL international) for streptavidin-HRP conjugates or 1 mg/ml p-nitrophenyl phosphate disodium salt hexahydrate (Sigma; catalog no: N2765) for streptavidin-AP conjugates. Optical density was measured using the VersaMax™ microplate spectrophotometer (Molecular Devices, Sunnyvale, California).

2.3.8. Histopathology and immunohistochemistry

Upon animal euthanasia and experimental organ excision, a portion of the indicated organ was collected in formalin solution (10% formaldehyde in 1X PBS) for tissue fixation. Formalin-fixed tissue samples were then embedded in wax, processed, subjected to 3 µm sections and stained with hematoxylin and eosin (H&E) for histopathological analyses. Thereafter, stained sections were mounted onto microscopic slides using a xylene-based mounting medium for image acquisition and quantification using the Nikon Eclipse 90i (Nikon) microscope with the Nikon NIS-Elements advanced imaging software (Nikon Corporation).

2.3.9. Statistical analyses

All data represented was analyzed using GraphPad Prism 6.0 with the use of the unpaired student *t-test* (two-tailed with equal variance). A $*p$ value of less than 0.05 was considered significant, depicting $**p < 0.01$, $***p < 0.001$ and $****p < 0.0001$.

2.4. Results

2.4.1. The neomycin cassette in the published Lyl1-deficient ($Lyl1^{Mg}$) mouse has been omitted, yet they remain viable and express no physiological difference compared to wild-type mice

$Lyl1^{Mg}$ mice were received from Prof. Barbara Kee's laboratory from the University of Chicago on a C57BL/6 background and back-crossed three generations to in-house C57BL/6J strain. Using the primers provided, genotyping instructions were followed according to Kee's laboratory. However, this provided no indication of the presence/absence of the Lyl1 mutant allele since the provided primers and PCR protocol yielded no band (data not shown). Referring to Goodell's $Lyl1^{Mg}$ generation paper [107], alternate primers were designed, targeting upstream and downstream of the Lyl1 gene which resulted in an ~900bp band

instead of the expected ~3kb (data not shown). This band was sequenced using the following primer pair: Lyl1-forward 5' – CCC CTT CCT CAA CAG TGT CTA C – 3' with Lyl1-reverse 5' – TAT GGC TTG GTC TGC GCT TC – 3' and demonstrated complete removal of the neomycin cassette along with one loxP site (*Figure 2.1 A*). It is unknown as to how this occurred, nonetheless, based on the new allele, accurately targeted primers could be designed, resulting in successfully genotyping all litters using the multiplex PCR method (*Figure 2.1 B*). Later, animal fitness between the littermate control, hereon referred to as wild-type (WT), and $Lyl1^{Mg}$ (hereon referred to as $Lyl1^{-/-}$) are evaluated by first investigating the physiological parameters including body weight (*Figure 2.1 C*), organ weight (*Figure 2.1 D*) and cell numbers (*Figure 2.1 E*) of which no difference was observed. To confirm the global deletion of Lyl1, we examined Lyl1 expression in the liver, lung, lymph node (LN), spleen and thymus by qPCR in both WT and $Lyl1^{-/-}$ mice (*Figure 2.1 F*). It was evident that Lyl1 has been removed from the entire immune system. Additionally, publicly available databases, including the Genotype-Tissue Expression (GTEx) consortium [139] and the Functional Annotation of the Mammalian genome 5 (FANTOM5) [102], show that, aside from blood, Lyl1 is most abundantly expressed in the spleen in humans and murine models, respectively. This expression pattern was also confirmed in *Figure 2.1 F*.

2.4.2. Lyl1-deficiency causes imbalances during thymopoiesis, however, express similar single positive T-cells compared to WT

Given the significant role of Lyl1 during thymopoiesis and consequently T-lymphocyte development [122], the thymus immune cell population was initially investigated (*Figure 2.2*). This data confirms the role of Lyl1 during thymopoiesis given the imbalance between WT and $Lyl1^{-/-}$ during the double negative (DN) stages of T-cell development (*Figure 2.2 A-B*). However, when comparing the single positive (SP) mature $CD4^+$ and $CD8^+$ populations between WT and $Lyl1^{-/-}$, these cells demonstrate to populate the thymic tissue comparably. Although a slight decrease in $Lyl1^{-/-}$ $CD8^+$ percentages (*Figure 2.2 A*) was observed, this did not translate to cell numbers (*Figure 2.2 B*). A histopathological assessment of the tissue showed no difference in tissue structure between WT and $Lyl1^{-/-}$ mice (*Figure 2.2 C*). Therefore, this data suggest, and confirms Goodell's thymic characterization [122], that although there is an imbalance during the DN stages of T-cell development between WT and $Lyl1^{-/-}$ mice, these imbalances are not reflected in mature T-cell specifications.

2.4.3. Lung and lymph node (LN) immune cell populations are comparable between WT and Lyl1-knockout mice

Tissue characterization on mature cells, aside from the thymus, was only previously examined in the bone marrow and spleen of which the B-cells ($CD19^+B220^+$) and myeloid cells, characterized by granulocytes and macrophages using Mac1 and Gr1 markers, demonstrated comparable expression patterns between WT and $Lyl1^{-/-}$ mice [122]. Therefore, to identify the effects of Lyl1-deficiency on alternate components of the immune system, an extensive organ characterization was performed by examining the effects of Lyl1-deficiency on myeloid and lymphoid cell development and recruitment in various tissues. In the absence of Lyl1, the lung myeloid populations (*Figure 2.3 A*) reveal differences in percentages, however, this effect was not translated to cell numbers (*Figure 2.3 A lower panel*). Additionally, the lung lymphoid cell population numbers (*Figure 2.3 B-E*) are comparable between WT and $Lyl1^{-/-}$ mice. Moreover, histopathological assessment on alveolar spacing show that Lyl1-deficient lungs experience no excess inflammation, or lack thereof (*Figure 2.3 F-G*). Therefore, this data suggests that the absence of Lyl1 has slight effects on lung cell recruitment at steady state. Similarly, the LN myeloid (*Figure 2.4 A*) and lymphoid (*Figure 2.4 B-E*) cell populations, including the $CD4^+$ and $CD8^+$ subpopulations (*Figure 2.4 C-D*) involving memory as well as the $CD4^+$ PD1/KLRG1 positive/negative T-cell populations (*Figure 2.4E)* are comparable between the two mouse models. Together, this data show that Lyl1-deficient lungs and LN demonstrate no considerable defects in myeloid and lymphoid cell recruitment when compared to WT mice. Thus, providing a platform for studying the role of this gene in various lung targeting infectious diseases without underlying complications.

2.4.4. Globally deleted Lyl1 and WT mice demonstrate comparable immune cell populations in the spleen and liver tissues

To examine additional secondary organs, myeloid and lymphoid immune cell recruitment in both the spleen (*Figure 2.5*) and the liver (*Figure 2.6*) of WT and $Lyl1^{-/-}$ mice were investigated. The percentage and number of myeloid and lymphoid immune cell populations (*Figure 2.5 A-B*), as well as $CD4^+$ and $CD8^+$ T-cell memory (*Figure 2.5 C-D*) recruited to the spleen were comparable between the two mouse models. Kupffer cells, dendritic cells and various other myeloid cells recruited to the liver are independent of Lyl1 at steady state (*Figure 2.6 A*). Furthermore, Lyl1-deficiency does not impair lymphoid cell recruitment to the liver (*Figure 2.6 B-E*), nor does it influence the microscopic anatomy of the spleen (*Figure 2.5 E*) or the liver (*Figure 2.6 F*). Therefore, our data suggest that $Lyl1^{-/-}$ mice can be used to study the relationship between Lyl1 and various systemic infectious diseases that target the spleen and the liver.

2.4.5. The cytokine/antibody profile is minimally affected by the absence of Lyl1 at steady state

Increased cytokine expressions are clear indicators of disease or stress [140]. Therefore, investigating cytokine production in the absence of Lyl1 would assist in understanding whether the Lyl1-deficient mice suffer from any immunological imbalance without this transcription factor. To address this, cytokine expression in the lung, spleen, liver and serum was investigated in both WT and $Lyl1^{-/-}$ mice. Overall, Lyl1-deficient murine models do not display any alarming immunological imbalances evident in most Th1, Th2 and Th17 response associated cytokine levels in all organs in comparison to WT mice. Although lung and liver IL-6 (*Figure 2.7 A, E*), as well as splenic IL-5 (*Figure 2.7 D*), suggest significant induction in $Lyl1^{-/-}$ mice, the overall expression levels were considerably low or the effects were not consistently observed across all organs at steady state. Notably, the only cytokines representing significant upregulation in the absence of Lyl1 is splenic IL-2 and IL-4 expression (*Figure 2.7 C-D*). Additionally, the effects of Lyl1-deficiency on antibody production and cytokine release into the bloodstream were investigated. No differences in antibody concentrations (*Figure 2.7 G*) and cytokine levels, aside from IL-10, (*Figure 2.7 H*) between WT and $Lyl1^{-/-}$ mice. However, although our data suggest a slight increase in IL-10 release into the bloodstream, the level of IL-10 expressed in tissues remain comparable to WT (*Figure 2.7 H*).

Collectively, our data demonstrate no immunological imbalance in mice deficient of the Lyl1 transcription factor. Lyl1-deficient mice exhibit comparable mature myeloid and lymphoid cell development in all represented organs at steady state as well as cytokine and antibody concentrations in comparison to WT mice.

2.5. Discussion and Conclusion

It is evident that the $Lyl1^{Mg}$ mouse strain published in Goodell's paper [107] did not retain the exact genetic composition on the Lyl1 loci and thus differs from the mouse housed at the UCT Animal Facility. However, since the changes in genetic composition was within the plasmid, the mice were still viable and fertile. As a result of plasmid genetic modification, the primer pair provided by Barbara Kee's laboratory and the primer pair used in Goodell's paper to genotype the $Lyl1^{Mg}$ mouse was unsuccessful. This mouse model was generated in Texas, however, it was received by our laboratory from an alternate experimental laboratory based in Chicago. Therefore, it is possible that the mouse could potentially have been crossed with an embryonic Cre-expressing mouse strain, and by accidentally inducing the Cre-LoxP system, it globally removed the entire sequence between the loxP sites. Therefore, we aimed to re-characterize the effects of Lyl1-deficiency, especially on the adult immune system, at a steady state. With the re-evaluation of Lyl1-deficient mice at naïve state, our data suggest no gross defect in tissue homeostasis which is evident

in total cellular recruitment and organ weight *(Figure 2.1 D-E*). Upon confirmation of Lyl1 deletion in various organs, it was interesting to observe the lowest expression of Lyl1 to be in the thymus, albeit its significant role in thymic progenitor homeostasis [122] (*Figure 2.1 F*). Thus, indicating an under-appreciated role of the Lyl1 gene in other immune processes. Given its role in T-cell development and the importance of T-cells in infectious models, we initially investigated thymic responses in the absence of Lyl1 (*Figure 2.2*). Our data demonstrate clear imbalances in double-negative (DN) thymocytes between WT and Lyl1$^{-/-}$ which confirms Zohren and co-authors' data describing a blockage in the transition of DN1 to DN2 in Lyl1$^{-/-}$ thymus. Additionally, the same authors prove that Lyl1-deficiency does not impair later developmental thymopoiesis which is evident in comparable single positive (SP) CD4^{+} and CD8^{+} populations irrespective of imbalanced DN thymocytes. Thus, although the genetic composition on the Lyl1 loci differs to the published Lyl1$^{-/-}$ mouse, our data support the published conclusion that there are potential existing compensatory mechanisms for Lyl1-deficiency during thymopoiesis in later T-cell development stages [122].

To further characterize the effects of Lyl1-deficiency at a steady state, we examined Lyl1-deficient lungs, lymph nodes, spleen, liver and serum to obtain a broad spectrum of the effect of globally deleted Lyl1 on myeloid and lymphoid cell recruitment and inflammation (*Figure 2.3 – 2.6*). Overall, we concluded no significant changes in all the above-mentioned organs. Furthermore, mice deficient of Lyl1 does not experience any changes in tissue structure evident in the absence of tissue pathology (all histopathological assessed organs). We do have to note the statistical significance represented in some populations including lung myeloid percentage (*Figure 2.3 A*), lung CD4^{+} memory percentage (*Figure 2.3 C*), and occasional lymph node (*Figure 2.4*) and liver (*Figure 2.6*) percentages. Despite the differences observed in percentages, there are similar total cell numbers between WT and Lyl1$^{-/-}$ lung, lymph node and liver tissues (*Figure 2.1 E*). Hence, this does not translate to the absolute cell number of immune populations when they are back-calculated. Therefore, it is also important for the significance to be translated to cell numbers as it reflects the absolute number of positively stained cells. Thus, to consider biologically meaningful significance, we view both percentage and cell numbers collectively. Hence, our conclusion is represented as no significant difference in the recruitment of various cell populations between WT and Lyl1$^{-/-}$ lungs, lymph nodes, spleen and liver. Furthermore, we examined cytokine response in the lung, spleen and liver of WT and Lyl1$^{-/-}$ mice (*Figure 2.7 A-F*) of which we concluded no major differences between the two mouse models. However, IL-2 and IL-4 does appear to be significantly induced in Lyl1-deficient mice compared to WT at a steady state in the spleen (*Figure 2.7 C-D*). This could be the contributing compensatory mechanism, in the absence of Lyl1, to induce comparable SP T-cells in secondary lymphoid organs. IL-4 has been reported to promote T-cell survival [141]. Therefore, the increased levels of IL-4 in the absence of Lyl1 could potentially serve as a compensatory mechanism for impaired T-cell development.

More compelling is the enhanced IL-2 expression in Lyl1$^{-/-}$ spleens. IL-2 is a known T-cell growth factor [142] and has been reported to display a distinct relationship with the paralog of Lyl1, known as Stem Cell Leukemia (Scl) [143]. This paper demonstrates that Scl expression in IL-2$^{-/-}$ mice is significantly downregulated [143]. Thus, given the 82% amino acid identity between Lyl1 and Scl [110, 111], there has been a reported hypothesis of compensatory mechanisms between the two transcription factors of which could be presented here. This could be represented by increased IL-2 to induce Scl expression to compensate for the inability of T-cell development in the absence of Lyl1 (*Figure 2.2*). It should be stressed that differences in IL-2 levels were not observed in the non-lymphoid tissues, liver and lung (*Figure 2.7 A, E*). Moreover, the statistical significance represented in IL-6, IL-4 and IL-5 as well as serum IL-10 were considered rather insignificant due to expression differences to be less than two-fold and the differences were not consistently present in all tissues. Aside from IL-10, immunological responses in the serum displayed no change in antibody and cytokine release in the bloodstream when comparing the two mouse strains (*Figure 2.7 G-H*).

In summary, the Lyl1^{Mg} mouse strain is viable, fertile and displays minimal changes in immunological parameters when examining adult thymus, lung, lymph node, spleen and liver immune cell populations, histopathology and secreted cytokine/antibodies. Thus, the Lyl1 globally deleted mouse strain can be effectively used for infectious studies that are organ-specific or systemic to identify the role of Lyl1 during various infectious models.

2.6. Acknowledgements

We express gratitude to the UCT Animal Research Facility and Ms. Munadia Ansarie for the breeding, genotyping and maintenance of mice as well as the technical staff. Ms. Zarinah Sonday, Mr. Marlon Petersen and Mr. George Jacobs for the maintenance of the laboratory. Furthermore, we thank Ms. Lizette Fick and Ms. Raygaana Jacobs for their excellent histological services.

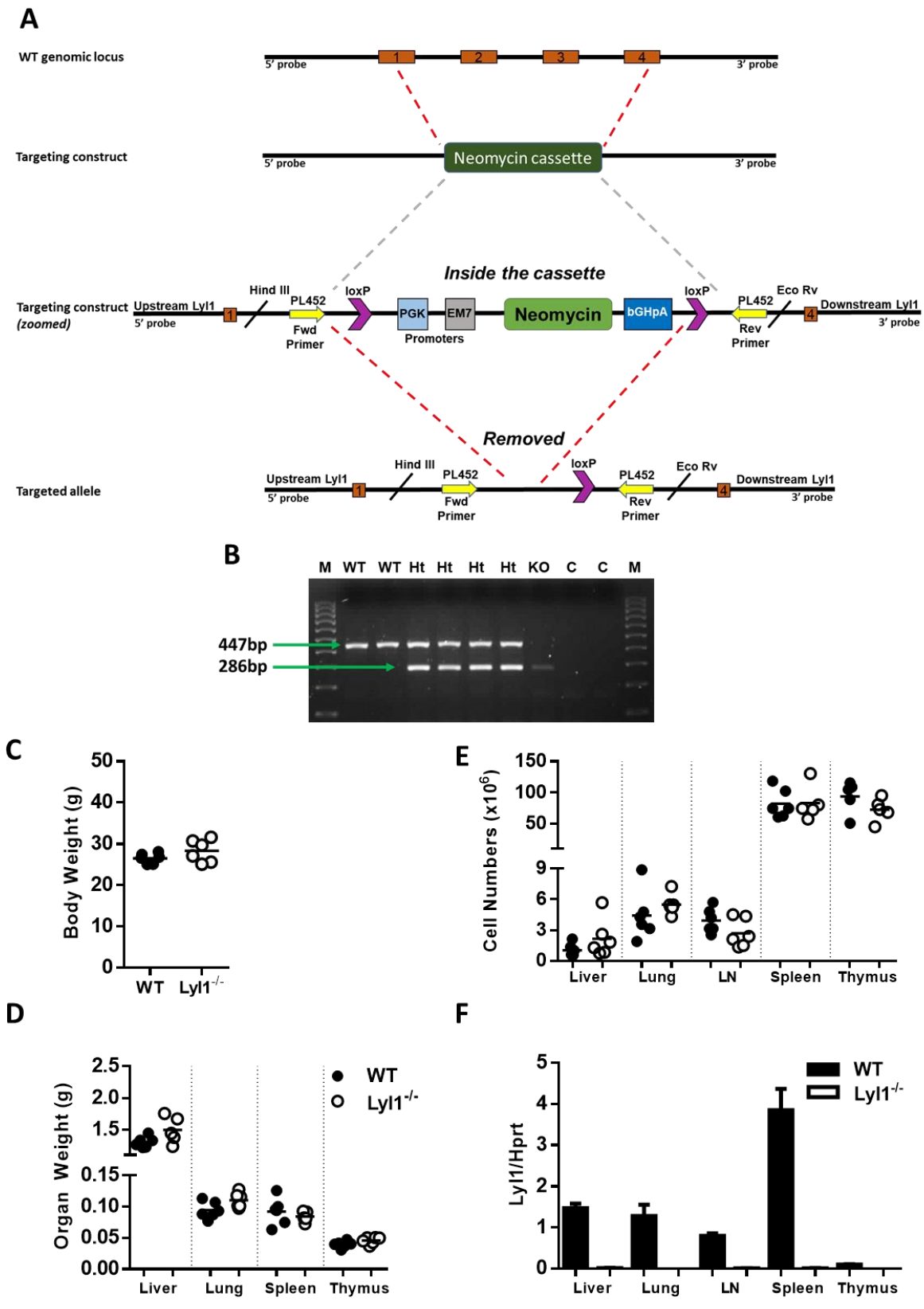

Figure 2.1. **Confirmed globally deleted Lyl1$^{-/-}$ mice experience no physiological differences compared to wild-type (WT) mice. (A)** Proposed and published targeting construct was shown to be altered by

amplifying and sequencing Lyl1. **(B)** Primer design for mice genotyping was confirmed by PCR and gel electrophoresis demonstrating the marker (M), wild type (WT), heterozygous (Ht), knockout (KO) and negative control (water; C). Low signal in KO band due to diluted positive control. **(C-F)** Naïve WT and Lyl1$^{-/-}$ mice (n = 6 mice/group) were sacrificed and compared for **(C)** body weight, **(D)** organ weight, **(E)** cell numbers as well as **(F)** mRNA expression in harvested organs. Error bar denotes Mean ±SEM and line denotes Mean. Data shown is representative of 2 independent experiments. Unpaired student t-test analysis to determine significance/insignificance.

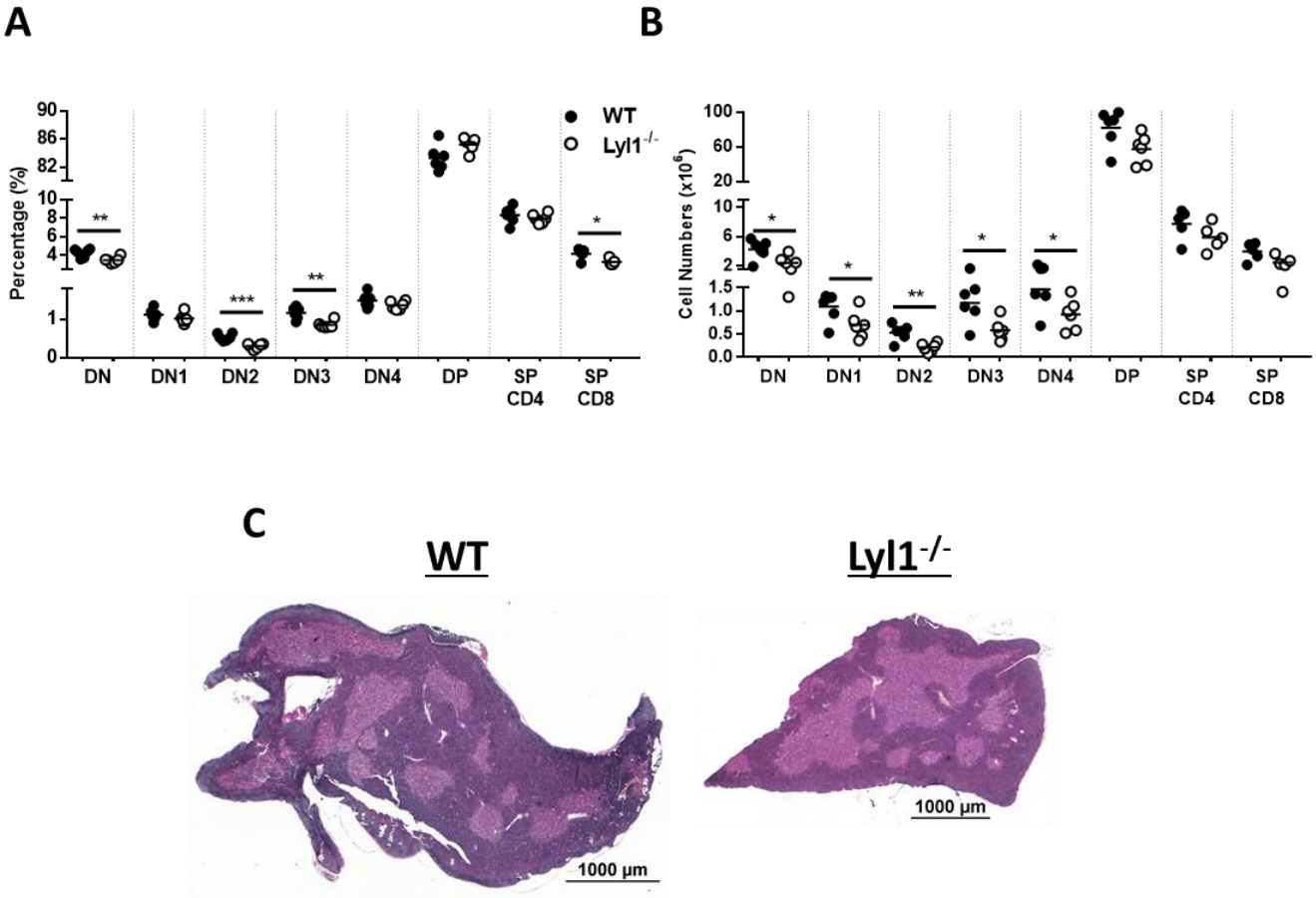

Figure 2.2. **Lyl1-deficient mice experience a perturbance in thymopoiesis, but comparable single positive T-cells.** The thymus was collected from both naïve WT and Lyl1$^{-/-}$ mice (n = 6 mice/group) and subjected to single cell suspension after which they were surface stained to analyze the **(A)** percentage and **(B)** cell numbers by flow cytometry. Surface markers of the different lymphoid cell populations are as follows (according to the gating strategy in ***Appendix A***): Double negative (DN) = CD4^{-}CD8^{-}; DN1 = CD44^{+}CD4^{-}CD8^{-}CD25^{-}; DN2 = CD44^{+}CD25^{+}CD4^{-}CD8^{-}; DN3 = CD25^{+}CD4^{-}CD8^{-}CD44^{-}; DN4 = CD4^{-}CD8^{-}CD44^{-}CD25^{-}; Double positive (DP) = CD4^{+}CD8^{+}; single positive (SP) CD4^{+} = CD4^{+}CD8^{-}; SP CD8^{+} = CD8^{+}CD4^{-}. **(C)** Representative H&E histopathology section (x20) for collected thymus. Line denotes Mean. Data shown is representative of 2 independent experiments. Unpaired student t-test analysis at *p < 0.05, **p < 0.01, ***p < 0.001 to determine significance.

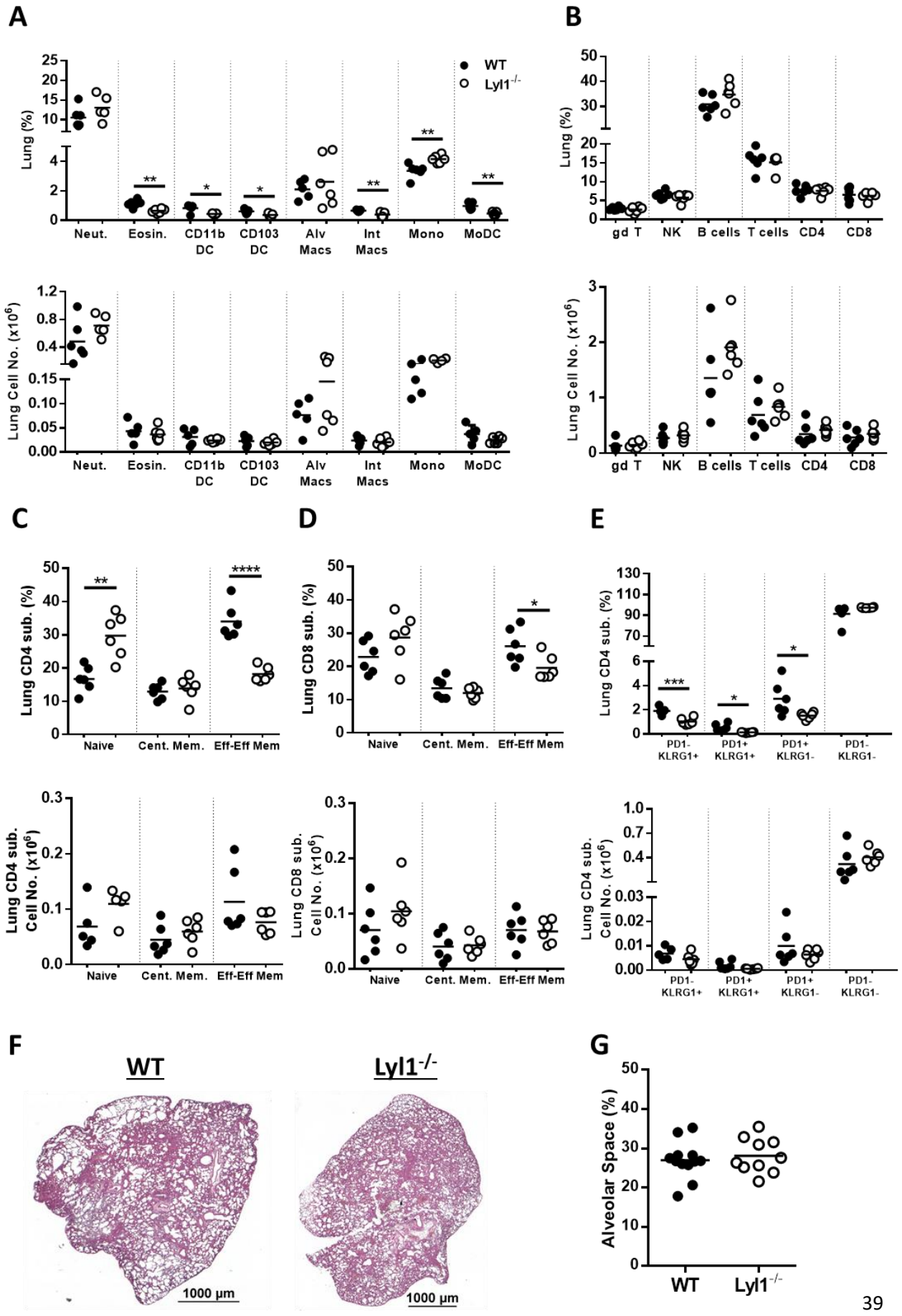
A
B
C
D
E
F
G
WT
Lyl1-/-
Lung (%)
Lung Cell No. (x10^6)
Neut.
Eosin.
CD11b DC
CD103 DC
Alv Macs
Int Macs
Mono
MoDC
gd T
NK
B cells
T cells
CD4
CD8
Lung CD4 sub. (%)
Lung CD8 sub. (%)
Lung CD4 sub. Cell No. (x10^6)
Lung CD8 sub. Cell No. (x10^6)
Naive
Cent. Mem.
Eff-Eff Mem
Lung CD4 sub. (%)
Lung CD4 sub. Cell No. (x10^6)
PD1- KLRG1+
PD1+ KLRG1+
PD1+ KLRG1-
PD1- KLRG1-
WT
Lyl1-/-
1000 µm
1000 µm
Alveolar Space (%)
WT
Lyl1-/-

Figure 2.3*. Naïve lung immune cell populations in the absence of Lyl1 is similar to WT.** Collected lungs from both WT and $Lyl1^{-/-}$ naïve mice (n = 6 mice/group) were subjected to single cell suspension for downstream flow cytometric analysis investigating the **(A)** myeloid and **(B-E)** lymphoid populations. Surface markers of the different lung myeloid cell populations are as follows (according to the gating strategy in ***Appendix C): Neutrophils (Neut.) = $Ly6G^{+}CD11b^{+}$; Eosinophils (Eosin.) = $SiglecF^{+}CD11b^{+}CD64^{-}$; $CD11b^{+}$ DC = $CD11c^{+}MHCII^{+}CD11b^{+}CD64^{-}$; $CD103^{+}$ DC = $CD11c^{+}MHCII^{+}CD103^{+}CD64^{-}$; Alveolar Macrophages (Alv. Macs) = $CD64^{+}MerTK^{+}SiglecF^{+}CD11c^{+}$; Interstitial Macrophages (Int. Macs) = $CD64^{+}MerTK^{+}SiglecF^{+}CD11b^{+}$ $CD11c^{-}$; Monocytes (Mono) = $Ly6G^{+}CD11b^{+}CD64^{-}$; Monocyte-derived DC (MoDC) = $CD64^{+}CD11b^{+}CD11c^{+}$. Surface markers of the different lung lymphoid cell populations are as follows (according to the gating strategy in ***Appendix B***): gamma delta T-cells (gd T) = $CD3^{+}gdTCR^{+}$; NK cells = $NK1.1^{+}CD3^{-}$; B-cells = $CD19^{+}CD3^{-}$; T-cells = $CD3^{+}CD19^{-}$; $CD4^{+}$ T-cells = $CD3^{+}CD4^{+}$; $CD8^{+}$ T-cells = $CD3^{+}CD8^{+}$; $CD4^{+}$ naïve = $CD3^{+}CD4^{+}CD62L^{+}CD44^{-}$; $CD4^{+}$ Central Memory = $CD3^{+}CD4^{+}CD62L^{+}CD44^{+}$; $CD4^{+}$ Effector/Effector Memory = $CD3^{+}CD4^{+}CD44^{+}CD62L^{-}$; $CD8^{+}$ naïve = $CD3^{+}CD8^{+}CD62L^{+}CD44^{-}$; $CD8^{+}$ Central Memory = $CD3^{+}CD8^{+}CD62L^{+}CD44^{+}$; $CD8^{+}$ Effector/Effector Memory = $CD3^{+}CD8^{+}CD44^{+}$ $CD62L^{-}$; $CD4^{+}$ $PD1^{-}$ $KLRG1^{+}$ T-cells = $CD3^{+}CD4^{+}KLRG1^{+}PD1^{-}$; $CD4^{+}$ $PD1^{+}KLRG1^{+}$ T-cells = $CD3^{+}CD4^{+}KLRG1^{+}PD1^{+}$; $CD4^{+}$ $PD1^{+}KLRG1^{-}$ T-cells = $CD3^{+}CD4^{+}PD1^{+}KLRG1^{-}$; $CD4^{+}$ $PD1^{-}KLRG1^{-}$ T-cells = $CD3^{+}CD4^{+}KLRG1^{-}$ $PD1^{-}$. **(F)** Representative H&E histopathology section (x20) for collected lung with **(G)** alveolar space quantification. Line denotes Mean. Data shown is representative of 2 independent experiments. Unpaired student t-test analysis at $*p < 0.05$, $**p < 0.01$, $***p < 0.001$, $****p < 0.0001$ to determine significance.

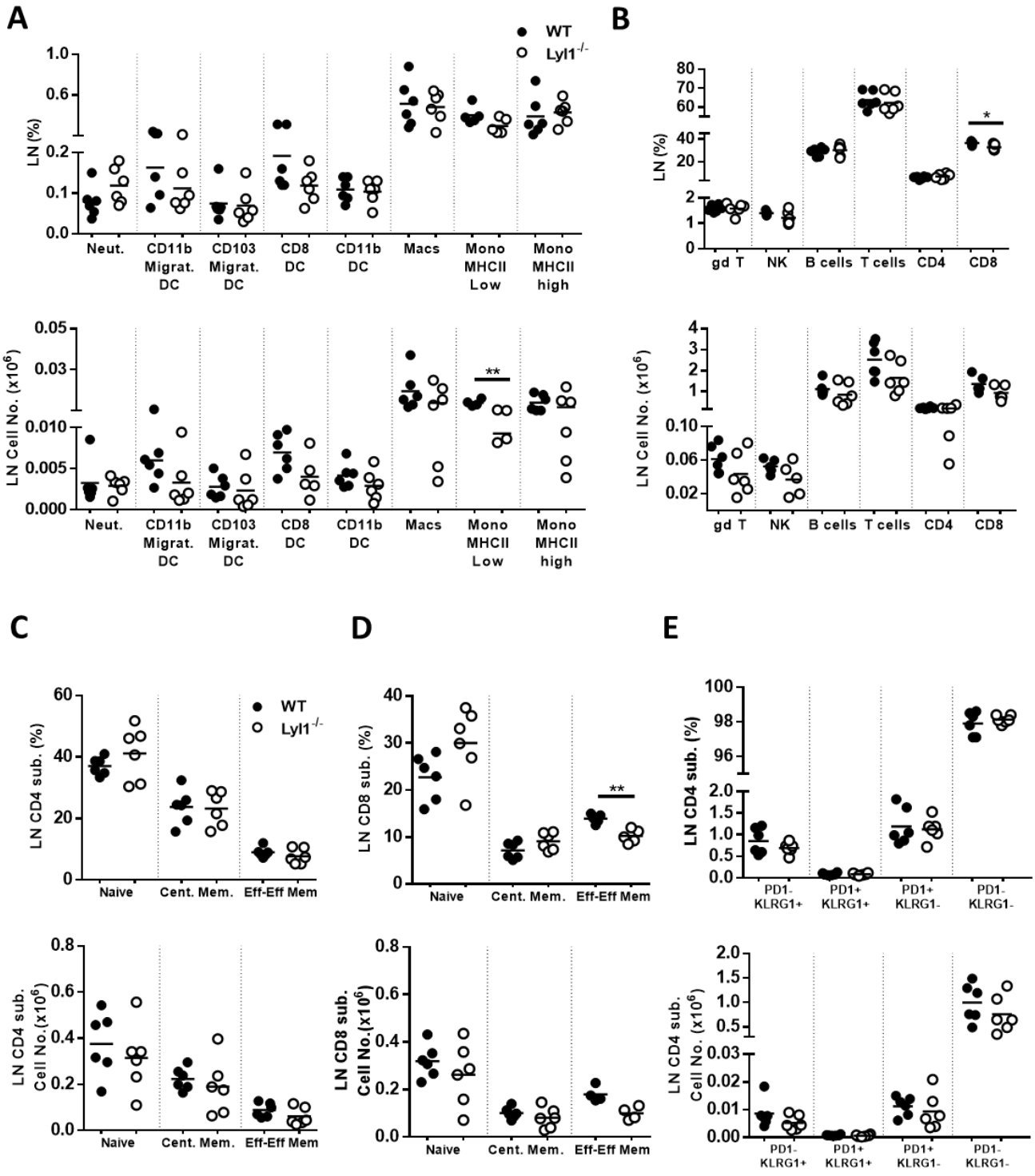

Figure 2.4*. Immune cell population in the lymph node (LN) of Lyl1$^{-/-}$ is comparable to that of WT mice.** LN was collected from both WT and Lyl1$^{-/-}$ naïve mice (*n* = 6 mice/group) and subjected to single cell suspension for downstream flow cytometric analysis investigating the **(A)** myeloid and **(B-E)** lymphoid populations. Surface markers of the different LN myeloid cell populations are as follows (according to the gating strategy in ***Appendix D): Neutrophils (Neut.) = Ly6G^{+}CD11b^{+}; CD11b^{+} Migratory DC = CD11c^{+}MHCII^{high}CD11b^{+}CD103^{-}; CD103^{+} Migratory DC = CD11c^{+}MHCII^{high}CD103^{+}CD11b^{-}; CD8^{+}

Resident DC = $CD11c^{+}MHCII^{low}CD8^{+}CD11b^{-}$; $CD11b^{+}$ Resident DC = $CD11c^{+}MHCII^{low}CD11b^{+}CD8^{-}$; Macrophages (Macs) = $F4/80^{+}CD11b^{+}$; Monocytes (Mono MHCII low) = $Ly6C^{+}MHCII^{low}$; Monocytes (Mono MHCII high) = $Ly6C^{+}MHCII^{high}$. Surface markers of the different LN lymphoid cell populations are as follows (according to the gating strategy in ***Appendix B***): gamma delta T-cells (gd T) = $CD3^{+}gdTCR^{+}$; NK cells = $NK1.1^{+}CD3^{-}$; B-cells = $CD19^{+}CD3^{-}$; T-cells = $CD3^{+}CD19^{-}$; $CD4^{+}$ T-cells = $CD3^{+}CD4^{+}$; $CD8^{+}$ T-cells = $CD3^{+}CD8^{+}$; $CD4^{+}$ naïve = $CD3^{+}CD4^{+}CD62L^{+}CD44^{-}$; $CD4^{+}$ Central Memory = $CD3^{+}CD4^{+}CD62L^{+}CD44^{+}$; $CD4^{+}$ Effector/Effector Memory = $CD3^{+}CD4^{+}CD44^{+}CD62L^{-}$; $CD8^{+}$ naïve = $CD3^{+}CD8^{+}CD62L^{+}CD44^{-}$; $CD8^{+}$ Central Memory = $CD3^{+}CD8^{+}CD62L^{+}CD44^{+}$; $CD8^{+}$ Effector/Effector Memory = $CD3^{+}CD8^{+}CD44^{+}$ $CD62L^{-}$; $CD4^{+}$ $PD1^{-}KLRG1^{+}$ T-cells = $CD3^{+}CD4^{+}KLRG1^{+}PD1^{-}$; $CD4^{+}$ $PD1^{+}KLRG1^{+}$ T-cells = $CD3^{+}CD4^{+}KLRG1^{+}PD1^{+}$; $CD4^{+}$ $PD1^{+}KLRG1^{-}$ T-cells = $CD3^{+}CD4^{+}PD1^{+}KLRG1^{-}$; $CD4^{+}$ $PD1^{-}KLRG1^{-}$ T-cells = $CD3^{+}CD4^{+}KLRG1^{-}PD1^{-}$. Line denotes Mean. Data shown is representative of 2 independent experiments. Unpaired student t-test analysis at $*p < 0.05$, $**p < 0.01$ to determine significance.

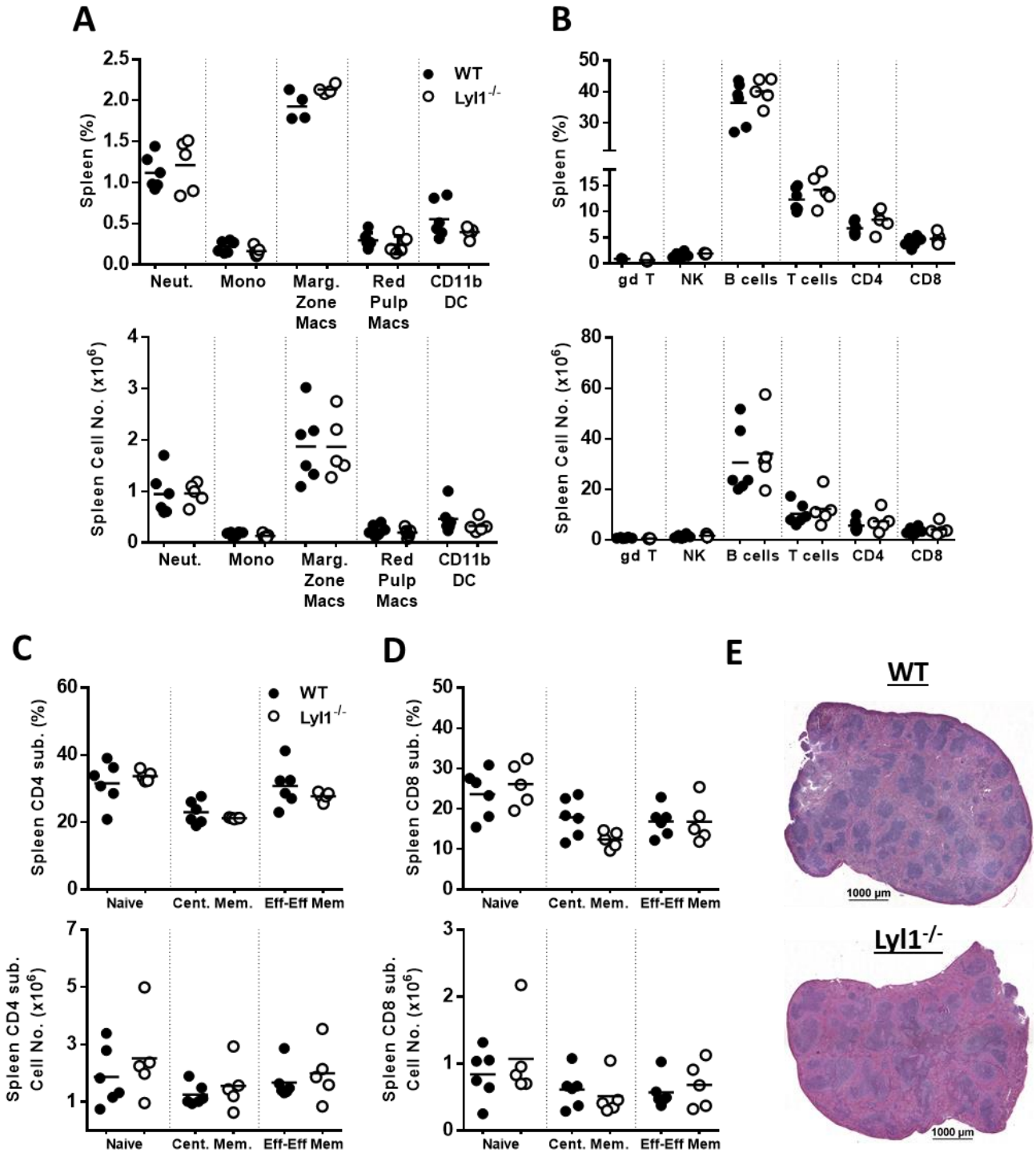

Figure 2.5*. Lyl1$^{-/-}$ spleens show no defect in immune cell population in comparison to WT spleens.** Spleens from both WT and Lyl1$^{-/-}$ naïve mice (n = 6 mice/group) were harvested and processed for single cell suspension for downstream flow cytometric analysis investigating the **(A)** myeloid and **(B-D)** lymphoid populations. Surface markers of the different spleen myeloid cell populations are as follows (according to the gating strategy in ***Appendix E): Neutrophils (Neut.) = Ly6G^{+}CD11b^{+}; Monocytes (Mono) = CD11b^{+}; Ly6C^{+}CD11c^{-}; Marginal Zone Macrophages (Marg. Zone Macs) = CD11b^{high}F4/80^{low}CD11c^{-}; Red Pulp

Macrophages (Red Pulp Macs) = F4/80^{high}CD11b^{low}CD11c^{-}; CD11b^{+} DC = CD11c^{+}MHCII^{+}CD11b^{+}. Surface markers of the different spleen lymphoid cell populations are as follows (according to the gating strategy in ***Appendix B***): gamma delta T-cells (gd T) = CD3^{+}gdTCR^{+}; NK cells = NK1.1^{+}CD3^{-}; B-cells = CD19^{+}CD3^{-}; T-cells = CD3^{+}CD19^{-}; CD4^{+} T-cells = CD3^{+}CD4^{+}; CD8^{+} T-cells = CD3^{+}CD8^{+}; CD4^{+} naïve = CD3^{+}CD4^{+}CD62L^{+}CD44^{-}; CD4^{+} Central Memory = CD3^{+}CD4^{+}CD62L^{+}CD44^{+}; CD4^{+} Effector/Effector Memory = CD3^{+}CD4^{+}CD44^{+}CD62L^{-}; CD8^{+} naïve = CD3^{+}CD8^{+}CD62L^{+}CD44^{-}; CD8^{+} Central Memory = CD3^{+}CD8^{+}CD62L^{+}CD44^{+}; CD8^{+} Effector/Effector Memory = CD3^{+}CD8^{+}CD44^{+}CD62L^{-}. **(E)** Representative H&E histopathology section (x20) for collected spleen. Line denotes Mean. Data shown is representative of 2 independent experiments. Unpaired student t-test analysis to determine significance/insignificance.

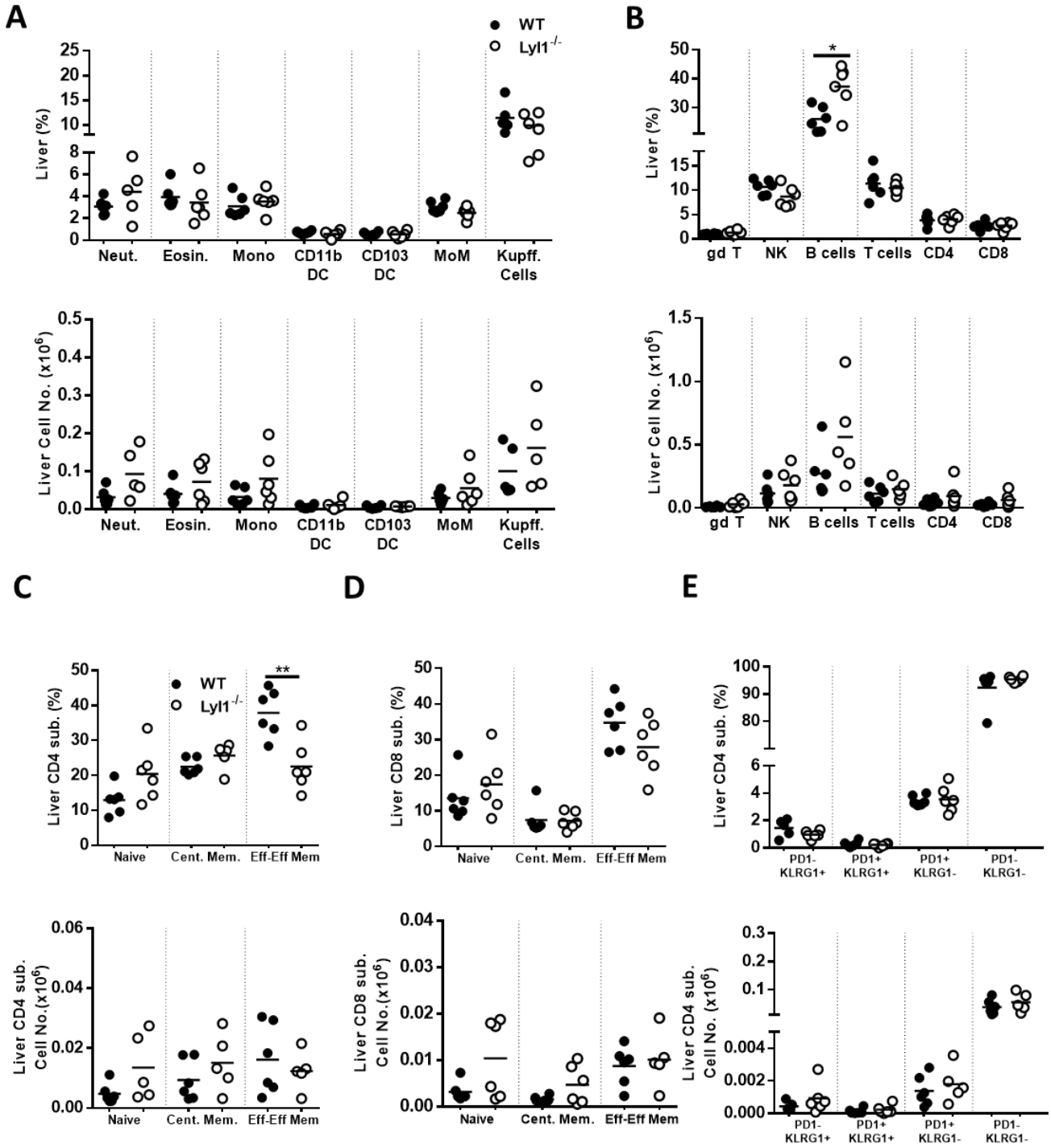
A
WT
Lyl1-/-
Liver (%)
Neut.
Eosin.
Mono
CD11b DC
CD103 DC
MoM
Kupff. Cells
Liver Cell No. (x10^6)
B
*
gd T
NK
B cells
T cells
CD4
CD8
C
**
Liver CD4 sub. (%)
Naive
Cent. Mem.
Eff-Eff Mem
Liver CD4 sub. Cell No.(x10^6)
D
Liver CD8 sub. (%)
Liver CD8 sub. Cell No.(x10^6)
E
Liver CD4 sub. (%)
PD1- KLRG1+
PD1+ KLRG1+
PD1+ KLRG1-
PD1- KLRG1-
Liver CD4 sub. Cell No. (x10^6)
F
WT
Lyl1-/-
1000 µm

Figure 2.6*. Liver immune cell population is comparable between Lyl1$^{-/-}$ and WT mice.** WT and Lyl1$^{-/-}$ naïve livers (n = 6 mice/group) were collected, digested and processed into a single cell suspension for downstream flow cytometric analysis investigating the **(A)** myeloid and **(B-E)** lymphoid populations. Surface markers of the different liver myeloid cell populations are as follows (according to the gating strategy in ***Appendix F): Neutrophils (Neut.) = Ly6G^{+}CD11b^{+}; Eosinophils (Eosin.) = CD11b^{+}SiglecF^{+}; Monocytes (Mono) = CD11b^{+}; Ly6C^{+}; CD11b^{+} DC = CD11c^{+}MHCII^{+}CD11b^{+}CD103^{-}; CD103^{+} DC = CD11c^{+}MHCII^{+}CD11b^{-}CD103^{+}; Monocyte-derived Macrophages (MoM) = CD11b^{+}F4/80^{low}CD11c^{-}Ly6C^{-}; Kupffer cells (Kupff. Cells) = F4/80^{+}CD11b^{low}. Surface markers of the different liver lymphoid cell populations are as follows (according to the gating strategy in ***Appendix B***): gamma delta T-cells (gd T) = CD3^{+}gdTCR^{+}; NK cells = NK1.1^{+}CD3^{-}; B-cells = CD19^{+}CD3^{-}; T-cells = CD3^{+}CD19^{-}; CD4^{+} T-cells = CD3^{+}CD4^{+}; CD8^{+} T-cells = CD3^{+}CD8^{+}; CD4^{+} naïve = CD3^{+}CD4^{+}CD62L^{+}CD44^{-}; CD4^{+} Central Memory = CD3^{+}CD4^{+}CD62L^{+}CD44^{+}; CD4^{+} Effector/Effector Memory = CD3^{+}CD4^{+}CD44^{+}CD62L^{-}; CD8^{+} naïve = CD3^{+}CD8^{+}CD62L^{+}CD44^{-}; CD8^{+} Central Memory = CD3^{+}CD8^{+}CD62L^{+}CD44^{+}; CD8^{+} Effector/Effector Memory = CD3^{+}CD8^{+}CD44^{+}CD62L^{-}. **(F)** Representative H&E histopathology section (x20) for collected liver. Line denotes Mean. Data shown is representative of 2 independent experiments. Unpaired student t-test analysis at *$p < 0.05$, **$p < 0.01$ to determine significance.

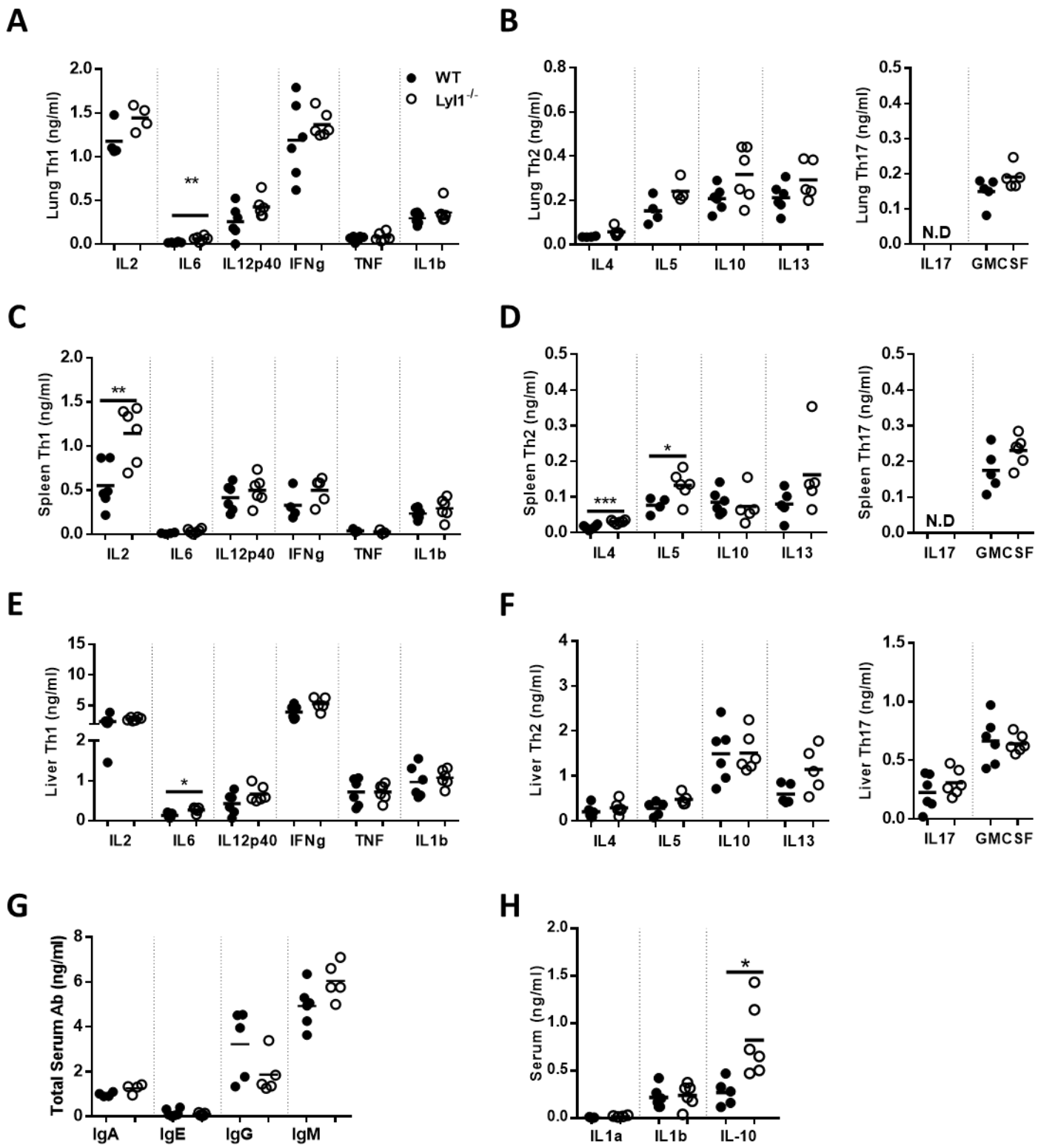

***Figure 2.7*. Lyl1-deficiency has minimal effect on the immune cytokine/antibody profile compared to WT mice at steady state.** Supernatants from organ homogenates (n = 6 mice/group) were analyzed by means of ELISA for Th1, Th2 and Th17 cytokines in the **(A, B)** lung, **(C, D)** spleen and the **(E, F)** liver. Serum **(G)** antibody and **(H)** cytokine ELISA was also performed. Only datapoints above the detection limit for each cytokine are visually represented. Line denotes Mean. Data shown is representative of 2 independent experiments. Unpaired student t-test analysis at $*p < 0.05$, $**p < 0.01$ to determine significance.

CHAPTER 3: Manuscript in preparation

Lymphoblastic leukemia 1 (Lyl1): It is more than just a cancer gene

Shelby-Sara Jones[1,2], Mumin Ozturk[1,2], Nathan Kieswetter[1,2], Sibongiseni Poswayo[1,2], Harukazu Suzuki[4], Suraj P. Parihar[1,2,3], Reto Guler[1,2,3*], Frank Brombacher[1,2,3*]

[1] International Centre for Genetic Engineering and Biotechnology, Cape Town Component, Cape Town 7925, South Africa.

[2] Department of Pathology, University of Cape Town, Institute of Infectious Diseases and Molecular Medicine (IDM), Division of Immunology and South African Medical Research Council (SAMRC) Immunology of Infectious Diseases, Faculty of Health Sciences, University of Cape Town, Cape Town 7925, South Africa.

[3]Wellcome Centre for Infectious Diseases Research in Africa (CIDRI-Africa), Institute of Infectious Disease and Molecular Medicine (IDM), Faculty of Health Sciences, University of Cape Town, Cape Town 7925, South Africa.

[4]RIKEN Center for Integrative Medical Sciences, Yokohama, Japan.

*Correspondence: Frank Brombacher, frank.brombacher@icgeb.org and Reto Guler, reto.guler@uct.ac.za

Keywords: Lyl1$^{-/-}$, LPS, *Listeria monocytogenes (Lm)*

3.1. Abstract

The discovery of Lymphoblastic leukemia 1 (Lyl1) in 1989 initiated the release of numerous publications describing the relationship between Lyl1 and various leukemia models. Since then, the effects of this transcription factor in other disease models has not been explored. Here, we demonstrate the first distinct role for Lyl1 in non-leukemia environments. Our data reveal a significant downregulation of Lyl1 in response to various bacterial infections and pattern recognition receptor-stimulations. Furthermore, we show that the downregulation is a consequence of host regulation through various MAPk and NFκB subunits. However, using Lyl1-deleted murine models, we establish the requirement for Lyl1 to reduce host susceptibility to *Listeria monocytogenes* (*Lm*). Collectively, our data demonstrate a significant role for this well-known cancer transcription factor and its potential to contribute to bacterial clearance.

3.2. Introduction

A bHLH transcription factor, Lymphoblastic leukemia 1 (Lyl1), has been extensively explored in leukemia after its discovery upon chromosomal translocation t(7;19)(q35;p13) with the T-cell receptor β gene during T-cell Acute Lymphoblastic Leukemia (T-ALL) [105]. Given its ectopic expression in T-ALL, many believed this transcription factor to exhibit great oncogenic potential [131]. However, more recently, Lukov and co-authors demonstrated a rather indirect oncogenic potential of Lyl1 by reporting how Lyl1 predisposed the host towards lymphoma after which secondary mutations occurred to eventually develop cancer [130]. Since its discovery in 1989 [106], studying the relationship between Lyl1 and cancer development resulted in many publications over the years. These publications were a result of either using human cell lines or evaluating Lyl1 expression levels in leukemia patients with the intention of using this transcription factor as a potential target for therapy. These included the use of the Jurkat T-cell line to establish the interaction of Lyl1 with NFκB p50/p105 [119], HEK 293T-cell line to identify the capability of MAP kinases to phosphorylate Lyl1 [125] as well as to show the regulation of angiopoietin-2 (ANG-2) expression by Lyl1 in human endothelial cells [121]. Furthermore, the oncogenic potential of Lyl1 was also shown in Acute Myeloid Leukemia (AML) by examining AML-diagnosed patients [132], in addition to using both AML patients and K562 cell-line to demonstrate the interaction between Lyl1 and CREB1 [120].

Given the 78% conservation of this transcription factor from human to mouse [144], numerous reports involved the use of murine models. Today, there are two available Lyl1-deleted mouse models, $Lyl1^{LacZ}$ and $Lyl1^{Mg}$, whereby either only the HLH-expressing fourth exon has been removed [110] or the entire gene has been deleted [107], respectively. These mouse models have demonstrated the importance of Lyl1 in hematopoietic function in addition to establishing distinct roles to its paralog, Scl/Tal1 (Stem Cell

Leukemia/T-cell Acute Lymphoblastic Leukemia 1). Lyl1 has been shown to be less essential than Scl/Tal1 during early hematopoiesis and is unable to compensate for the loss of Scl/Tal1 [110]. However, Lyl1 is important for maintaining adult hematopoietic stem cell function [118]. In addition to many other studies, Lyl1 has been shown to play a significant role in thymopoiesis and T-cell development [122] and thus research on this transcription factor is solely explored in blood cancers. However, although Zohren and co-authors confirm the distinct role for Lyl1 in the lymphoid specification and the maintenance of early T-lineage progenitors [122], they also demonstrate comparable single positive T-cells in the thymus and suggest a potential compensatory mechanism [122]. Therefore, although Lyl1 serves a significant role in hematopoietic function, the comparable single positive T-cells, as well as the data presented in the previous chapter, suggest a relatively functional adult immune system at a steady state independent of Lyl1.

Since Lyl1-deficient animals do not exhibit any underlying defects during homeostasis, based on assessing cytokine release and cellular recruitment in various organs (*Chapter 2, unpublished data*), we aimed to explore the effects of this transcription factor in an alternate disease model. Therefore, we initially accessed the international collaborative ZENBU database which included various CAGE (Cap Analysis of Gene Expression) transcriptomics datasets in response to diverse cell states, including *Mtb*-infected cells from the FANTOM5 consortium [103]. The rapid change in the expression pattern of Lyl1 in response to bacterial infections was especially interesting since the differential expression of Lyl1 was the complete opposite to what is usually observed during leukemia. With the aim of uncovering an alternate role for Lyl1, here, we demonstrate the first non-leukemia Lyl1-related study in addition to its unique function in intracellular bacterial infections such as *Listeria monocytogenes* (*Lm*).

Overall, our research reveals that the regulation of Lyl1 expression is not pathway-specific but rather co-regulated pre-transcriptionally by all MAPk subunits as well as NFκB. Additionally, we show that Lyl1 does not regulate the activation of these transcription factors in return. Furthermore, although Lyl1 activity contributes to disease progression in leukemia, the absence of Lyl1 during *Lm* infection results in host susceptibility. Thus, our data suggest an alternative role for Lyl1 during bacterial infections, aside from its well-known oncogenic function in leukemia.

3.3. Methods

3.3.1. Mouse strains

To study the function of Lymphoblastic leukemia 1 (Lyl1), we acquired a Lyl1 global knockout mouse whereby the entire coding region was deleted using a lox-P-flanked Neomycin cassette. This mouse ($Lyl1^{Mg/Mg}$) was generated by the Margaret A. Goodell laboratory at Baylor College of Medicine, Houston,

Texas [107] by injecting the correctly targeted clones into blastocytes of 129 AB2.2 mice and further back-crossed to the C57BL/6 strain for ten generations. Once received at the University of Cape Town (UCT), Lyl1$^{Mg/Mg}$ was back-crossed with in-house C57BL/6J strains for three generations to generate Lyl1$^{-/-}$, Lyl1$^{-/+}$ and littermate control, Lyl1$^{+/+}$ in the Animal Research Facility, UCT. Animals were housed, monitored and experimentally handled within strict accordance with the guidelines approved by the Animal Research Ethics Board of UCT. All experiments included mice aged 8 – 12 weeks and were sex-matched.

3.3.2. Ethical statement

All animals used in this study were subjected to experimental procedures that were in strict accordance with the South African National Standard (SANS 10386:2008) and the Animal Research Ethics Committee of the Faculty of Health Sciences, University of Cape Town (Protocol Permit No: 015/040 and 019/023).

3.3.3. Bone marrow-derived macrophages (BMDM) generation and infection

Bone marrow-derived macrophages (BMDM) were generated from 8-12 weeks old wild-type (WT) and Lyl1-deficient mice as previously described [145]. Briefly, bone marrow from the femurs were collected and differentiated into macrophages using sterile tissue grade Petri dishes containing Plutznik media (DMEM containing 30% L929 cell conditioned medium, 10% fetal calf serum, 5% horse serum, 1 mM sodium pyruvate, 2 mM L-glutamine, 0.1 mM β-mercaptoethanol, 100 U/ml penicillin G, and 100 µg/ml streptomycin) for 10 days. Thereafter, macrophages were harvested and seeded into 24-well plates ($7.5x10^5$ cells/well; Nunc, Denmark) for downstream infection for RNA collection and rested overnight at 37°C with 5% CO_2. Overnight adhered macrophages were either infected with BCG, H37Rv, HN878, CDC1551, N72 *Mtb* strains or heat-killed *Mtb* with MOI:1 and with MOI:10 for *Listeria monocytogenes* (*Lm*) infected macrophages. For *Mtb*-infected cells, RNA was collected at 2-, 4-, 12- and 24-hours post-infection and *Lm*-infected cells at 1-, 3-, 6- and 12-hours post-infection with 350 µl of RLT lysis buffer to determine mRNA expressions.

3.3.4. Generation and infection/stimulation of monocyte-derived macrophages (MDM)

The isolation and generation of peripheral blood mononuclear cells (PBMC) and monocyte-derived macrophages (MDM) were performed as previously described for the FANTOM6 consortium [146]. Briefly, PBMC were isolated using Histopaque®-10771 (Sigma-Aldrich) and blood was collected in VACUETTE® K_2E blood collection tubes (Greiner Bio-one). Later, PBMC were used to generate MDM

by seeding $10x10^6$ cells/well in 12-well plates (Nunc) and incubated at 37°C with 5% CO_2 and 70% RH for 2 hours to allow for monocyte adhesion. Non-adherent cells were removed, and adherent cells were incubated in X-VIVO™ 15 serum-free hematopoietic medium (supplemented with 1% penicillin-streptomycin) for 7 days with media change at day 3. This allowed for the differentiation of monocytes into MDM. Thereafter, MDM were either infected with *Mtb* HN878 (at MOI:5) for 4 hours, *Lm* (MOI:10) for 1 hour or stimulated with LPS (100 ng/ml) after which the cells were harvested for mRNA expression analysis by qPCR.

3.3.5. BMDM pathway stimulation and inhibition

Generated BMDM as described above were seeded into either 96-well plates ($1.5x10^5$ cells/well; Nunc, Denmark) for viability assays, 24-well plates ($7.5x10^5$ cells/well; Nunc, Denmark) for RNA collection/isolation of stimulated/inhibited cells, or 6-well plates ($3x10^6$ cells/well; Nunc, Denmark) for protein collection for western blot applications and rested overnight at 37°C with 5% CO_2. Thereafter, overnight seeded macrophages were subjected to titration and viability test for all the agonists including cGAMP (20, 100, 500 nM; Sigma Aldrich), CpG ODN 1668 (20, 100 and 500 nM; InvivoGen), LPS (20, 100, 500 ng/ml; Sigma-Aldrich) MDP (4, 20, 100 µg/ml; Sigma-Aldrich), Pam_3CSK_4 (20, 100, 500 ng/ml; Tocris) or TDM (4, 20 and 100 µg/ml; Sigma-Aldrich), of which 100 nM, 500 nM, 100 ng/ml, 20 µg/ml, 100 ng/ml and 20 µg/ml, respectively, was used in all downstream applications. For RNA isolation, cells were harvested with 350 µl of RLT lysis buffer at 1-, 2-, 4-, 6-, 12- and 24-hours after stimulation, whereas protein was collected with RIPA buffer (150 mM NaCl, 0.1% Triton X-100, 0.5% Sodium deoxycholate, 0.1% SDS and 50 mM Tris, pH 8), including protease (Sigma Aldrich; catalogue no: #P8340) and phosphatase (Roche; catalogue no: 04 906 837 001) inhibitor cocktails. Supernatants were collected for ELISA analysis. To capture nascent RNA, $4x10^6$ cells/well were seeded in a 6-well plate and manufacturer instructions were followed according to the Click-iT™ Nascent RNA capture kit (catalog No. C10365) to trace nascent RNA using ethylene uridine (EU). For pathway inhibition studies, BMDM were seeded for the same applications described above for 24 hours and were exposed to NFκB inhibitor (Bay11-7082; 7.5 µM; Sigma-Aldrich), p38 MAPk inhibitor (SB 203580; 5 µM; Tocris), JNK MAPk inhibitor (SP600125; 10 µM; Sigma-Aldrich), ERK1/2 MAPk inhibitor (FR180204; 10 µM; Sigma-Aldrich) or MSK1/2 inhibitor (SB 747651A dihydrochloride; 10 µM ; Tocris) for one hour. Thereafter, they were stimulated with 100 ng/ml LPS to induce the downregulation of Lyl1. RNA lysates were collected as described above.

3.3.6. Quantitative real-time polymerase chain reaction (qRT-PCR)

Samples were collected with 350 µl of RLT lysis buffer and later RNA was extracted using the RNeasy Mini Kit (Qiagen catalogue no. 74106) and normalized to 300 ng. Thereafter, RNA was reverse transcribed by the Transcriptor First Strand complementary DNA (cDNA) Synthesis Kit (Roche catalogue no. 04 379 012 001) using both anchored oligo dT primers and random hexamer primers according to the manufacturer instructions to yield cDNA. Later, various transcripts were amplified by qPCR using LightCycler® 480 SYBR Green I Master Mix (with primer pairs listed in *Appendix G*) in the LightCycler® 480 Instrument II (Roche). Primer pairs, listed in *Appendix G* with their respective PCR conditions, were purchased from Integrated DNA Technologies (IDT; Coralville, Iowa, United States). The PCR reaction was first pre-incubated for 5 minutes at 95°C followed by amplification (denaturing (D) for 10 seconds; annealing (A) for 15 seconds; extension (E) for 15 seconds and the final acquisition step (S) for 1 second) for 45 cycles. All targeted expressions were normalized to Hprt expression levels.

3.3.7. Western blot

Sodium dodecyl sulfate polyacrylamide gel electrophoresis (SDS-PAGE) and Western Blot analysis was executed as previously described in [92]. Briefly, total cell lysates were assessed for protein content using the BCA Protein Assay Kit (ThermoFisher Scientific Pierce™; catalog no. 23225) as per the manufacturer instructions. A total of 20 – 40 µg of protein was combined with 1X loading dye (2% SDS, 5% 2-mercaptoethanol, 10% glycerol, 0.002% bromophenol blue, 0.62 M Tris-HCl, pH 6.8), boiled at 100°C for 5 minutes and loaded onto a 12% separating SDS – PAGE gel (Mini-PROTEAN® system; Bio-Rad). Subsequently, the protein was transferred onto a nitrocellulose membrane (Amersham Biosciences) using the Mini Trans-Blot® Cell system (Bio-Rad), followed by membrane blocking with 5% w/v BSA, 1X TBS (20 mM Tris with 150 mM NaCl) and 0.1% Tween20 (blocking buffer) for 2 hours on a shaker at room temperature. Later, the membrane was probed with either p38 MAPK (D13E1) XP® (Cell Signaling Technology; Catalog no.: CST8690S), Phospho-p38 MAPK (Thr180/Tyr182) (D3F9) XP® (Cell Signaling Technology; Catalog no.: CST4511S), SAPK/JNK Antibody (Cell Signaling Technology; Catalog no.: CST9252S), Phospho-SAPK/JNK (Thr183/Tyr185) (G9) (Cell Signaling Technology; Catalog no.: CST9255S), NFκB p65 (D14E12) XP® (Cell Signaling Technology; Catalog no.: CST8242S), Phospho-NFκB p65 (Ser536) (93H1) XP® (Cell Signaling Technology; Catalog no.: CST3033S), NFκB p50/p105 (Clone 1N19, ZooMAb®) (Sigma Aldrich; Catalog no.: ZRB2082) or GAPDH (Sant Cruz Biotechnology; Catalog no.: sc-47724) primary antibodies using the manufacturer recommended dilutions in 5% BSA blocking buffer at 4°C overnight. Thereafter, the membrane was incubated in respective HRP-conjugated secondary antibody (diluted 1:10 000 in blocking buffer), goat anti-rabbit IgG H&L (HRP) pre-absorbed

or goat anti-mouse IgG H&L (HRP) pre-absorbed (both from Abcam; catalog no: ab7090 or ab97040, respectively) at room temperature for 1 hour. Immunoblots were developed using the KPL LumiGLO® Reserve Chemiluminescent Substrate Kit (SeraCare Life Sciences; catalog no: 5430-0042(54-61-02)) on the iBright FL1000 Imaging System (ThermoFisher Scientific). Densitometry analysis was performed using the built-in iBright FL1000 Imaging System after which each band was normalized to Gapdh. Data represented as normalized values and the fold change is representative of $Lyl1^{-/-}$ normalized experimental value to the normalized WT control value.

3.3.8. *Listeria monocytogenes* (*Lm*) infection in mice

As previously described [147], mice were intraperitoneally infected with $1.9x10^6$ CFU/mouse for mortality and $2x10^5$ CFU/mouse for time-course experiments. Bacterial loads, physiological parameters and flow cytometric analysis was performed on indicated organs as directed [138, 147].

3.3.9. Measurement of nitric oxide and cytokines/chemokine in culture supernatants and homogenates

Nitric oxide in infected cell culture supernatants was measured using the Griess reagent assay. Briefly, cell supernatants were incubated with 1% sulfanilamide in 2.5% phosphoric acid for 10 minutes at room temperature in the dark, followed by 0.1% naphthyl-ethylene-diamine in 2.5% phosphoric acid for another 10 minutes. BMDM cell culture, organ homogenates, as well as serum cytokines and chemokines were examined using the standard sandwich ELISA protocol (coating and detection antibodies obtained from BD Biosciences, BioLegend and R&D Scientific) using either TMB Microwell Peroxidase Substrate (KPL international) for streptavidin-HRP conjugates or 1 mg/ml p-nitrophenyl phosphate disodium salt hexahydrate (Sigma; catalog no: N2765) for streptavidin-AP conjugates. Optical density was measured using the VersaMax™ microplate spectrophotometer (Molecular Devices, Sunnyvale, California).

3.3.10. Flow cytometry

Collected *Lm*-infected organs were subjected to collagenase digestion in preparation for single-cell suspension as described previously [138]. Cells were surface stained for the identification of the lymphoid and myeloid populations in the spleen and liver. The following antibodies, purchased from BD Biosciences, BioLegend and eBioScience, were used to surface phenotype various cell populations: PD-1 (FITC); CD4

(BV421/V450); CD44 (PE); NK1.1 (APC-Cy7); CD3 (A700); CXCR5 (PE-Cy7); CD62L (APC); CD19 (PerCP-Cy5.5); CD8 (V500); KLRG1 (BV786); CD64 (PE-Cy7); Ly6C (PerCP-Cy5.5); CD11b (V450); MHC II (A700); CD11c (APC); SiglecF (APC-Cy7); Ly6G (FITC); MerTK (BV786); CD103 (PE); F4/80 (PE-Cy7); CD169 (APC-eFluor780). Cells were stained and acquired according to [138] using the BD LSR Fortessa (BD Biosciences Immunocytochemistry Systems), and the data analysis was performed with FlowJo v10.6.1 Software (Treestar, US). All panels are outlined in the appendix: *B*-liver and spleen lymphoid; *E*-spleen myeloid and *F*-liver myeloid.

3.3.11. Statistical analyses

All data represented was analyzed using GraphPad Prism 6.0 with the use of the unpaired student *t-test* (two-tailed with equal variance). A $*p$ value of less than 0.05 was considered significant, depicting $**p < 0.01$, $***p < 0.001$ and $****p < 0.0001$.

3.4. Results

3.4.1. Lyl1 expression is significantly downregulated in response to bacterial infections and immune stimulants

The data extracted from the latest FANTOM5 project demonstrating CAGE sequencing of diverse cellular environments, proved a significant reduction in Lyl1 expression in both M1 (IFNγ) and M2 (IL-13/IL-4) macrophage subsets after *Mtb* HN878 infection *in vitro* (*Figure 3.1 A*) [101, 102]. This was later confirmed in human monocyte-derived macrophages (MDM) in the current ongoing FANTOM6 compilation (publicly available on the Zenbu-FANTOM6 database: https://fantom.gsc.riken.jp/zenbu/reports/#FANTOM6) (*Figure 3.1 B*). The above-mentioned data was all extracted from databases, however, the validation experiments were performed by our laboratory. Given the significant downregulation of this transcription factor, we originally hypothesized an immune evasion mechanism. Therefore, we examined whether the downregulation was virulence-dependent. *Figure 3.1 C* demonstrates similar Lyl1 downregulation patterns between various *Mtb* strains during *in vitro* infection. Additionally, bone marrow-derived macrophages (BMDM) infected with heat-killed *Mtb* also downregulated Lyl1 expression (*Figure 3.1 D*). Thus, these two experiments suggest that the downregulation of Lyl1 is virulence-independent, and therefore, potentially not a consequence of *Mtb* evasion. Further FANTOM6 data revealed the downregulation of Lyl1 after LPS stimulation in human macrophages *in vitro* (*Figure 3.1 E*). Moreover, Lyl1 expression during *Listeria monocytogenes* (*Lm*)

infection in BMDM (*Figure 3.1 F left panel*) and MDM (*Figure 3.1 F right panel*) demonstrated a trended and significant reduction in Lyl1, respectively. To validate this data in an *in vivo* model, mice were either subjected to septic shock by LPS, or *Lm*, after which, in both settings a depletion of Lyl1 in the liver, spleen and peritoneal fluid of septic shock mice (*Figure 3.1 G*) and in the spleen of *Lm*-infected mice (*Figure 3.1 H*) was observed. Collectively, this data suggests that the downregulation of Lyl1 is not a consequence of an immune evasion mechanism caused by *Mtb*, but rather a host regulatory mechanism to potentially control infections and/or stress. This is evident in the reduction of Lyl1 during *Mtb* and *Lm* infection as well as septic shock both *in vitro* and *in vivo* murine models as well as *in vitro* human macrophages.

3.4.2. MAPk and NFκB signaling pathways are key regulators of Lyl1 expression

Given the downregulation of Lyl1 in all the above-tested bacterial infections and immune stimulants, we suspect host regulation of Lyl1 expression in response to danger signals. Therefore, we aimed to investigate which signaling cascade regulates Lyl1 expression in response to various immune stimulants by initially identifying a specific pathway targeted to Lyl1 downregulation (*Figure 3.2 A*). Using a titration method, Lyl1 expression in BMDM across various activated pathways was examined. This included the STING (by cGAMP), TLR9 (by CpG ODN), TLR4 (by LPS), NOD2 (by MDP), TLR2 (by Pam_3Csk_4) and the Mincle pathway (by TDM) of which Lyl1 downregulation was observed in all pathways (*Figure 3.2 A*). Cell toxicity was assessed (*Figure S3.1 A*), and pathway activation was confirmed by means of mRNA (*Figure S3.1 B-D*) and marker protein expression (*Figure S3.2 A-D*). Prior to exploring a common denominator between these pathways, we investigated whether the downregulation of this transcription factor is pre- or post-transcriptional. With the use of a kit designed to examine nascent RNA, we confirmed pre-transcriptional downregulation of Lyl1 given the significant decline in nascent Lyl1 expression (*Figure 3.2 B left panel*) in confirmed (IL-6 induced) LPS-stimulated BMDM (*Figure 3.2 B right panel*). Finally, we examined Lyl1 activity in primary murine macrophages in response to various MAPk and NFκB family member inhibitors *in vitro*. With the use of p38 MAPk, ERK1/2 MAPk, JNK MAPk and NFκB inhibitors, pathway inhibition was confirmed by proving the downregulation of downstream genes (*Figure S3.3*), after which a co-regulatory function of Lyl1 expression between all these transcription factors was identified (*Figure 3.2 C*). Exposing these macrophages to various inhibitor cocktails, we observe p38 MAPk to potentially exhibit the largest contributing regulator given the expression of Lyl1 appearing to be the highest when inhibiting p38 MAPk. However, all these kinases, as well as NFκB, control Lyl1 expression as once all are inhibited simultaneously in LPS-stimulated macrophages, Lyl1 expression is comparable to that of unstimulated (*Figure 3.2 C*). To confirm this, we investigated downstream of these kinases and inhibited MSK1/2 in the presence of LPS stimulation (*Figure 3.2 D-E*). Inhibiting MSK1/2 proved a partial recovery

of Lyl1 expression in LPS-stimulated macrophages. Thus, altogether, this data show that Lyl1 is indeed regulated by various host signaling pathways. However, this regulation is not pathway-specific but rather controlled by combinatorial MAP kinases and NFκB activity.

3.4.3. Lyl1-deficient macrophages are less inflammatory in response to LPS *in vitro*

After identifying the regulators of Lyl1 expression, the effects of LPS on Lyl1-deficient macrophages were investigated. Initially, confirmation of the genetic deletion of Lyl1 was performed (*Figure 3.3 A*) followed by cell toxicity of various pattern recognition receptor (PRR) agonists in Lyl1$^{-/-}$ macrophages (*Figure 3.3 B*). Lyl1-knockout macrophages experienced no toxicity in response to the agonists. Later, by means of mRNA expression and cytokine release, the inflammatory response of Lyl1-deficient macrophages in response to LPS was explored (*Figure 3.3 C-F*). Interestingly, although we demonstrate host regulation of Lyl1 in response to LPS, we also show a less inflammatory response in Lyl1$^{-/-}$ macrophages. This is evident in reduced Nos2 and nitrite (*Figure 3.3 C*) as well as both mRNA expression and cytokine releasing IL-6 (*Figure 3.3 D*), IL-1β (*Figure 3.3 E*) and TNFα (*Figure 3.3 F*). Therefore, as the host regulates Lyl1 expression in LPS-stimulated macrophages, Lyl1 also regulate various macrophage responses to LPS, which is evident in differential cytokine responses in the absence of Lyl1.

3.4.4. MAPk and NFκB p50-p65 signaling pathways are not regulated by Lyl1

Given the significant changes in immunological responses in Lyl1-deficient macrophages when exposed to LPS stimulation, we investigated potential components of the immune system that Lyl1 could regulate. Since Lyl1 expression is regulated by MAPk and NFκB transcription factors in addition to published data proving the interaction between Lyl1 and MAPk [125] as well as Lyl1 and NFκB [119], we hypothesized the regulation of these transcription factors by Lyl1. Since p38 MAPk significantly contributes to Lyl1 regulation (*Figure 3.2 C*), we initially explored this transcription factor (*Figure 3.4 A-B*), in addition to JNK/SAPK MAPk (*Figure 3.4 A, C*) and NFκB2 (p65) (*Figure 3.4 A, D*) to which we discovered no significant difference in expression and phosphorylation patterns between LPS-stimulated WT and Lyl1-deficient macrophages. To confirm the complete ineffective activity of Lyl1 on NFκB, protein expression levels of another subunit of the NFκB family, NFκB1 (p50/p105), was analyzed of which we conclude no regulatory effect of Lyl1 on NFκB1 (*Figure 3.4 A, E*). Thus, collectively, these western blots demonstrate the consistent expression and activation of these transcription factors in macrophages to be independent of Lyl1.

3.4.5. Lyl1-deficient mice are more susceptible to *Lm* infection *in vivo*

Upon macrophage LPS-stimulation, activating the TLR4 pathway, Lyl1-deficient macrophages appeared to be less bactericidal by releasing less pro-inflammatory cytokines (*Figure 3.3 C-F*). To examine the effect of a bacterial infection in a Lyl1-deficient host, WT and $Lyl1^{-/-}$ mice were initially subjected to a lethal dose of *Lm* for mortality assessment. Mice deficient in Lyl1 succumbed to the infection significantly earlier compared to WT and heterozygous $Lyl1^{+/-}$ mice (*Figure 3.5 A*). Thereafter, to investigate the immunological effects of *Lm* on Lyl1-deficient hosts, WT and $Lyl1^{-/-}$ mice were exposed to *Lm* for 3 days (3dpi) at $4x10^4$ CFU/mouse after which the spleen and the liver were harvested. Three-day *Lm* exposure did not reveal many physical nor cellular differences between WT and $Lyl1^{-/-}$ (*Figure 3.5 B-F*), aside from slightly smaller livers in Lyl1-knockout mice (*Figure 3.5 D*) and increased cell numbers in Lyl1-deficient spleens (*Figure 3.5 E*). Furthermore, although a less inflammatory response during LPS-stimulated macrophages *in vitro* (*Figure 3.3 C-F*) was observed, Lyl1-deficient spleens were rather more inflammatory compared to WT (*Figure 3.5 H*). These included a significant induction of IL12p40, IFNβ, TGFβ and IL-17. Interestingly, Lyl1-deficient livers either appear to be unaffected or experience a reduction in Th17 cytokines (*Figure 3.5 G*). Additionally, the serum cytokine profile displayed no significant differences between WT and $Lyl1^{-/-}$ mice during listeriosis (*Figure 3.5 I*).

Moreover, with the use of flow cytometry, the myeloid and lymphoid population recruitment patterns between WT and Lyl1-knockout mice in both the liver and the spleen in response to *Lm* 3 days post-infection were explored (*Figure 3.6*). The myeloid population of Lyl1-deficient livers proved to be unaffected compared to WT mice (*Figure 3.6 A*). However, the spleens of $Lyl1^{-/-}$ mice exhibit a significant increase in conventional dendritic cells (DC) reflected in both percentage and cell numbers (*Figure 3.6 B*). In order to validate biological significance, we consider both the percentage and its translation to absolute cell numbers. Thus, although a slight increase in neutrophil and monocyte cell numbers in the spleen was observed, this did not translate to percentage. Interestingly, $Lyl1^{-/-}$ mice exhibited reduced NK cells in the liver (*Figure 3.6 C*). This was also evident in splenocyte percentages, however, the effect was not translated to cell numbers (*Figure 3.6 E*). Finally, the effect of a 3-day exposure to *Lm* on T-cell memory was examined of which not many differences between WT and Lyl1-knockout mice were revealed, aside from increased naïve $CD4^+$ T-cells in Lyl1-deficient spleens (*Figure 3.6 F*). Altogether, our data demonstrate a clear susceptible phenotype of Lyl1-deficient murine models compared to WT in response to *Lm*. This susceptibility is evident in Lyl1-deficient mice surrendering to listeriosis significantly earlier, accompanied by an increased cytokine response and conventional dendritic cells in the spleens of $Lyl1^{-/-}$ mice along with a reduction of NK cells and Th17 cytokines in Lyl1-deficient livers when compared to WT.

3.5. Discussion and Conclusion

The identification of Lyl1 as a gene of interest during *Mycobacterium tuberculosis (Mtb)* infection was based on searching transcriptomics datasets for immune evasion genes specifically affected by *Mtb*. Analyzing the CAGE transcriptomics data from the FANTOM5 project, it was evident that Lyl1 was significantly downregulated within 4 hours of *Mtb* exposure. The gene expression of this transcription factor was almost to a point of complete depletion in both M1 (IFNγ) and M2 (IL-13/IL-4) macrophage subsets *in vitro* (*Figure 3.1 A*) [104]. Thus, Lyl1 presented itself as a potential *Mtb* immune evasion gene. However, with the intention of confirming this effect, not only did we demonstrate this downregulation as virulence-independent (*Figure 3.1 C-D*), but we also identified the same response in LPS-stimulated monocytes (*in vitro*) (*Figure 3.1 E*), septic shock (*in vivo*) (*Figure 3.1 G*) as well as *Listeria monocytogenes* (*Lm*)-infected BMDM, MDM (*in vitro*) (*Figure 3.1 F*) and murine *in vivo* kinetics (*Figure 3.1 H*). Although different from what we originally hypothesized, we were still intrigued by the radical change in expression patterns of this transcription factor in response to bacterial infections and septic shock.

As previously mentioned, and evident in the name, this transcription factor has been extensively studied in various leukemia models and clinical samples, demonstrating a significant contribution to cancer development. The overexpression of this transcription factor has been shown to have either direct or indirect oncogenic potential [130-132]. Cancer patients exhibit significantly increased levels of Lyl1 [131, 148]. Thus, to observe the complete opposite, and largely significant, expression pattern in response to bacterial infections was rather interesting. Since the regulation of this transcription factor was independent of bacterial species as well as the induction of septic shock (*Figure 3.1*), we instead investigated a host regulatory effect of Lyl1 in response to these danger signals. By process of elimination and confirmation of agonist toxicity and pathway activation (*Figure S3.1, S3.2*), we discovered that the regulation of Lyl1 was not pathway-specific, neither was it regulated by one component of the pattern recognition signals (*Figure 3.2*). Rather, in addition to a previous report that demonstrates the phosphorylation of Lyl1 by MAPk [125], we show the regulation of Lyl1 in response to LPS to be via MAPk (p38, ERK1/2 and JNK) and NFκB pathways (*Figure 3.2 C*).

After confirmed Lyl1-deletion in isolated BMDM (*Figure 3.3 A*), we investigated the importance of this transcription factor in response to an LPS-induced stressful environment *in vitro*. Evidently, macrophages deficient in the Lyl1 transcription factor prove to be less inflammatory (*Figure 3.3 C-F*). Since cancer studies have presented a negative connotation to the presence of this potentially oncogenic transcription factor with respect to disease progression, in addition to host regulation of this transcription factor and reduced cytokine response in our experimental setup, we hypothesized that a Lyl1 globally-deleted mouse would be more protected against bacterial infections. However, after subjecting $Lyl1^{-/-}$ mice to *Lm*, they

displayed a more susceptible phenotype by succumbing earlier to a lethal dose of *Lm* (*Figure 3.5 A*). Furthermore, Lyl1-deficient spleens exhibited an increased inflammatory response (*Figure 3.5 H*), as well as increased recruitment of conventional dendritic cells (*Figure 3.6 B*), whereas the liver experienced a reduction in Th17 response (*Figure 3.5 G*) in addition to less NK cell recruitment (*Figure 3.6 C*) compared to WT mice. Pron and co-authors describe dendritic cells as the early targets for *Lm* infection and tend to facilitate bacterial spread [149] after which Neuenhahn and co-authors show that $CD8^+$ dendritic cells are required for effective entry of the *Lm* bacterium into the spleen [150]. Here, we show significantly increased $CD8^+$ and $CD11b^+$ dendritic cells in Lyl1-deficient spleens (*Figure 3.6 B*) which could potentially contribute to increased susceptibility by enhancing bacterial spread through the provision of increased *Lm* harboring cells. Furthermore, previous studies have shown that the activation of NK cells could promote *Lm* virulence, thus rendering the host more susceptible to listeriosis infection [151, 152]. However, at the same time NK cells are also known to serve an important role in innate immune responses to various pathogens, including bacterial microbes [153]. Our data demonstrate a significant decrease in NK cells in Lyl1-deficient livers compared to WT in response to *Lm* (*Figure 3.6 C*). This could also explain the reduced GM-CSF levels in the liver (*Figure 3.5 G*) given that NK cells commonly produce GM-CSF as a means to contribute to innate immunity [154]. Furthermore, studies have shown that IL-17 reduces *Lm* bacterial burden in the liver [155]. Here, we show a significant reduction in IL-17 in Lyl1-deficient livers (*Figure 3.5 G*) which could also contribute to $Lyl1^{-/-}$ host susceptibility. However, although the previously mentioned publication does not demonstrate the relationship between spleen IL-17 and listeriosis, one must note the increased IL-17 in Lyl1-deficient spleens (*Figure 3.5 H*). Supporting the well-known dendritic cell and IL-12 correlation [149], with increasing splenic conventional dendritic cells, we also observe increased splenic IL-12p40 (*Figure 3.5 H*). Furthermore, Lyl1-deficient spleens also experience increased IFNβ and TGFβ which are known innate responses to *Lm* infection to assist in bacterial clearance [156, 157].

Aside from all these immunological markers of susceptibility in Lyl1-knockout mice, the fact that we do not observe a clear increase in bacterial burden (*Figure 3.5 F*) could be that we addressed an early timepoint (3 days post-infection). It is possible that later time points would render a stronger immunological marker and bacterial burden phenotype. However, when investigating later time points, Ly1l-deficient mice began succumbing to the infection prior to the experimental endpoint (data not shown but evident in mortality). With a lower infectious dose, it might be possible to investigate a later timepoint. Furthermore, the bacterial burden observed in WT and $Lyl1^{-/-}$ macrophages in response to an *in vitro Lm* infection is similar (*Figure 3.5 J*). It is possible that because *Lm* is a fast-growing organism that could overexert immunological responses in a rapid manner, unlike the slow-growing *Mtb*, we thus could not detect differences in bacterial burden *in vivo* (*Figure 3.5 F*) and *in vitro* (*Figure 3.5 J*). Nonetheless, with these

immunological markers in combination with the mortality, it is evident that in the absence of Lyl1, rather than inducing a protective phenotype, the host becomes significantly susceptible to *Lm* infection.

Although the activity of Lyl1 during leukemia tends to promote disease progression, it appears that Lyl1 activity is instead required to limit host susceptibility to bacterial infections. Therefore, although we identified the pathways responsible for regulating Lyl1 expression, we ideally sought to identify the pathways that Lyl1 regulate, given the absence of it renders host susceptibility. The relationship between Lyl1 with various components of the immune system has been vaguely studied, including the regulation of Lyl1 by Ets and GATA factors [111], as well as how Lyl1 regulates CREB1 [120], ANG-2 [121] and spleen erythropoiesis [126]. Furthermore, Lyl1-knockout mice demonstrate increased lung vascular permeability [124] as well as maintain primitive erythropoiesis [135]. However, there is no clear pathway for Lyl1 activity at steady state nor during cancer, much less during bacterial infections. Thus, with this intention, we investigated whether Lyl1 regulates any of the MAPk and NFκB family components by examining protein expression and phosphorylation in Lyl1-deficient macrophages (*Figure 3.4*). Although these kinases and NFκB regulate Lyl1 expression, Lyl1 does not seem to regulate these transcription factors in return. According to Ferrier and co-authors, there is a distinct relationship between Lyl1 and NFκB1 (p50/p105) [119]. However, to our surprise, we did not see any differences in the expression levels of NFκB1 between LPS-stimulated WT and Lyl1-deficient macrophages (*Figure 3.4 A, E*). We speculate that the use of a human Jurkat T-cell line could induce a different response to primary murine cells (BMDM), although murine Lyl1 protein is highly conserved to human Lyl1 protein (78%) [144]. Alternatively, given that although we see a similar expression pattern of Lyl1 in response to LPS compared to bacterial infections, we have to consider the less inflammatory response observed in LPS-induced Lyl1-deficient macrophages which is the opposite effect of what we observe during *Lm in vivo*. This could potentially be a result of LPS inducing TLR4 specifically, whereas *Lm* stimulates various pathways *in vivo* [158], especially TLR2 [159]. Therefore, rendering a different response in the absence of Lyl1 compared to *in vitro* LPS-stimulated macrophages. It should also be noted that Lyl1 can exhibit various functions in different cell types that can mask pro-inflammatory roles of Lyl1 in macrophages.

In conclusion, we have shown that a well-known cancer gene has the potential to contribute to bacterial clearance, whether it be directly or indirectly. However, when exposed to danger signals, the host selectively downregulates this transcription factor, yet in turn rendering itself more susceptible to infection. This is evident in the imbalanced immune responses to *in vivo Lm* infection when compared to WT mice. Furthermore, we demonstrate that Lyl1 is indeed regulated by both MAPk and NFκB pathways and we eliminate the potential regulation of these transcription factors by Lyl1 in response to LPS *in vitro*. However, further research needs to be performed to understand the mechanism behind how and why the

host selectively downregulates Lyl1 in response to these bacterial infections. For many years, Lyl1 was not considered to serve a role in other disease models, much less be required rather than eliminated to limit disease progression. Since the overexpression of this transcription factor leads to tumour development, and its elimination promotes bacterial progression, identifying a distinct pathway and regulatory mechanisms would be of high importance if one were to consider targeting this transcription factor or downstream genes for various forms of therapy.

3.6. Acknowledgements

We express gratitude to the UCT Animal Research Facility and Ms. Munadia Ansarie for the breeding, genotyping and maintenance of mice as well as the technical staff. Ms. Zarinah Sonday, Mr. Marlon Petersen and Mr. George Jacobs for the maintenance of the laboratory.

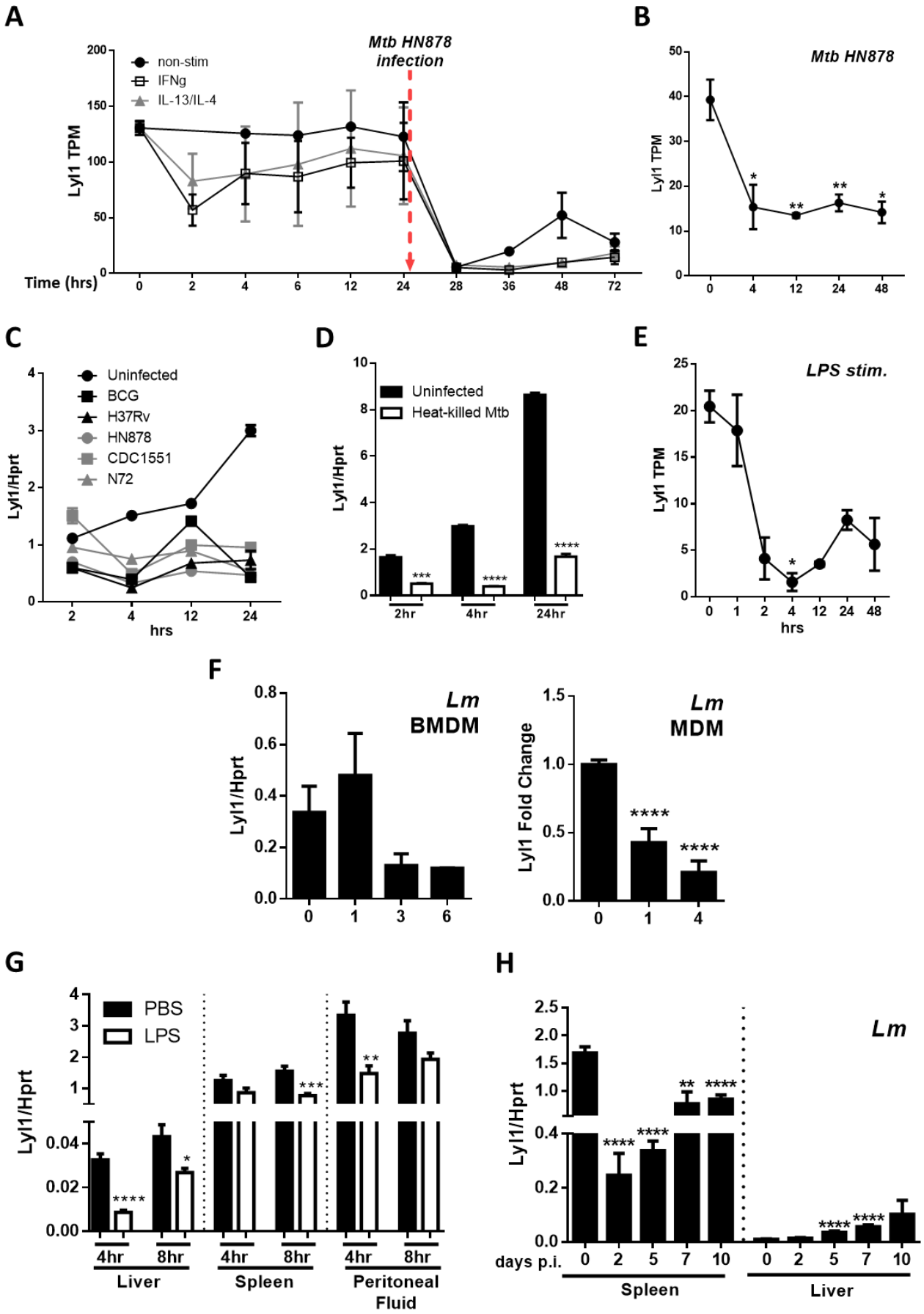
A
Mtb HN878 infection
non-stim
IFNg
IL-13/IL-4
Lyl1 TPM
Time (hrs)
B
Mtb HN878
Lyl1 TPM
C
Uninfected
BCG
H37Rv
HN878
CDC1551
N72
Lyl1/Hprt
hrs
D
Uninfected
Heat-killed Mtb
Lyl1/Hprt
2hr
4hr
24hr
E
LPS stim.
Lyl1 TPM
hrs
F
Lm
BMDM
Lyl1/Hprt
Lm
MDM
Lyl1 Fold Change
G
PBS
LPS
Lyl1/Hprt
4hr
8hr
Liver
Spleen
Peritoneal Fluid
H
Lm
Lyl1/Hprt
days p.i.
Spleen
Liver

Figure 3.1. **Lyl1 is downregulated in multiple immune stimulated environments *in vitro* and *in vivo*.** **(A)** Expression kinetics (represented as Tags Per Million (TPM)) of Lyl1 in *Mtb* HN878 infected mouse bone marrow-derived macrophage (BMDM) data were extracted from the Zenbu-FANTOM5 database and **(B)** human monocyte-derived macrophage (MDM) data were extracted from the Zenbu-FANTOM6 database. **(C)** BMDM were either subjected to various indicated *Mtb* strains, as well as **(D)** heat killed *Mtb* at MOI:1. **(E)** LPS-stimulated human monocyte-derived macrophage (MDM) data were extracted from the Zenbu-FANTOM6 database. **(F)** BMDM were infected with *Listeria monocytogenes* (*Lm*) with MOI:10 for RNA collection (*left panel*) and MDM derived from healthy participants were infected with *Lm* with MOI:10 to measure Lyl1 expression kinetics (*right panel*). **(G)** C57BL/6 mice were administered either 10 mg/kg LPS or 1X PBS by intraperitoneal injection (n = 6 mice/group) after which indicated organs were collected at 4- and 8-hours post-administration for RNA isolation to measure Lyl1 expression. **(H)** A total of $2x10^5$ CFU/mouse of *Lm* was intraperitoneally injected into C57BL/6 mice (n = 3 mice/group) after which the spleen and liver were collected at indicated time points for RNA isolation. Error bar denotes Mean ±SEM. Data shown are representative of 2-4 independent experiments. Unpaired student t-test analysis at $*p < 0.05$, $**p < 0.01$, $***p < 0.001$, $****p < 0.0001$ to determine significance.

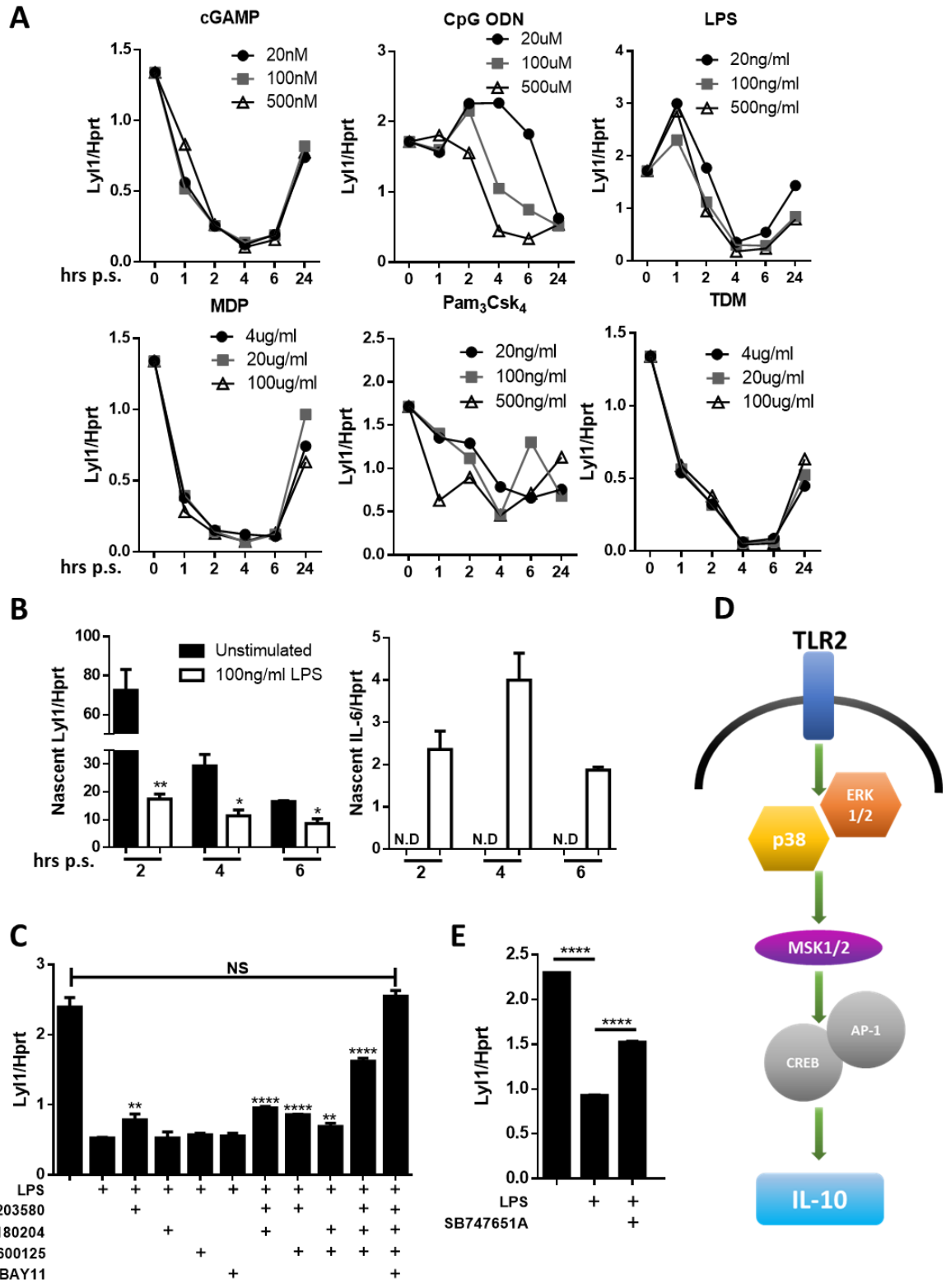

Figure 3.2. **Lyl1 expression is downregulated by MAPk and NFkB signaling pathways in macrophages. (A)** BMDM were exposed to either cGAMP, CpG ODN, LPS, MDP, Pam3Csk4 or TDM at various indicated concentrations. RNA was collected at indicated time points. **(B)** BMDM were stimulated with LPS (or unstimulated) and simultaneously tagged with biotinylated ethynyl uridine (EU)

followed by RNA pulldown for nascent RNA collection. qPCR was performed on synthesized cDNA to check for Lyl1 expression (*left panel*) and IL-6 (*right panel*) to confirm LPS stimulation. **(C)** BMDM were exposed to various inhibitor cocktails including 5 µM SB203580 (p38 MAPk inhibitor), 10 µM FR180204 (ERK1/2 MAPk inhibitor), 10 µM SP600125 (JNK MAPk inhibitor) and 7.5 µM BAY11 7084 (NFkB inhibitor) as well as **(E)** 10 µM SB747651A (MSK1/2 inhibitor) for 1 hour prior to 100 ng/ml LPS stimulation. **(D)** Schematic of MSK1/2-CREB pathway. Error bar denotes Mean ±SEM. Data shown are representative of 2-4 independent experiments. Unpaired student t-test analysis at *$p < 0.05$, **$p < 0.01$, ***$p < 0.001$, ****$p < 0.0001$ to determine significance.

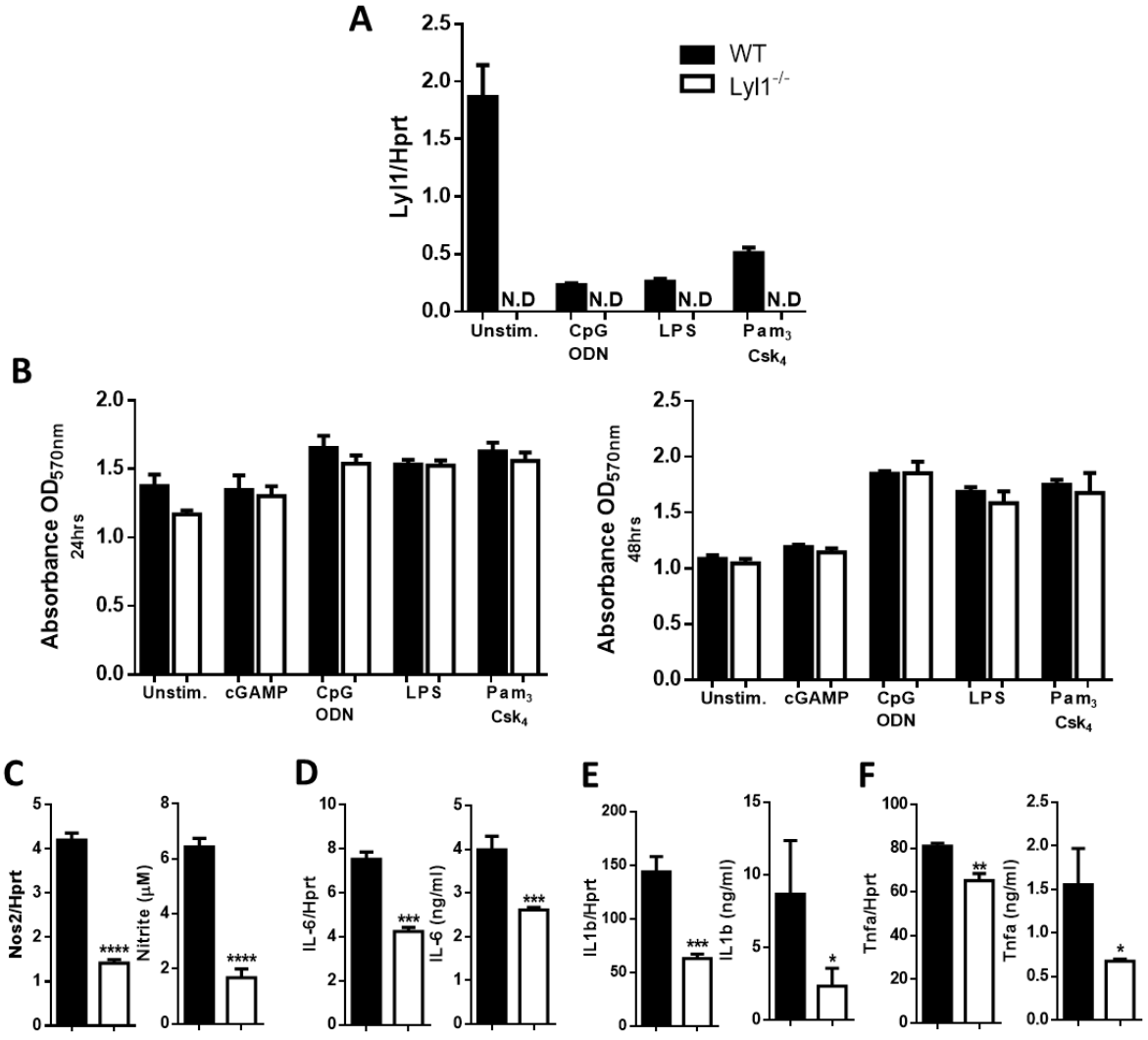

Figure 3.3. **Pro-inflammatory responses are reduced in LPS-stimulated Lyl1$^{-/-}$ macrophages *in vitro*.** **(A)** WT and Lyl1$^{-/-}$ BMDM were exposed to either 500 nM CpG ODN, 100 ng/ml LPS or 100 ng/ml Pam_3Csk_4 for 6 hours after which RNA was collected and Lyl1-deletion was confirmed. **(B)** Cell viability of indicated agonists at 24 (*left panel*) and 48 hours (*right panel*). **(C-F)** Indicated cytokines were assessed in 100 ng/ml LPS-stimulated WT and Lyl1$^{-/-}$ BMDM by intracellular mRNA expression at 6 hours and extracellular protein in supernatants by ELISA at 48 hours. Error bar denotes Mean ±SEM. Data shown are representative of 2-4 independent experiments. Unpaired student t-test analysis at *$p < 0.05$, **$p < 0.01$, ***$p < 0.001$, ****$p < 0.0001$ to determine significance.

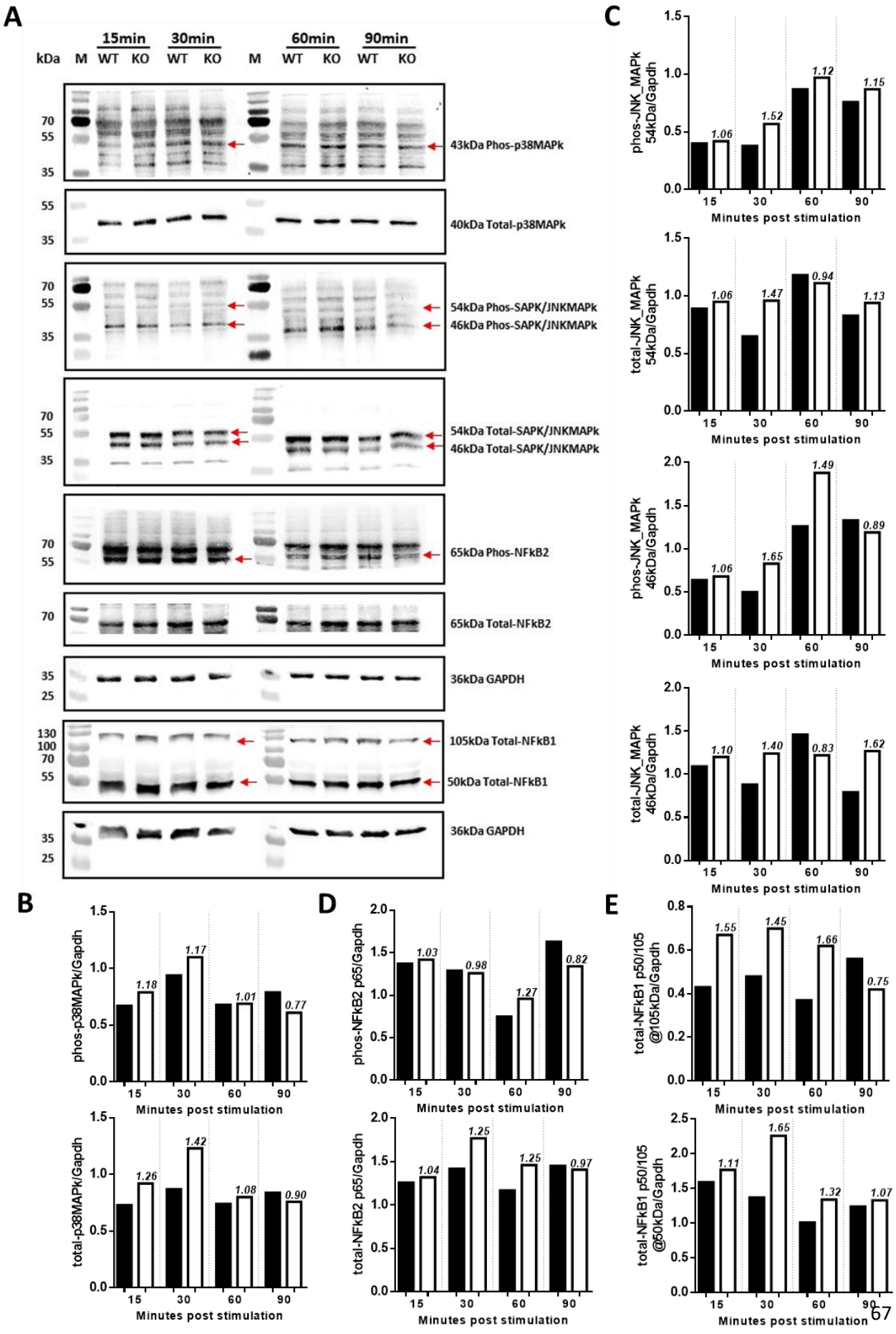
A
15min
30min
60min
90min
kDa M WT KO WT KO M WT KO WT KO
70
55
35
43kDa Phos-p38MAPk
55
35
40kDa Total-p38MAPk
70
55
35
54kDa Phos-SAPK/JNKMAPk
46kDa Phos-SAPK/JNKMAPk
70
55
35
54kDa Total-SAPK/JNKMAPk
46kDa Total-SAPK/JNKMAPk
70
55
65kDa Phos-NFkB2
70
65kDa Total-NFkB2
35
25
36kDa GAPDH
130
100
70
55
105kDa Total-NFkB1
50kDa Total-NFkB1
35
25
36kDa GAPDH
C
phos-JNK_MAPk 54kDa/Gapdh
1.06 1.52 1.12 1.15
Minutes post stimulation
total-JNK_MAPk 54kDa/Gapdh
1.06 1.47 0.94 1.13
Minutes post stimulation
phos-JNK_MAPk 46kDa/Gapdh
1.06 1.65 1.49 0.89
Minutes post stimulation
total-JNK_MAPk 46kDa/Gapdh
1.10 1.40 0.83 1.62
Minutes post stimulation
B
phos-p38MAPk/Gapdh
1.18 1.17 1.01 0.77
Minutes post stimulation
total-p38MAPk/Gapdh
1.26 1.42 1.08 0.90
Minutes post stimulation
D
phos-NFkB2 p65/Gapdh
1.03 0.98 1.27 0.82
Minutes post stimulation
total-NFkB2 p65/Gapdh
1.04 1.25 1.25 0.97
Minutes post stimulation
E
total-NFkB1 p50/105 @105kDa/Gapdh
1.55 1.45 1.66 0.75
Minutes post stimulation
total-NFkB1 p50/105 @50kDa/Gapdh
1.11 1.65 1.32 1.07
Minutes post stimulation

***Figure 3.4*. Lyl1 activity does not regulate MAP kinase and p50-p65 NFκB pathways.** WT and Lyl1$^{-/-}$ BMDM were stimulated with 100 ng/ml LPS and protein lysates were collected at indicated time points. **(A)** Western blot analysis on 30µg loaded protein was performed using phospho-p38 MAPk, total-p38 MAPk, phospho-SAPK/JNK MAPk, total-SAPK/JNK MAPk, phospho-NFκB2 (p65), total-NFκB2 (p65), total-NFκB1 (p50/p105), as well as Gapdh primary antibodies. **(B-E)** Densitometry analysis was performed on protein-specific bands, normalized to Gapdh to confirm expression differences. Fold change values are indicative of the normalized Lyl1$^{-/-}$ experimental value to the normalized WT control value.

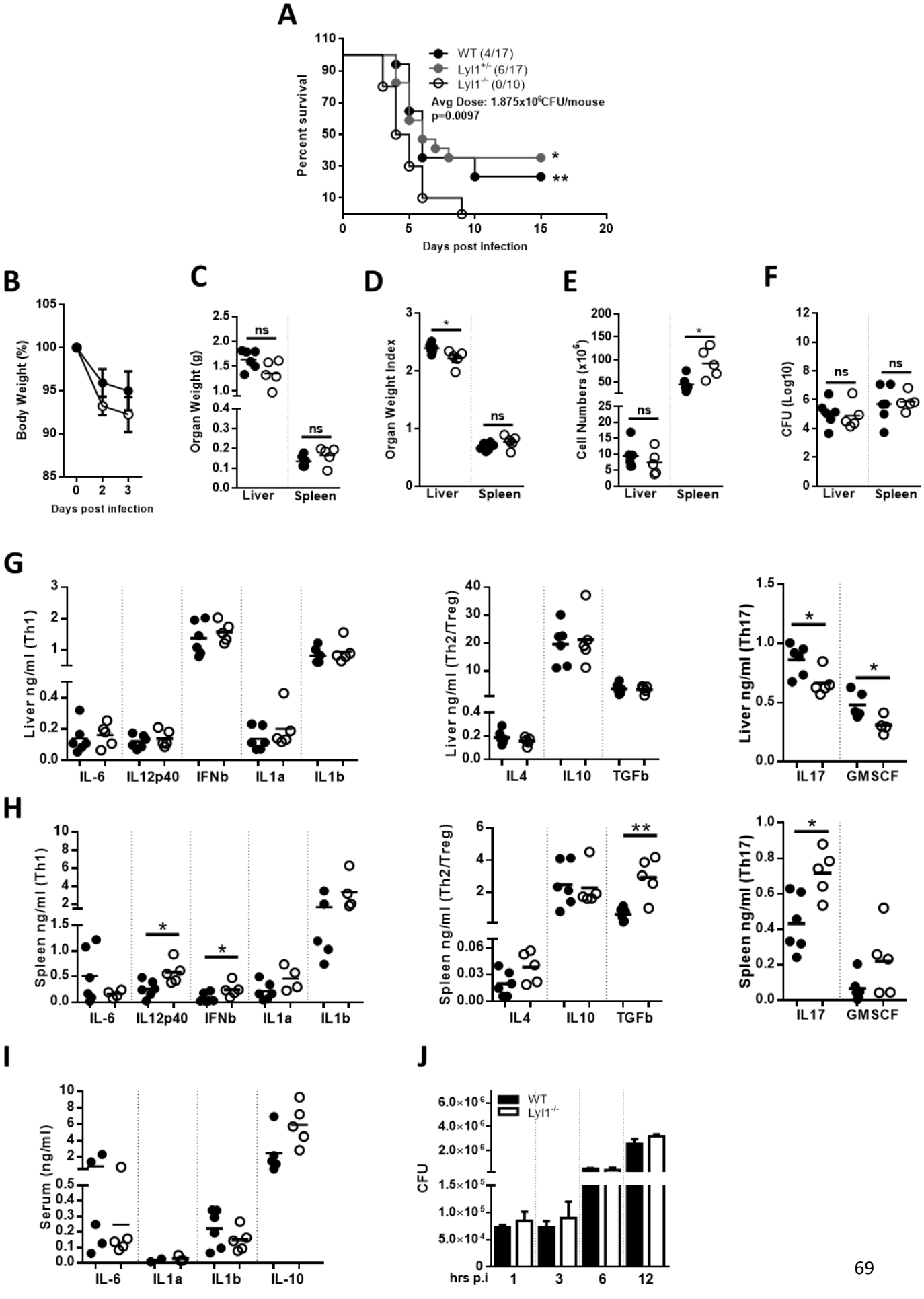
A
Percent survival
Days post infection
WT (4/17)
Lyl1+/- (6/17)
Lyl1-/- (0/10)
Avg Dose: 1.875x10^6CFU/mouse
p=0.0097
B
Body Weight (%)
Days post infection
C
Organ Weight (g)
Liver
Spleen
ns
D
Organ Weight Index
E
Cell Numbers (x10^6)
F
CFU (Log10)
G
Liver ng/ml (Th1)
IL-6
IL12p40
IFNb
IL1a
IL1b
Liver ng/ml (Th2/Treg)
IL4
IL10
TGFb
Liver ng/ml (Th17)
IL17
GMSCF
H
Spleen ng/ml (Th1)
Spleen ng/ml (Th2/Treg)
Spleen ng/ml (Th17)
I
Serum (ng/ml)
IL-10
J
CFU
WT
Lyl1-/-
hrs p.i
1
3
6
12

Figure 3.5. **Mice are more susceptible to *Listeria monocytogenes* (*Lm*) in the absence of Lyl1 compared to WT mice *in vivo*. (A)** A survival study (n = 10-17 mice/group) by intraperitoneally injecting WT, Lyl1$^{+/-}$ and Lyl1$^{-/-}$ mice with 1.9x10^{6} CFU/mouse *Lm*. **(B-H)** Littermate control and Lyl1$^{-/-}$ mice were intraperitoneally injected with 4x10^{4} CFU/mouse *Lm* (n = 5 mice/group) and sacrificed 3 days post-infection (3dpi) to compare **(B)** body weight, **(C)** organ weight, **(D)** relative organ weight index, **(E)** cell numbers and **(F)** CFU. **(G-H)** Supernatants from organ homogenates were analyzed by means of ELISA for Th1, Th2 and Th17 associated cytokines in the **(G)** liver and the **(H)** spleen. **(I)** ELISA was performed on the serum collected from both WT and Lyl1$^{-/-}$ mice at 3dpi. **(J)** Bone marrow cells of naïve wild-type (WT) and Lyl1$^{-/-}$ mice were harvested and subsequently infected with *Lm* MOI:10. These cells were later lysed at 1, 3, 6 and 12 hours post-infection to plate for intracellular bacterial burden. Line denotes Mean. Data shown are representative of 2-4 independent experiments. Unpaired student t-test analysis at *p < 0.05, **p < 0.01 to determine significance.

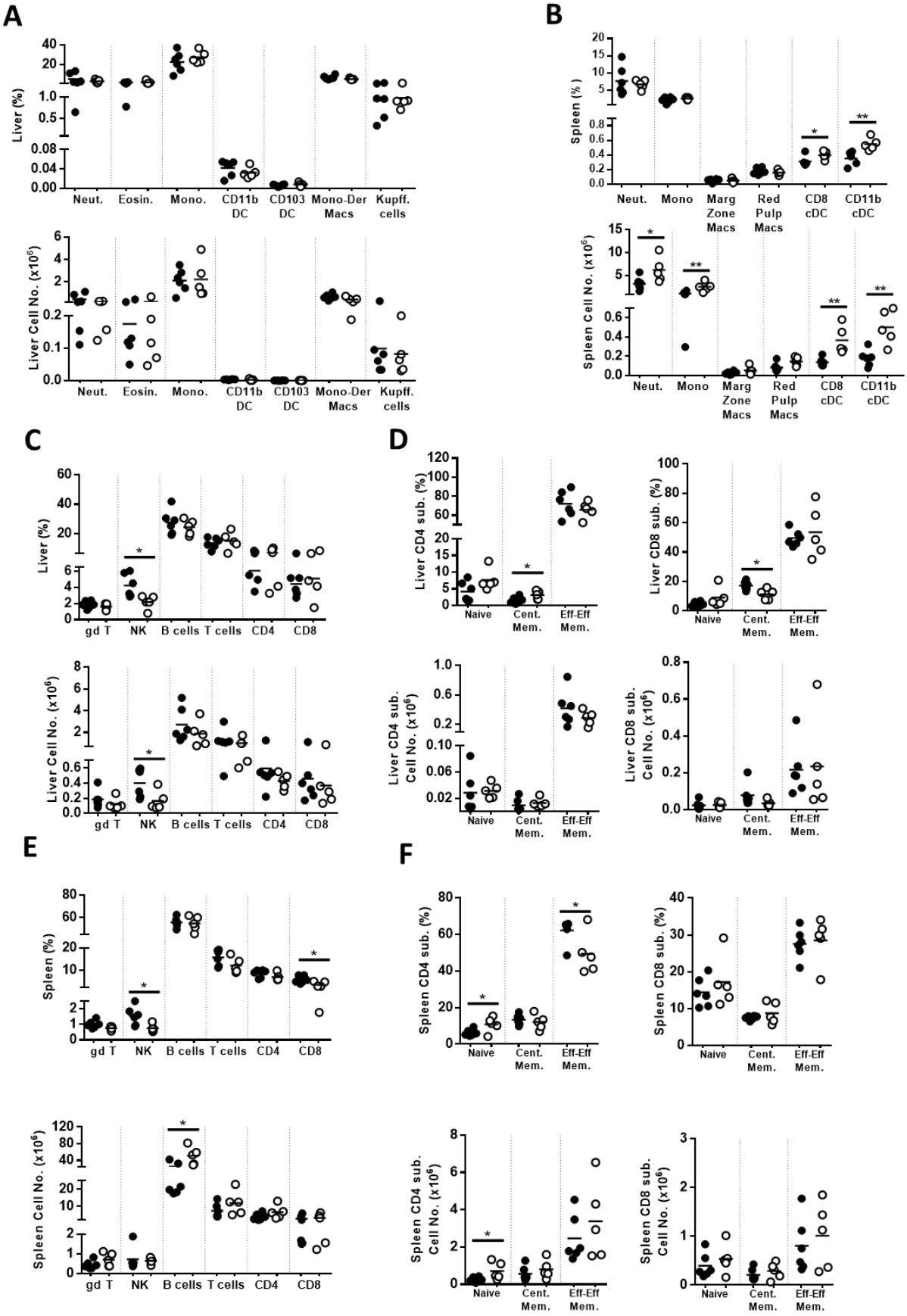
A
Liver (%)
Neut.
Eosin.
Mono.
CD11b DC
CD103 DC
Mono-Der Macs
Kupff. cells
Liver Cell No. (x10^6)
B
Spleen (%)
Neut.
Mono
Marg Zone Macs
Red Pulp Macs
CD8 cDC
CD11b cDC
Spleen Cell No. (x10^6)
C
Liver (%)
gd T
NK
B cells
T cells
CD4
CD8
Liver Cell No. (x10^6)
D
Liver CD4 sub. (%)
Naive
Cent. Mem.
Eff-Eff Mem.
Liver CD8 sub. (%)
Liver CD4 sub. Cell No. (x10^6)
Liver CD8 sub. Cell No. (x10^6)
E
Spleen (%)
Spleen Cell No. (x10^6)
F
Spleen CD4 sub. (%)
Spleen CD8 sub. (%)
Spleen CD4 sub. Cell No. (x10^6)
Spleen CD8 sub. Cell No. (x10^6)

Figure 3.6. **Lyl1$^{-/-}$ mice display increased dendritic cell recruitment in spleen and decreased NK cell recruitment in the liver.** Littermate control and Lyl1$^{-/-}$ mice were intraperitoneally injected with 4x10^4 CFU/mouse *Lm* (*n* = 5 mice/group) and sacrificed 3 days post infection (3dpi). **(A-B)** Single cell suspension for **(A)** liver and **(B)** spleen tissue was analyzed for percentage and total cell numbers in the myeloid and lymphoid **(C-D)** liver and **(E-F)** spleen populations. Surface markers of the different liver myeloid cell populations are as follows (according to the gating strategy in ***Appendix F***): Neutrophils (Neut.) = Ly6G$^+$CD11b$^+$; Eosinophils (Eosin.) = CD11b$^+$SiglecF$^+$; Monocytes (Mono) = CD11b$^+$; Ly6C$^+$; CD11b$^+$ DC = CD11c$^+$MHCII$^+$CD11b$^+$CD103$^-$; CD103$^+$ DC = CD11c$^+$MHCII$^+$CD11b$^-$CD103$^+$; Monocyte-derived Macrophages (MoM) = CD11b$^+$F4/80^{low}CD11c$^-$Ly6C$^-$; Kupffer cells (Kupff. Cells) = F4/80$^+$CD11b^{low}. Surface markers of the different spleen myeloid cell populations are as follows (according to the gating strategy in ***Appendix E***): Neutrophils (Neut.) = Ly6G$^+$CD11b$^+$; Monocytes (Mono) = CD11b$^+$; Ly6C$^+$CD11c$^-$; Marginal Zone Macrophages (Marg. Zone Macs) = CD11b^{high}F4/80^{low}CD11c$^-$; Red Pulp Macrophages (Red Pulp Macs) = F4/80^{high}CD11b^{low}CD11c$^-$; CD8$^+$ DC = CD11c$^+$MHCII$^+$CD8$^+$CD11b$^-$; CD11b$^+$ DC = CD11c$^+$MHCII$^+$CD11b$^+$CD8$^-$. Surface markers of the different liver and spleen lymphoid cell populations are as follows (according to the gating strategy in ***Appendix B***): gamma delta T-cells (gd T) = CD3$^+$gdTCR$^+$; NK cells = NK1.1$^+$CD3$^-$; B-cells = CD19$^+$CD3$^-$; T-cells = CD3$^+$CD19$^-$; CD4$^+$ T-cells = CD3$^+$CD4$^+$; CD8$^+$ T-cells = CD3$^+$CD8$^+$; CD4$^+$ naïve = CD3$^+$CD4$^+$CD62L$^+$CD44$^-$; CD4$^+$ Central Memory = CD3$^+$CD4$^+$CD62L$^+$CD44$^+$; CD4$^+$ Effector/Effector Memory = CD3$^+$CD4$^+$CD44$^+$CD62L$^-$; CD8$^+$ naïve = CD3$^+$CD8$^+$CD62L$^+$CD44$^-$; CD8$^+$ Central Memory = CD3$^+$CD8$^+$CD62L$^+$CD44$^+$; CD8$^+$ Effector/Effector Memory = CD3$^+$CD8$^+$CD44$^+$CD62L$^-$. Line denotes Mean. Data shown is representative of 2 independent experiments. Unpaired student t-test analysis at *$p < 0.05$, **$p < 0.01$ to determine significance.

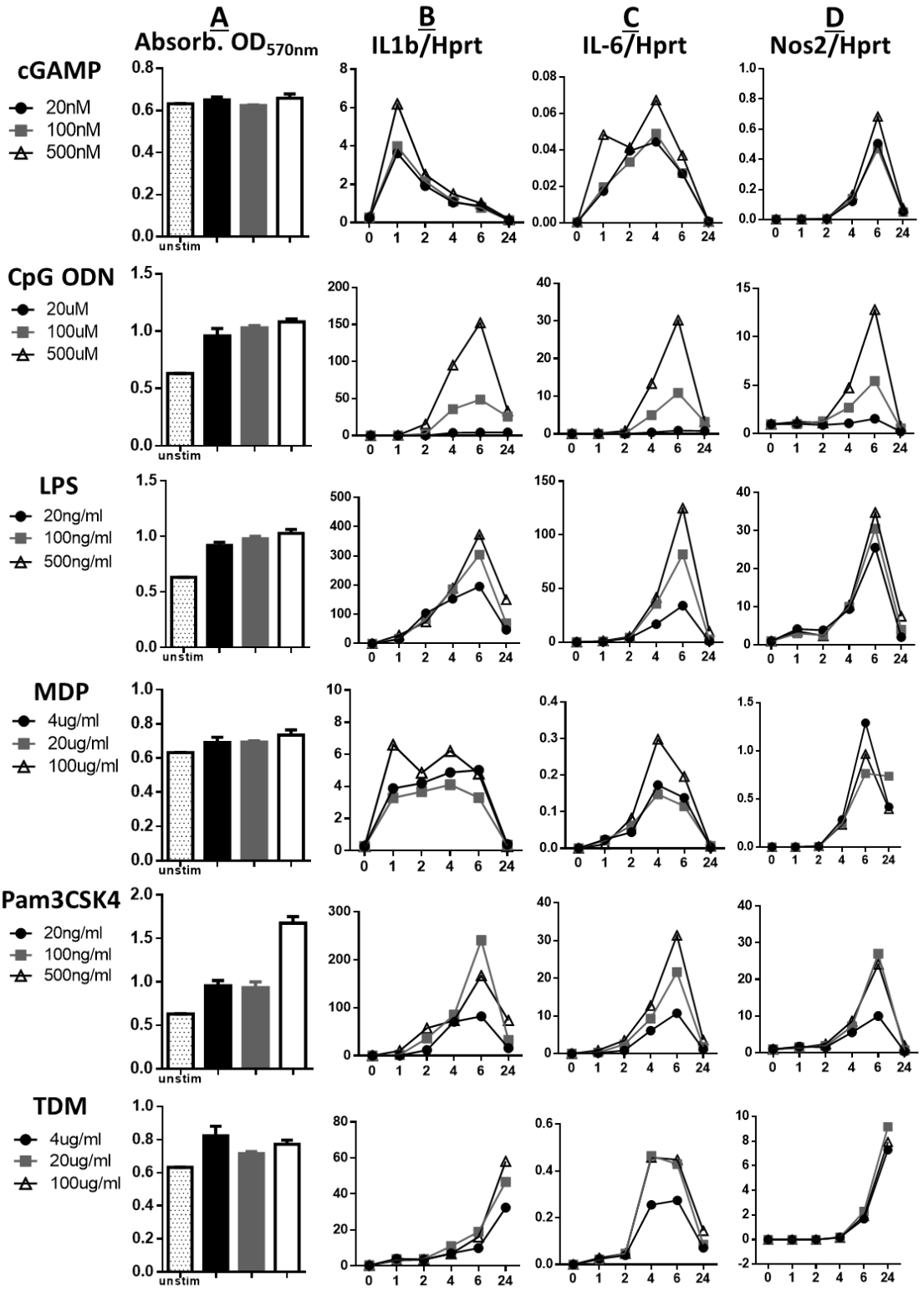

Figure S3.1. **All agonists induced the targeted pathway and demonstrated no cell toxicity.** BMDM were exposed to either cGAMP, CpG ODN, LPS, MDP, Pam_3Csk_4 or TDM at various indicated concentrations. **(A)** A viability assay was performed at 48hrs. **(B-D)** RNA was collected at indicated time points for mRNA expression. Error bar denotes Mean ±SEM. Data shown are representative of 3-4 independent experiments.

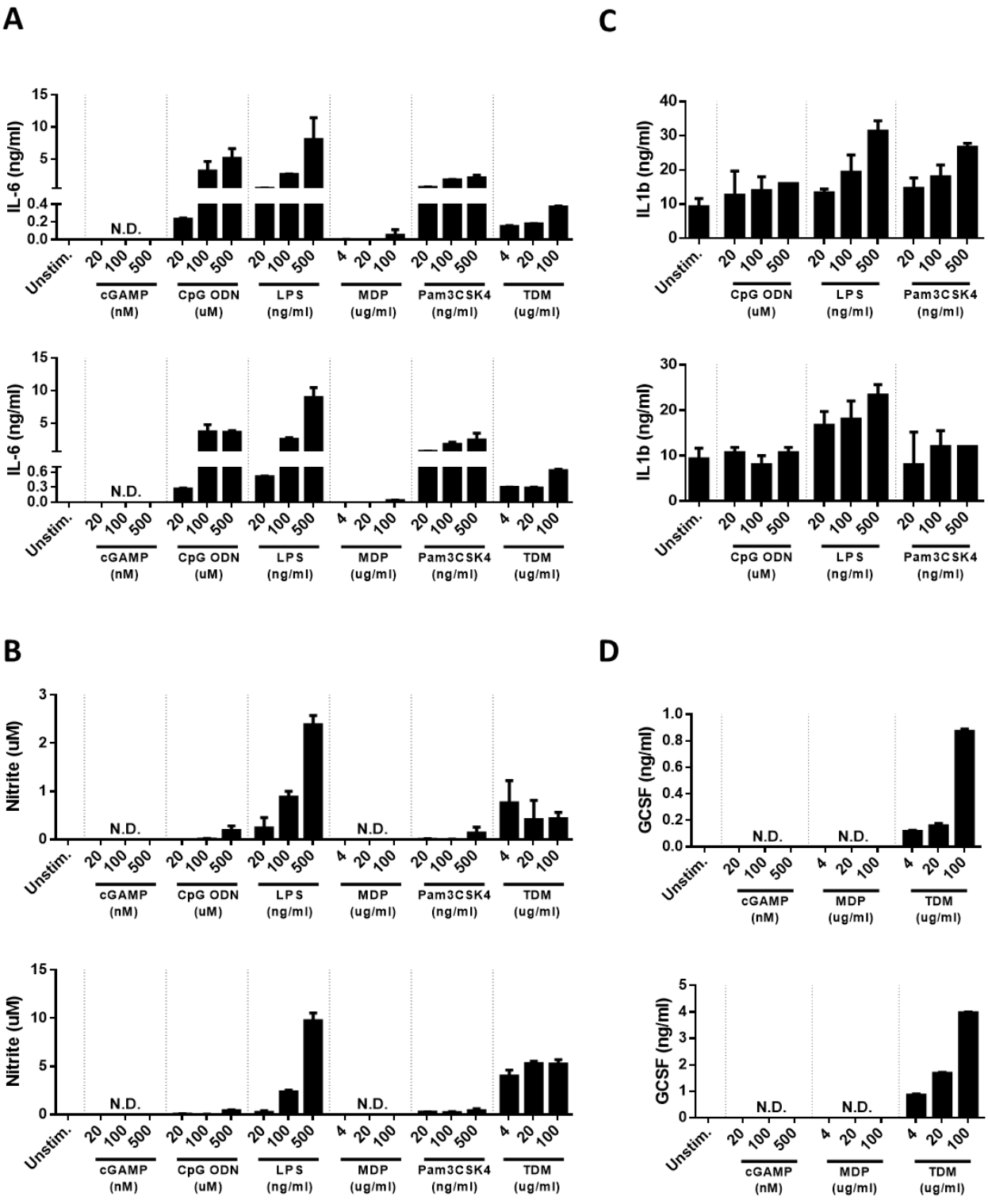

Figure S3.2. **All agonists induced the target pro-inflammatory cytokine production.** BMDM were exposed to either cGAMP, CpG ODN, LPS, MDP, Pam_3Csk_4 or TDM at various indicated concentrations. **(A-D)** Supernatants were collected and investigated for cytokine release by ELISA at 24 hours **(***upper panel***)** and 48 hours **(***lower panel***)**. Error bar denotes Mean ±SEM. Data shown are representative of 3-4 independent experiments. Unpaired student t-test to determine significance/insignificance.

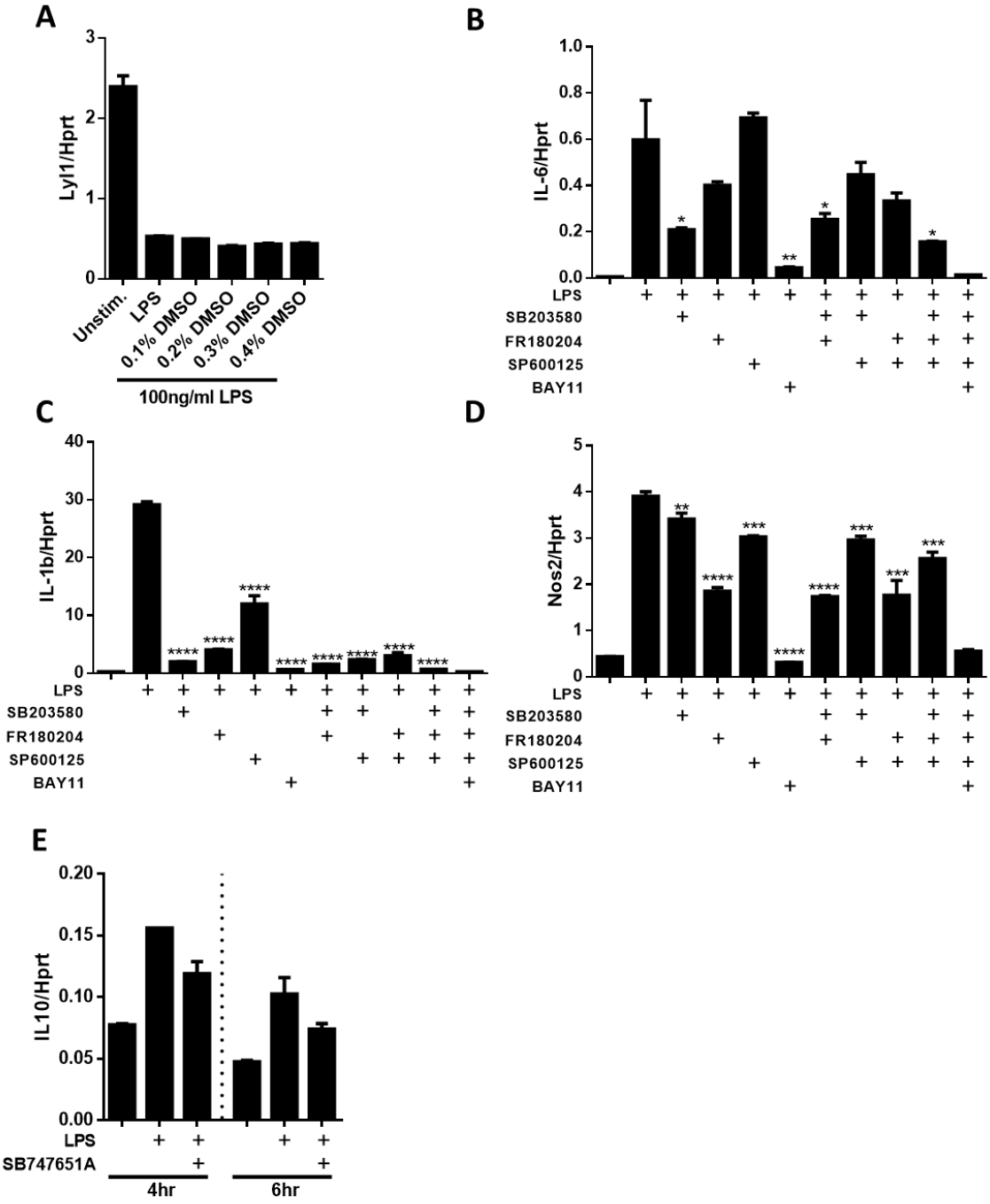

Figure S3.3. **Cytokine gene expression evaluation confirms the inhibition of various MAPk subunits, NFκB and MSK1/2 during *in vitro* experiments.** Bone marrow cells of naïve C57BL/6 mice were harvested and differentiated. **(A)** DMSO effects on Lyl1 expression was assessed at 4 hours. **(B-D)** BMDM were exposed to various inhibitor cocktails including 5 µM SB203580 (MAPk p38 inhibitor), 10 µM FR180204 (MAPk ERK1/2 inhibitor), 10 µM SP600125 (MAPk JNK inhibitor) and 7.5 µM BAY11-7084 (NFkB inhibitor) as well as **(E)** 10 µM SB747651A (MSK1/2 inhibitor) for 1 hour prior to 100ng/ml LPS stimulation. **(B-E)** Cells were harvested for RNA isolation and mRNA expression after 4 hours of LPS stimulation. Error bar denotes Mean ±SEM. Data shown are representative of 2-4 independent experiments. Unpaired student t-test analysis at *$p < 0.05$, **$p < 0.01$, ***$p < 0.001$, ****$p < 0.0001$ to determine significance.

CHAPTER 4: Manuscript in preparation

Lyl1-deficiency promotes inflammatory responses and increased bacterial burden in response to *Mycobacterium tuberculosis* infection

Shelby-Sara Jones[1,2], Mumin Ozturk[1,2], Nathan Kieswetter[1,2], Harukazu Suzuki[4], Reto Guler[1,2,3*], Frank Brombacher[1,2,3*]

[1] International Centre for Genetic Engineering and Biotechnology, Cape Town Component, Cape Town 7925, South Africa.

[2] Department of Pathology, University of Cape Town, Institute of Infectious Diseases and Molecular Medicine (IDM), Division of Immunology and South African Medical Research Council (SAMRC) Immunology of Infectious Diseases, Faculty of Health Sciences, University of Cape Town, Cape Town 7925, South Africa.

[3]Wellcome Centre for Infectious Diseases Research in Africa (CIDRI-Africa), Institute of Infectious Disease and Molecular Medicine (IDM), Faculty of Health Sciences, University of Cape Town, Cape Town 7925, South Africa.

[4]RIKEN Center for Integrative Medical Sciences, Yokohama, Japan.

*Correspondence: Frank Brombacher, frank.brombacher@icgeb.org and Reto Guler, reto.guler@uct.ac.za

Keywords: Lyl1$^{-/-}$, *Mycobacterium tuberculosis* (*Mtb*), susceptibility, neutrophils

4.1. Abstract

The use of host-directed therapies (HDT) has shown to be promising in developing new therapies to treat tuberculosis (TB). With the use of next-generation sequencing in conjunction with cap analysis gene expression (CAGE), Lymphoblastic leukemia 1 (Lyl1) was identified as a potential HDT target for TB given the significant downregulation of this transcription factor in both M1 (IFNγ) and M2 (IL-13/IL-4) *Mtb*-infected macrophages. Here, we demonstrate host susceptibility with increased bacterial burdens in response to the *Mtb* HN878 strain in the absence of Lyl1 in primary macrophages and mouse models. We show that Lyl1-deficiency promotes an exaggerated inflammatory response with increasing chemokine secretion and neutrophil recruitment to the lungs, in combination with reduced anti-inflammatory responses. We further show that Lyl1 may not be used as a marker of chronic TB in whole blood, however, acute upper respiratory viral infections decrease Lyl1 expression levels significantly. Collectively, our data establish a role for Lyl1 during *Mtb* infection and therefore provides the potential for Lyl1 to be fully explored to delineate downstream pathways for a potential HDT for TB.

4.2. Introduction

Tuberculosis (TB), caused by *Mycobacterium tuberculosis* (*Mtb*), results in over a million deaths annually. For 2018, the World Health Organization (WHO) reported a total of 10 million TB-infected patients, of which 1.5 million died [56]. The remarkable ability of this bacteria to manipulate and exploit cellular host responses for its survival and virulence continues to encourage further investigation into therapeutics that can overcome this persistent bacteria [160]. Since Robert Koch's tubercle bacillus discovery in 1882, extensive research has been dedicated to the expulsion of this disease in infected patients. However, with growing years and various treatment regimens, the bacteria is continuously developing resistance, rendering it more virulent in some cases [161]. Recently, researchers investigated host-directed therapy (HDT) as a means of circumventing the bacteria's manipulative and adaptive nature. These studies aim to develop adjunctive anti-TB therapies that would enhance the hosts immune response to effectively eradicate the bacteria with reduced tissue damage [83, 162]. A holistic approach to identifying potential HDT targets would be the use of genome-wide transcriptional deep sequencing of total RNA in conjunction with cap analysis gene expression (CAGE). The FANTOM (Functional Annotation of Mammalian Genome) consortium has implemented these techniques to provide a transcriptional network of various diseased cell states in both human and murine cells [101-103]. Our research group contributed specifically to FANTOM5 whereby, with the use of CAGE, various differentially expressed genes were identified in *Mtb*-infected M1 (IFNγ) and M2 (IL-13/IL-4) BMDM. Of these targets, the Lymphoblastic leukemia 1

(Lyl1) gene was especially interesting given its significant downregulation in both M1 and M2 macrophages as early as 4 hours post-infection [104].

Lymphoblastic leukemia 1 (Lyl1) is a basic helix-loop-helix (bHLH) family transcription factor that was initially identified due to its chromosomal translocation in T-cell leukemia [106]. The bHLH domain of Lyl1 is highly conserved, sharing 82% of amino acid identity, to that of Scl/Tal1 which is also known to play a role in the development of T-cell leukemia [110, 163]. Downstream research explored the importance of these transcription factors in response to leukemia as well as identifying comparable and individual roles of each gene, including its significance in hematopoiesis [164]. For many years, Lyl1 was hypothesized to harbour oncogenic potential due to its chromosomal mutation and significant overexpression in leukemia malignancies [106]. However, research has shown that Lyl1 is not directly oncogenic, but rather predisposes mice towards lymphoma after which secondary mutations occur to develop cancer [130]. These studies demonstrate that Lyl1 has the potential to alter immune regulation significantly in response to leukemia.

However, Lyl1 has only been explored in leukemia, demonstrating a significant upregulation of this transcription factor in cancer patients [148]. Therefore, it was interesting to discover, through the FANTOM5 project, the significant downregulation of this transcription factor in all macrophage subsets in response to *Mtb* [102, 104]. Host-directed therapy is becoming a widespread approach in developing 'intelligent drugs' to circumvent *Mtb* host manipulation and exploitation [162]. Therefore, given the considerable expressional change in this transcription factor in response to *Mtb*, we investigated the role and importance of this gene in response to mycobacteria.

In this study, we show that Lyl1-deficient mouse models are highly susceptible to hypervirulent *Mtb* HN878. Globally deleted Lyl1 mice experience increased bacterial burden accompanied by a highly inflammatory response. This is represented by an increase in cytokine and chemokine secretion as well as neutrophil recruitment to the lungs of Lyl1-deficient mice compared to wild-type (WT). Given the changes in the immune profile in $Lyl1^{-/-}$ mice compared WT in response to *Mtb*, our study highlights the requirement of Lyl1 during *Mtb* infection.

4.3. Methods

4.3.1. Mouse strains

To study the function of Lymphoblastic leukemia 1 (Lyl1), we acquired a Lyl1 global knockout mouse whereby the entire coding region was deleted using a lox-P-flanked Neomycin cassette. This mouse ($Lyl1^{Mg/Mg}$) was generated by the Margaret A. Goodell laboratory at Baylor College of Medicine, Houston, Texas [107] by injecting the correctly targeted clones into blastocytes of 129 AB2.2 mice and further back-

crossed to the C57BL/6 strain for ten generations. Once received at the University of Cape Town (UCT), $Lyl1^{Mg/Mg}$ was back-crossed with in-house C57BL/6J strains for three generations to generate $Lyl1^{-/-}$, $Lyl1^{-/+}$ and littermate control, $Lyl1^{+/+}$ in the Animal Research Facility, UCT. Animals were housed, monitored and experimentally handled within strict accordance with the guidelines approved by the Animal Research Ethics Board of UCT. All experiments included mice aged 8 – 12 weeks and were sex-matched.

4.3.2. Ethical statement

All animals used in this study were subjected to experimental procedures that were in strict accordance with the South African National Standard (SANS 10386:2008) and the Animal Research Ethics Committee of the Faculty of Health Sciences, University of Cape Town (Protocol Permit No: 015/040 and 019/023).

4.3.3. Bone marrow-derived macrophages (BMDM) generation, activation and infection *in vitro*

Bone marrow-derived macrophages (BMDM) were generated from 8-12 weeks old wild-type (WT) and Lyl1-deficient mice as per [145]. Briefly, bone marrow from the femurs was collected and differentiated into macrophages using sterile tissue grade Petri dishes containing Plutznik media (DMEM containing 30% L929 cell–conditioned medium, 10% fetal calf serum, 5% horse serum, 1 mM sodium pyruvate, 2 mM L-glutamine, 0.1 mM β-mercaptoethanol, 100 U/ml penicillin G, and 100 µg/ml streptomycin) for 10 days. Thereafter, macrophages were harvested and seeded into either 96-well plates ($1.5x10^5$ cells/well; Nunc, Denmark) for downstream infections or 24-well plates ($7.5x10^5$ cells/well; Nunc, Denmark) for RNA collection/isolation. Thereafter, seeded macrophages were activated by the addition of 100 ng/ml LPS (Sigma-Aldrich) accompanied by a media control and rested overnight at 37°C with 5% CO_2. Steady state and/or activated macrophages were later infected with hypervirulent *Mtb* HN878 with MOI:1 for 3 and 6 days for bacterial loads and cytokine concentration in supernatants (ELISA) or for 4-, 12- and 24-hours post-infection to determine mRNA expressions.

4.3.4. *Mtb* infection in mice (*in vivo*)

Anesthetized mice were intranasally infected with either *Mtb* HN878 or mCherry-H37Rv by administering 25 µl per nasal cavity. The actual inoculum dose was determined one day post-infection. Bacterial loads, physiological parameters, flow cytometric and histopathological analyses were performed on indicated organs as directed [138], however, briefly described below.

4.3.5. Bacterial loads in BMDM and organs

At various indicated timepoints, lysed BMDM (in 0.05% Triton X-100) and organ homogenates were subjected to 10-fold dilutions and plated on Middlebrook 7H10 agar plates supplemented with 10% OADC and 0.5% glycerol. Plates were incubated at 37°C for 14 – 21 days and the CFU for cell culture and organ enumerated.

4.3.6. Quantitative real-time polymerase chain reaction (qRT-PCR)

Plated cells were collected with 350 µl of RLT lysis buffer designed to extract RNA using the RNeasy Mini Kit (Qiagen catalogue no. 74106). RNA was extracted according to the manufacturer instructions and normalized to 300 ng. Thereafter, RNA was reverse transcribed by the Transcriptor First Strand complementary DNA (cDNA) Synthesis Kit (Roche catalogue no. 04 379 012 001) using both anchored oligo dT primers and random hexamer primers according to the manufacturer instructions to yield cDNA. Later, various transcripts were amplified by qPCR using LightCycler® 480 SYBR Green I Master Mix (with primer pairs listed in *Appendix G*) in the LightCycler® 480 Instrument II (Roche). Primer pairs, listed in *Appendix G* with their respective PCR conditions, were purchased from Integrated DNA Technologies (IDT; Coralville, Iowa, United States). The PCR reaction was first pre-incubated for 5 minutes at 95°C followed by amplification (denaturing (D) for 10 seconds; annealing (A) for 15 seconds; extension (E) for 15 seconds and the final acquisition step (S) for 1 second) for 45 cycles. All targeted expressions were normalized to Hprt expression levels.

4.3.7. Measurement of nitric oxide and cytokines/chemokine in culture supernatants and homogenates

Nitric oxide in infected cell culture supernatants was measured using the Griess reagent assay. Briefly, cell supernatants were incubated with 1% sulfanilamide in 2.5% phosphoric acid for 10 minutes at room temperature in the dark, followed by 0.1% naphthyl-ethylene-diamine in 2.5% phosphoric acid for another 10 minutes. BMDM cell culture and organ homogenates cytokines and chemokines were examined using the standard sandwich ELISA protocol (coating and detection antibodies obtained from BD Biosciences, BioLegend and R&D Scientific) using either TMB Microwell Peroxidase Substrate (KPL international) for streptavidin-HRP conjugates or 1 mg/ml p-nitrophenyl phosphate disodium salt hexahydrate (Sigma; catalog no: N2765) for streptavidin-AP conjugates. Optical density was measured using the VersaMax™ microplate spectrophotometer (Molecular Devices, Sunnyvale, California).

4.3.8. Flow cytometry

Collected *Mtb*-infected organs were subjected to collagenase digestion in preparation for single-cell suspension as described previously [138]. Cells were surface-stained for the identification of the lymphoid and myeloid populations in the lung and lymph node. The following antibodies, purchased from BD Biosciences, BioLegend and eBioScience, were used to surface phenotype various cell populations: PD-1 (FITC); CD4 (BV421/V450); CD44 (PE); NK1.1 (APC-Cy7); CD3 (A700); CXCR5 (PE-Cy7); CD62L (APC); CD19 (PerCP-Cy5.5); CD8 (V500); KLRG1 (BV786); CD64 (PE-Cy7); Ly6C (PerCP-Cy5.5); CD11b (V450); MHC II (A700); CD11c (APC); SiglecF (APC-Cy7); Ly6G (FITC); MerTK (BV786); CD103 (PE); F4/80 (PE-Cy7); CD169 (APC-eFluor780). Cells were stained and acquired according to [138] using the BD LSR Fortessa (BD Biosciences Immunocytochemistry Systems), and the data analysis was performed with FlowJo v10.6.1 Software (Treestar, US). Cell sorting was performed in the biosafety level 3 lab with BD FACSAria Fusion to sort *Mtb*-harbouring ($mCherry^{+}$) neutrophil, monocyte, alveolar macrophage and recruited macrophage populations. All panels are outlined in the appendix: *B*-lung and lymph node lymphoid; *C*-lung myeloid and *D*-lymph node myeloid.

4.3.9. Histopathology and immunohistochemistry

Upon animal euthanasia and experimental organ excision, a fraction of the indicated organ was collected in formalin solution (10% formaldehyde in 1X PBS) for tissue fixation. Formalin-fixed tissue samples were then embedded in wax, processed, subjected to 3 µm sections and stained with hematoxylin and eosin (H&E) for histopathological analyses. Furthermore, various organs were processed for immunohistochemistry using either iNOS (Abcam) on 3 µm sections. Thereafter, stained sections were mounted onto microscopic slides using a xylene-based mounting medium for image acquisition and quantification using the Nikon Eclipse 90i (Nikon) microscope with the Nikon NIS-Elements advanced imaging software (Nikon Corporation).

4.3.10. Data deposition

The FANTOM5 CAGE data is publicly available (http://fantom.gsc.riken.jp/5) and can be interactively explored using the in-house Zenbu portal (https://fantom.gsc.riken.jp/zenbu/). Data from the other published databases, including the TB Gambia Cohort (PMID 22046420), TB SA and UK Cohort (PMID 20725040) and the Viral USA Cohort (PMID 26070066), was all manually extracted, organized and sorted using Microsoft Excel® and represented using GraphPad Prism 6.

4.3.11. Statistical analyses

All data represented was analyzed using GraphPad Prism 6.0 with the use of the student *t-test* (two-tailed with equal variance). A $*p$ value of less than 0.05 was considered significant, depicting $**p < 0.01$, $***p < 0.001$ and $****p < 0.0001$.

4.4. Results

4.4.1. Lyl1 is required to circumvent *Mtb* infection in macrophages *in vitro*

The discovery of increased susceptibility in Lyl1-deficient mice in response to *Listeria monocytogenes* (*Lm*) infection, supported by various immunological differences when compared to wild-type (WT) mice (*Chapter 3, unpublished data*), initiated the interest in fully exploring the effects of *Mycobacterium tuberculosis* (*Mtb*) on Lyl1-deficient hosts. Bone marrow-derived macrophages (BMDM) were generated from WT and Lyl1$^{-/-}$ mice. Thereafter, these BMDM were either subjected to media or 100 ng/ml LPS overnight for macrophage activation and later, both groups were exposed to *Mtb* HN878 with MOI:1 *in vitro* (*Figure 4.1 A-B*). Although the host downregulates Lyl1 in response to immune stimulating environments, it was interesting to observe an increase in intracellular bacterial burden in Lyl1-deficient macrophages compared to WT macrophages (*Figure 4.1 A*). This detrimental effect of *Mtb* HN878 on BMDM without Lyl1 indicates the requirement for Lyl1 to kill the bacteria effectively. Downstream effects of Lyl1-deficiency in response to *Mtb* HN878 were investigated intracellularly through mRNA expression levels by qPCR (*Figure 4.1 C*) as well as extracellularly using ELISA methods to assess for protein secretion (*Figure 4.1 B*). Interestingly, significant differences between WT and Lyl1$^{-/-}$ mRNA levels were observed as early as 4 hours post-infection (*Figure 4.1 C*). Inducible nitric oxide synthase (Nos2) mRNA was slightly increased in Lyl1$^{-/-}$ macrophages in comparison to WT. However, this did not translate to nitric oxide release in the supernatants of these *Mtb*-infected BMDM (*Figure 4.1 B*). Overall, an increase in cytokine response was established in Lyl1$^{-/-}$ BMDM, including IL-1α, IL-1β and TNFα both intracellularly and extracellularly, as well as IL-10 and chemokine Cxcl1 intracellularly. Contrastingly, there was a significant decrease in IL-12p40 cytokine release in LPS-activated *Mtb*-infected Lyl1$^{-/-}$ BMDM compared to WT (*Figure 4.1 B*). Thus, although the host regulates Lyl1 in response to *Mtb* HN878, this data demonstrates that, due to the increased bacterial burden as well as the significant change in immune profile in the absence of Lyl1, this transcription factor is indeed required for the reduction of *Mtb* bacterial burden *in vitro*.

4.4.2. Lyl1$^{-/-}$ mice are highly susceptible to chronic hypervirulent *Mtb* HN878 infection *in vivo*

With increased bacterial burden in Lyl1$^{-/-}$ BMDM in comparison to WT in response to *Mtb* HN878, we investigated whether Lyl1 is required for the eradication of *Mtb in vivo* and whether Lyl1-deficiency would yield overall *in vivo* host susceptibility. WT and Lyl1$^{-/-}$ mice were intranasally infected with *Mtb* HN878 at approximately 200 CFU/mouse for mortality and 100 CFU/mouse for time-point experiments (3, 6 and 10 weeks post-infection). A lethal dose of *Mtb* HN878 resulted in Lyl1$^{-/-}$ mice succumbing to the hypervirulent *Mtb* HN878 infection as early as 3 months post infection compared to 5.5 months for WT mice (*Figure 4.2 A*). This translated to increased bacterial burden in Lyl1-deficient lung and spleen (*Figure 4.2 B*), accompanied by enlarged organs when normalized to mouse weight (*Figure 4.2 D*) during chronic infection (6 and 10 weeks post-infection). There was no significant change, although there was an increasing trend, in the number of cells recruited to Lyl1-deficient lungs compared to WT at 6 weeks and 10 weeks post-infection (*Figure 4.2 E*). However, interestingly, upon chronic infection, the number of cells present in the lymph node were significantly decreased in the absence of Lyl1 (*Figure 4.2 E*). Together, the data above show that the host displays extreme susceptibility in the absence of Lyl1 in response to chronic hypervirulent *Mtb* HN878 infection. This could be a consequence of either increased bacterial growth or increased cellular recruitment to the site of infection. Potentially, this could be a consequence of both immune evasion and host regulatory responses, yielding Lyl1$^{-/-}$ mice to surrender to the infection significantly earlier than WT mice.

4.4.3. The absence of Lyl1 increases neutrophil recruitment during chronic hypervirulent *Mtb* HN878 infection *in vivo*

Since Lyl1-deficiency promotes increased bacterial burden and host susceptibility in response to *Mtb* HN878 infection, we aimed to investigate the differences in cellular recruitment patterns between WT and Lyl1$^{-/-}$ mice to highlight the potential causative or consequences of host susceptibility in Lyl1-deficient mice. Lyl1 has been reported to play a significant role in T- and B-cell development [122] and the observed phenotype is during chronic infection whereby the adaptive immunity is activated. Therefore, upon euthanasia at indicated time-points, flow cytometric analysis of the distribution of lymphoid cells in the lungs (*Figure 4.3*) and the lymph nodes (*Figure S4.1*) of WT and Lyl1$^{-/-}$ mice was investigated. Surprisingly, the lymphoid percentages in Lyl1-deficient *Mtb*-infected lungs were comparable to that of WT lungs (*Figure 4.3 A*), including CD4^{+} T-cell memory subpopulations (*Figure 4.4 A*). A further investigation into T-cell memory presented an increase in lung CD8^{+} effector/effector memory in Lyl1$^{-/-}$ mice compared to WT, however, this was not translated to cell numbers (*Figure 4.4 B*). The same lymphoid populations in the lymph nodes were investigated (*Figure S4.1*) and given the significant downregulation

of total cell numbers in the absence of Lyl1 (*Figure 4.2 D*), as suspected, there was a decrease in the absolute number of cells in all lymph node lymphoid cells in Lyl1$^{-/-}$ mice (*Figure S4.1 B*). However, when examining the percentage of lymph node lymphoid cells, the only difference reflected in percentages was the upregulation of CD4^{+} central memory and effector/effector memory at 3 weeks post-infection and subsequent downregulation of CD8^{+} central memory at 6 weeks post-infection (*Figure S4.2 A-B*). Thereafter, the myeloid population at all indicated time-points were investigated (*Figure 4.5 A-B*). Interestingly, during chronic infection, there was a consistent increase in neutrophil and monocyte recruitment in the lungs of Lyl1-deficient mice when examining the percentage (*Figure 4.5 A bottom panel*) and the cell numbers (*Figure 4.5 B bottom panel*) compared to WT mice (10 weeks post-infection). Three-week *Mtb* HN878 exposure does not induce any significant myeloid population cell changes in Lyl1-deficient mice compared to WT mice (*Figure 4.5 A-B upper panels*). Collectively, the data suggest that although Lyl1 is important for the development of various components of the lymphoid population, the absence of this transcription factor does not affect the recruitment of these cells to the site of infection in response to hypervirulent *Mtb* HN878. However, the loss of Lyl1 does indeed induce neutrophil and monocyte recruitment to the site of infection, which could potentially contribute to the host's weakened position in response to *Mtb* HN878 infection.

4.4.4. Lyl1-deficiency alters cytokine-chemokine secretion and promotes lung inflammation/pathology in response to hypervirulent *Mtb* HN878 infection *in vivo*

To identify the signaling mechanisms that are not only responsible for increased bacterial burden (*Figure 4.2 B*) but also responsible for the excessive neutrophil recruitment (*Figure 4.5 A-B*) in the absence of Lyl1, cytokine and chemokine expression levels were investigated in *Mtb* HN878 infected lung homogenates of both WT and Lyl1$^{-/-}$ mice. As observed in the physical and cellular parameters as well as the flow cytometric analysis, no differences in the cytokine and chemokine response to *Mtb* HN878 were observed at 3 weeks post-infection (3wpi) in Lyl1$^{-/-}$ lungs compared to WT (*Figure 4.6 A, B, C upper panels and 4.7 A*). At 6 weeks post-infection (6wpi), a significant increase in IL-12p40, IFNγ, IL-1α (*Figure 4.6 A middle panel*) as well as a reduction in GM-CSF (*Figure 4.6 C middle panel*) was observed in Lyl1-deficient lungs compared to WT. At 10 weeks post-infection there was a significant reduction in IFNβ and IFNγ (*Figure 4.6 A bottom panel*) in Lyl1-deficient lungs compared to WT lungs. Consistent between 6 and 10 weeks post-infection is the significant increase in IL-1α (*Figure 4.6 A*) accompanied by a decrease in GM-CSF (*Figure 4.6 C*) in the absence of Lyl1. Additionally, IL-1β is also induced in Lyl1-deficient lungs at 10 weeks post-infection (*Figure 4.6 A bottom panel*). Contrary to the cytokines, the release of chemokines in the lungs of Lyl1$^{-/-}$ infected mice was consistent between 6 and 10 weeks post-infection (*Figure 4.7 B, C*).

Chemokines, including Cxcl1 and Cxcl5, were significantly induced upon *Mtb* HN878 infection at both 6 and 10 weeks post-infection in the absence of Lyl1 compared to WT.

It is known that *Mtb* bacterial growth can induce lung pathology [165]. It has also been reported that, simultaneously, *Mtb* can cause an undesired and ineffective inflammatory response to the lungs and thus resulting in severe lung damage [166]. Therefore, due to the increased lung bacterial burden and the increased neutrophil recruitment, a histopathological analysis using H&E staining to determine lung pathology/inflammation was performed on WT and Lyl1$^{-/-}$ lungs (*Figure 4.8*). With the increased bacterial burden and neutrophil recruitment in the lungs of Lyl1$^{-/-}$ mice, increased pathology and inflammation, especially at 10 weeks post-infection (*Figure 4.8 E*), was observed. This is directly proportional to the level of iNOS present in the highly inflamed lungs by which we observe a significant increase in iNOS levels in Lyl1-deficient lungs compared to WT (*Figure 4.8 F*). Thus, the data above suggests that the excessive neutrophil chemo-attractant secretion accompanied by increased neutrophil recruitment in the absence of Lyl1 could potentially be compromising the immune system for effective eradication of *Mtb* HN878.

4.4.5. Lyl1-deficient neutrophils, monocytes and macrophages experience a significantly different cytokine profile *in vivo* compared to WT in response to *Mtb* H37Rv infection

Given the significant increase in lung bacterial burden and changes observed in the myeloid populations of Lyl1-deficient mice, we investigated *Mtb* localization and individual cellular responses using fluorescent reporter mCherry-H37Rv strain. WT and Lyl1$^{-/-}$ mice were intranasally infected with mCherry-H37Rv at 230 CFU/mouse for 6 weeks. The increased CFU levels in Lyl1$^{-/-}$ mice exposed to the *Mtb* H37Rv laboratory strain compared to WT mice, indicates a greater susceptibility in the absence of Lyl1. *Mtb* H37Rv is less virulent than the hypervirulent W-Beijing lineage *Mtb* HN878 [167]. When comparing both the mCherry-H37Rv (*Figure 4.9 A*) and HN878 (*Figure 4.2 B*) 6 weeks post-infection results, it is clear that the *Mtb* H37Rv did not induce a strong phenotype and thus failed to provide a clear understanding of individual cell function. Therefore, when examining Mtb localization in the myeloid population (*Appendix C* with the addition of mCherry^{+}myeloid cell^{+}), the slight significant increase in bacterial load in response to *Mtb* H37Rv was not sufficient to identify potential differences in intracellular *Mtb* localization in individual *Mtb* infected myeloid cells since an even distribution of *Mtb* between WT and Lyl1$^{-/-}$ myeloid cells was observed (*Figure 4.9 B*). Differentially recruited myeloid cells (neutrophils, monocytes) and *Mtb*-harbouring macrophages were sorted after which RNA was extracted, cDNA was synthesized, and various gene expressions were analyzed by qPCR. Lyl1-deletion was confirmed across all sorted cell types (*Figure 4.9 C*). Interestingly, with an influx of neutrophils to the lung in the Lyl1$^{-/-}$ mice compared to the WT mice

(*Figure 4.5*), its signaling mechanisms were significantly downregulated in the absence of Lyl1. Aside from Tnf, which was notably increased in Lyl1-deficient neutrophils, these included Il10, Il6, Ifn1 and Nos2 (*Figure 4.9 D, F, G, K*). In addition, Lyl1-deficient monocytes expressed reduced IL-10, IL-6, Ifnb1, Il1α, as well as Tnf. Both alveolar and interstitial macrophages in Lyl1$^{-/-}$ mice expressed increased levels of Cxcl1 (*Figure 4.9 E*) which could potentially induce the influx of neutrophils to the site of infection. Interestingly, Il6 in Lyl1-deficient alveolar macrophages was significantly reduced in comparison to WT. However, this phenotype was completely reversed in interstitial macrophages whereby the level of Il6 in Lyl1-deficient mice is significantly increased compared to WT mice (*Figure 4.9 F*). Furthermore, alveolar and interstitial macrophages in Lyl1$^{-/-}$ lungs express reduced Il10 compared to WT lungs (*Figure 4.9 D*), in addition to reduced Ifnb1, Il1β and Nos2 in alveolar macrophages and Il1α in interstitial macrophages. Collectively, although the infection with mCherry-H37Rv did not induce a strong susceptibility phenotype, represented by CFU (*Figure 4.9 A*), in Lyl1$^{-/-}$ mice compared to *Mtb* HN878, it is evident that Lyl1-deficiency influences the proinflammatory gene expression profile of neutrophils, monocytes and macrophages which could contribute to disease progression. It is also noticeable that the expression profile for these eight genes analyzed in *Figure 4.9* differs within the myeloid subsets, indicating various effects of Lyl1-deficiency in these subsets, hence revealing a complex picture.

4.4.6. Lyl1 cannot be used as a biomarker for TB diagnosis

Given the significant changes in immunological responses to *Mtb* infection in the absence of Lyl1 in murine models, by accessing various cohort databases, we investigated if Lyl1 can be used as a biomarker for TB diagnosis. We initially investigated the gene signature profile comparing healthy, latently infected and active TB individuals in a Gambia, West Africa cohort (*Figure 4.10 A*) [168]. This data, in conjunction with a subsequent whole blood transcriptomics dataset examining specifically neutrophilic high-burdened TB patients in South Africa (SA) and the United Kingdom (UK) [169], revealed no changes in the gene expression of Lyl1 in the blood (*Figure 4.10 B*). Furthermore, to identify whether Lyl1 can be used as a biomarker for alternate acute diseases besides cancer and TB, we accessed a viral transcriptomics dataset and investigated Lyl1 expression in USA Rhinovirus and Influenza A infected patients [170]. Interestingly, systemic viral infections resulted in a significant downregulation in Lyl1 gene expression in both Rhinovirus and Influenza A infected patients as well as co-infected patients (*Figure 4.10 C*). Collectively, this data demonstrates that Lyl1 cannot be used as a biomarker for TB diagnosis. However, changes in Lyl1 gene expression in response to viral infections offers great potential for Lyl1 and viral diagnosis if the relationship between Lyl1 and viral pathogens are fully explored.

4.5. Discussion and Conclusion

With the downregulation of Lyl1 expression during *Mtb* HN878 infection observed in the BMDM CAGE transcriptomics data [103, 104] and the identification of a role for Lyl1 in bacterial infections using *Lm* (*Chapter 3, unpublished data*), we investigated the implications of *Mtb* HN878 infection in Lyl1-deficient BMDM and mouse models. Globally deleted Lyl1 mice succumbed to *Mtb* HN878 infection significantly sooner than WT mice, indicating host susceptibility in the absence of Lyl1 (*Figure 4.2 A*). In both an *in vitro* and an *in vivo* model, Lyl1-deficiency resulted in a significant increase in bacterial burden in macrophages (*Figure 4.1 A*), lung and spleen (*Figure 4.2 B*). However, this effect was only observed during more chronic stages. This was evident in vast immunological differences observed at 10 weeks post-infection compared to 3 weeks post-infection as well as a weaker response in mice infected with *Mtb* H37Rv (*Figure 4.9 A*) compared to *Mtb* HN878 (*Figure 4.2 B*) at 6 weeks post-infection.

One of the indications of host susceptibility was the visually smaller mediastinal lymph nodes in $Lyl1^{-/-}$ mice (data not shown) which was translated to the reduced number of cells present in the mediastinal lymph node (*Figure 4.2 E*). Given the comparable cell numbers observed in naïve WT and $Lyl1^{-/-}$ mice (*Chapter 2, unpublished data*), we can confidently express that the reduced number of cells in the lung draining lymph nodes is a consequence of the *Mtb* infection in Lyl1-knockout mice and not because of an underlying genetic defect. The direct mechanism as to how and why this occurred is unclear. However, since Lyl1 plays a significant role in T- and B-cell development [122], we thus hypothesized a decreased number of total lymph node cells due to reduced lymphoid cell recruitment to infected lymph nodes and lungs. Surprisingly, lymphoid cell percentages in the lymph nodes (*Figure S4.1, S4.2*) and lungs (*Figure 4.3, 4.4*) were comparable between WT and Lyl1-deficient mice aside from changes in lymph node T-cell memory (*Figure S4.2*). However, these changes in memory T-cells are not reflected at the site of infection as well as the slight changes observed in lung $CD8^{+}$ memory T-cells were not translated to cell numbers (*Figure 4.4 B*). Contrastingly, Lyl1-deficiency significantly influences myeloid cell recruitment to the lungs (*Figure 4.5*). The changes observed in Lyl1-deficient myeloid populations were rather pro-inflammatory as a significant induction of neutrophil and monocyte numbers were observed in the lungs of *Mtb*-infected mice, especially at 10 weeks post-infection (*Figure 4.5 A-B*). Similarly, a significant increase in macrophage percentage in Lyl1-deficient lymph nodes was observed (*Figure S4.3*). Thus, although there appears to be a significant decrease in the total number of cells present in the lymph node in response to *Mtb* infection, the percentage of cell subsets present in the lymph node are either comparable between the two genotypes or increased in $Lyl1^{-/-}$ mice.

This effect on the myeloid population was quite interesting since Lyl1 is known to serve a role in the development of T-lymphocytes. Additionally, greater immunological differences are observed at later,

chronic timepoints whereby the adaptive immunity is activated. Therefore, to determine the best timepoint to investigate differences in *Mtb* localization and individual cellular responses were challenging. Unfortunately, infecting WT and Lyl1$^{-/-}$ mice with mCherry-H37Rv for 6 weeks (*Figure 4.9 A*) was not enough to induce as a strong phenotype as *Mtb* HN878 (*Figure 4.2 A*). However, although *Mtb* appeared to infect and replicate at comparable levels between WT and Lyl1$^{-/-}$ mice (*Figure 4.9 A-B*), significant differences were observed in the individual cellular cytokine gene expression in the absence of this transcription factor compared to WT (*Figure 4.9 C-K*). Therefore, with an overall increase in inflammatory responses in the absence of Lyl1, both *in vitro* (*Figure 4.1 B-C*) and *in vivo* (*Figure 4.6 A-C*), in response to *Mtb* infection, it is evident that Lyl1-deficiency impacts various immunological responses during *Mtb* infection. Analyzing these differences in the cytokine profile *in vitro* and *in vivo* could assist in deciphering the cause of host susceptibility to *Mtb* infection.

It is well known that IL-1α and IL-1β are required to provide immunity against *Mtb* infection [171, 172]. However, these pro-inflammatory cytokines present in unregulated levels are also capable of driving pathology during *Mtb* infection [173, 174]. Further studies have also demonstrated the regulation of IL-1 by various interferons [172, 173, 175]. Mayer-Barber and co-authors describe the inhibition of monocyte, macrophage and dendritic cell-secreted IL-1 by type I interferons, whereas type II interferons only regulate IL-1 secreted by monocytes and macrophages in response to *Mtb* infection [172]. Here, we demonstrate significant changes in IL-1 and interferon expression levels between WT and Lyl1$^{-/-}$ mice in response to *Mtb*. We observe consistently increased IL-1α and IL-1β during *in vitro* (*Figure 4.1 B-C*) and chronic *in vivo* (*Figure 4.6 A-C*) infections. In our *in vitro* study, we observe IL-1 mRNA induction as early as 4 hours post-infection (*Figure 4.1 C*), suggesting that the upregulation of IL-1 is independent on CFU but rather dependent on the Lyl1 transcription factor. Given the inhibitory effects of interferon, it was interesting to observe an increase in IL-1 expression and IFNγ in Lyl1-deficient lungs at 6 weeks post-infection (*Figure 4.6 A*). However, according to Mayer-Barker and co-authors, IFNγ only regulates monocyte-macrophage secreting IL-1 [172]. Therefore, since we show that Lyl1-deficient monocytes and macrophages are defective in secreting IL-1 at 6 weeks post-infection (*Figure 4.9 I-J*), the induced IL-1 expression observed in Lyl1-deficient lungs at 6 weeks post-infection (*Figure 4.6 A*) could potentially be secreted from an alternate cell type. Thus, the observed induction of potentially regulative IFNγ is not reflected in reduced or regulated IL-1 expression in Lyl1$^{-/-}$ lungs at 6 weeks post-infection (*Figure 4.6 A*). However, at 10 weeks post-infection, we observe a significant downregulation of both IFNβ and IFNγ in Lyl1-deficient lungs, accompanied by uncontrollably increased levels of IL-1α and IL-1β (*Figure 4.6 A*). The shortage of interferon type I and II results in unregulated and overexpressed pro-inflammatory IL-1α and IL-1β. Since Lyl1-deficient monocytes and macrophages do not show increased expression of these cytokines *in vivo*, it is possible that augmented IL-1 secretion is sourced from dendritic cells [176]. Therefore, the

overexpression of these pro-inflammatory cytokines in Lyl1-deficient hosts could contribute to severe lung pathology during *Mtb* infection. This data supports a previous publication describing the overexpression of IL-1, as a consequence of iNOS depletion, leading to increased pathology and mortality in *Mtb*-infected mice [174].

Additionally, although we observe slightly induced levels of Nos2 in *Mtb*-infected Lyl1-deficient macrophages (*Figure 4.1 C*), as well as histopathological iNOS analysis at 6 and 10 weeks post-infection (*Figure 4.8 D, F*), a significant decrease in nitrite levels in Lyl1-deficient macrophages was observed (*Figure 4.1 B*). Nos2 functions in catalyzing the generation of nitric oxide (NO) by converting L-arginine to L-citrulline. However, this enzymatic process can be interrupted by arginase activity and in turn reduce the level of NO production by competing with iNOS/Nos2 for available L-arginine [177, 178]. Therefore, although we demonstrate a slight increase in Nos2 gene expression, the ability for it to synthesize NO has been inhibited in the absence of Lyl1. Given the described importance of Nos2 during *Mtb* infection [179], as well as the previous report describing Nos2-deficiency yielding increased IL-1 expression [174], this reduction in nitrite levels could potentially be a causative agent in promoting increased bacterial burden in $Lyl1^{-/-}$ macrophages *in vitro*. Furthermore, a reduction in NO has been shown to result in reduced apoptosis [180]. Therefore, the observed decrease in NO in $Lyl1^{-/-}$ macrophages (*Figure 4.1 B*) could reduce apoptosis and thus, further contributing to the increased bacterial burden in the absence of $Lyl1^{-/-}$. We also speculate that even though there are increased Nos2 mRNA levels, the decreased NO levels suggest that there is a decrease in the L-Arginine substrate. This would ultimately point toward increased arginase activity. On the other hand, the increased iNOS protein levels observed in tissue by immunohistochemistry staining can be the result of increased bacterial burdens in Lyl1-knockout mice (*Figure 4.8 D, F*).

Furthermore, although an increase in iNOS activity is observed in histopathological analysis, neutrophilic and alveolar macrophage Nos2 levels are significantly downregulated in the absence of Lyl1 (*Figure 4.9 K*). During *Mtb* infection, neutrophils are known for their ability to produce nitrogen intermediates to limit pathogen survival and dissemination, as well as function in phagocytosing the mycobacterium and facilitating in mycobacterial clearance [181]. Furthermore, alveolar macrophages are also known to induce nitrogen radicals as the first defenders against *Mtb* [178]. Therefore, the reduction in neutrophilic and alveolar macrophage Nos2 secretion ability in the absence of Lyl1 could contribute to significant host susceptibility. Interestingly, our data demonstrates significant neutrophil recruitment to Lyl1-deficient lungs during *Mtb* infection (*Figure 4.5 A-B*). This is supported by increased macrophage Cxcl1 expression and overall Cxcl1 and Cxcl5 upregulation in $Lyl1^{-/-}$ lungs at 6 and 10 weeks post-infection (*Figure 4.7 B-C*) [182, 183]. Additionally, an increase in neutrophilic TNFα (*Figure 4.9 H*) also supports the influx of neutrophils in the absence of Lyl1 since, along with many other immune cells, neutrophils are

also influenced by their own secreted products in an autocrine manner. This includes the secretion of TNFα to facilitate neutrophil migration and propagate inflammation to site of infection [184]. Additionally, an influx of neutrophils into *Mtb*-infected lungs has also been shown to promote mycobacterial progression and active disease [185]. Here, we demonstrate an increasing chemokine release (*Figure 4.7 B-C*) in conjunction with increased neutrophil recruitment (*Figure 4.5 A-B*) to the lungs of Lyl1$^{-/-}$ mice. This is accompanied by a reduction in Lyl1-deficient neutrophilic Nos2 levels (*Figure 4.9 K*). Thus, an increase in neutrophil recruitment, together with reduced cellular Nos2 production, would contribute to not only inflammation, but bacterial growth as well.

Given that alveolar macrophages are the first *Mtb* targeted cells [59], its inability to secrete nitric oxide (*Figure 4.9 K*) could ultimately aid in bacterial replication. One way to explain alveolar macrophage defectivity is the reduction of GM-CSF levels in the absence of Lyl1 (*Figure 4.6 C*). Previous reports have demonstrated a distinct relationship between GM-CSF, alveolar macrophages and bacterial clearance in the lungs [186, 187]. In the absence of GM-CSF, macrophages become more permissive to *Mtb* growth [97, 187] as GM-CSF has been shown to play a role in the proliferation, maintenance and function of alveolar macrophages [186, 188]. The reduction in GM-CSF levels in Lyl1-deficient lungs could result in defective alveolar macrophage function. This is evident in reduced alveolar macrophage cytokine secretion in Lyl1-deficient mice during *Mtb* infection (*Figure 4.9 D-K*), including IL-1β, which has been shown, at regulated levels, to play a significant role in providing protection against *Mtb* infection [189]. Furthermore, the requirement for GM-CSF for IL-6 production by macrophages has been shown [190], in addition to *Mtb* manipulating the immune response by inducing the release of IL-6 by *Mtb*-infected macrophages to limit the response of uninfected macrophages to IFNγ [191]. Therefore, the reduction in IL-6 in Lyl1-deficient alveolar macrophages could be a consequence of reduced GM-CSF (*Figure 4.9 F*).

Furthermore, changes in additional cytokines that are also indicative of Lyl1$^{-/-}$ host susceptibility include differential expression of IL-10. Many studies have shown that the induction of IL-10 reduces resistance against *Mtb* infection, by limiting effective inflammatory responses [192, 193]. However, contrasting reports have also described that the absence of IL-10 can promote *Mtb* progression given the lack of regulation of inflammatory responses [194] which is what we observe in Lyl1$^{-/-}$ mice. Lyl1-deficient neutrophils, monocytes as well as alveolar and interstitial macrophages all exhibit reduced anti-inflammatory IL-10 secretion abilities after 6 weeks post-infection (*Figure 4.9 D*). Therefore, potentially contributing, or lack thereof, to the inflammatory response observed in Lyl1-deficient mice. The conflicting IL-10 expression induction in Lyl1-deficient macrophages *in vitro* could be explained by the increasing severity of Lyl1-deletion with chronic disease. Furthermore, the induction of IL-10 is observed as early as 4 hours post *in vitro* infection and as the disease progressed at 12 hours, the induction of IL-10 compared

to WT is lost (*Figure 4.1 C*). Therefore, it is possible that Lyl1-deficient hosts' anti-inflammatory components become less effective with disease progression. This is further supported by the initial upregulation of IL-1 regulative IFNγ at 6 weeks post-infection, followed by reduced IFNγ at 10 weeks post-infection (*Figure 4.6 A*).

Although Lyl1-deficiency induces significant changes in the immune profile in response to *Mtb*, it cannot be used as a biomarker for TB in whole blood as various TB cohort studies demonstrate no difference in Lyl1 expression in whole blood between infected and healthy patients (*Figure 4.10 A-B*). This may be due to the fact that the effects of Lyl1-deficiency observed during chronic, hypervirulent environments are not necessarily systemically represented. Interestingly, we do observe Lyl1 gene expression changes in response to more acute systemically represented viral infections, suggesting a further role for this transcription factor in response to viral pathogens (*Figure 4.10 C*).

To conclude, Lyl1-deficient mice are significantly more susceptible to chronic hypervirulent *Mtb* HN878 infection. This is evident in significantly increased bacterial burden and multiple inflammatory responses including the upregulation of chemokines and pro-inflammatory cytokines in combination with increased neutrophilic recruitment to Lyl1-deficient lungs. Furthermore, Lyl1-deficient neutrophils and macrophages appear to be defective in producing Nos2 which could contribute to the inability of $Lyl1^{-/-}$ mice to eradicate *Mtb*. Since the inflammatory response observed in the lungs is not only sourced from macrophages and neutrophils, it would be interesting to investigate the functionality of the lymphoid population. Although there are no differences in lymphoid cell recruitment between WT and $Lyl1^{-/-}$ mice, given the significant changes in immune profile observed in the absence of this transcription factor and the role it plays in T-cell development, it is possible that the functionality of these lymphoid cells could play a significant role in contributing to host susceptibility. Collectively, we demonstrate a significant requirement for Lyl1 in the ability to control *Mtb* infection in mouse models and that the absence of this transcription factor promotes disease progression by facilitating uncontrolled inflammatory responses. Therefore, it is possible that Lyl1 has regulatory potential by interacting with various components of the immune system to control *Mtb* infection. Thus, although further investigation in discovering the mechanism by which Lyl1 limits *Mtb* progression is required, our data highlights this key transcription factor and the potential of its surrounding immune regulators to serve as an HDT target for TB.

4.6. Acknowledgements

We express gratitude to the UCT Animal Research Facility and Ms. Munadia Ansarie for the breeding, genotyping and maintenance of mice as well as the technical staff. Ms. Zarinah Sonday, Mr. Marlon

Petersen and Mr. George Jacobs for the maintenance of the laboratory. Furthermore, we thank Ms. Lizette Fick and Ms. Raygaana Jacobs for their excellent histological services.

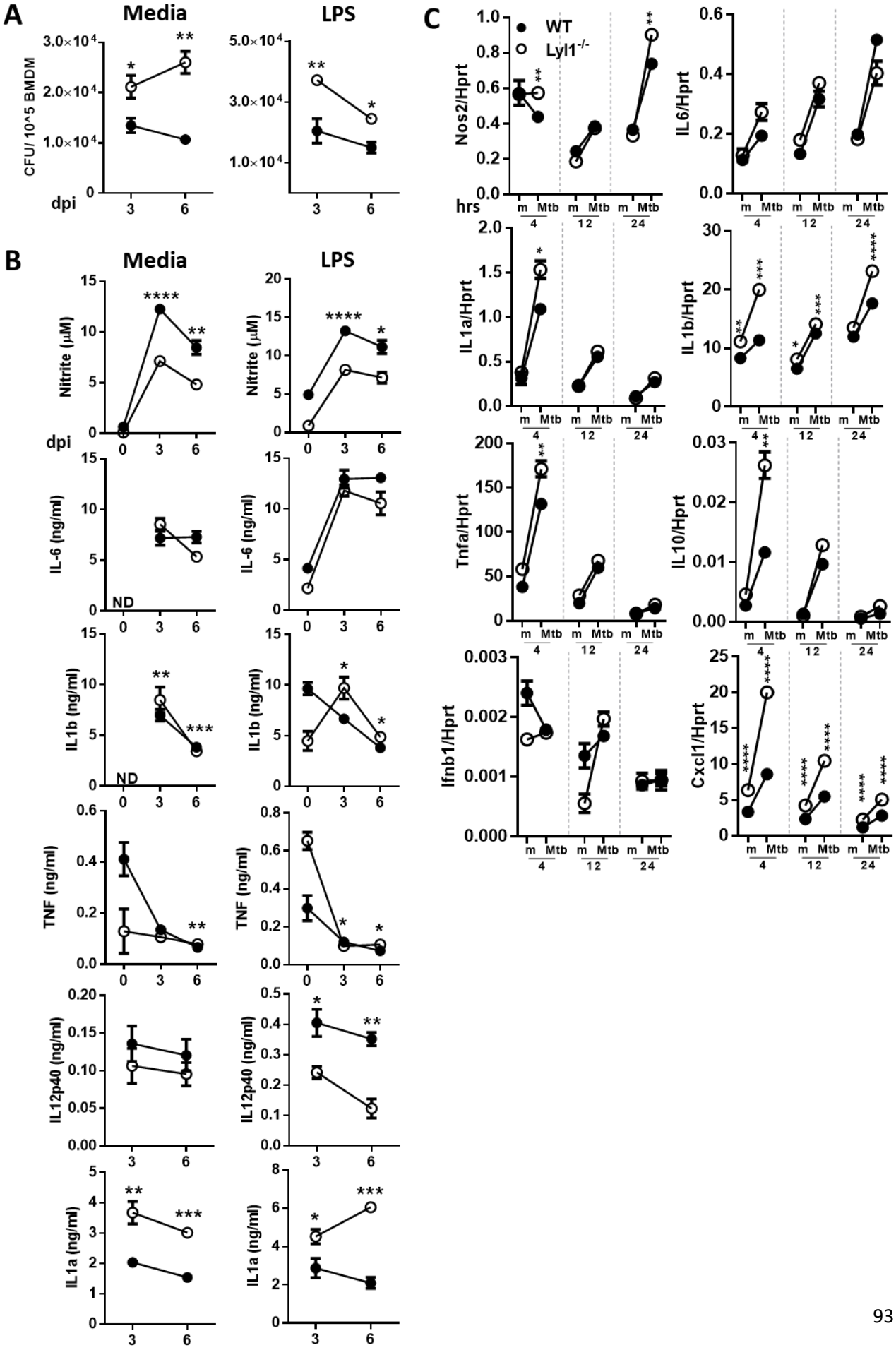
A
Media
LPS
CFU/ 10^5 BMDM
dpi
B
Media
LPS
Nitrite (μM)
IL-6 (ng/ml)
IL1b (ng/ml)
TNF (ng/ml)
IL12p40 (ng/ml)
IL1a (ng/ml)
ND
C
WT
Lyl1-/-
hrs
Nos2/Hprt
IL6/Hprt
IL1a/Hprt
IL1b/Hprt
Tnfa/Hprt
IL10/Hprt
Ifnb1/Hprt
Cxcl1/Hprt
m
Mtb

Figure 4.1. **Lyl1-deficiency increases macrophage bacterial burden with differential effects on proinflammatory gene expression in response to hypervirulent *Mtb* HN878 *in vitro*.** Bone marrow cells of naïve wild-type (WT) and Lyl1$^{-/-}$ mice were harvested and differentiated for relative experiments. **(A-B)** Bone marrow-derived macrophage (BMDM) cells were subjected to either media or 100 ng/ml LPS after which they were infected with *Mtb* HN878 with MOI:1. **(A)** Lysed cells (3 or 6 days post infection) were plated for intracellular bacterial burden and **(B)** supernatants (3 or 6 days post infection) were collected for cytokine production by ELISA. **(C)** RNA was collected from WT and Lyl1$^{-/-}$ BMDM infected with *Mtb* HN878 (MOI:1) at 4, 12 and 24 hours, synthesized to cDNA by two-step PCR and subjected to qPCR for mRNA expression. Data represented demonstrates technical replicates and the error bar denotes Mean ±SEM. If no variation detected in technical replicates, no error bar is displayed. Data shown is representative of 2-4 independent experiments. Unpaired student t-test analysis at $*p < 0.05$, $**p < 0.01$, $***p < 0.001$, $****p < 0.0001$ to determine significance.

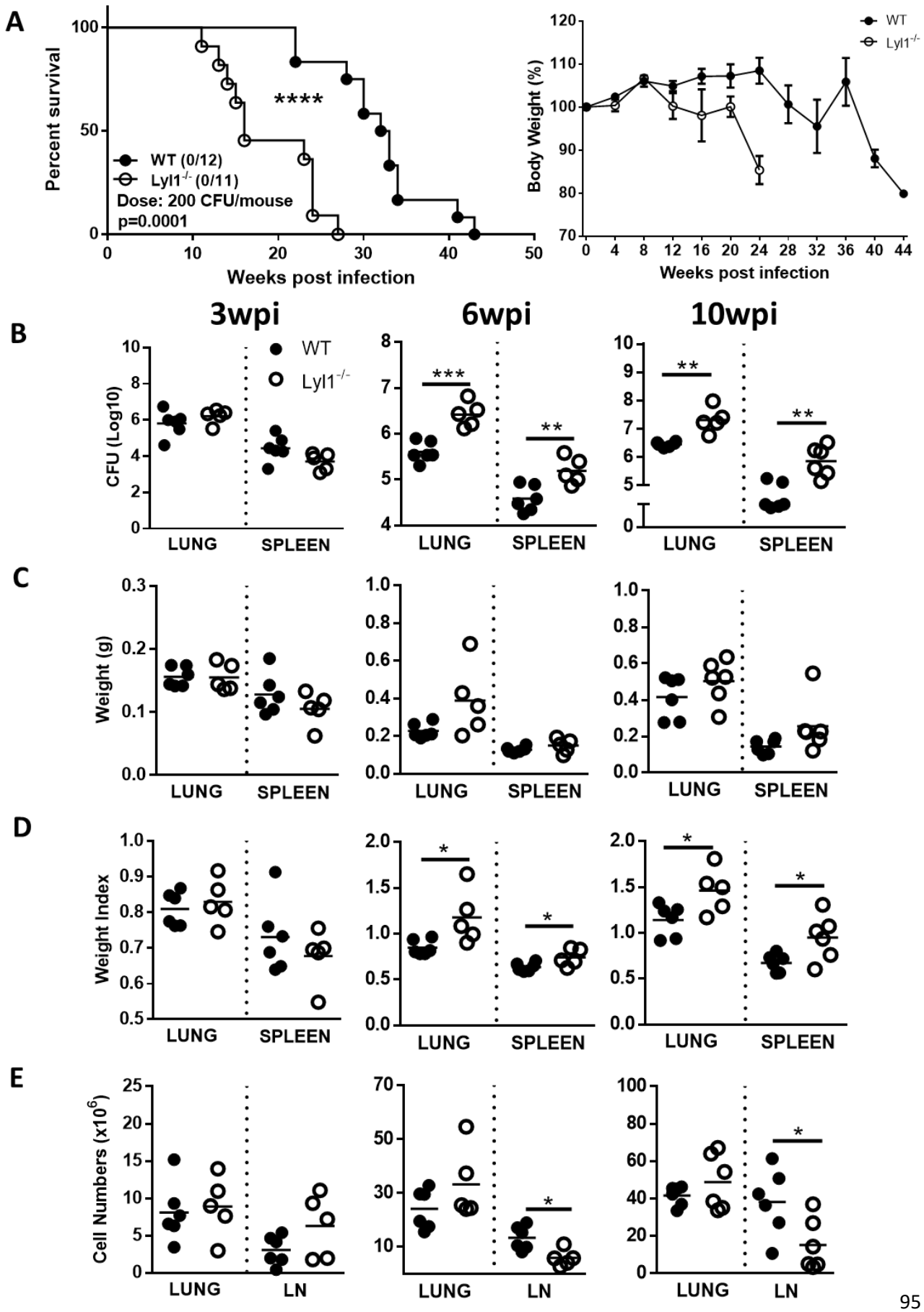
A
Percent survival
Weeks post infection
****
WT (0/12)
Lyl1-/- (0/11)
Dose: 200 CFU/mouse
p=0.0001
Body Weight (%)
WT
Lyl1-/-
Weeks post infection
B
3wpi
6wpi
10wpi
CFU (Log10)
WT
Lyl1-/-
LUNG
SPLEEN
C
Weight (g)
D
Weight Index
E
Cell Numbers (x10^6)
LUNG
LN

Figure 4.2. **Lyl1-deletion renders increased susceptibility to hypervirulent *Mtb* HN878 infection *in vivo*.** **(A)** Survival study. Littermate control (WT) and Lyl1$^{-/-}$ mice were intranasally infected with *Mtb* HN878 at 200 CFU/mouse (n = 11-12 mice/group). Mantel-Cox survival analysis with log-rank test P = 0.0001, WT vs Lyl1$^{-/-}$. **(B-E)** WT and Lyl1$^{-/-}$ mice were infected with 100 CFU/mouse intranasally with *Mtb* HN878 (n = 5-6 mice/group) and sacrificed at either 3-, 6- or 10- weeks post infection to determine **(B)** lung and spleen CFU burden, **(C)** lung and spleen weight and **(D)** weight index and **(E)** lung and lymph node cell numbers. Line denotes Mean. Data shown is representative of 2-4 independent experiments. Unpaired student t-test analysis at *$p < 0.05$, **$p < 0.01$, ***$p < 0.001$ to determine significance.

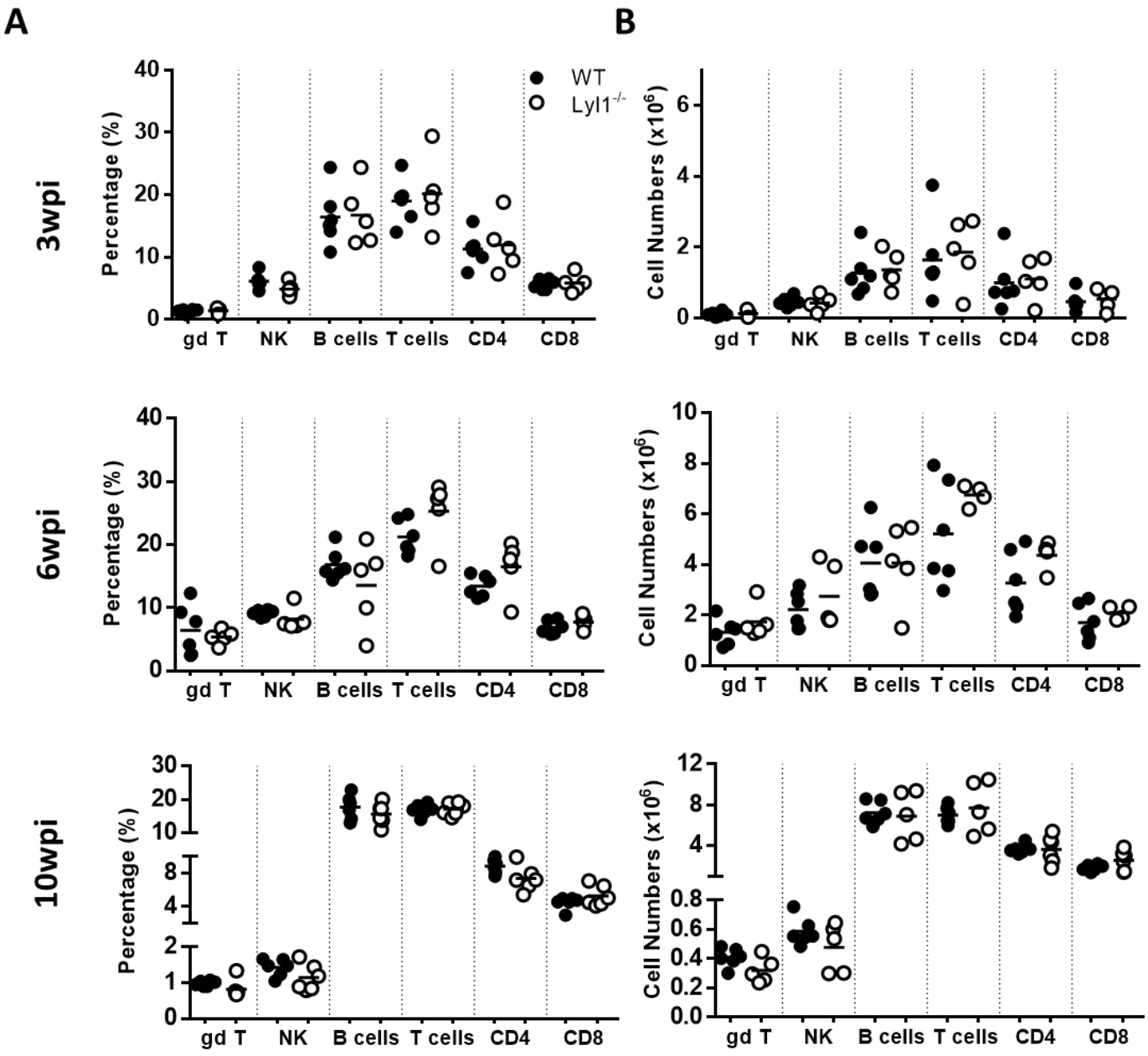

Figure 4.3. **No differences in the lung lymphoid population is observed after hypervirulent *Mtb* HN878 infection in the absence of Lyl1**. **(A-B)** Littermate control (WT) and Lyl1$^{-/-}$ mice were infected with 100 CFU/mouse intranasally with *Mtb* HN878 (*n* = 5-6 mice/group) and sacrificed at either 3-, 6- or 10-weeks post infection. Using flow cytometry, single cell suspension of lung tissue was analyzed for **(A)** percentage and **(B)** total cell numbers of the lymphoid cell population at indicated timepoints. Surface markers of the different cell populations are as follows (according to the gating strategy ***Appendix B***): gamma delta T-cells (gd T) = CD3$^+$gdTCR$^+$; NK cells = NK1.1$^+$CD3$^-$; B-cells = CD19$^+$CD3$^-$; T-cells = CD3$^+$CD19$^-$; CD4$^+$ T-cells = CD3$^+$CD4$^+$; CD8$^+$ T-cells = CD3$^+$CD8$^+$. Line denotes Mean. Data shown is representative of 2-3 independent experiments.

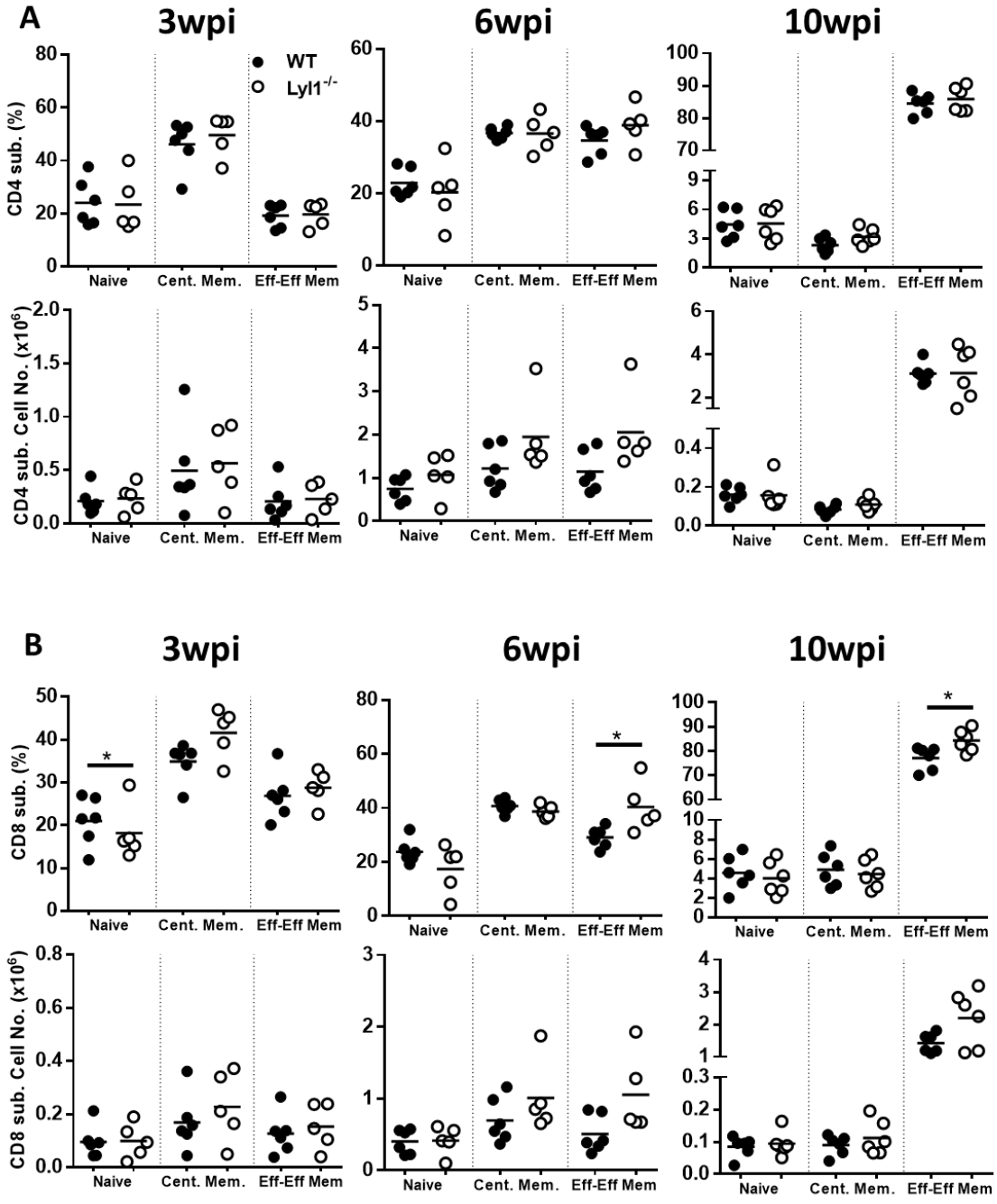

Figure 4.4. **Lyl1-deficiency does not impair lung T-cell memory in response to *Mtb* HN878 infection.** **(A-B)** Littermate control (WT) and Lyl1$^{-/-}$ mice were infected with 100 CFU/mouse intranasally with *Mtb* HN878 (*n* = 5-6 mice/group) and sacrificed at either 3-, 6- or 10-weeks post infection. Using flow cytometry, single cell suspension of lung tissue was analyzed for percentage and absolute cell numbers of the **(A)** lung CD4$^+$ T-cell and **(B)** CD8$^+$ T-cell subset at indicated timepoints. Surface markers of the different cell populations are as follows (according to the gating strategy ***Appendix B***): CD4$^+$ naïve = CD3$^+$CD4$^+$CD62L$^+$CD44$^-$; CD4$^+$ Central Memory = CD3$^+$CD4$^+$CD62L$^+$CD44$^+$; CD4$^+$ Effector/Effector Memory = CD3$^+$CD4$^+$CD44$^+$CD62L$^-$; CD8$^+$ naïve = CD3$^+$CD8$^+$CD62L$^+$CD44$^-$; CD8$^+$ Central Memory = CD3$^+$CD8$^+$CD62L$^+$CD44$^+$; CD8$^+$ Effector/Effector Memory = CD3$^+$CD8$^+$CD44$^+$ CD62L$^-$. Line denotes Mean. Data shown is representative of 2-3 independent experiments. Unpaired student t-test analysis at *$p < 0.05$ to determine significance.

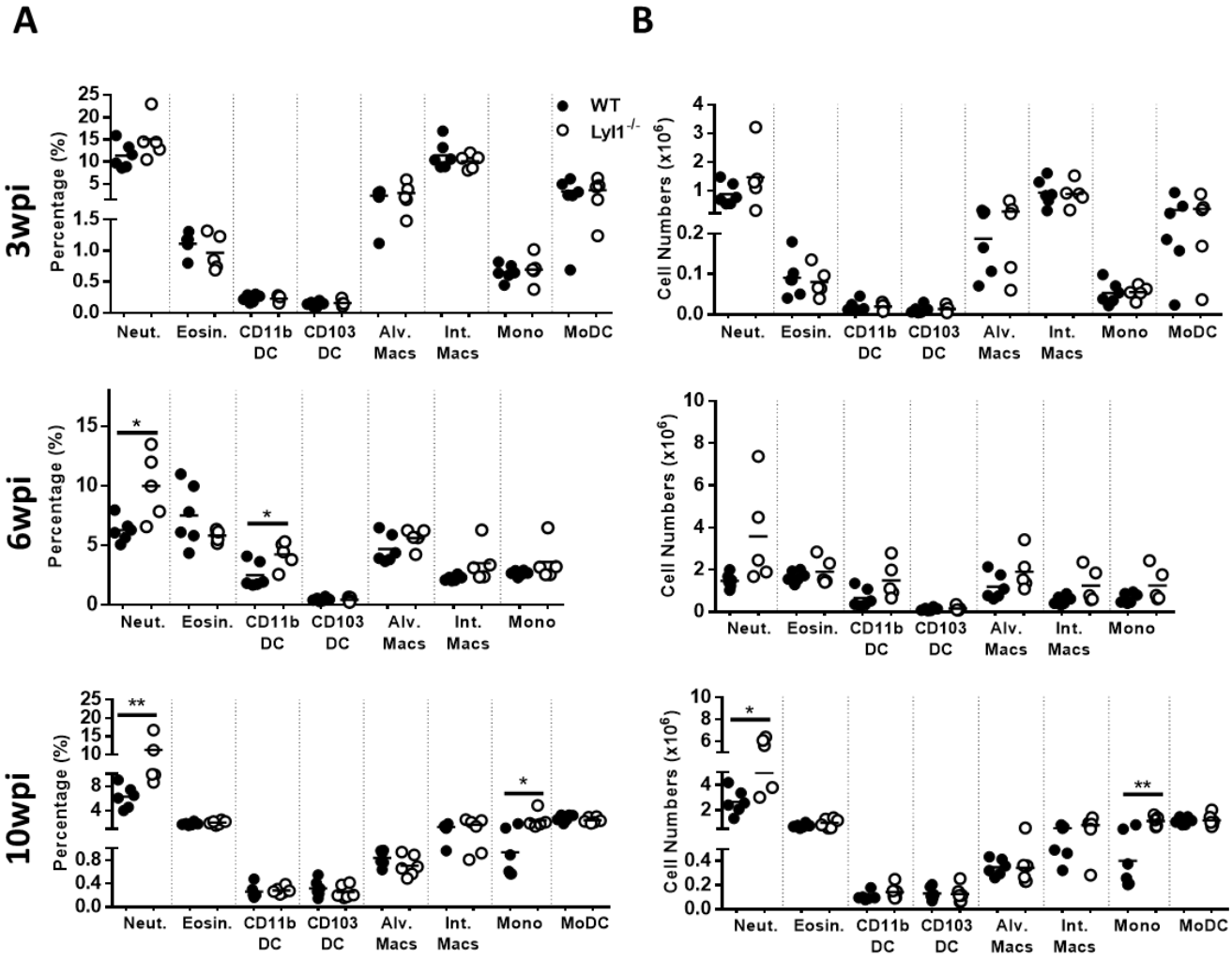

Figure 4.5. **Lyl1-deletion enhances lung neutrophil and monocyte recruitment in response to chronic hypervirulent *Mtb* HN878 *in vivo*. (A-B)** Littermate control (WT) and Lyl1$^{-/-}$ mice were infected with 100 CFU/mouse intranasally with *Mtb* HN878 (n = 5 mice/group) and sacrificed at either 3-, 6- or 10-weeks post infection. Using flow cytometry, single cell suspension of lung tissue was analyzed for **(A)** percentage and **(B)** total cell numbers of the myeloid cell population at indicated timepoints. Surface markers of the different cell populations are as follows (according to the gating strategy ***Appendix C***): Neutrophils (Neut.) = Ly6G$^+$CD11b$^+$; Eosinophils (Eosin.) = SiglecF$^+$CD11b$^+$CD64$^-$; CD11b$^+$ DC = CD11c$^+$MHCII$^+$CD11b$^+$CD64$^-$; CD103$^+$ DC = CD11c$^+$MHCII$^+$CD103$^+$CD64$^-$; Alveolar Macrophages (Alv. Macs) = CD64$^+$MerTK$^+$SiglecF$^+$CD11c$^+$; Interstitial Macrophages (Int. Macs) = CD64$^+$MerTK$^+$SiglecF$^+$CD11b$^+$ CD11c$^-$; Monocytes (Mono) = Ly6G$^+$CD11b$^+$CD64$^-$; Monocyte-derived DC (MoDC) = CD64$^+$CD11b$^+$CD11c$^+$. Line denotes Mean. Data shown is representative of 2-3 independent experiments. Unpaired student t-test analysis at *$p < 0.05$, **$p < 0.01$ to determine significance.

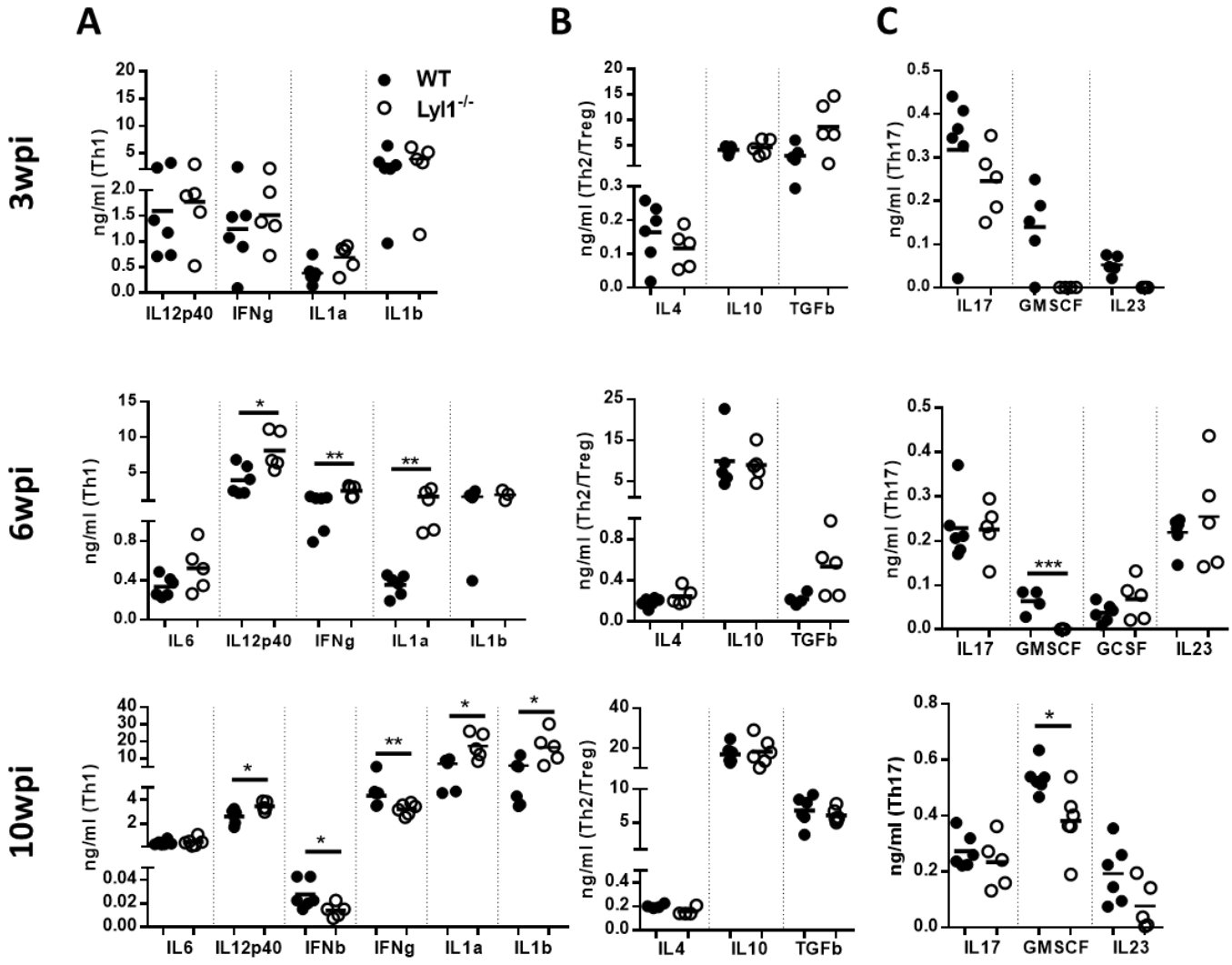

Figure 4.6. **Lyl1-deletion promotes inflammatory responses during chronic hypervirulent *Mtb* HN878 *in vivo*. (A-C)** Littermate control (WT) and Lyl1$^{-/-}$ mice were infected with 100 CFU/mouse intranasally with *Mtb* HN878 (n = 5 mice/group) and sacrificed at either 3-, 6- or 10-weeks post infection. Supernatants from lung homogenates were analyzed by means of ELISA for **(A)** Th1 cytokines, **(B)** Th2 and T regulating cytokine, **(C)** and finally Th17 cytokines. Line denotes Mean. Data shown is representative of 2-3 independent experiments. Unpaired student t-test analysis at *p < 0.05, **p < 0.01 to determine significance.

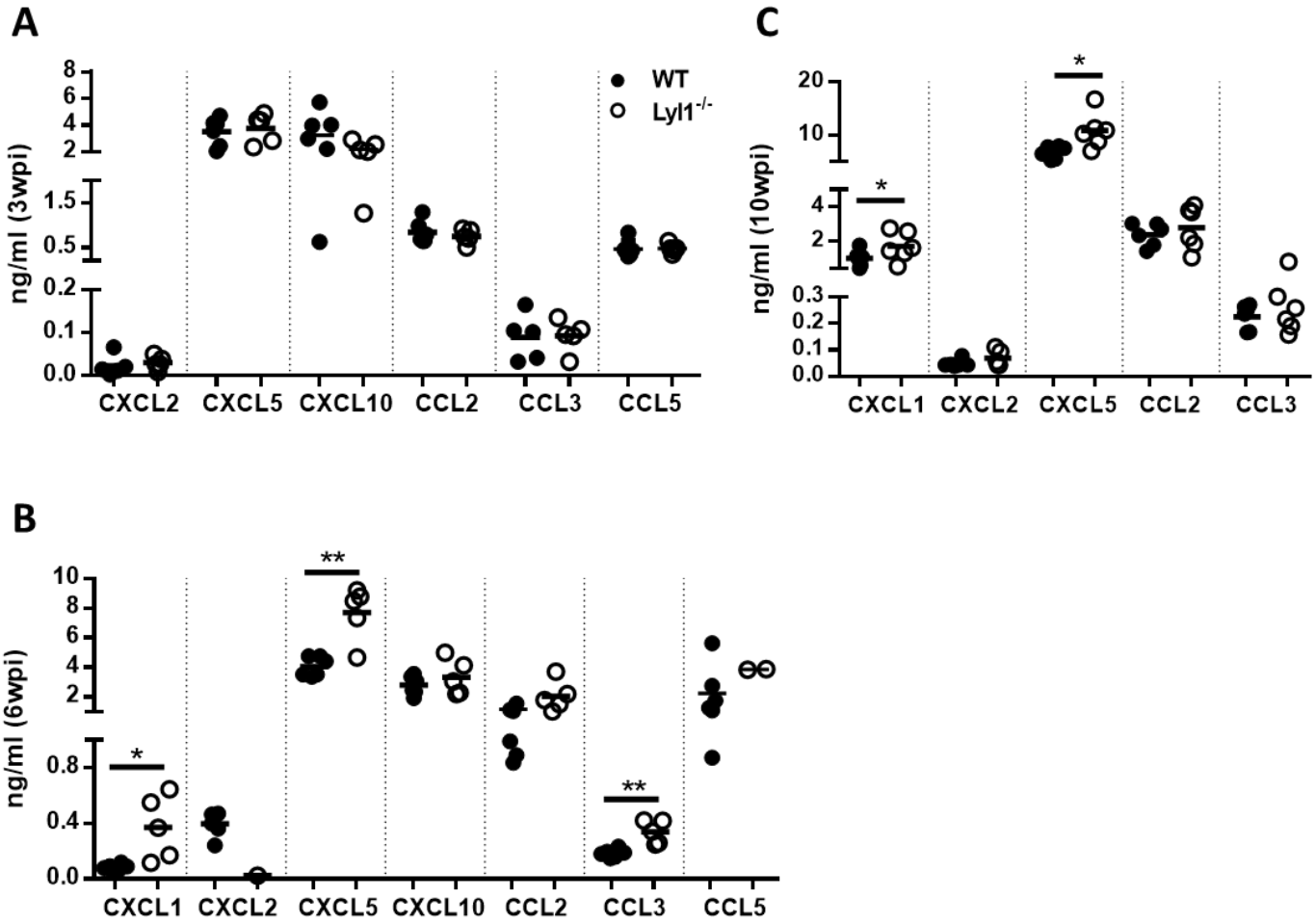

Figure 4.7. **Lyl1-deletion induces CXCL1 and CXCL5 levels in response to chronic hypervirulent *Mtb* HN878 *in vivo*. (A-C)** Littermate control (WT) and Lyl1$^{-/-}$ mice were infected with 100 CFU/mouse intranasally with *Mtb* HN878 (n = 5 mice/group) and sacrificed at either 3-, 6- or 10-weeks post infection. Supernatants from lung homogenates were analyzed, by ELISA, for chemokine release at **(A)** 3 weeks post infection, **(B)** 6 weeks post infection and **(C)** 10 weeks post infection. Line denotes Mean. Data shown is representative of 2-3 independent experiments. Unpaired student t-test analysis at *$p < 0.05$, **$p < 0.01$ to determine significance.

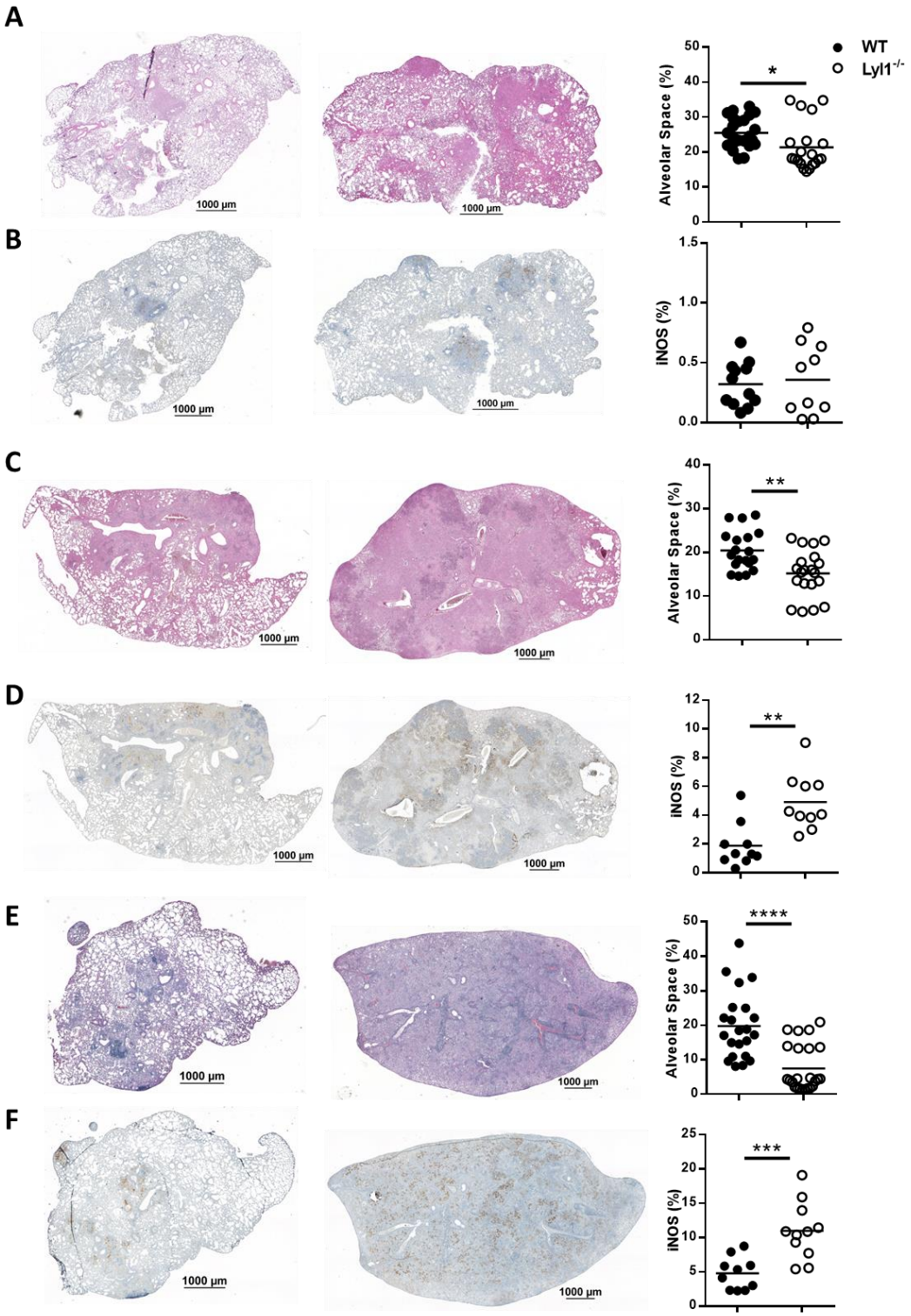

Figure 4.8. **Lyl1-deficiency induces severe lung inflammation during chronic hypervirulent *Mtb* HN878 infection. (A-F)** Littermate control (WT) and Lyl1$^{-/-}$ mice were infected with 100 CFU/mouse intranasally with *Mtb* HN878 (n = 5 mice/group) and sacrificed at either 3-, 6- or 10-weeks post infection. Representative H&E histopathology lung section (20x) along with quantification at **(A)** 3 weeks post infection, **(C)** 6 weeks post infection and **(E)** 10 weeks post infection. Representative iNOS histopathology lung section (10x) along with quantification at **(B)** 3 weeks post infection, **(D)** 6 weeks post infection and **(F)** 10 weeks post infection. Line denotes Mean. Data shown is representative of 2-3 independent experiments. Unpaired student t-test analysis at *$p < 0.05$, **$p < 0.01$, ***$p < 0.001$, ****$p < 0.0001$ to determine significance.

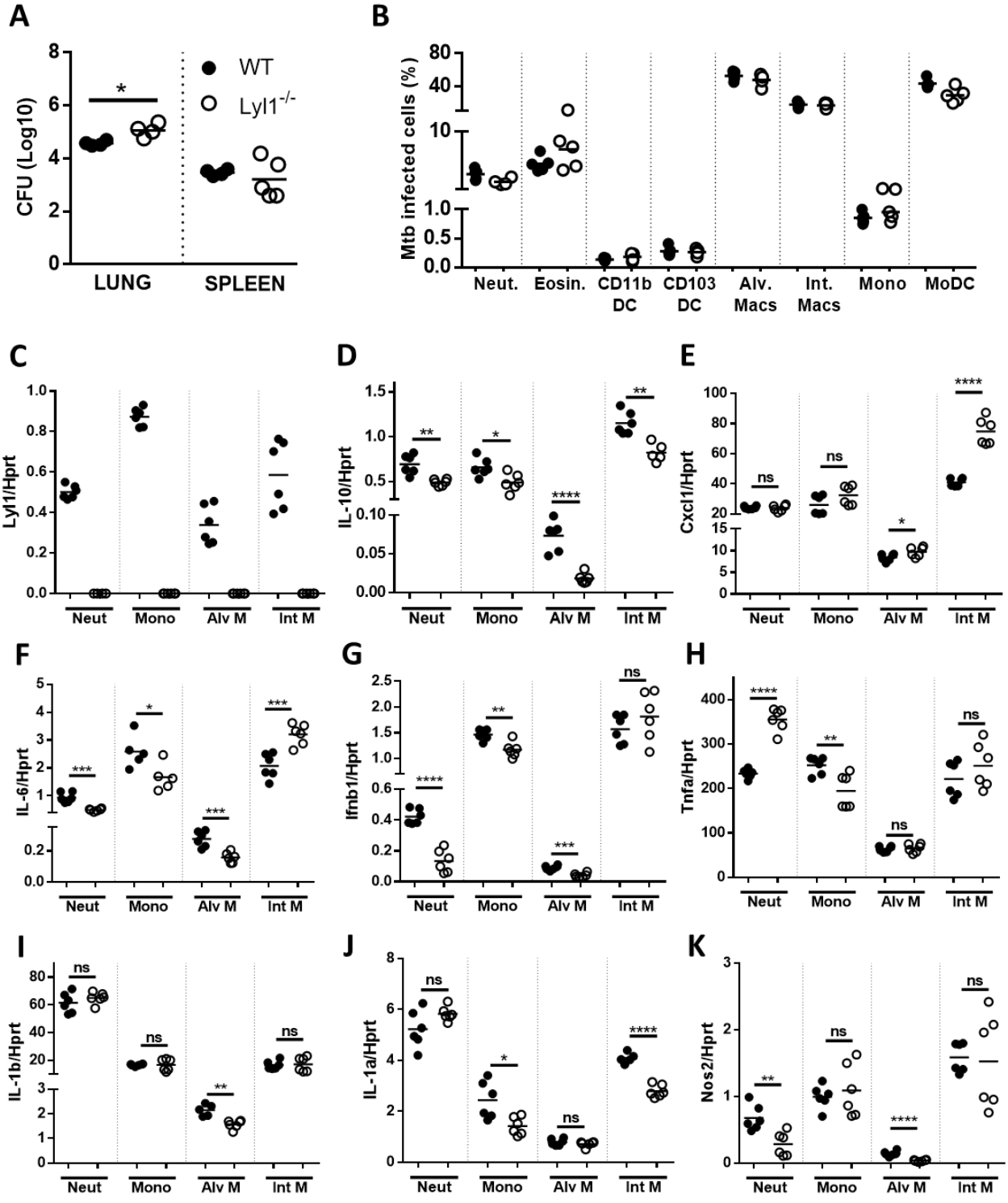

Figure 4.9. **Lyl1-deficiency alters myeloid cell cytokine gene expression in response to *Mtb* H37Rv.** Littermate control (WT) and Lyl1$^{-/-}$ mice were intranasally infected with mCherry tagged H37Rv *Mtb* at 230 CFU/mouse (n = 5 mice/group) and sacrificed at 6 weeks post infection. **(A)** Bacterial burden using lung and spleen homogenates. **(B)** Flow cytometric analysis of single cell suspended lung tissue to assess

for individually infected cells using the following markers (according to the gating strategy ***Appendix C***): Neutrophils (Neut.) = mCherry^{+}Ly6G^{+}CD11b^{+}; Eosinophils (Eosin.) = mCherry^{+}SiglecF^{+}CD11b^{+}CD64^{-}; CD11b^{+} DC = mCherry^{+}CD11c^{+}MHCII^{+}CD11b^{+}CD64^{-}; CD103^{+} DC = mCherry^{+}CD11c^{+}MHCII^{+}CD103^{+}CD64^{-}; Alveolar Macrophages (Alv. Macs) = mCherry^{+}CD64^{+}MerTK^{+}SiglecF^{+}CD11c^{+}; Interstitial Macrophages (Int. Macs) = mCherry^{+}CD64^{+}MerTK^{+}SiglecF^{+}CD11b^{+} CD11c^{-}; Monocytes (Mono) = mCherry^{+}Ly6G^{+}CD11b^{+}CD64^{-}; Monocyte-derived DC (MoDC) = mCherry^{+}CD64^{+}CD11b^{+}CD11c^{+}. **(C-K)** The mRNA profile performed by qPCR on sorted cells including neutrophils (neut.), monocytes (mono), alveolar macrophages (alv M) and interstitial macrophages (int M). Line denotes Mean. Data shown is representative of 2 independent experiments. Unpaired student t-test analysis at *$p < 0.05$, **$p < 0.01$, ***$p < 0.001$, ****$p < 0.0001$ to determine significance.

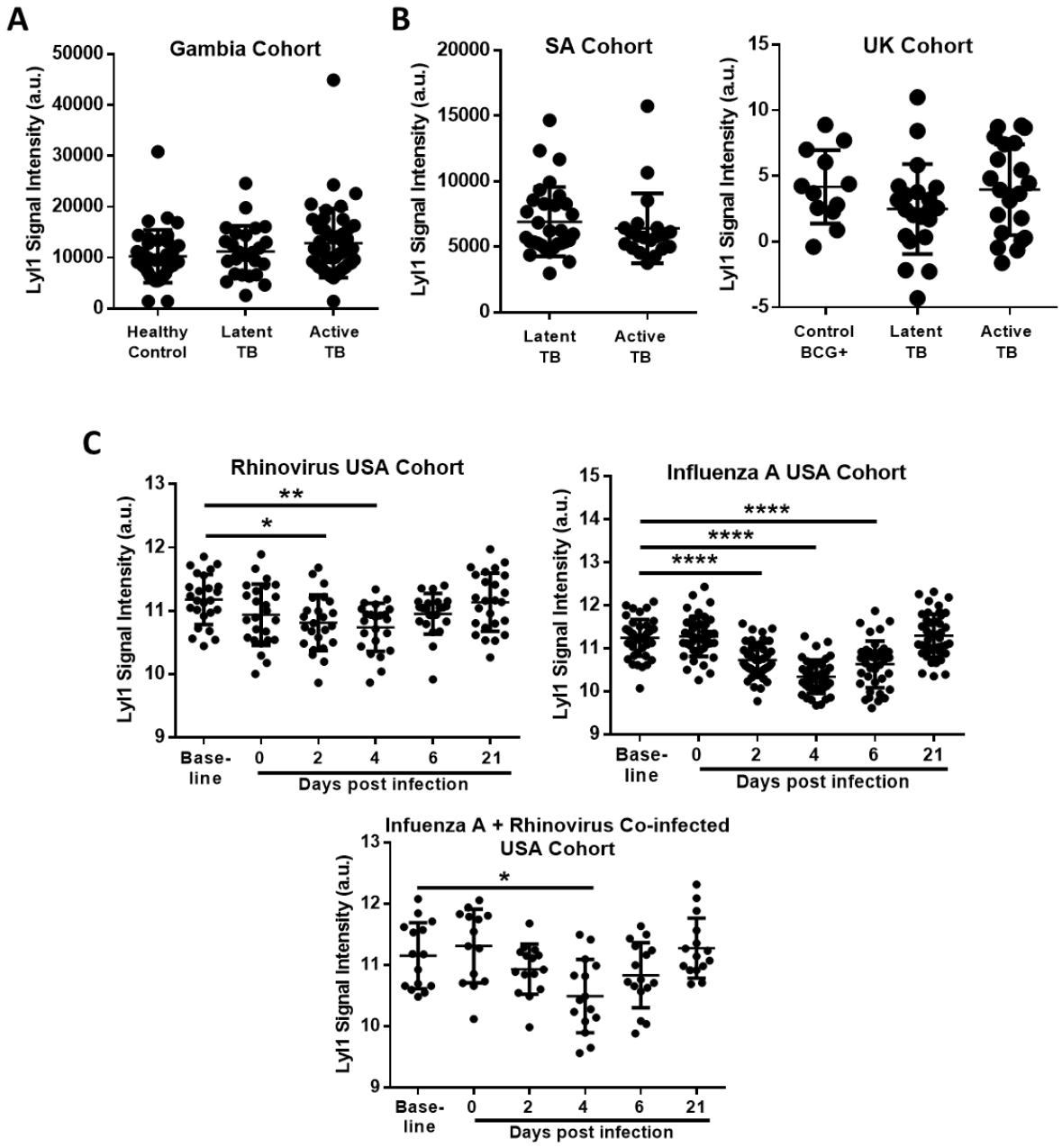

Figure 4.10. **Lyl1 cannot be used as a biomarker for TB diagnosis but has great potential for viral infected patients.** All represented data was extracted from publicly available databases. **(A)** Data was manually extracted, organized and sorted from the publicly available TB Gambia Cohort (PMID 22046420). **(B)** Data was manually extracted, organized and sorted from the publicly available TB South Africa (SA) and United Kingdom (UK) Cohort (PMID 20725040). **(C)** Data was manually extracted, organized and sorted from the publicly available USA Rhinovirus and Influenza A Cohort (PMID 26070066). Kruskal-Wallis test analysis at $*p < 0.05$, $**p < 0.01$, $***p < 0.001$, $****p < 0.0001$ to determine significance.

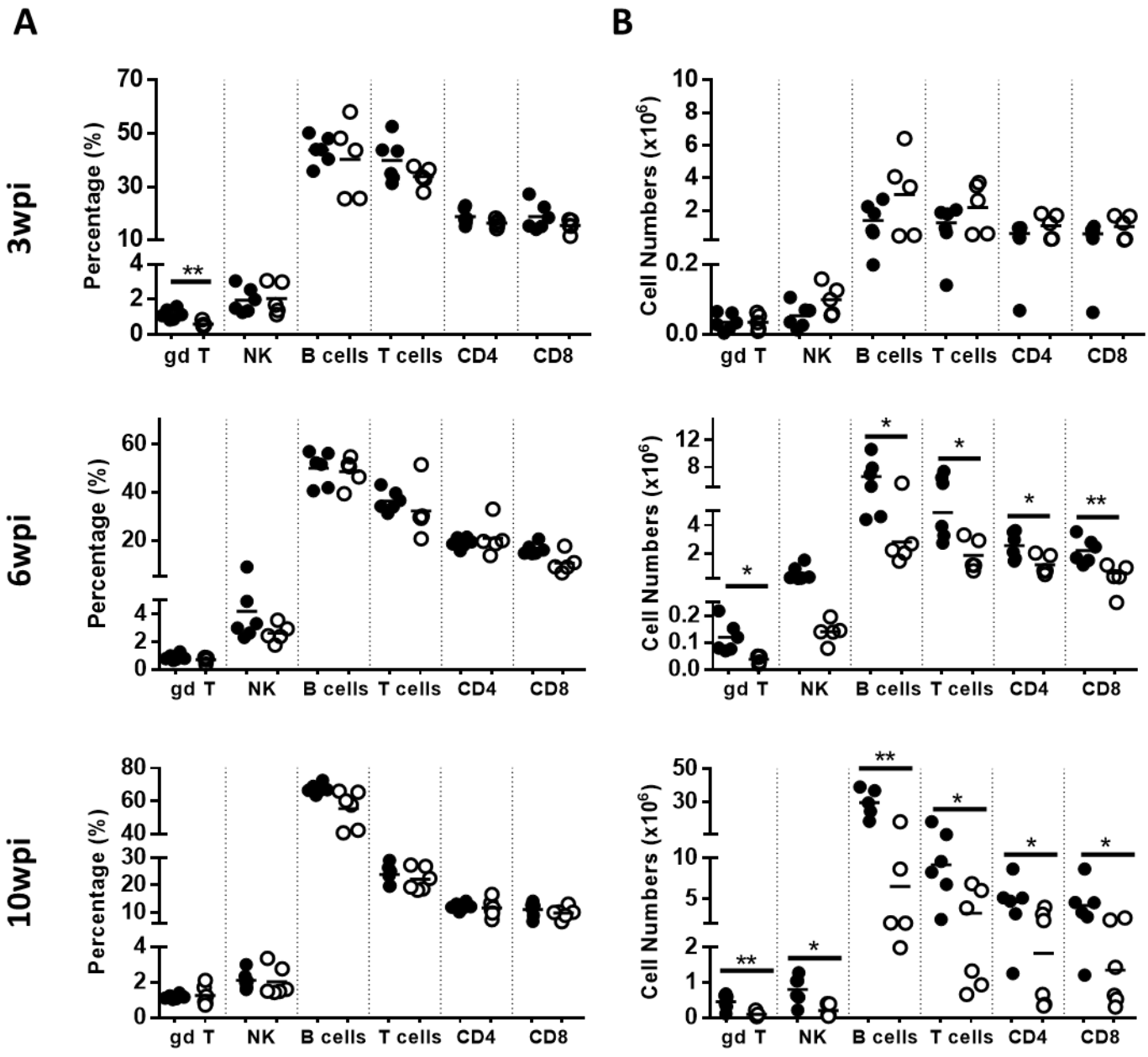

Figure S4.1. **No changes in the lymph node (LN) lymphoid population was observed after hypervirulent *Mtb* HN878 infection (*in vivo*) in the absence of Lyl1**. **(A-B)** Littermate control (WT) and Lyl1$^{-/-}$ mice were infected with 100 CFU/mouse intranasally with *Mtb* HN878 (n = 5 mice/group) and sacrificed at either 3-, 6- or 10-weeks post infection. Using flow cytometry, single cell suspension of LN tissue was analyzed for **(A)** percentage and **(B)** total cell numbers of the lymphoid cell population at indicated timepoints. Surface markers of the different cell populations are as follows (according to the gating strategy in ***Appendix B***): gamma delta T-cells (gd T) = CD3$^+$gdTCR$^+$; NK cells = NK1.1$^+$CD3$^-$; B-cells = CD19$^+$CD3$^-$; T-cells = CD3$^+$CD19$^-$; CD4$^+$ T-cells = CD3$^+$CD4$^+$; CD8$^+$ T-cells = CD3$^+$CD8$^+$. Line denotes Mean. Data shown is representative of 2-3 independent experiments. Student t-test analysis at *$p < 0.05$, **$p < 0.01$ to determine significance.

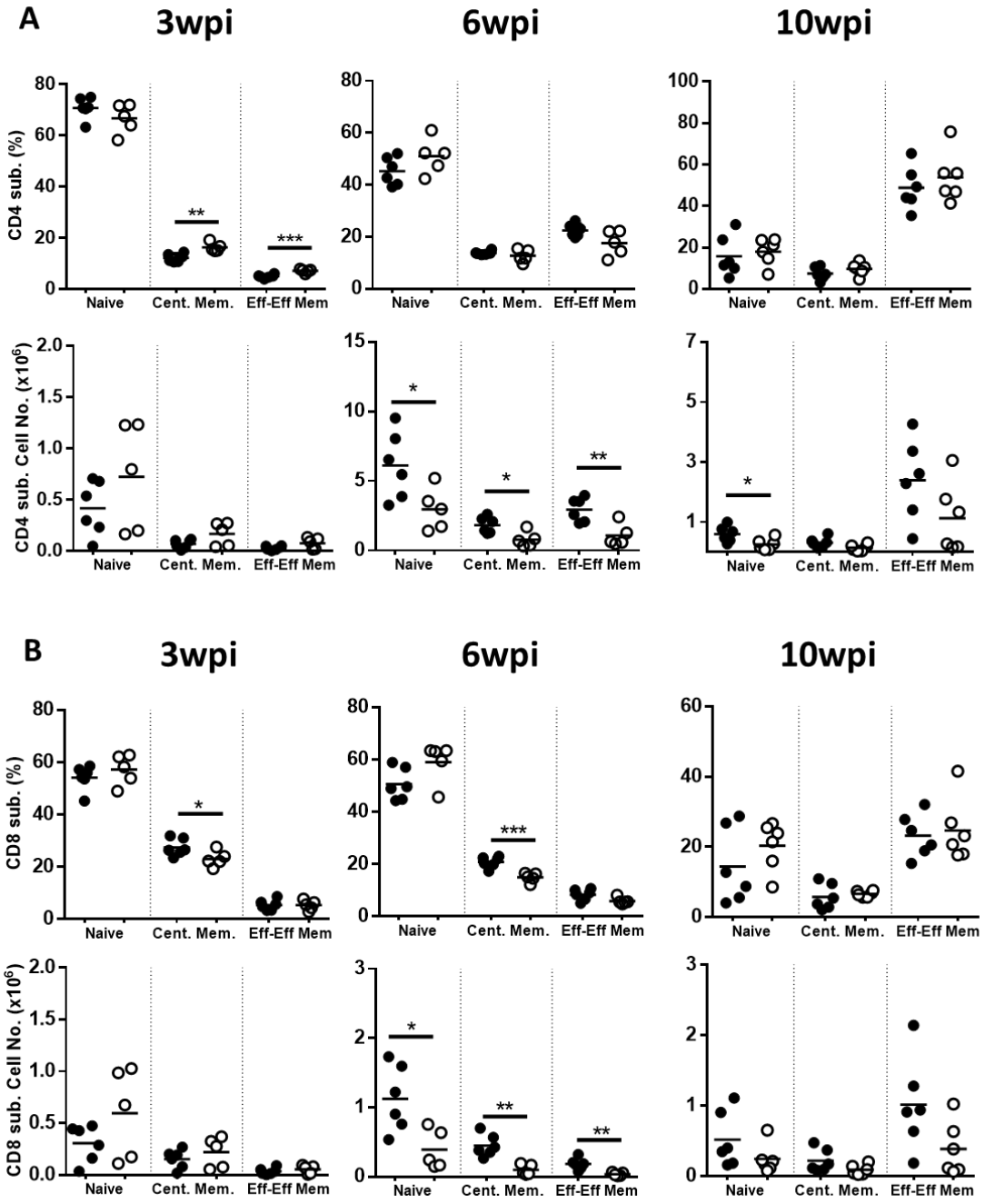

Figure S4.2. **Changes in T-cell memory was observed in Lyl1$^{-/-}$ lymph nodes (LN) after hypervirulent *Mtb* HN878 infection**. **(A-B)** Littermate control (WT) and Lyl1$^{-/-}$ mice were infected with 100 CFU/mouse intranasally with *Mtb* HN878 (n = 5 mice/group) and sacrificed at either 3-, 6- or 10-weeks post infection. Using flow cytometry, single cell suspension of LN tissue was analyzed for percentage and total cell numbers of the LN **(A)** CD4$^+$ T-cell and **(B)** CD8$^+$ T-cell subset lymphoid cell population at indicated timepoints. Surface markers of the different cell populations are as follows (according to the gating strategy in ***Appendix B***): CD4$^+$ naïve = CD3$^+$CD4$^+$CD62L$^+$CD44$^-$; CD4$^+$ Central Memory = CD3$^+$CD4$^+$CD62L$^+$CD44$^+$; CD4$^+$ Effector/Effector Memory = CD3$^+$CD4$^+$CD44$^+$CD62L$^-$; CD8$^+$ naïve = CD3$^+$CD8$^+$CD62L$^+$CD44$^-$; CD8$^+$ Central Memory = CD3$^+$CD8$^+$CD62L$^+$CD44$^+$; CD8$^+$ Effector/Effector Memory = CD3$^+$CD8$^+$CD44$^+$ CD62L$^-$. Line denotes Mean. Data shown is representative of 2-3 independent experiments. Student t-test analysis at *$p < 0.05$, **$p < 0.01$, ***$p < 0.001$ to determine significance.

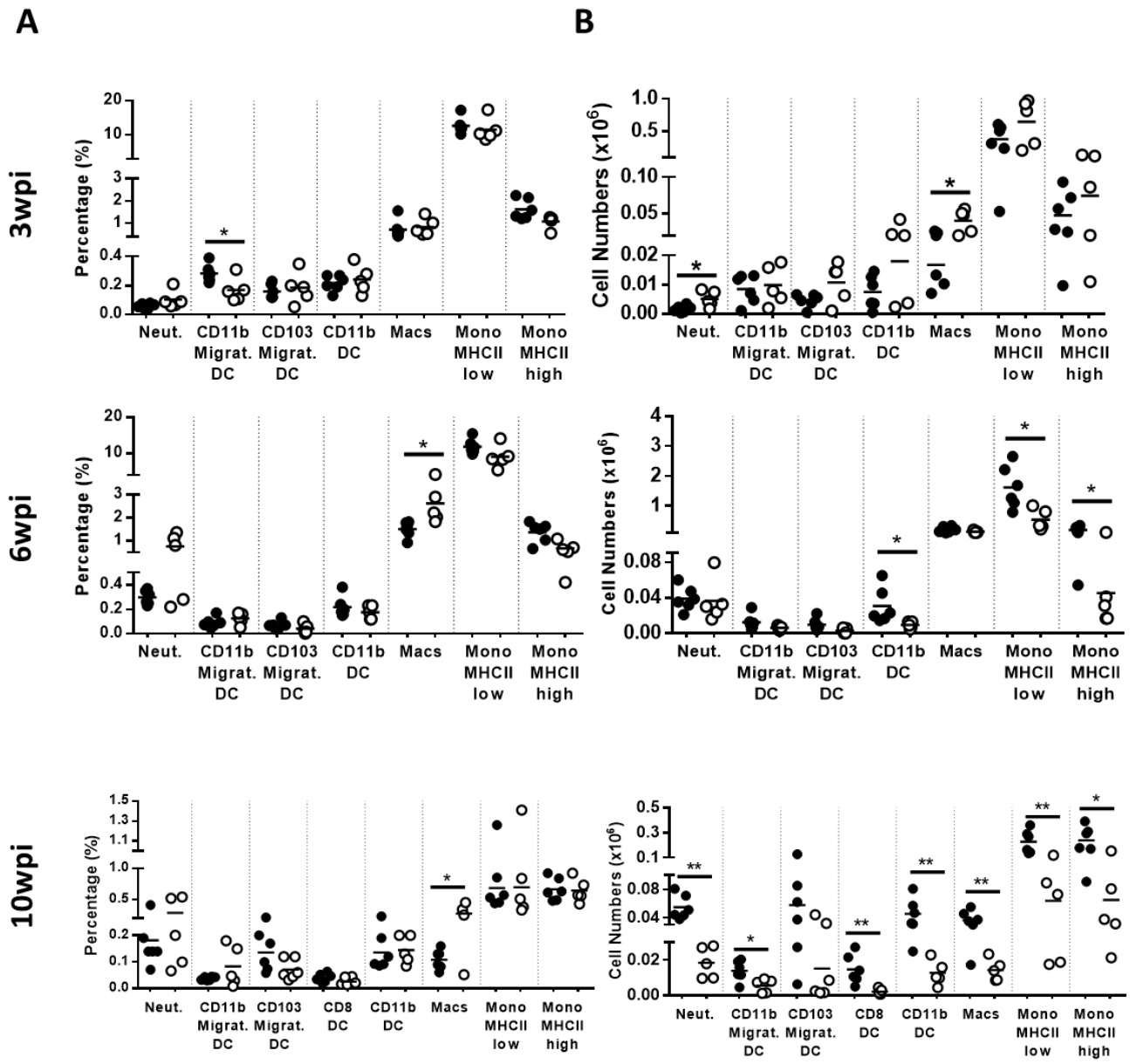

Figure S4.3. **Lyl1-deletion enhances macrophage recruitment to the lymph nodes (LN) in response to chronic hypervirulent *Mtb* HN878**. **(A-B)** Littermate control (WT) and Lyl1$^{-/-}$ mice were infected with 100 CFU/mouse intranasally with *Mtb* HN878 (n = 5 mice/group) and sacrificed at either 3-, 6- or 10-weeks post infection. Using flow cytometry, single cell suspension of LN tissue was analyzed for **(A)** percentage and **(B)** total cell numbers of the myeloid cell population at indicated timepoints. Surface markers of the different cell populations are as follows (according to the gating strategy in ***Appendix D)***: Neutrophils (Neut.) = Ly6G^{+}CD11b^{+}; CD11b^{+} Migratory DC = CD11c^{+}MHCII^{high}CD11b^{+}CD103^{-}; CD103^{+} Migratory DC = CD11c^{+}MHCII^{high}CD103^{+}CD11b^{-}; CD8^{+} Resident DC = CD11c^{+}MHCII^{low}CD8^{+}CD11b^{-}; CD11b^{+} Resident DC = CD11c^{+}MHCII^{low}CD11b^{+}CD8^{-}; Macrophages (Macs) = F4/80^{+}CD11b^{+}; Monocytes (Mono MHCII low) = Ly6C^{+}MHCII^{low}; Monocytes (Mono MHCII high) = Ly6C^{+}MHCII^{high}. Line denotes Mean. Data shown is representative of 2-3 independent experiments. Student t-test analysis at *$p < 0.05$, **$p < 0.01$ to determine significance.

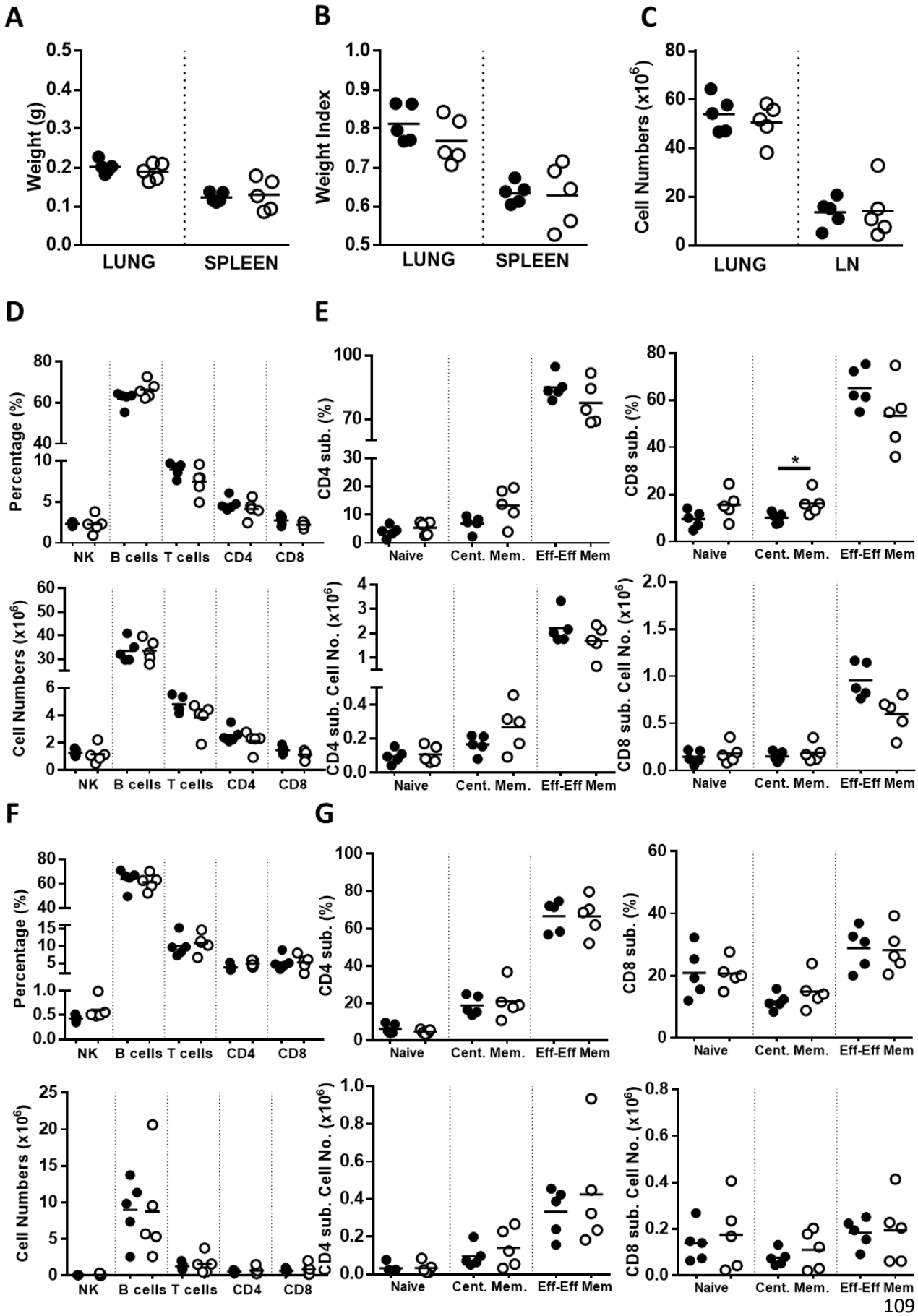
A
Weight (g)
LUNG
SPLEEN
B
Weight Index
LUNG
SPLEEN
C
Cell Numbers (x10^6)
LUNG
LN
D
Percentage (%)
NK
B cells
T cells
CD4
CD8
Cell Numbers (x10^6)
E
CD4 sub. (%)
CD8 sub. (%)
CD4 sub. Cell No. (x10^6)
CD8 sub. Cell No. (x10^6)
Naive
Cent. Mem.
Eff-Eff Mem
*
F
G

Figure S4.4*. Lyl1-deficient lymphoid population is unaffected by *Mtb* H37Rv infection after 6 weeks**. **(A-G)** Littermate control (WT) and Lyl1$^{-/-}$ mice were intranasally infected with mCherry tagged H37Rv *Mtb* at 230 CFU/mouse (n = 5 mice/group) and sacrificed at 6 weeks post infection to determine **(A)** lung and spleen weight, **(B**) weight index and **(C)** lung and lymph node (LN) cell numbers. Using flow cytometry, single cell suspension tissue was analyzed for percentage and total cell numbers of the lymphoid cell population at indicated timepoints for **(D)** lung and **(F)** LN. Surface markers of the different cell populations are as follows (according to the gating strategy in ***Appendix B): gamma delta T-cells (gd T) = CD3$^+$gdTCR$^+$; NK cells = NK1.1$^+$CD3$^-$; B-cells = CD19$^+$CD3$^-$; T-cells = CD3$^+$CD19$^-$; CD4$^+$ T-cells = CD3$^+$CD4$^+$; CD8$^+$ T-cells = CD3$^+$CD8$^+$. Further lymphoid T-cell subsets (CD4$^+$ and CD8$^+$) was analyzed for percentage and total cell numbers of the **(E)** lung and the **(G)** LN at indicated timepoints. Surface markers of the different cell populations are as follows (according to the gating strategy in ***Appendix B***): CD4$^+$ naïve = CD3$^+$CD4$^+$CD62L$^+$CD44$^-$; CD4$^+$ Central Memory = CD3$^+$CD4$^+$CD62L$^+$CD44$^+$; CD4$^+$ Effector/Effector Memory = CD3$^+$CD4$^+$CD44$^+$CD62L$^-$; CD8$^+$ naïve = CD3$^+$CD8$^+$CD62L$^+$CD44$^-$; CD8$^+$ Central Memory = CD3$^+$CD8$^+$CD62L$^+$CD44$^+$; CD8$^+$ Effector/Effector Memory = CD3$^+$CD8$^+$CD44$^+$ CD62L$^-$. Line denotes Mean. Data shown is representative of 2 independent experiments. Student t-test analysis at $*p < 0.05$ to determine significance.

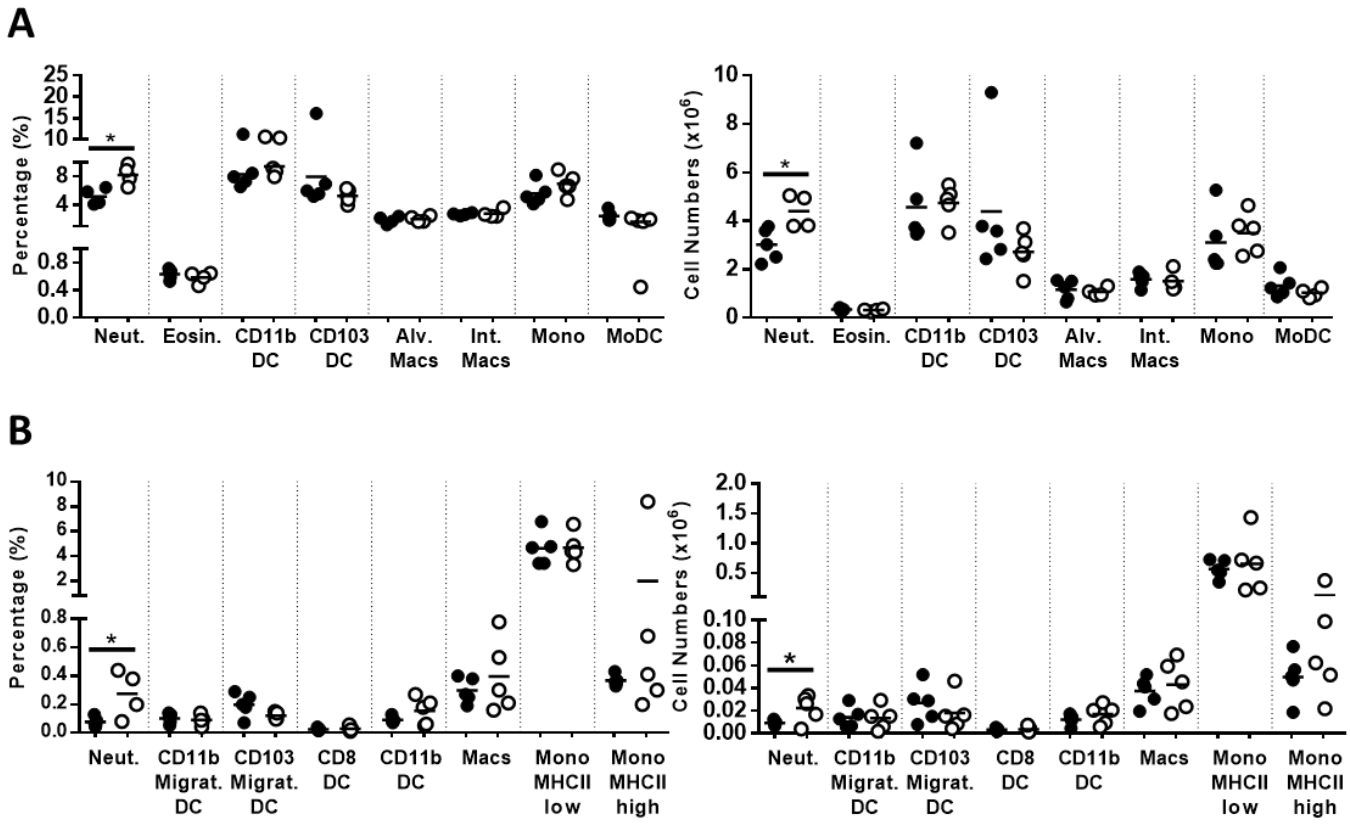

Figure S4.5*. Neutrophil recruitment is enhanced during *Mtb* H37Rv infection in the absence of Lyl1.** **(A-B)** Littermate control (WT) and Lyl1$^{-/-}$ mice were intranasally infected with mCherry tagged H37Rv *Mtb* at 230 CFU/mouse (n = 5 mice/group) and sacrificed at 6 weeks post infection. Using flow cytometry, single cell suspension tissue was analyzed for percentage and total cell numbers of the myeloid cell population at indicated timepoints for **(A)** lung and **(B)** LN. Surface markers of the different cell populations are as follows (for lung according to the gating strategy in ***Appendix C): Neutrophils (Neut.) = Ly6G$^+$CD11b$^+$; Eosinophils (Eosin.) = SiglecF$^+$CD11b$^+$CD64$^-$; CD11b$^+$ DC = CD11c$^+$MHCII$^+$CD11b$^+$CD64$^-$; CD103$^+$ DC = CD11c$^+$MHCII$^+$CD103$^+$CD64$^-$; Alveolar Macrophages (Alv. Macs) = CD64$^+$MerTK$^+$SiglecF$^+$CD11c$^+$; Interstitial Macrophages (Int. Macs) = CD64$^+$MerTK$^+$SiglecF$^+$CD11b$^+$ CD11c$^-$; Monocytes (Mono) = Ly6G$^+$CD11b$^+$CD64$^-$; Monocyte-derived DC (MoDC) = CD64$^+$CD11b$^+$CD11c$^+$, (for LN according to the gating strategy in ***Appendix D***): Neutrophils (Neut.) = Ly6G$^+$CD11b$^+$; CD11b$^+$ Migratory DC = CD11c$^+$MHCII^{high}CD11b$^+$CD103$^-$; CD103$^+$ Migratory DC = CD11c$^+$MHCII^{high}CD103$^+$CD11b$^-$; CD8$^+$ Resident DC = CD11c$^+$MHCII^{low}CD8$^+$CD11b$^-$; CD11b$^+$ Resident DC = CD11c$^+$MHCII^{low}CD11b$^+$CD8$^-$; Macrophages (Macs) = F4/80$^+$CD11b$^+$; Monocytes (Mono MHCII low) = Ly6C$^+$MHCII^{low}; Monocytes (Mono MHCII high) = Ly6C$^+$MHCII^{high}. Line denotes Mean. Data shown is representative of 2 independent experiments. Student t-test analysis at *$p < 0.05$, **$p < 0.01$ to determine significance.

Concluding Remarks

The aim of the work presented in this thesis was to identify and characterize the novel candidate gene, Lymphoblastic leukemia 1 (Lyl1), in macrophage-specific pathogen killing effector functions during bacterial infections. To achieve this, initial characterization of immune cell recruitment, cytokine/antibody concentrations and histopathology in the thymus, lymph nodes, lungs, spleen and liver of $Lyl1^{-/-}$ mice at a steady state was performed. We confirmed the role of Lyl1 during thymopoiesis as well as a compensatory mechanism for the development of comparable single positive $CD4^+$ and $CD8^+$ T-cells in the absence of Lyl1. Aside from splenic IL-2 induction, of which we argue as the compensatory mechanism to achieve single positive $CD4^+$ and $CD8^+$ T-cells in the absence of Lyl1, we conclude minimal significant immunological differences in adult $Lyl1^{-/-}$ mice compared to littermate control/WT mice. This availed the $Lyl1^{-/-}$ mouse for any further infectious disease studies without any underlying conditions.

By investigating Lyl1 expression patterns in different macrophage-stimulated environments, as well as demonstrating host susceptibility to both *Mtb* and *Lm* infection in the absence of Lyl1, we prove that the downregulation of Lyl1 is not bacterial specific. We do, however, show that Lyl1 is regulated by the host. Though, instead of providing protection by regulating Lyl1 to induce a pro-inflammatory response, the absence of the gene rather induces an exaggerated inflammatory response providing a favourable environment for bacterial growth.

The requirement for this transcription factor during bacterial infections is rather conflicting considering that the overexpression of this gene promotes tumour development. Although we identified Lyl1 regulation by MAPk and NFκB in response to LPS, further investigation into Lyl1 regulatory targets is required to fully explore the mechanism responsible for exacerbated inflammation during bacterial infections in the absence of Lyl1. The future work will involve RNA-Seq of wild type and Lyl1-deficient macrophages in response to *Mtb* infection to holistically understand Lyl1 regulatory mechanisms in macrophages. The absence of chromatin immunoprecipitation (ChIP) grade antibodies has also hindered our progress to perform ChIP-PCR experiments of Lyl1 target gene promoters. In fact, we have tried four different commercially available mouse Lyl1 specific antibodies; but none of them proved to be specific to Lyl1.

We further demonstrate that Lyl1 cannot be used as a biomarker in whole blood for TB since patients suffering from TB does not systemically show differentially expressed Lyl1. However, we reveal that Lyl1 has great potential to serve as biomarkers in whole blood for viral infections, including influenza and rhinovirus. We argue that TB is rather slow progressing and differences in immunological markers are observed at chronic stages whereas influenza and rhinovirus are considered acute diseases allowing for genetic differences to be observed systemically.

The data presented in this thesis demonstrate clear differential expression of Lyl1 in response to immune-stimulants and bacterial infection. Further data collection also proves the downregulation of this transcription factor during viral infections. Therefore, we prove non-leukemia involved novel functions of Lyl1 using intracellular bacterial infections as a model and thus, reveal an under-appreciated role for the Lyl1 gene in various immune responses. However, given that the overexpression and underexpression of Lyl1 could be detrimental to the host, it is important to further investigate the targets and regulative components surrounding this transcription factor. Therefore, the significant changes in Lyl1 expression patterns provide great potential in further establishing a role for this gene in various disease models to identify genetic targets for the development of host-directed therapies.

References

1. Centers for Disease Control and Prevention, *Antibiotic resistance threats in the United States, 2013.* Atlanta, GA: US, Department of Health and Human Services, CDC, 2013.
2. Willyard, C., *The drug-resistant bacteria that pose the greatest health threats.* Nature News, 2017. **543**(7643): p. 15-15.
3. Centers for Disease Control and Prevention, *Antibiotic resistance threats in the United States, 2019.* Atlanta, GA: US, Department of Health and Human Services, CDC, 2019.
4. Ventola, C.L., *The antibiotic resistance crisis: part 1: causes and threats.* Pharmacy and Therapeutics, 2015. **40**(4): p. 277-83.
5. Michael, C.A., D. Dominey-Howes, and M. Labbate, *The antimicrobial resistance crisis: causes, consequences, and management.* Frontiers in Public Health, 2014. **2**: p. 145-145.
6. Gandhi, N., A. Moll, A. Sturm, R. Pawinski, T. Govender, U. Lalloo, K. Zeller, J. Andrews, and G. Friedland, *Extensively drug-resistant tuberculosis as a cause of death in patients co-infected with tuberculosis and HIV in a rural area of South Africa.* Lancet, 2006. **368**: p. 1575-80.
7. Muñoz-Carrillo, J.L., F. Rodríguez, O. Coronado, M. García, and J. Cordero, *Physiology and Pathology of Innate Immune Response Against Pathogens*, in *Physiology and Pathology of Immunology*, N. Rezaei, Editor. 2017, IntechOpen: London, UK. p. 99-134.
8. Giamarellos-Bourboulis, E.J. and M. Raftogiannis, *The immune response to severe bacterial infections: consequences for therapy.* Expert Review of Anti-Infective Therapy, 2012. **10**(3): p. 369-80.
9. Kawai, T. and S. Akira, *The role of pattern-recognition receptors in innate immunity: update on Toll-like receptors.* Nature Immunology, 2010. **11**(5): p. 373-384.
10. Stamm, C.E., A.C. Collins, and M.U. Shiloh, *Sensing of Mycobacterium tuberculosis and consequences to both host and bacillus.* Immunological Reviews, 2015. **264**(1): p. 204-219.
11. Weiss, G. and U.E. Schaible, *Macrophage defense mechanisms against intracellular bacteria.* Immunological Reviews, 2015. **264**(1): p. 182-203.
12. Franken, L., M. Schiwon, and C. Kurts, *Macrophages: sentinels and regulators of the immune system.* Cellular Microbiology, 2016. **18**(4): p. 475-487.
13. Collins, H.L. and S.H.E. Kaufmann, *Acquired Immunity against Bacteria*, in *Immunology of Infectious Diseases*, Stefan H. E. Kaufmann, Alan Sher, and R. Ahmed., Editors. 2002, American Society of Microbiology: Washington, DC, USA. p. 207-222.
14. Chaplin, D.D., *Overview of the immune response.* The Journal of allergy and clinical immunology, 2010. **125**(2): p. S3-S23.
15. Gordon, S., *Phagocytosis: The Legacy of Metchnikoff.* Cell, 2016. **166**(5): p. 1065-1068.
16. Gordon, S., A. Plüddemann, and F. Martinez Estrada, *Macrophage heterogeneity in tissues: phenotypic diversity and functions.* Immunological Reviews, 2014. **262**(1): p. 36-55.
17. Marakalala, M.J., F.O. Martinez, A. Plüddemann, and S. Gordon, *Macrophage Heterogeneity in the Immunopathogenesis of Tuberculosis.* Frontiers in Microbiology, 2018. **9**(1028): p. 1-15.
18. Epelman, S., K.J. Lavine, and G.J. Randolph, *Origin and functions of tissue macrophages.* Immunity, 2014. **41**(1): p. 21-35.
19. Mills, C.D., K. Kincaid, J.M. Alt, M.J. Heilman, and A.M. Hill, *M-1/M-2 macrophages and the Th1/Th2 paradigm.* The Journal of Immunology, 2000. **164**(12): p. 6166-73.
20. Mantovani, A., A. Sica, S. Sozzani, P. Allavena, A. Vecchi, and M. Locati, *The chemokine system in diverse forms of macrophage activation and polarization.* Trends in Immunology, 2004. **25**(12): p. 677-686.
21. Nathan, C.F., H.W. Murray, M.E. Wiebe, and B.Y. Rubin, *Identification of interferon-gamma as the lymphokine that activates human macrophage oxidative metabolism and antimicrobial activity.* The Journal of Experimental Medicine, 1983. **158**(3): p. 670-89.

22. Stein, M., S. Keshav, N. Harris, and S. Gordon, *Interleukin 4 potently enhances murine macrophage mannose receptor activity: a marker of alternative immunologic macrophage activation.* The Journal of Experimental Medicine, 1992. **176**(1): p. 287-292.
23. Anderson, C. and D. Mosser, *A novel phenotype for an activated macrophage: The type 2 activated macrophage.* Journal of Leukocyte Biology, 2002. **72**: p. 101-6.
24. Kadl, A., A.K. Meher, P.R. Sharma, M.Y. Lee, A.C. Doran, S.R. Johnstone, M.R. Elliott, F. Gruber, J. Han, W. Chen, et al., *Identification of a novel macrophage phenotype that develops in response to atherogenic phospholipids via Nrf2.* Circulation Research, 2010. **107**(6): p. 737-46.
25. Gleissner, C.A., I. Shaked, K.M. Little, and K. Ley, *CXC chemokine ligand 4 induces a unique transcriptome in monocyte-derived macrophages.* The Journal of Immunology, 2010. **184**(9): p. 4810-8.
26. Orecchioni, M., Y. Ghosheh, A.B. Pramod, and K. Ley, *Macrophage Polarization: Different Gene Signatures in M1(LPS+) vs. Classically and M2(LPS–) vs. Alternatively Activated Macrophages.* Frontiers in Immunology, 2019. **10**(1084): p. 1-14.
27. Martinez, F.O. and S. Gordon, *The M1 and M2 paradigm of macrophage activation: time for reassessment.* F1000 Prime Reports, 2014. **6**: p. 13-26.
28. Benoit, M., B. Desnues, and J.L. Mege, *Macrophage polarization in bacterial infections.* The Journal of Immunology, 2008. **181**(6): p. 3733-9.
29. Gordon, S., *Alternative activation of macrophages.* Nature Reviews Immunology, 2003. **3**(1): p. 23-35.
30. Murray, P.J., J.E. Allen, S.K. Biswas, E.A. Fisher, D.W. Gilroy, S. Goerdt, S. Gordon, J.A. Hamilton, L.B. Ivashkiv, T. Lawrence, et al., *Macrophage activation and polarization: nomenclature and experimental guidelines.* Immunity, 2014. **41**(1): p. 14-20.
31. Wynn, T.A., A. Chawla, and J.W. Pollard, *Macrophage biology in development, homeostasis and disease.* Nature, 2013. **496**(7446): p. 445-455.
32. Gautier, E.L., T. Shay, J. Miller, M. Greter, C. Jakubzick, S. Ivanov, J. Helft, A. Chow, K.G. Elpek, S. Gordonov, et al., *Gene-expression profiles and transcriptional regulatory pathways that underlie the identity and diversity of mouse tissue macrophages.* Nature Immunology, 2012. **13**(11): p. 1118-28.
33. Gordon, S. and A. Plüddemann, *Tissue macrophages: heterogeneity and functions.* BMC Biology, 2017. **15**(1): p. 53-71.
34. Ashida, H., H. Mimuro, M. Ogawa, T. Kobayashi, T. Sanada, M. Kim, and C. Sasakawa, *Cell death and infection: a double-edged sword for host and pathogen survival.* Journal of Cell Biology, 2011. **195**(6): p. 931-42.
35. Martin, C.J., M.G. Booty, T.R. Rosebrock, C. Nunes-Alves, D.M. Desjardins, I. Keren, S.M. Fortune, H.G. Remold, and S.M. Behar, *Efferocytosis is an innate antibacterial mechanism.* Cell Host Microbe, 2012. **12**(3): p. 289-300.
36. Frank, D. and J.E. Vince, *Pyroptosis versus necroptosis: similarities, differences, and crosstalk.* Cell Death and Differentiation, 2019. **26**(1): p. 99-114.
37. Daniel, T.M., *The history of tuberculosis.* Respiratory Medicine, 2006. **100**(11): p. 1862-1870.
38. Hayman, J., *Mycobacterium ulcerans: an infection from Jurassic time?* Lancet, 1984. **2**(8410): p. 1015-6.
39. Rothschild, B.M., L.D. Martin, G. Lev, H. Bercovier, G.K. Bar-Gal, C. Greenblatt, H. Donoghue, M. Spigelman, and D. Brittain, *Mycobacterium tuberculosis Complex DNA from an Extinct Bison Dated 17,000 Years before the Present.* Clinical Infectious Diseases, 2001. **33**(3): p. 305-311.
40. Hershkovitz, I., H.D. Donoghue, D.E. Minnikin, G.S. Besra, O.Y. Lee, A.M. Gernaey, E. Galili, V. Eshed, C.L. Greenblatt, E. Lemma, et al., *Detection and molecular characterization of 9,000-year-old Mycobacterium tuberculosis from a Neolithic settlement in the Eastern Mediterranean.* PLoS One, 2008. **3**(10): p. 3426-3432.
41. Kapur, V., T.S. Whittam, and J.M. Musser, *Is Mycobacterium tuberculosis 15,000 years old?* The Journal of Infectious Diseases, 1994. **170**(5): p. 1348-9.

42. Barberis, I., N.L. Bragazzi, L. Galluzzo, and M. Martini, *The history of tuberculosis: from the first historical records to the isolation of Koch's bacillus.* Journal of Preventive Medicine and Hygiene, 2017. **58**(1): p. 9-12.
43. Doetsch, R.N., *Benjamin Marten and his "New Theory of Consumptions".* Microbiological reviews, 1978. **42**(3): p. 521-528.
44. Roguin, A., *Rene Theophile Hyacinthe Laënnec (1781-1826): the man behind the stethoscope.* Clinical Medicine and Research, 2006. **4**(3): p. 230-235.
45. Daniel, T.M., *Hermann Brehmer and the origins of tuberculosis sanatoria.* International Journal of Tuberculosis and Lung Disease, 2011. **15**(2): p. 161-2.
46. Daniel, T.M., *Jean-Antoine Villemin and the infectious nature of tuberculosis.* International Journal of Tuberculosis and Lung Disease, 2015. **19**(3): p. 267-8.
47. Koch, R., *The Etiology of Tuberculosis.* Reviews of Infectious Diseases, 1982. **4**(6): p. 1270-1274.
48. Luca, S. and T. Mihaescu, *History of BCG Vaccine.* Maedica, 2013. **8**(1): p. 53-58.
49. Schatz, A., E. Bugle, and S.A. Waksman, *Streptomycin, a Substance Exhibiting Antibiotic Activity Against Gram-Positive and Gram-Negative Bacteria.⁎†.* Proceedings of the Society for Experimental Biology and Medicine, 1944. **55**(1): p. 66-69.
50. Lehmann, J., *The Treatment of Tuberculosis in Sweden with Para-Aminosalicylic Acid (PAS): A Review.* Diseases of the Chest, 1949. **16**(6): p. 684-703.
51. Crofton, J., *Chemotherapy of pulmonary tuberculosis.* British Medical Journal, 1959. **1**(5138): p. 1610-1614.
52. Margalith, P. and G. Beretta, *Rifomycin. XI. taxonomic study on streptomyces mediterranei nov. sp.* Mycopathologia et mycologia applicata, 1960. **13**(4): p. 321-330.
53. Thomas, J.P., C.O. Baughn, R.G. Wilkinson, and R.G. Shepherd, *A New Synthetic Compound with Antituberculous Activity in Mice: Ethambutol (Dextro-2, 2'- (Ethylenediimino)-di-1-Butanol).* American Review of Respiratory Disease, 1961. **83**(6): p. 891-893.
54. *Short-course chemotherapy in pulmonary tuberculosis. A controlled trial by the British Thoracic and Tuberculosis Association.* Lancet, 1976. **2**(7995): p. 1102-4.
55. World Health Organization. *The End TB Strategy*. 2015 [cited 2020 17 June]; Available from: https://www.who.int/tb/strategy/en/.
56. World Health Organization. *Global tuberculosis report 2019*. 2019 17 October 2019 [cited 2020 17 June]; Available from: https://www.who.int/tb/publications/global_report/en/.
57. Sulis, G., A. Roggi, A. Matteelli, and M.C. Raviglione, *Tuberculosis: epidemiology and control.* Mediterranean Journal of Hematology and Infectious Diseases, 2014. **6**(1): p. 2014070-2014070.
58. Seung, K.J., S. Keshavjee, and M.L. Rich, *Multidrug-Resistant Tuberculosis and Extensively Drug-Resistant Tuberculosis.* Cold Spring Harbor Perspectives in Medicine, 2015. **5**(9): p. 017863-017863.
59. Cohen, S.B., B.H. Gern, J.L. Delahaye, K.N. Adams, C.R. Plumlee, J.K. Winkler, D.R. Sherman, M.Y. Gerner, and K.B. Urdahl, *Alveolar Macrophages Provide an Early Mycobacterium tuberculosis Niche and Initiate Dissemination.* Cell Host and Microbe, 2018. **24**(3): p. 439-446.
60. Upadhyay, S., E. Mittal, and J.A. Philips, *Tuberculosis and the art of macrophage manipulation.* Pathogens and Disease, 2018. **76**(4): p. 1-12.
61. Manzanillo, P.S., M.U. Shiloh, D.A. Portnoy, and J.S. Cox, *Mycobacterium tuberculosis activates the DNA-dependent cytosolic surveillance pathway within macrophages.* Cell Host and Microbe, 2012. **11**(5): p. 469-480.
62. Marinho, F.V., S. Benmerzoug, S. Rose, P.C. Campos, J.T. Marques, A. Báfica, G. Barber, B. Ryffel, S.C. Oliveira, and V.F.J. Quesniaux, *The cGAS/STING Pathway Is Important for Dendritic Cell Activation but Is Not Essential to Induce Protective Immunity against Mycobacterium tuberculosis Infection.* Journal of Innate Immunity, 2018. **10**(3): p. 239-252.
63. Murray, E.G.D., R.A. Webb, and M.B.R. Swann, *A disease of rabbits characterised by a large mononuclear leucocytosis, caused by a hitherto undescribed bacillus Bacterium monocytogenes (n.sp.).* The Journal of Pathology and Bacteriology, 1926. **29**(4): p. 407-439.

64. Pirie, J.H.H., *Listeria: Change of Name for a Genus Bacteria.* Nature, 1940. **145**(3668): p. 264-264.
65. Seeliger, H.P.R., *Listeriosis — History and actual developments.* Infection, 1988. **16**(2): p. S80-S84.
66. Reiss, H.J., J. Potel, and A. Krebs, *[Granulomatosis infantiseptica; a general infection of infants and the newborn characterized by the presence of miliary granuloma].* Zeitschrift für die gesamte innere Medizin und ihre Grenzgebiete, 1951. **6**(15-16): p. 451-7.
67. Seeliger, H.P.R., *Listeriosis*. English edition ed. 1961, Basel, New York: Karger.
68. Hof, H., *History and epidemiology of listeriosis.* FEMS Immunology and Medical Microbiology, 2003. **35**(3): p. 199-202.
69. Schlech, W.F., 3rd, P.M. Lavigne, R.A. Bortolussi, A.C. Allen, E.V. Haldane, A.J. Wort, A.W. Hightower, S.E. Johnson, S.H. King, E.S. Nicholls, et al., *Epidemic listeriosis--evidence for transmission by food.* The New England Journal of Medicine, 1983. **308**(4): p. 203-6.
70. Mackaness, G.B., *The influence of immunologically committed lymphoid cells on macrophage activity in vivo.* The Journal of Experimental Medicine, 1969. **129**(5): p. 973-992.
71. Parihar, V.S., G. Lopez-Valladares, M.L. Danielsson-Tham, I. Peiris, S. Helmersson, M. Unemo, B. Andersson, M. Arneborn, E. Bannerman, S. Barbuddhe, et al., *Characterization of human invasive isolates of Listeria monocytogenes in Sweden 1986-2007.* Foodborne Pathogens and Disease, 2008. **5**(6): p. 755-61.
72. World Health Organization. *2000 - Listeria in France: Disease Outbreak Report*. 2000 [cited 2020 19 June]; Available from: https://www.who.int/csr/don/2000_02_29/en/.
73. Canadian Government. *Report of the Independent Investigator into the 2008 Listeriosis Outbreak*. 2009 [cited 2020 24 June]; Available from: https://www.canada.ca/en/news/archive/2009/07/report-independent-investigator-into-2008-listeriosis-outbreak.html.
74. McCollum, J.T., A.B. Cronquist, B.J. Silk, K.A. Jackson, K.A. O'Connor, S. Cosgrove, J.P. Gossack, S.S. Parachini, N.S. Jain, P. Ettestad, et al., *Multistate Outbreak of Listeriosis Associated with Cantaloupe.* The New England Journal of Medicine, 2013. **369**(10): p. 944-953.
75. Thomas, J., N. Govender, K.M. McCarthy, L.K. Erasmus, T.J. Doyle, M. Allam, A. Ismail, N. Ramalwa, P. Sekwadi, G. Ntshoe, et al., *Outbreak of Listeriosis in South Africa Associated with Processed Meat.* The New England Journal of Medicine, 2020. **382**(7): p. 632-643.
76. Centers for Disease and Control. *Outbreak of Listeria Infections*. 2019 [cited 2020 19 June]; Available from: https://www.cdc.gov/listeria/outbreaks/monocytogenes-08-19/index.html.
77. World Health Organization. *Listeriosis – South Africa: Disease Outbreak News*. 2018 [cited 2020 19 June]; Available from: https://www.who.int/csr/don/28-march-2018-listeriosis-south-africa/en/.
78. Pamer, E.G., *Immune responses to Listeria monocytogenes.* Nature Reviews Immunology, 2004. **4**(10): p. 812-823.
79. Edelson, B.T. and E.R. Unanue, *MyD88-dependent but Toll-like receptor 2-independent innate immunity to Listeria: no role for either in macrophage listericidal activity.* The Journal of Immunology, 2002. **169**(7): p. 3869-75.
80. Seki, E., H. Tsutsui, N.M. Tsuji, N. Hayashi, K. Adachi, H. Nakano, S. Futatsugi-Yumikura, O. Takeuchi, K. Hoshino, S. Akira, et al., *Critical roles of myeloid differentiation factor 88-dependent proinflammatory cytokine release in early phase clearance of Listeria monocytogenes in mice.* The Journal of Immunology, 2002. **169**(7): p. 3863-8.
81. Guler, R. and F. Brombacher, *Host-directed drug therapy for tuberculosis.* Nature Chemical Biology, 2015. **11**(10): p. 748-751.
82. Kaufmann, S.H.E., A. Dorhoi, R.S. Hotchkiss, and R. Bartenschlager, *Host-directed therapies for bacterial and viral infections.* Nature Reviews Drug Discovery, 2018. **17**(1): p. 35-56.
83. Tobin, D.M., *Host-Directed Therapies for Tuberculosis.* Cold Spring Harbor Perspectives in Medicine, 2015. **5**(10): p. 021196-021212.

84. Palucci, I. and G. Delogu, *Host Directed Therapies for Tuberculosis: Futures Strategies for an Ancient Disease.* Chemotherapy, 2018. **63**(3): p. 172-180.
85. Bourigault, M.L., R. Vacher, S. Rose, M.L. Olleros, J.P. Janssens, V.F. Quesniaux, and I. Garcia, *Tumor necrosis factor neutralization combined with chemotherapy enhances Mycobacterium tuberculosis clearance and reduces lung pathology.* American Journal of Clinical and Experimental Immunology, 2013. **2**(1): p. 124-34.
86. Stanley, S.A., A.K. Barczak, M.R. Silvis, S.S. Luo, K. Sogi, M. Vokes, M.-A. Bray, A.E. Carpenter, C.B. Moore, N. Siddiqi, et al., *Identification of Host-Targeted Small Molecules That Restrict Intracellular Mycobacterium tuberculosis Growth.* PLOS Pathogens, 2014. **10**(2): p. 1003946-1003962.
87. Chun, R., J. Adams, and M. Hewison, *Immunomodulation by vitamin D: Implications for TB.* Expert Review of Clinical Pharmacology, 2011. **4**: p. 583-91.
88. Kolloli, A. and S. Subbian, *Host-Directed Therapeutic Strategies for Tuberculosis.* Frontiers in medicine, 2017. **4**: p. 171-171.
89. Wejse, C., V.F. Gomes, P. Rabna, P. Gustafson, P. Aaby, I.M. Lisse, P.L. Andersen, H. Glerup, and M. Sodemann, *Vitamin D as supplementary treatment for tuberculosis: a double-blind, randomized, placebo-controlled trial.* American Journal of Respiratory and Critical Care Medicine, 2009. **179**(9): p. 843-50.
90. Vilaplana, C., E. Marzo, G. Tapia, J. Diaz, V. Garcia, and P.J. Cardona, *Ibuprofen therapy resulted in significantly decreased tissue bacillary loads and increased survival in a new murine experimental model of active tuberculosis.* The Journal of Infectious Diseases, 2013. **208**(2): p. 199-202.
91. Mihaylova, B., J. Emberson, L. Blackwell, A. Keech, J. Simes, E.H. Barnes, M. Voysey, A. Gray, R. Collins, and C. Baigent, *The effects of lowering LDL cholesterol with statin therapy in people at low risk of vascular disease: meta-analysis of individual data from 27 randomised trials.* Lancet, 2012. **380**(9841): p. 581-90.
92. Parihar, S.P., R. Guler, R. Khutlang, D.M. Lang, R. Hurdayal, M.M. Mhlanga, H. Suzuki, A.D. Marais, and F. Brombacher, *Statin therapy reduces the mycobacterium tuberculosis burden in human macrophages and in mice by enhancing autophagy and phagosome maturation.* The Journal of Infectious Diseases, 2013. **209**(5): p. 754-763.
93. de Vallière, S., G. Abate, A. Blazevic, R.M. Heuertz, and D.F. Hoft, *Enhancement of innate and cell-mediated immunity by antimycobacterial antibodies.* Infection and Immunity, 2005. **73**(10): p. 6711-20.
94. Burel, J.G., M. Babor, M. Pomaznoy, C.S. Lindestam Arlehamn, N. Khan, A. Sette, and B. Peters, *Host Transcriptomics as a Tool to Identify Diagnostic and Mechanistic Immune Signatures of Tuberculosis.* Frontiers in Immunology, 2019. **10**: p. 221-221.
95. Ehrt, S., D. Schnappinger, S. Bekiranov, J. Drenkow, S. Shi, T.R. Gingeras, T. Gaasterland, G. Schoolnik, and C. Nathan, *Reprogramming of the macrophage transcriptome in response to interferon-gamma and Mycobacterium tuberculosis: signaling roles of nitric oxide synthase-2 and phagocyte oxidase.* Journal of Experimental Medicine, 2001. **194**(8): p. 1123-40.
96. Saliba, A.-E., S. C Santos, and J. Vogel, *New RNA-seq approaches for the study of bacterial pathogens.* Current Opinion in Microbiology, 2017. **35**: p. 78-87.
97. Bryson, B.D., T.R. Rosebrock, F.G. Tafesse, C.Y. Itoh, A. Nibasumba, G.H. Babunovic, B. Corleis, C. Martin, C. Keegan, P. Andrade, et al., *Heterogeneous GM-CSF signaling in macrophages is associated with control of Mycobacterium tuberculosis.* Nature Communications, 2019. **10**(1): p. 2329-2340.
98. Pisu, D., L. Huang, J.K. Grenier, and D.G. Russell, *Dual RNA-Seq of Mtb-Infected Macrophages In Vivo Reveals Ontologically Distinct Host-Pathogen Interactions.* Cell Reports, 2020. **30**(2): p. 335-350.
99. Stark, R., M. Grzelak, and J. Hadfield, *RNA sequencing: the teenage years.* Nature Reviews Genetics, 2019. **20**(11): p. 631-656.

100. Dunham, I., A. Kundaje, S.F. Aldred, P.J. Collins, C.A. Davis, F. Doyle, C.B. Epstein, S. Frietze, J. Harrow, R. Kaul, et al., *An integrated encyclopedia of DNA elements in the human genome.* Nature, 2012. **489**(7414): p. 57-74.
101. Forrest, A.R.R., H. Kawaji, M. Rehli, J. Kenneth Baillie, M.J.L. de Hoon, V. Haberle, T. Lassmann, I.V. Kulakovskiy, M. Lizio, M. Itoh, et al., *A promoter-level mammalian expression atlas.* Nature, 2014. **507**(7493): p. 462-470.
102. Noguchi, S., T. Arakawa, S. Fukuda, M. Furuno, A. Hasegawa, F. Hori, S. Ishikawa-Kato, K. Kaida, A. Kaiho, M. Kanamori-Katayama, et al., *FANTOM5 CAGE profiles of human and mouse samples.* Scientific Data, 2017. **4**: p. 170112-170122.
103. Lizio, M., J. Harshbarger, H. Shimoji, J. Severin, T. Kasukawa, S. Sahin, I. Abugessaisa, S. Fukuda, F. Hori, S. Ishikawa-Kato, et al., *Gateways to the FANTOM5 promoter level mammalian expression atlas.* Genome Biology, 2015. **16**: p. 22-36.
104. Roy, S., S. Schmeier, B. Kaczkowski, E. Arner, T. Alam, M. Ozturk, O. Tamgue, S.P. Parihar, H. Kawaji, M. Itoh, et al., *Transcriptional landscape of Mycobacterium tuberculosis infection in macrophages.* Sci Rep, 2018. **8**(1): p. 6758-6771.
105. Cleary, M.L., J.D. Mellentin, J. Spies, and S.D. Smith, *Chromosomal translocation involving the beta T cell receptor gene in acute leukemia.* The Journal of Experimental Medicine, 1988. **167**(2): p. 682-687.
106. Mellentin, J.D., S.D. Smith, and M.L. Cleary, *lyl-1, a novel gene altered by chromosomal translocation in T cell leukemia, codes for a protein with a helix-loop-helix DNA binding motif.* Cell, 1989. **58**(1): p. 77-83.
107. Souroullas, G.P. and M.A. Goodell, *A new allele of Lyl1 confirms its important role in hematopoietic stem cell function.* Genesis, 2011. **49**(6): p. 441-8.
108. Miyamoto, A., X. Cui, L. Naumovski, and M.L. Cleary, *Helix-loop-helix proteins LYL1 and E2a form heterodimeric complexes with distinctive DNA-binding properties in hematolymphoid cells.* Molecular and Cellular Biology, 1996. **16**(5): p. 2394-2401.
109. Begley, C.G., P.D. Aplan, S.M. Denning, B.F. Haynes, T.A. Waldmann, and I.R. Kirsch, *The gene SCL is expressed during early hematopoiesis and encodes a differentiation-related DNA-binding motif.* Proceedings of the National Academy of Sciences of the United States of America, 1989. **86**(24): p. 10128-32.
110. Capron, C., Y. Lecluse, A.L. Kaushik, A. Foudi, C. Lacout, D. Sekkai, I. Godin, O. Albagli, I. Poullion, F. Svinartchouk, et al., *The SCL relative LYL-1 is required for fetal and adult hematopoietic stem cell function and B-cell differentiation.* Blood, 2006. **107**(12): p. 4678-86.
111. Chan, W.Y.I., G.A. Follows, G. Lacaud, J.E. Pimanda, J.-R. Landry, S. Kinston, K. Knezevic, S. Piltz, I.J. Donaldson, L. Gambardella, et al., *The paralogous hematopoietic regulators Lyl1 and Scl are coregulated by Ets and GATA factors, but Lyl1 cannot rescue the early Scl–/– phenotype.* Blood, 2006. **109**(5): p. 1908-1916.
112. Visvader, J.E., Y. Fujiwara, and S.H. Orkin, *Unsuspected role for the T-cell leukemia protein SCL/tal-1 in vascular development.* Genes and Development, 1998. **12**(4): p. 473-9.
113. Robb, L., N.J. Elwood, A.G. Elefanty, F. Köntgen, R. Li, L.D. Barnett, and C.G. Begley, *The scl gene product is required for the generation of all hematopoietic lineages in the adult mouse.* The EMBO journal, 1996. **15**(16): p. 4123-4129.
114. Bradley, C.K., E.A. Takano, M.A. Hall, J.R. Göthert, A.R. Harvey, C.G. Begley, and J.A. van Eekelen, *The essential haematopoietic transcription factor Scl is also critical for neuronal development.* European Journal of Neuroscience, 2006. **23**(7): p. 1677-89.
115. Mikkola, H.K., J. Klintman, H. Yang, H. Hock, T.M. Schlaeger, Y. Fujiwara, and S.H. Orkin, *Haematopoietic stem cells retain long-term repopulating activity and multipotency in the absence of stem-cell leukaemia SCL/tal-1 gene.* Nature, 2003. **421**(6922): p. 547-51.
116. Curtis, D.J., M.A. Hall, L.J. Van Stekelenburg, L. Robb, S.M. Jane, and C.G. Begley, *SCL is required for normal function of short-term repopulating hematopoietic stem cells.* Blood, 2004. **103**(9): p. 3342-3348.

117. Giroux, S., A.L. Kaushik, C. Capron, A. Jalil, C. Kelaidi, F. Sablitzky, D. Dumenil, O. Albagli, and I. Godin, *lyl-1 and tal-1/scl, two genes encoding closely related bHLH transcription factors, display highly overlapping expression patterns during cardiovascular and hematopoietic ontogeny.* Gene Expression Patterns, 2007. **7**(3): p. 215-26.
118. Souroullas, G.P., J.M. Salmon, F. Sablitzky, D.J. Curtis, and M.A. Goodell, *Adult hematopoietic stem and progenitor cells require either Lyl1 or Scl for survival.* Cell Stem Cell, 2009. **4**(2): p. 180-6.
119. Ferrier, R., R. Nougarede, S. Doucet, B. Kahn-Perles, J. Imbert, and D. Mathieu-Mahul, *Physical interaction of the bHLH LYL1 protein and NF-kappaB1 p105.* Oncogene, 1999. **18**(4): p. 995-1005.
120. San-Marina, S., Y. Han, F. Suarez Saiz, M.R. Trus, and M.D. Minden, *Lyl1 interacts with CREB1 and alters expression of CREB1 target genes.* Biochimica et Biophysica Acta, 2008. **1783**(3): p. 503-17.
121. Deleuze, V., R. El-Hajj, E. Chalhoub, C. Dohet, V. Pinet, P. Couttet, and D. Mathieu, *Angiopoietin-2 is a direct transcriptional target of TAL1, LYL1 and LMO2 in endothelial cells.* PLoS One, 2012. **7**(7): p. 40484-40498.
122. Zohren, F., G.P. Souroullas, M. Luo, U. Gerdemann, M.R. Imperato, N.K. Wilson, B. Göttgens, G.L. Lukov, and M.A. Goodell, *The transcription factor Lyl-1 regulates lymphoid specification and the maintenance of early T lineage progenitors.* Nature Immunology, 2012. **13**(8): p. 761-769.
123. San-Marina, S., Y. Han, J. Liu, and M.D. Minden, *Suspected leukemia oncoproteins CREB1 and LYL1 regulate Op18/STMN1 expression.* Biochimica et Biophysica Acta, 2012. **1819**(11-12): p. 1164-72.
124. Pirot, N., H. Delpech, V. Deleuze, C. Dohet, M. Courtade-Saïdi, C. Basset-Léobon, E. Chalhoub, D. Mathieu, and V. Pinet, *Lung endothelial barrier disruption in Lyl1-deficient mice.* American Journal of Physiology-Lung Cellular and Molecular Physiology, 2014. **306**(8): p. 775-785.
125. Lukov, G.L. and M.A. Goodell, *LYL1 degradation by the proteasome is directed by a N-terminal PEST rich site in a phosphorylation-independent manner.* PLoS One, 2010. **5**(9): p. 12692-12699.
126. Capron, C., C. Lacout, Y. Lécluse, O. Wagner-Ballon, A.L. Kaushik, E. Cramer-Bordé, F. Sablitzky, D. Duménil, and W. Vainchenker, *LYL-1 deficiency induces a stress erythropoiesis.* Experimental Hematology, 2011. **39**(6): p. 629-42.
127. McCormack, M.P., B.J. Shields, J.T. Jackson, C. Nasa, W. Shi, N.J. Slater, C.S. Tremblay, T.H. Rabbitts, and D.J. Curtis, *Requirement for Lyl1 in a model of Lmo2-driven early T-cell precursor ALL.* Blood, 2013. **122**(12): p. 2093-103.
128. Ferrando, A.A., D.S. Neuberg, J. Staunton, M.L. Loh, C. Huard, S.C. Raimondi, F.G. Behm, C.-H. Pui, J.R. Downing, and D.G. Gilliland, *Gene expression signatures define novel oncogenic pathways in T cell acute lymphoblastic leukemia.* Cancer Cell, 2002. **1**(1): p. 75-87.
129. Zhong, Y., L. Jiang, H. Hiai, S. Toyokuni, and Y. Yamada, *Overexpression of a transcription factor LYL1 induces T- and B-cell lymphoma in mice.* Oncogene, 2007. **26**(48): p. 6937-47.
130. Lukov, G.L., L. Rossi, G.P. Souroullas, R. Mao, and M.A. Goodell, *The expansion of T-cells and hematopoietic progenitors as a result of overexpression of the lymphoblastic leukemia gene, Lyl1 can support leukemia formation.* Leukemia Research, 2011. **35**(3): p. 405-12.
131. Meng, Y.S., H. Khoury, J.E. Dick, and M.D. Minden, *Oncogenic potential of the transcription factor LYL1 in acute myeloblastic leukemia.* Leukemia, 2005. **19**(11): p. 1941-7.
132. Meng, Y.S., X.J. Hu, and W. Liu, *Knockdown of LYL1 impaired proliferation of CD34(+) myeloid leukemia cells.* Leukemia and Lymphoma, 2009. **50**(11): p. 1896-9.
133. Curtis, D.J., J.M. Salmon, and J.E. Pimanda, *Concise review: Blood relatives: formation and regulation of hematopoietic stem cells by the basic helix-loop-helix transcription factors stem cell leukemia and lymphoblastic leukemia-derived sequence 1.* Stem Cells, 2012. **30**(6): p. 1053-8.
134. Porcher, C., W. Swat, K. Rockwell, Y. Fujiwara, F. Alt, and S. Orkin, *The T Cell Leukemia Oncoprotein SCL/tal-1 Is Essential for Development of All Hematopoietic Lineages.* Cell, 1996. **86**: p. 47-57.

135. Chiu, S.K., J. Saw, Y. Huang, S.E. Sonderegger, N.C. Wong, D.R. Powell, D. Beck, J.E. Pimanda, C.S. Tremblay, and D.J. Curtis, *A novel role for Lyl1 in primitive erythropoiesis.* Development, 2018. **145**(19): p. 1-9.
136. Mohrs, M., B. Ledermann, G. Kohler, A. Dorfmuller, A. Gessner, and F. Brombacher, *Differences between IL-4- and IL-4 receptor alpha-deficient mice in chronic leishmaniasis reveal a protective role for IL-13 receptor signaling.* The Journal of Immunology, 1999. **162**(12): p. 7302-8.
137. Herbert, D.R., C. Holscher, M. Mohrs, B. Arendse, A. Schwegmann, M. Radwanska, M. Leeto, R. Kirsch, P. Hall, H. Mossmann, et al., *Alternative macrophage activation is essential for survival during schistosomiasis and downmodulates T helper 1 responses and immunopathology.* Immunity, 2004. **20**(5): p. 623-35.
138. Guler, R., S.P. Parihar, S. Savvi, E. Logan, A. Schwegmann, S. Roy, N.E. Nieuwenhuizen, M. Ozturk, S. Schmeier, and H. Suzuki, *IL-4Rα-Dependent Alternative Activation of Macrophages Is Not Decisive for Mycobacterium tuberculosis Pathology and Bacterial Burden in Mice.* PloS one, 2015. **10**(3): p. 0121070-0121084.
139. Consortium, G.T., *The Genotype-Tissue Expression (GTEx) project.* Nature genetics, 2013. **45**(6): p. 580-585.
140. Whicher, J.T. and S.W. Evans, *Cytokines in disease.* Clinical Chemistry, 1990. **36**(7): p. 1269-1281.
141. Silva-Filho, J.L., C. Caruso-Neves, and A.A.S. Pinheiro, *IL-4: an important cytokine in determining the fate of T cells.* Biophysical reviews, 2014. **6**(1): p. 111-118.
142. Malek, T.R., A. Yu, V. Vincek, P. Scibelli, and L. Kong, *CD4 Regulatory T Cells Prevent Lethal Autoimmunity in IL-2Rbeta-Deficient Mice: Implications for the Nonredundant Function of IL-2.* Immunity, 2002. **17**(2): p. 167-178.
143. Giampaolo, S., G. Wójcik, E. Serfling, and A.K. Patra, *Interleukin-2-regulatory T cell axis critically regulates maintenance of hematopoietic stem cells.* Oncotarget, 2017. **8**(18): p. 29625-29642.
144. Kuo, S.S., J.D. Mellentin, N.G. Copeland, D.J. Gilbert, N.A. Jenkins, and M.L. Cleary, *Structure, chromosome mapping, and expression of the mouse Lyl-1 gene.* Oncogene, 1991. **6**(6): p. 961-968.
145. Roy, S., R. Guler, S.P. Parihar, S. Schmeier, B. Kaczkowski, H. Nishimura, J.W. Shin, Y. Negishi, M. Ozturk, and R. Hurdayal, *Batf2/Irf1 induces inflammatory responses in classically activated macrophages, lipopolysaccharides, and mycobacterial infection.* The Journal of Immunology, 2015. **194**(12): p. 6035-6044.
146. Tamgue, O., L. Gcanga, M. Ozturk, L. Whitehead, S. Pillay, R. Jacobs, S. Roy, S. Schmeier, M. Davids, Y.A. Medvedeva, et al., *Differential Targeting of c-Maf, Bach-1, and Elmo-1 by microRNA-143 and microRNA-365 Promotes the Intracellular Growth of Mycobacterium tuberculosis in Alternatively IL-4/IL-13 Activated Macrophages.* Frontiers in Immunology, 2019. **10**(421): p. 1-16.
147. Parihar, S.P., R. Guler, D.M. Lang, H. Suzuki, A.D. Marais, and F. Brombacher, *Simvastatin enhances protection against Listeria monocytogenes infection in mice by counteracting Listeria-induced phagosomal escape.* PloS one, 2013. **8**(9): p. 75490-75501.
148. Kim, S.I., J.W. Lee, N. Lee, M. Lee, H.S. Kim, H.H. Chung, J.W. Kim, N.H. Park, Y.S. Song, and J.S. Seo, *LYL1 gene amplification predicts poor survival of patients with uterine corpus endometrial carcinoma: analysis of the Cancer genome atlas data.* BMC Cancer, 2018. **18**(1): p. 494-504.
149. Pron, B., C. Boumaila, F. Jaubert, P. Berche, G. Milon, F. Geissmann, and J.L. Gaillard, *Dendritic cells are early cellular targets of Listeria monocytogenes after intestinal delivery and are involved in bacterial spread in the host.* Cellular Microbiology, 2001. **3**(5): p. 331-40.
150. Neuenhahn, M., K.M. Kerksiek, M. Nauerth, M.H. Suhre, M. Schiemann, F.E. Gebhardt, C. Stemberger, K. Panthel, S. Schröder, T. Chakraborty, et al., *CD8alpha+ dendritic cells are required for efficient entry of Listeria monocytogenes into the spleen.* Immunity, 2006. **25**(4): p. 619-30.

151. Humann, J. and L.L. Lenz, *Activation of naive NK cells in response to Listeria monocytogenes requires IL-18 and contact with infected dendritic cells.* The Journal of immunology 2010. **184**(9): p. 5172-5178.
152. Clark, S.E., H.C. Filak, B.S. Guthrie, R.L. Schmidt, A. Jamieson, P. Merkel, V. Knight, C.M. Cole, D.H. Raulet, and L.L. Lenz, *Bacterial Manipulation of NK Cell Regulatory Activity Increases Susceptibility to Listeria monocytogenes Infection.* PLOS Pathogens, 2016. **12**(6): p. 1005708-1005729.
153. Moretta, A., E. Marcenaro, S. Parolini, G. Ferlazzo, and L. Moretta, *NK cells at the interface between innate and adaptive immunity.* Cell Death and Differentiation, 2008. **15**(2): p. 226-233.
154. Vivier, E., D.H. Raulet, A. Moretta, M.A. Caligiuri, L. Zitvogel, L.L. Lanier, W.M. Yokoyama, and S. Ugolini, *Innate or adaptive immunity? The example of natural killer cells.* Science, 2011. **331**(6013): p. 44-49.
155. Hamada, S., M. Umemura, T. Shiono, K. Tanaka, A. Yahagi, M.D. Begum, K. Oshiro, Y. Okamoto, H. Watanabe, K. Kawakami, et al., *IL-17A produced by gammadelta T cells plays a critical role in innate immunity against listeria monocytogenes infection in the liver.* The Journal of immunology, 2008. **181**(5): p. 3456-3463.
156. Theisen, E. and J.-D. Sauer, *Listeria monocytogenes-Induced Cell Death Inhibits the Generation of Cell-Mediated Immunity.* Infection and Immunity, 2017. **85**(1): p. 00733-16.
157. Nakane, A., M. Asano, S. Sasaki, S. Nishikawa, T. Miura, M. Kohanawa, and T. Minagawa, *Transforming growth factor beta is protective in host resistance against Listeria monocytogenes infection in mice.* Infection and immunity, 1996. **64**(9): p. 3901-3904.
158. Corr, S.C. and L.A.J. O'Neill, *Listeria monocytogenes infection in the face of innate immunity.* Cellular Microbiology, 2009. **11**(5): p. 703-709.
159. Machata, S., S. Tchatalbachev, W. Mohamed, L. Jänsch, T. Hain, and T. Chakraborty, *Lipoproteins of Listeria monocytogenes are critical for virulence and TLR2-mediated immune activation.* The Journal of Immunology, 2008. **181**(3): p. 2028-35.
160. Sakula, A., *Robert Koch: centenary of the discovery of the tubercle bacillus, 1882.* Thorax, 1982. **37**(4): p. 246-51.
161. Dookie, N., S. Rambaran, N. Padayatchi, S. Mahomed, and K. Naidoo, *Evolution of drug resistance in Mycobacterium tuberculosis: a review on the molecular determinants of resistance and implications for personalized care.* The Journal of antimicrobial chemotherapy, 2018. **73**(5): p. 1138-1151.
162. Guler, R. and F. Brombacher, *Host-directed drug therapy for tuberculosis.* Nat Chem Biol, 2015. **11**(10): p. 748-51.
163. Visvader, J., C.G. Begley, and J.M. Adams, *Differential expression of the LYL, SCL and E2A helix-loop-helix genes within the hemopoietic system.* Oncogene, 1991. **6**(2): p. 187-94.
164. Pirot, N., V. Deleuze, R. El-Hajj, C. Dohet, F. Sablitzky, P. Couttet, D. Mathieu, and V. Pinet, *LYL1 activity is required for the maturation of newly formed blood vessels in adulthood.* Blood, 2010. **115**(25): p. 5270-9.
165. Sakamoto, K., *The Pathology of Mycobacterium tuberculosis Infection.* Veterinary Pathology, 2012. **49**(3): p. 423-439.
166. Muefong, C.N. and J.S. Sutherland, *Neutrophils in Tuberculosis-Associated Inflammation and Lung Pathology.* Frontiers in Immunology, 2020. **11**(962): p. 1-9.
167. Manca, C., L. Tsenova, A. Bergtold, S. Freeman, M. Tovey, J.M. Musser, C.E. Barry, V.H. Freedman, and G. Kaplan, *Virulence of a Mycobacterium tuberculosis clinical isolate in mice is determined by failure to induce Th1 type immunity and is associated with induction of IFN-α/β.* Proceedings of the National Academy of Sciences, 2001. **98**(10): p. 5752-5757.
168. Maertzdorf, J., M. Ota, D. Repsilber, H.J. Mollenkopf, J. Weiner, P.C. Hill, and S.H. Kaufmann, *Functional correlations of pathogenesis-driven gene expression signatures in tuberculosis.* PLoS One, 2011. **6**(10): p. 26938-26946.

169. Berry, M.P.R., C.M. Graham, F.W. McNab, Z. Xu, S.A.A. Bloch, T. Oni, K.A. Wilkinson, R. Banchereau, J. Skinner, R.J. Wilkinson, et al., *An interferon-inducible neutrophil-driven blood transcriptional signature in human tuberculosis.* Nature, 2010. **466**(7309): p. 973-977.
170. Zhai, Y., L.M. Franco, R.L. Atmar, J.M. Quarles, N. Arden, K.L. Bucasas, J.M. Wells, D. Niño, X. Wang, G.E. Zapata, et al., *Host Transcriptional Response to Influenza and Other Acute Respiratory Viral Infections--A Prospective Cohort Study.* PLOS Pathogens, 2015. **11**(6): p. 1004869-1004898.
171. Guler, R., S.P. Parihar, G. Spohn, P. Johansen, F. Brombacher, and M.F. Bachmann, *Blocking IL-1α but not IL-1β increases susceptibility to chronic Mycobacterium tuberculosis infection in mice.* Vaccine, 2011. **29**(6): p. 1339-1346.
172. Mayer-Barber, K.D., B.B. Andrade, D.L. Barber, S. Hieny, C.G. Feng, P. Caspar, S. Oland, S. Gordon, and A. Sher, *Innate and adaptive interferons suppress IL-1α and IL-1β production by distinct pulmonary myeloid subsets during Mycobacterium tuberculosis infection.* Immunity, 2011. **35**(6): p. 1023-1034.
173. Mayer-Barber, K.D. and B. Yan, *Clash of the Cytokine Titans: counter-regulation of interleukin-1 and type I interferon-mediated inflammatory responses.* Cellular and Molecular Immunology, 2017. **14**(1): p. 22-35.
174. Mishra, B.B., V.A.K. Rathinam, G.W. Martens, A.J. Martinot, H. Kornfeld, K.A. Fitzgerald, and C.M. Sassetti, *Nitric oxide controls the immunopathology of tuberculosis by inhibiting NLRP3 inflammasome-dependent processing of IL-1β.* Nature Immunology, 2013. **14**(1): p. 52-60.
175. Huang, Y., L.M. Blatt, and M.W. Taylor, *Type 1 interferon as an antiinflammatory agent: inhibition of lipopolysaccharide-induced interleukin-1 beta and induction of interleukin-1 receptor antagonist.* Journal of Interferon and Cytokine Research, 1995. **15**(4): p. 317-21.
176. Ainscough, J.S., G. Frank Gerberick, M. Zahedi-Nejad, G. Lopez-Castejon, D. Brough, I. Kimber, and R.J. Dearman, *Dendritic cell IL-1α and IL-1β are polyubiquitinated and degraded by the proteasome.* The Journal of Biological Chemistry, 2014. **289**(51): p. 35582-35592.
177. Rapovy, S.M., J. Zhao, R.L. Bricker, S.M. Schmidt, K.D.R. Setchell, and J.E. Qualls, *Differential Requirements for L-Citrulline and L-Arginine during Antimycobacterial Macrophage Activity.* The Journal of Immunology 2015. **195**(7): p. 3293-3300.
178. Jamaati, H., E. Mortaz, Z. Pajouhi, G. Folkerts, M. Movassaghi, M. Moloudizargari, I.M. Adcock, and J. Garssen, *Nitric Oxide in the Pathogenesis and Treatment of Tuberculosis.* Frontiers in Microbiology, 2017. **8**: p. 2008-2019.
179. MacMicking, J.D., R.J. North, R. LaCourse, J.S. Mudgett, S.K. Shah, and C.F. Nathan, *Identification of nitric oxide synthase as a protective locus against tuberculosis.* Proceedings of the National Academy of Sciences, 1997. **94**(10): p. 5243-5248.
180. Herbst, S., U.E. Schaible, and B.E. Schneider, *Interferon gamma activated macrophages kill mycobacteria by nitric oxide induced apoptosis.* PLoS One, 2011. **6**(5): p. e19105.
181. Gideon, H.P., J. Phuah, B.A. Junecko, and J.T. Mattila, *Neutrophils express pro- and anti-inflammatory cytokines in granulomas from Mycobacterium tuberculosis-infected cynomolgus macaques.* Mucosal Immunology, 2019. **12**(6): p. 1370-1381.
182. Nouailles, G., A. Dorhoi, M. Koch, J. Zerrahn, J. Weiner, K. Faé, F. Arrey, S. Kuhlmann, S. Bandermann, D. Loewe, et al., *CXCL5-secreting pulmonary epithelial cells drive destructive neutrophilic inflammation in tuberculosis.* The Journal of Clinical Investigation, 2014. **124 3**: p. 1268-82.
183. Sawant, K.V., R. Xu, R. Cox, H. Hawkins, E. Sbrana, D. Kolli, R.P. Garofalo, and K. Rajarathnam, *Chemokine CXCL1-Mediated Neutrophil Trafficking in the Lung: Role of CXCR2 Activation.* Journal of Innate Immunity, 2015. **7**(6): p. 647-658.
184. Lyadova, I.V., *Neutrophils in Tuberculosis: Heterogeneity Shapes the Way?* Mediators of Inflammation, 2017. **2017**: p. 8619307-8619307.
185. Eruslanov, E.B., I.V. Lyadova, T.K. Kondratieva, K.B. Majorov, I.V. Scheglov, M.O. Orlova, and A.S. Apt, *Neutrophil Responses to Mycobacterium tuberculosis Infection in Genetically Susceptible and Resistant Mice.* Infection and Immunity, 2005. **73**(3): p. 1744-1753.

186. Shibata, Y., P.Y. Berclaz, Z.C. Chroneos, M. Yoshida, J.A. Whitsett, and B.C. Trapnell, *GM-CSF regulates alveolar macrophage differentiation and innate immunity in the lung through PU.1*. Immunity, 2001. **15**(4): p. 557-67.
187. Stanley, E., G.J. Lieschke, D. Grail, D. Metcalf, G. Hodgson, J.A. Gall, D.W. Maher, J. Cebon, V. Sinickas, and A.R. Dunn, *Granulocyte/macrophage colony-stimulating factor-deficient mice show no major perturbation of hematopoiesis but develop a characteristic pulmonary pathology*. Proceedings of the National Academy of Sciences of the United States of America, 1994. **91**(12): p. 5592-5596.
188. Akagawa, K.S., K. Kamoshita, and T. Tokunaga, *Effects of granulocyte-macrophage colony-stimulating factor and colony-stimulating factor-1 on the proliferation and differentiation of murine alveolar macrophages.* The Journal of Immunology, 1988. **141**(10): p. 3383-90.
189. Jayaraman, P., I. Sada-Ovalle, T. Nishimura, A.C. Anderson, V.K. Kuchroo, H.G. Remold, and S.M. Behar, *IL-1β promotes antimicrobial immunity in macrophages by regulating TNFR signaling and caspase-3 activation.* The Journal of Immunology, 2013. **190**(8): p. 4196-4204.
190. Sonderegger, I., G. Iezzi, R. Maier, N. Schmitz, M. Kurrer, and M. Kopf, *GM-CSF mediates autoimmunity by enhancing IL-6-dependent Th17 cell development and survival.* The Journal of experimental medicine, 2008. **205**(10): p. 2281-2294.
191. Nagabhushanam, V., A. Solache, L.-M. Ting, C.J. Escaron, J.Y. Zhang, and J.D. Ernst, *Innate Inhibition of Adaptive Immunity: Mycobacterium tuberculosis-Induced IL-6 Inhibits Macrophage Responses to IFN-γ.* The Journal of Immunology, 2003. **171**(9): p. 4750-4757.
192. Redford, P.S., A. Boonstra, S. Read, J. Pitt, C. Graham, E. Stavropoulos, G.J. Bancroft, and A. O'Garra, *Enhanced protection to Mycobacterium tuberculosis infection in IL-10-deficient mice is accompanied by early and enhanced Th1 responses in the lung.* European Journal of Immunology, 2010. **40**(8): p. 2200-2210.
193. Beamer, G.L., D.K. Flaherty, B.D. Assogba, P. Stromberg, M. Gonzalez-Juarrero, R. de Waal Malefyt, B. Vesosky, and J. Turner, *Interleukin-10 promotes Mycobacterium tuberculosis disease progression in CBA/J mice.* The Journal of Immunology, 2008. **181**(8): p. 5545-50.
194. Higgins, D.M., J. Sanchez-Campillo, A.G. Rosas-Taraco, E.J. Lee, I.M. Orme, and M. Gonzalez-Juarrero, *Lack of IL-10 alters inflammatory and immune responses during pulmonary Mycobacterium tuberculosis infection.* Tuberculosis, 2009. **89**(2): p. 149-57.

Appendix

Appendix A

Thymus Lymphoid Gating Strategy

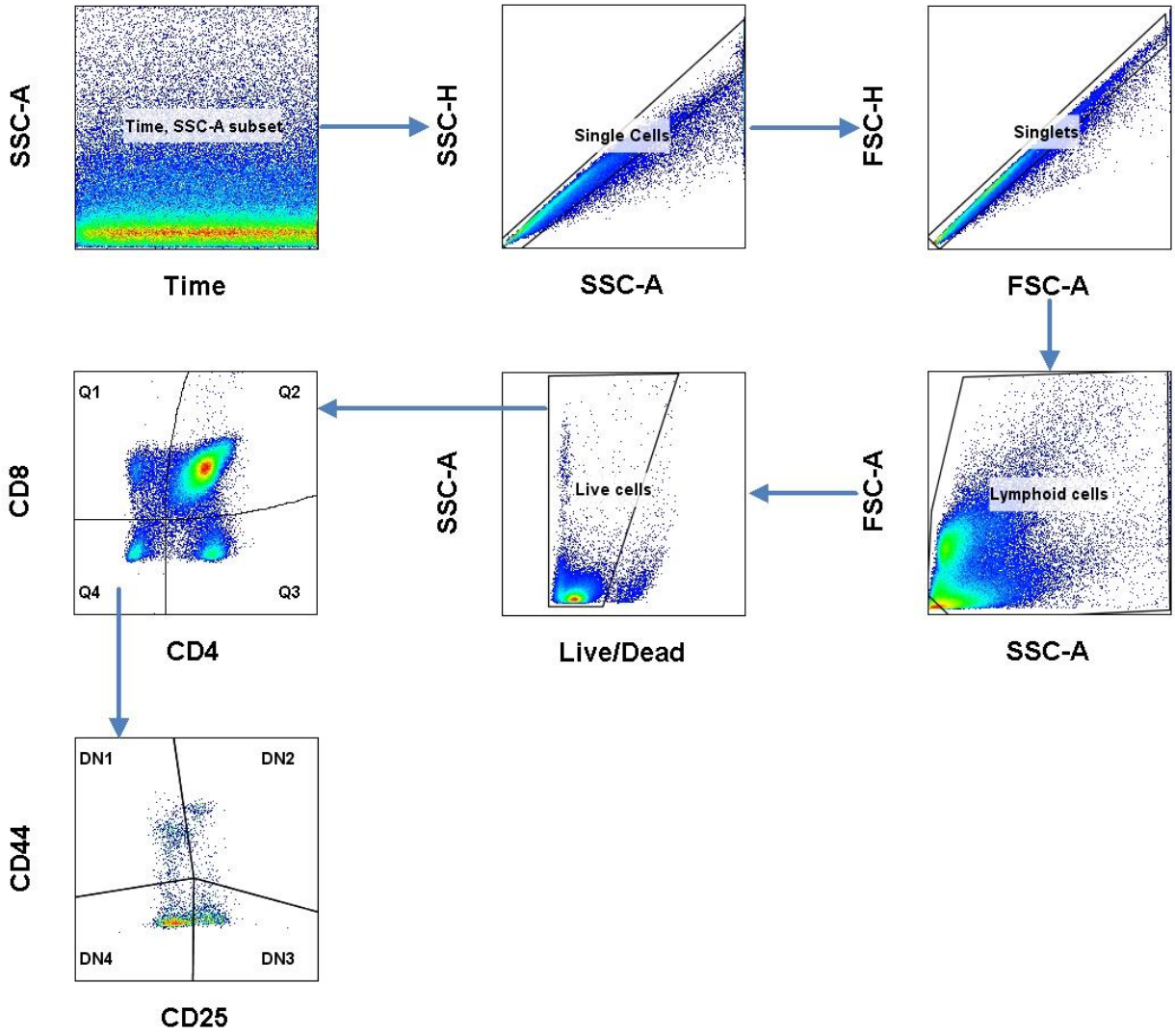

Appendix B

Lung, Lymph Node, Spleen & Liver Lymphoid Gating Strategy

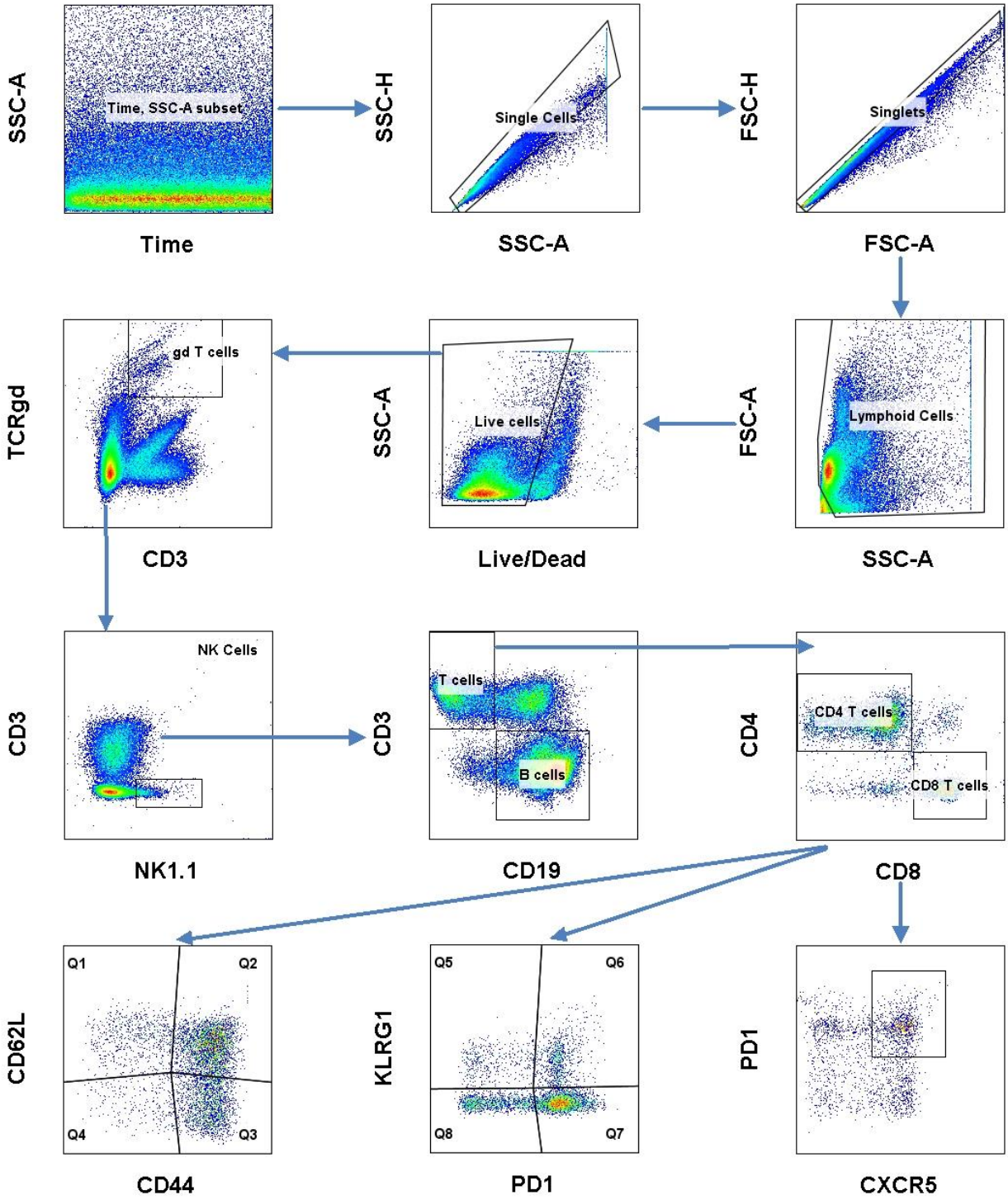

Appendix C

Lung Myeloid Gating Strategy

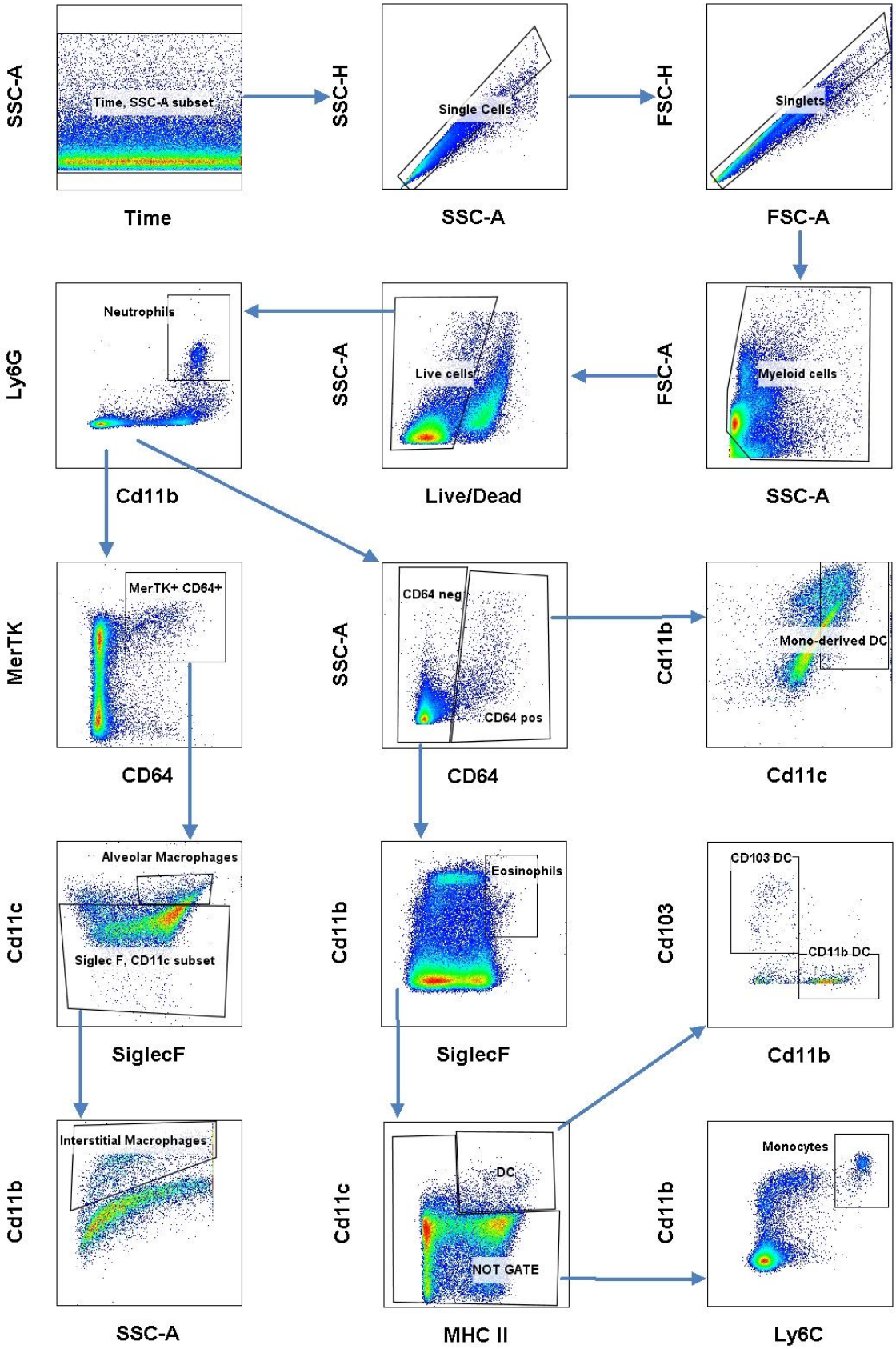

Appendix D

Lymph Node Myeloid Gating Strategy

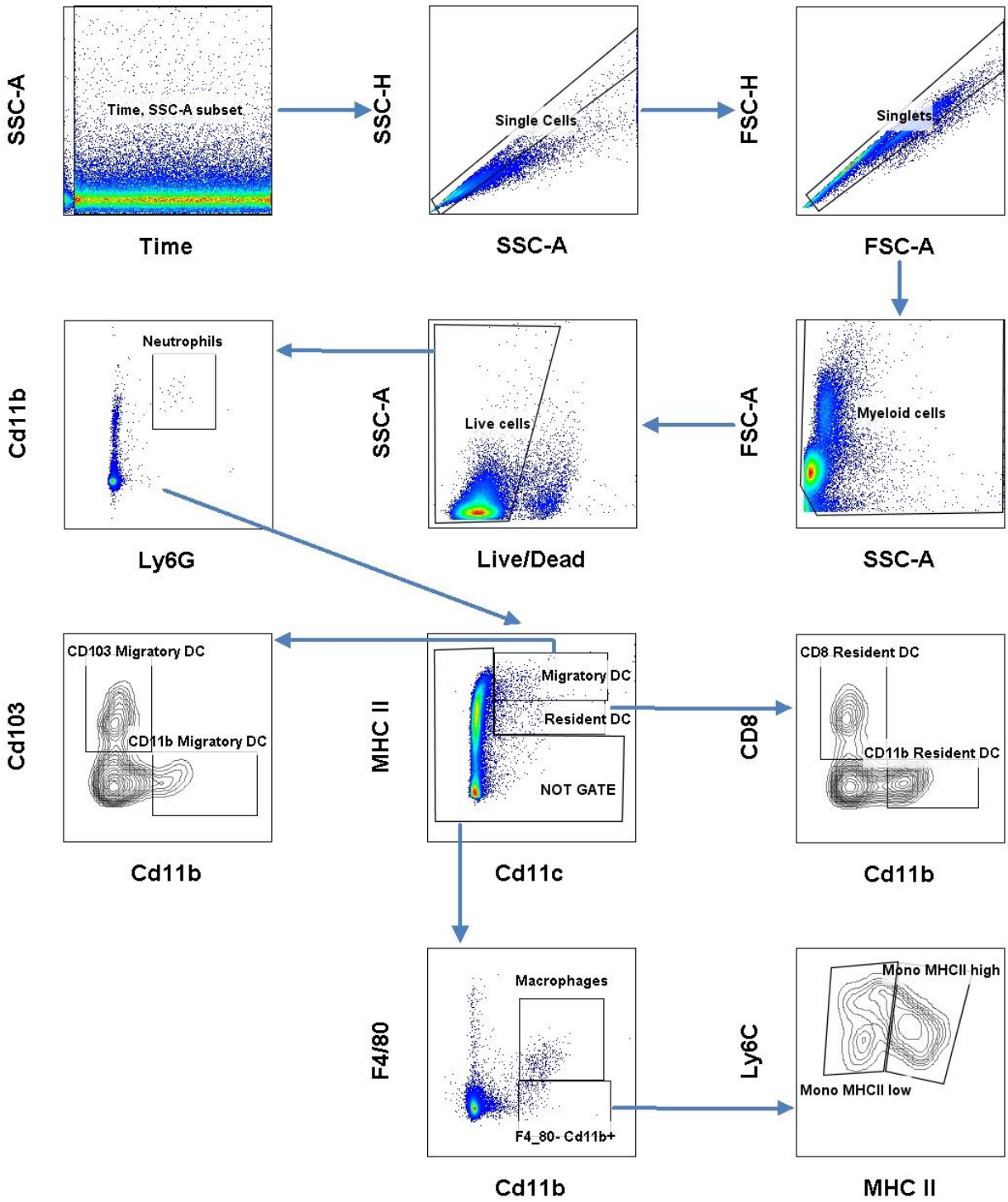

Appendix E

Liver Myeloid Gating Strategy

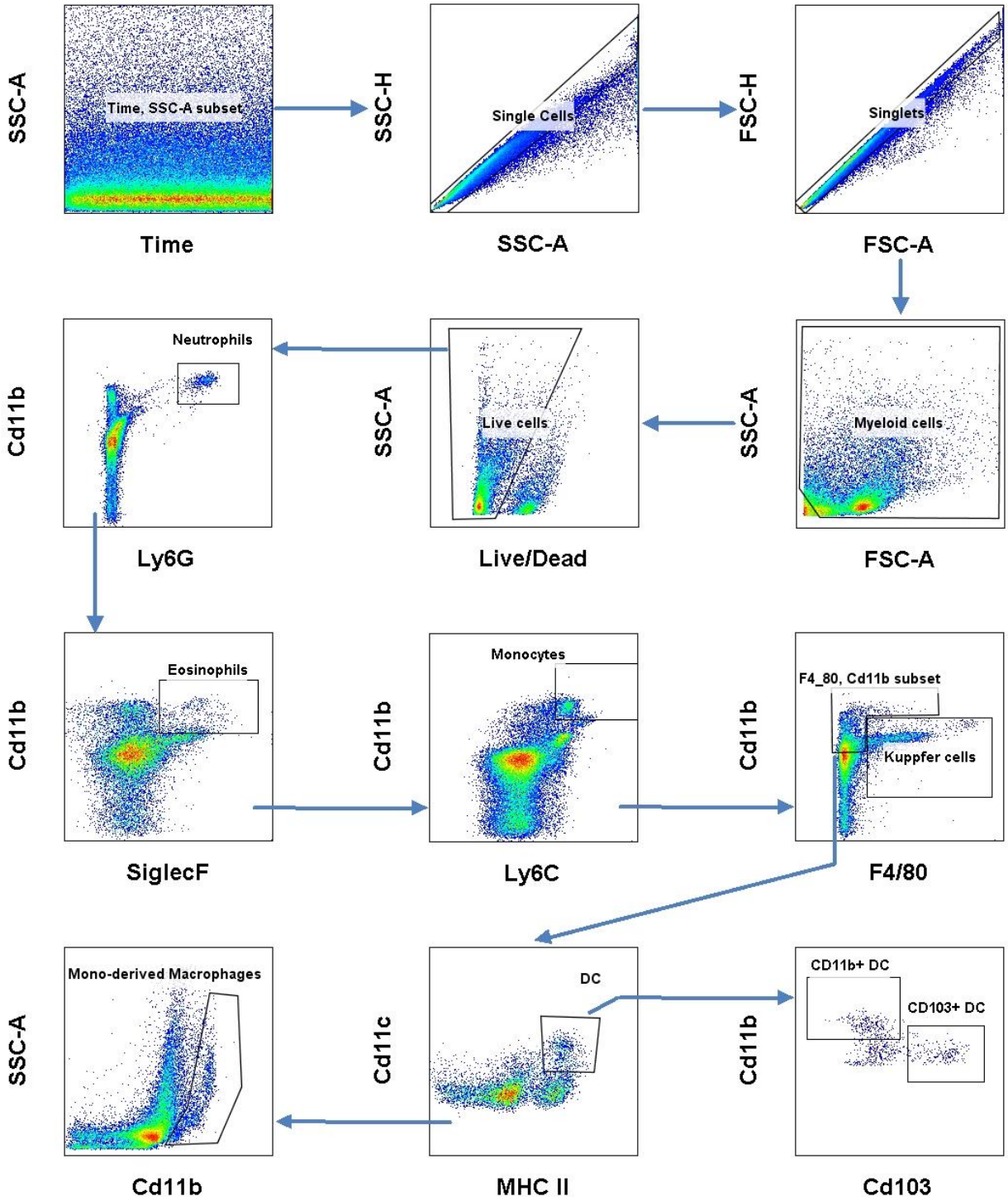

Appendix F

Spleen Myeloid Gating Strategy

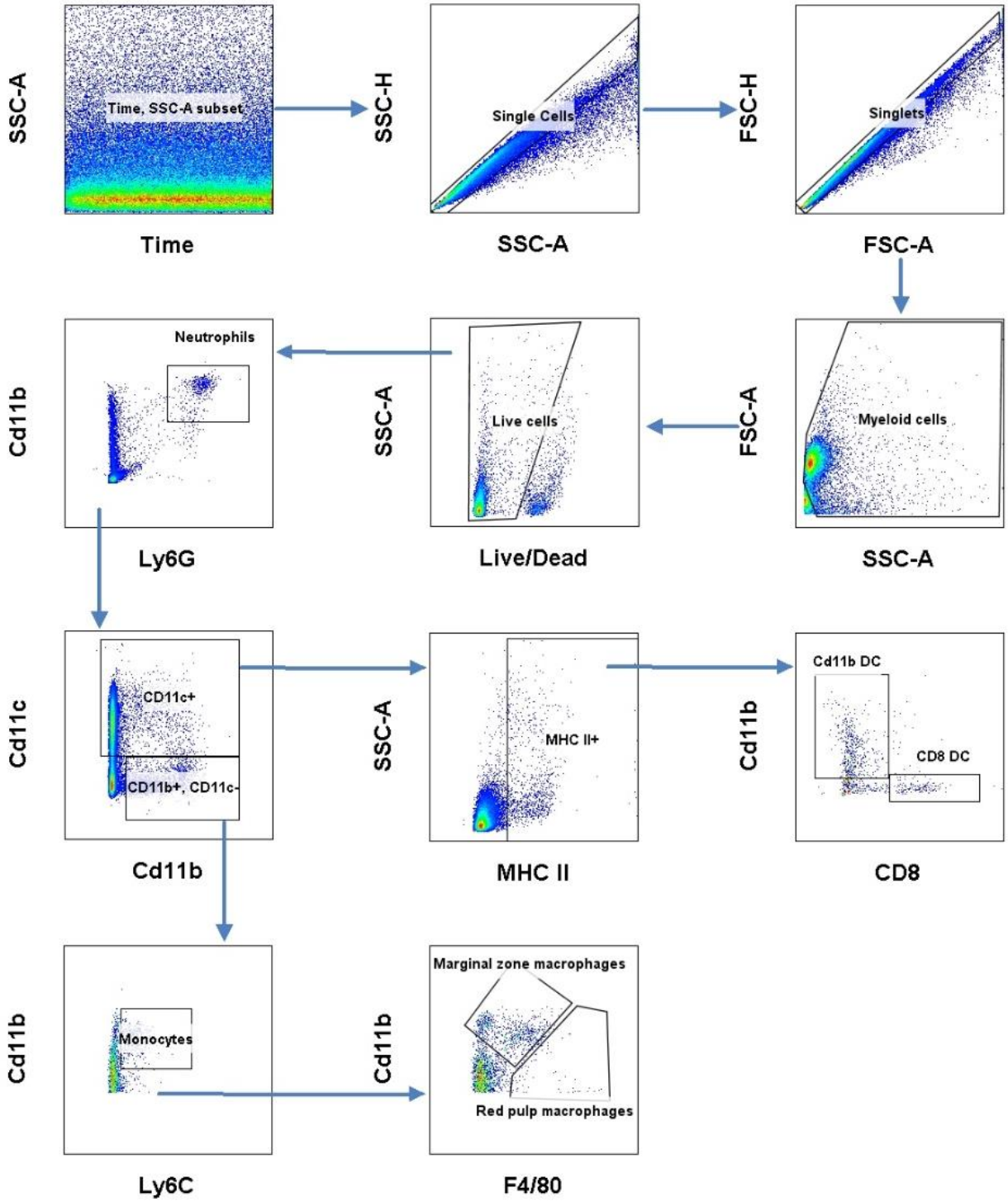

Appendix G

Gene Target	Primer Sequence	PCR Conditions	
Hprt – forward	5’ – GTT GGA TAT GCC CTT GAC – 3’	***D:*** 95°C	***A:*** 58°C
Hprt – reverse	5’ – AGG ACT AGA ACA CCT GCT – 3’	***E:*** 72°C	***S:*** 76°C
***HPRT – forward**	5’ – AGG CGA ACC TCT CGG CTT T – 3’	***D:*** 95°C	***A:*** 60°C
***HPRT – reverse**	5’ – AAG ACG TTC AGT CCT GTC CAT – 3’	***E:*** 72°C	***S:*** 80°C
Lyl1 – forward	5’ – CCC CTT CCT CAA CAG TGT CTA C – 3’	***D:*** 95°C	***A:*** 60°C
Lyl1 – reverse	5’ – TAT GGC TTG GTC TGC GCT TC – 3’	***E:*** 72°C	***S:*** 80°C
***LYL1 – forward**	5’ – CAT CTT CCC TAG CAG CCG GTT G – 3’	***D:*** 95°C	***A:*** 60°C
***LYL1 – reverse**	5’ – GTT GGT GAA CAC GCG CCG – 3’	***E:*** 72°C	***S:*** 80°C
Nos2 – forward	5’ – AAC TGC AAG AGA ACG GAG AAC G – 3’	***D:*** 95°C	***A:*** 64°C
Nos2 – reverse	5’ – AAC ATT CTG TGC TGT CCC AGT – 3’	***E:*** 72°C	***S:*** 80°C
TNFα – forward	5’ – TCT CAT CAG TTC TAT GGC CC – 3’	***D:*** 95°C	***A:*** 62°C
TNFα – reverse	5’ – GGG AGT AGA CAA GGT ACA AC – 3’	***E:*** 72°C	***S:*** 80°C
Ifnβ – forward	5’ – CAG CTC CAA GAA AGG ACG AAC – 3’	***D:*** 95°C	***A:*** 60°C
Ifnβ – reverse	5’ – GGC AGT GTA ACT CTT CTG CAT – 3’	***E:*** 72°C	***S:*** 80°C
Il-1α – forward	5’ – CGC TTG AGT CGG CAA AGA AAT C – 3’	***D:*** 95°C	***A:*** 60°C
Il-1α – reverse	5’ – ATA CTG TCA CCC GGC TCT CC – 3’	***E:*** 72°C	***S:*** 78°C
Il-1β – forward	5’ – TGC CAC CTT TTG ACA GTG ATG – 3’	***D:*** 95°C	***A:*** 60°C
Il-1β – reverse	5’ – ATG TGC TGC TGC GAG ATT TG – 3’	***E:*** 72°C	***S:*** 80°C
Il-6 – forward	5’ – GTT CTC TGG GAA ATC GTG GA – 3’	***D:*** 95°C	***A:*** 60°C
Il-6 – reverse	5’ – TGT ACT CCA GGT AGC TAT GG – 3’	***E:*** 72°C	***S:*** 76°C
Il-10 – forward	5’ – AGC CGG GAA GAC AAT AAC TG – 3’	***D:*** 95°C	***A:*** 60°C
Il-10 – reverse	5’ – CAT TTC CGA TAA GGC TTG G – 3’	***E:*** 72°C	***S:*** 80°C
CXCL1 – forward	5’ – ACT GCA CCC AAA CCG AAG TC – 3’	***D:*** 95°C	***A:*** 60°C
CXCL1 – reverse	5’ – TGG GGA CAC CTT TTA GCA TCT T – 3’	***E:*** 72°C	***S:*** 80°C
GM-CSF – forward	5’ – TGA ACC TCC TGG ATG ACA TG – 3’	***D:*** 95°C	***A:*** 60°C
GM-CSF – reverse	5’ – GTG TTT CAC AGT CCG TTT CC – 3’	***E:*** 72°C	***S:*** 80°C

*******Human primers;* ***D****-denaturing;* ***A****-annealing;* ***E****-extension;* ***S****-final step*